INVESTIGATING THE UPR IN FIBROTIC LUNG DISEASE

Investigating Strategies to Modulate Macrophage Function to Prevent the Progression of Fibrotic Lung Disease

By

EHAB AYAUB, Hon. B.Sc.

A Thesis Submitted to the School of Graduate Studies in Partial Fulfillment of the Requirements for the Degree Doctor of Philosophy

McMaster University

DOCTOR OF PHILOSOPHY (2017) McMaster University
Department of Medical Sciences Hamilton, Ontario, Canada

TITLE: Investigating strategies to modulate macrophage function to prevent the progression of fibrotic lung disease

AUTHOR: Ehab Ayaub, Hon. B.Sc. in Life Science (McMaster University)

SUPERVISOR: Dr. Kjetil Ask

NUMBER OF PAGES: xv, 270

ABSTRACT

Tissue fibrosis occurs in the advanced stages of various chronic diseases and can account for 45% of all deaths related to chronic diseases worldwide. The extracellular matrix (ECM) components comprising the fibrotic scar are primarily derived from myofibroblasts, which are contractile fibroblasts arising from the trans-differentiation of several cellular progenitors. Disturbances in immune cell infiltration and function could lead to the uncontrolled production of pro/anti-inflammatory mediators, which may alter the phenotype, state, and function of myofibroblasts progenitors, leading to aberrant wound repair and pathological fibrosis. A great deal of knowledge has implicated macrophages in the pathogenesis and exacerbation of the fibrotic process. Nonetheless, much remains to be elucidated on the potential mechanisms regulating macrophage accumulation and pro-fibrotic polarization, and whether these mechanisms can be further investigated to modulate tissue repair. The Endoplasmic reticulum (ER) stress has recently been implicated as a key mechanism that propagates the pathogenesis of the fibrotic process. How ER stress precisely impacts the fibrotic process is still unclear. This thesis partly explored how modulating the outcome of ER stress – the unfolded protein response (UPR), would affect the severity of lung fibrosis and addressed the role of IL-6 signalling in macrophages during fibrosis. The data demonstrated that UPR activation in pro-fibrotic macrophages and partial deficiency of Grp78, the master regulator of the UPR, abrogated pulmonary fibrotic changes and reduced the accumulation of pro-fibrotic (M2-like) macrophages. These findings were later associated with high TUNEL levels, 7AAD positive cells, Chop and cleaved caspase 3 levels, which are suggestive of GRP78

mediated apoptosis in this population. On the contrary, mice lacking a terminal UPR mediator of apoptosis, called Chop, had increased ECM deposition and greater persistence of non-apoptotic macrophages. These findings suggest that UPR-mediated macrophage polarization and apoptosis may alter lung wound repair processes. As IL-6 synergized the effect of IL-4 to promote a hyper M2 macrophage state, it provided a unique and compelling model to study the dynamics of macrophage alternative programming, which has set the stage to investigate whether the UPR was implicated in the generation of a hyper pro-fibrotic macrophage phenotype. This hyper M2 macrophage model led to the identification of ER expansion program and the IRE1-XBP1 arm of the UPR in pro-fibrotic macrophage polarization, and suggested an unprecedented *in vivo* role of IL-6 in priming macrophages in the injured lungs to possibly potentiate pathological wound repair. Looking forward, many questions remain to be answered in order to precisely identify the vital UPR axis regulating ER expansion in macrophages during pathological wound repair and to get closer to the understanding of whether the UPR modulates the pro-fibrotic/pro-resolving capacity of macrophages. Insights on these mechanisms may facilitate the development of therapeutics that better manage chronic fibrotic diseases which pose fatal consequences and increase public concern.

AKNOWLEDGMENTS

I have been fortunate to have had the opportunity to conduct this work and gain deeper insights into the fibrotic disease process. This work was not solely a one-individual's work, but rather a collaborative effort of many individuals, and would not have been possible without their support. First and foremost, a special acknowledgement to my supervisor, mentor and friend, Dr. Kjetil Ask. Your kindness and humility has no end and can speak for itself. Thank you for listening tirelessly to my ideas and for always believing in my potential. Thank you for giving me a lot of freedom in the lab and for draining your grant account, even at times of financial distress. You have always promoted positive thinking and strived to foster my scientific growth. It has been an absolute pleasure to work with you. Dr. Carl Richards, you have been my second supervisor during my Masters and Ph.D. Many of our discussions in the hallway and around the lab area have inspired me to become a better scientist and to push myself beyond my limits to accomplish my goals. Dr. Martin Stampfli, a massive thank you for continuing to peak my interest in immunology and for allowing me to be part of the immunology teaching assistant crew. To all of my committee members, including Dr. Mark Inman and Jeffrey Dickhout, thank you for your helpful advice and constructive criticism. To the members of the fibrosis group, Dr. Martin Kolb, Jack Gauldie and Peter Margetts, thank you for constantly raise my interest in fibrosis research and for always providing unique insights and perspectives to my work.

My deepest gratitude also goes to the technicians, students, and faculty at the Firestone Institute for Respiratory Health and the McMaster Immunology Research Centre for your immense friendship, invaluable time, great expertise and helpful discussions throughout the years. I am very indebted to Jane Ann Smith for exceptional technical assistance. You were instrumental to the success to all of my experiments. Talveer Mandur taught me that dawn-to-midnight days are possible and can be enjoyable most of the time. Josh McGrath, Steven Cass, Rocky Lai! Thank you for the many stimulating scientific and sports discussions over a pint of beer at Phoenix, Amanda Lee for being the best COMPS buddy, Anisha Dubey for being a wonderful friend and a Western blot guru, Rodrigo Jiménez-Saiz and Jewel Imani for being awesome squash mates and wonderful friends. Jewel and Dr. Fernando Botelho, you were key to the success of many of my long day FACS experiments, so thank you. To Anisha Dubey, Karun Tandon, Tina Nham, Chandak Upagupta, Pavithra Parasarathy and Hemisha Patel, thank you for being great friends and colleagues and for keeping me sane throughout the years. I wish you the very best from the bottom of my heart. I would also like to thank Hemisha Patel and Sauyoung Lee for their helpful edits and proofreading of this document. To James Murphy, I have had the immense pleasure overseeing your progress leading our industrial work and I am sure there is a bright future ahead of you. To the army of undergrads and co-op students that we had over the years, best of luck in your future endeavours and I hope you all do great in research, medical school and beyond. I would like to thank coffee, MDCL Timmies for serving coffee, and my mom, for making me coffee every morning. To my family and siblings, thank you for putting up with my

late night hours and for believing that I was actually doing work. To my parents who left war-torn Iraq, leaving everything behind and facing uncertainty, thank you for providing for me and my siblings. Thank you Canada for the incredible opportunities you provided.

TABLE OF CONTENTS

List of figures and Tables

None

List of abbreviations

AAMs	Alternatively activated macrophages
ADAM17	A disintegrin and metalloproteinase 17
AECs	Alveolar epithelial cells
AM	Alveolar macrophage
AE-IPF	Acute exacerbation of IPF
Akt1	Akt Serine/Threonine kinase 1
ATF6	Activating transcription factor 6
ATF4	Activating transcription factor 4
αSMA	Alpha smooth muscle actin
AEBSF	4-(2-Aminoethyl) benzenesulfonyl fluoride hydrochloride
BALF	Bronchoalveolar lavage fluid
BMDMs	Bone marrow-derived macrophages
C/EBPβ	CCAAT/enhancer binding protein β
CHOP	C/EBP homologous protein
Cst	Quasi-static compliance
eIF2	eukaryotic translation Initiation Factor 2
ER	Endoplasmic reticulum
EMT	Epithelial-to-mesenchymal transition
EndoMT	Endothelial-to-mesenchymal transformation
EDEM1	ER degradation enhancer, mannoside alpha-like 1
ECM	Extracellular matrix
Est	Quasi-static elastance
FVC	Forced vital capacity
GP130	Glycoprotein 130
GRP78	Glucose-regulated protein 78
IFNγ	Interferon gamma
IL-6	Interleukin 6
ILD	Interstitial lung disease
IRE1	Inositol-requiring enzyme 1
IPF	Idiopathic pulmonary fibrosis
K_{value}	Salazar-Knowles Parameter
LPS	Lipopolysaccharide
mIL-6Rα	Membrane-bound interleukin 6 receptor alpha
MIP-1α	Macrophage inflammatory protein 1-alpha
OSM	Oncostatin M
4-PBA	4-Phenyl butyrate acid
PV loop	Pressure-volume loop
PERK	Protein kinase RNA-like endoplasmic reticulum kinase
ROS	Reactive oxygen species
SatM	Segregated-nucleus-containing atypical monocytes
STAT3	Signal transducer and activator of transcription 3
STF	STF-083010
Tc2	Type II effector CD8+ cells
TNFα	Tumour necrosis factor alpha
TM	Tunicamycin
TGF-β1	Transforming growth factor beta 1
UPR	Unfolded protein response
XBP-1	X-box binding protein 1 (s = spliced or t = total)

Preface

The Ph.D. thesis shown in this document is presented in the "Sandwich" format as per the instructions illustrated in the "Guide for the Preparation of Master's and Doctoral Theses" provided by the School of Graduate Studies at McMaster University. Chapter 1 is an introduction chapter which contains general knowledge that ties together the three main studies presented in this document. Chapters 2-4 constitute the body of the work and include three independent but conceptually related studies investigating mechanisms and processes aimed at better understanding the implication of macrophages in modulating fibrogenesis. In these sections, I have primarily outlined the duration and status of the work, as well as my contributions. Details pertaining to the conception and design of the studies, performance of experiments, analysis and interpretation of the data, drafting of the manuscript, as well as editing and revising the manuscript are indicated in each chapter (2-4).

Chapter 1: This chapter contains introductory topics essential for the understanding of the rationale and objectives of the work in chapters (2-4).

Chapter 2: **Ayaub EA**, Kolb PS, Mohammed-ali Z, Tat V, Murphy J, Bellaye PS, Shimbori C, Boivin FJ, Lai R, Lynn EG, Lhotak S, Bridgewater D, Kolb MRJ, Inman MD, Dickhout JG, Austin RC, Ask K. GRP78 and CHOP modulate macrophage apoptosis and the development of

bleomycin-induced pulmonary fibrosis. *Journal of Pathology* 2016; 239: 411 – 425.

This work has been performed over the period of November 2012 – March 2016. I initiated this study at the start of my Masters and continued to work on it during my Ph.D. As the primary author, I designed and performed the majority of the experiments, analysed and interpreted most of the generated data, and drafted the manuscript. Experimental assistance was provided by undergraduate students (PSK, VT, JM), graduate students (ZM, RL, FJB) and post-doctoral fellows (PSB, CS, EGL). Dr. RCA and JGD provided the *Grp78*$^{+/-}$ mice and gave scientific input. Drs. MDI, MRJK and DB critically appraised the manuscript. KA overlooked the project, designed key experiments and edited the manuscript.

Chapter 3: **Ayaub EA**, Tandon K, Parthasarathy P, Dvorkin-Gheva A, Dubey A, Murphy J, Kolb PS, Lhotak S, Kolb MRJ, Austin RC, Richards CD, Ask K. IL-6 mediates ER expansion and hyperpolarization of alternatively activated macrophages**.** Manuscript to be submitted.

This work started in May 2015. As the primary author, I conceptualized the majority of the experiments, analysed and interpreted most of the generated data, and drafted the manuscript. Experimental assistance was provided by undergraduate students (PSK, JM) and graduate students (KT, PP). KT provided the human link by confirming the phenomena in the THP-1 human monocytic cell line. Dr. SL processed samples for

transmission electron microscopy and provided intellectual input with the interpretation of the images. Dr. AD assisted with the bioinformatics and generated the hierarchical clustering analysis of the immune/inflammatory and UPR related genes. Dr. RCA and MRJK gave scientific input. Dr. CDR provided the expertise in gp130-mediated IL-6 signalling. KA overlooked the project, designed key experiments and edited the manuscript.

Chapter 4: **Ayaub EA**, Dubey A, Imani J, Botelho F, Kolb MRJ, Richards CD, Ask K. Overexpression of OSM and IL-6 impacts the polarization of pro-fibrotic macrophages and the development of bleomycin-induced lung fibrosis. *Scientific reports* (August 2017). Manuscript in revision.

This work started in Nov 2015. As the primary author, I conceptualized the majority of the experiments in this project, analysed and interpreted most of the generated data, and drafted the manuscript. AD significantly contributed to this project by performing all the Western blots and helped to draft the manuscript. Experimental assistance was also provided by JI (Ph.D. student) and Dr. FB (Research associate) who both helped to interpret the results of the flow cytometry. Dr. MRJK provided intellectual input regarding fibrosis. Dr. CDR provided the expertise in gp130-mediated IL-6/OSM signalling, and with Dr. KA, overlooked the project, designed key experiments and edited the manuscript.

Chapter 5: This chapter includes the discussion of the three primary projects included in this thesis. The significance of the major findings has been highlighted while discussing how the generated data added new knowledge to the field. Potential implications and future directions have also been included.

Chapter 1

Introduction

Fibrotic lung disease – Overview

Fibrosis constitutes a major pathological process contributing to interstitial lung disease (ILD) progression and mortality. Idiopathic pulmonary fibrosis (IPF) is a chronic progressive lung disease, which is typically fatal within 2-3 years of diagnosis [1]. This disease is estimated to affect around 30,000 Canadians, where approximately 6000 new diagnoses are made every year [2]. A large portion of IPF patients experience accelerated disease progression and rapid decline in lung function, known as acute exacerbation of IPF (AE-IPF) [3, 4]. There are various triggers to AE-IPF, such as mechanical injury/stress, infections, as well exposure to environmental pollutants; it is now recognized that a hyper-active immune compartment may also influence the prognosis of the disease [4-6]. Although the origin and development of IPF remains to be fully understood, it is believed that fibrosis is associated with a progressive accumulation of myofibroblasts, specialized cells involved in secreting and depositing collagen and other extracellular matrix (ECM) proteins crucial for the scarring process [7-9]. The accumulation of scarring materials leads to increased stiffness in the lung which makes breathing increasingly more difficult.

Immune cell involvement and the role of inflammation in lung fibrosis have recently regained the attention of the medical and scientific community. Interestingly, while inflammatory mediators and immune cells are intricately involved in the pathogenesis of IPF, corticosteroid treatments have shown poor efficacy. The poor response does not necessarily equate a lack of involvement of the immune compartment, as there are many

inflammatory diseases in which anti-inflammatory therapies are ineffective [10, 11]. These findings raise potential for an alternate immune pathway, and suggest a need to precisely delineate specific targets to better understand the immune cell hypothesis in the progression of the fibrotic process. The immune cell hypothesis states that the rapid progression of fibrosis is mediated by episodic and possibly silent inflammatory events. More precisely, it is postulated that specific subsets of activated leukocytes (T cells, monocytes or macrophages) contribute to the steep progression of fibrosis by expressing factors that enhance the pro-fibrotic phenotype and function of structural cells, such as epithelial cell and fibroblasts. Recent progress in IPF therapeutics has been made in the form of two FDA approved drugs, Pirfenidone and Nintedanib, which slowed IPF disease progression, as demonstrated by their ability to significantly reduce the annual rate of decline in forced vital capacity (FVC), which is regarded as the primary end point in both trials [12, 13]. However, there are still unmet medical needs in many patients that continue have severe IPF. This suggests a need to further investigate targetable biological processes, which may lead to treatment options that have a profound effect on the progression of IPF.

Cellular contributors to lung fibrosis

The primary cell type that directly impacts the process of ECM buildup is the myofibroblast. Myofibroblasts are contractile fibroblasts that express smooth muscle actin stress fibers, and are known to efficiently synthesize collagen and other extracellular matrix proteins [14]. Although the exact cellular progenitor of myofibroblasts during

fibrosis is still unclear, myofibroblasts are generally thought to originate from the trans-differentiation of various cells types. Some of the most common progenitors include: Epithelial cells, through epithelial-to-mesenchymal transition (EMT) [15, 16]; endothelial cells, through endothelial-to-mesenchymal transition (EndoMT) [17, 18]; fibrocytes [19, 20]; and fibroblasts [21]. Mechanisms interfering with myofibroblast activities, such as proliferation or survival in the fibrotic milieu and ECM deposition, could impact the severity of fibrosis.

Aside from myofibroblasts, the accumulation of immune cell infiltrates including lymphocytes, macrophages, neutrophils and eosinophils have been associated with pathological changes in patients with usual interstitial pneumonia (UIP), a common feature of fibrotic lung disease [22]. Immune cells are believed to be the upstream cells that orchestrate the process of fibrogenesis, either through the secretion of pro-fibrotic mediators or through various actions that remain to be elucidated [23, 24]. In IPF, there have been long standing beliefs that immune cells are not initially required to develop fibrosis. With recent advancements of knowledge revolving around fibrosis, it is more increasingly recognized that immune cells can propagate the fibrotic process, especially in cases of infection and recurrent tissue injury to the epithelium/endothelium. Our goal is to identify, modulate and better understand the primary immune compartment that significantly alters myofibroblasts accumulation and pro-fibrotic function.

T cells in pulmonary fibrosis

Although the precise involvement of the adaptive immune compartment in pulmonary fibrosis remains controversial [25, 26], there is increasing evidence that T cells may influence fibrotic disease pathogenesis. In 2007, IPF research regained interest in T cells when Feghali-Bostwick et al. demonstrated that CD4 T lymphocytes from IPF patients have auto-reactive clonal expansion properties against IPF lung fibrotic extracts, not seen in healthy control lungs [27]. The authors demonstrated increased autoantibody production and augmented T cell proliferative capacity in response to cellular self-antigens derived from the fibrotic ECM. In many fibrotic lung diseases such as IPF and sarcoidosis, both CD4 and CD8 were present and activated [28, 29]. Furthermore, the shift of T cells towards the CD8 phenotype was associated with poor prognosis in IPF patients. Animals lacking T cells or CD28, a co-stimulatory signal required for T cell activation, experienced reduced fibroblast proliferation and ECM deposition during bleomycin-induced lung fibrosis [30], while reduced expression of CD28 on CD4+ T cells predicted poor survival [31], suggesting the complexity of T cell subtypes. Studies from IPF disease models such the bleomycin model suggest that the specialized subsets, Th1 and γδT cells, elicit anti-fibrotic effects in the animal model [32, 33], while those subsets with Th17 and Th2-mediated cells promote fibrotic effects [34, 35]. In the bleomycin-induced pulmonary fibrosis model, regulatory T cells (T_{regs}) had opposing roles during early and late phase of the disease [36, 37]. While T_{regs} contributed to enhanced fibrogenic potential during the inflammatory phase, they had a suppressive role during the chronic fibrotic stage of the disease. In the silica-induced lung fibrosis in mice, T_{regs} were recruited to the lung and were responsible for the production of the fibrogenic

cytokines, TGFβ1, IL-10, PDGF and IL-6 [38]. In the pulmonary interstitium of IPF lungs, CD4+ T cell ratio, favouring CD4+CCR4+ to CD4+CCR6+ cells, was associated with better FVC, further implicating this unique T-cell subset in preserving lung function, as displayed by better FVC [39]. Thus, unlike the pro-fibrotic and anti-fibrotic roles of the different CD4 class of effector cells, the number of CD8+ T cells has been correlated with poor prognosis in patients with pulmonary fibrosis [28, 29, 40]. Recently, IL-21 has been identified to control the differentiation of CD8+ T cells to IL-13-producing Tc2 cells, and thereby assigning IL-21-Tc2 axis as a key immune signalling pathway involved in fibrogenesis [41]. Overall, literature suggests that T cells have the capacity to either propagate or diminish the fibrotic process via the production of Th1/Th2 related factors or through close interaction and activation of myeloid or structural cells. What still remain partially unanswered is the exact mechanism or signal that allows T cells to gain a pro-fibrotic status during chronic repair processes.

Macrophage phenotypes and their contribution to lung fibrosis

Many of the mediators produced by T cells influence the phenotype and function of macrophages, which are regarded as prominent immune cells in fibrotic disorders, including pulmonary fibrosis. Macrophages are highly abundant in the bronchoalveolar lavage fluid (BALF) of IPF patients and display various phenotypes depending on the inflammatory milieu. In murine models, macrophages produce superoxide and hydroxide free radicals in response to bleomycin, leading to injured lung epithelium, an inflammatory cascade and fibrosis [42]. Macrophages have also been shown abundant in

areas of chronic inflammation and to play a role in altering fibroblast function by modulating fibroblasts pro-inflammatory and proliferative capacity [43, 44]. In response to their surroundings, macrophages polarize into various phenotypes depending on the signals in their microenvironment. Based on *in vitro* studies, it is acknowledged that there are two types of macrophages, the classically activated (M1) macrophage and the alternatively activated (M2) macrophage (AAM) [45]. In response to a common M1 macrophage stimulus, lipopolysaccharide (LPS) and interferon gamma IFNγ, M1 macrophages display anti-fibrotic/tumour properties by producing nitric oxide and other inflammatory mediators (TNFα, IL-6 and IL-1β) and enhancing T cell responses. M2 macrophages are mainly responsible for down-regulating inflammation through the release of anti-inflammatory cytokines as well as initiating tissue repair and remodelling events by synthesizing TGFβ1, VEGF and EGF [46, 47]. M2 macrophages are programmed by IL-4 and IL-13, and are characterized by the expression of CD206, arginase-1 (arg1), Ym-1, Fizz-1, CD163 and CCL18. Some of these markers are differentially and uniquely regulated between different species. For example, arginase-1 is solely regarded as a murine M2-related marker, while CCL18 is considered to be a human M2-produced chemokine. It has also been acknowledged that M2 macrophages can be further classified into different subtypes depending on the initial stimulus *in vitro* (such as M2a, M2b, M2c). Notably, M1 and M2 macrophages are opposite and well-defined extremes of macrophages that can be utilized *in vitro* in studying mechanisms encountered during pathological wound repair. In this thesis paper, the terms “M1” and “M2” macrophages are used to refer to macrophages in which the initial stimuli (*in vitro*)

are known to be LPS/IFNγ and IL-4/IL-13, respectively. For identification of *in vivo* macrophages expressing certain characteristics of M1 and/or M2 macrophages, as shown experimentally, these cells are referred to as M1-like or M2-like macrophages. Alternatively, the macrophage phenotype can be illustrated based on the positivity of the markers expressed on the cell (such as arg1+CD206+ macrophages).

Although there has been controversy regarding the wide range of immunomodulatory molecules that impact macrophage trophic function, it has been generally accepted that mediators resulting from alternative activation of macrophages could contribute to fibrotic processes. For example, during the acute exacerbation of IPF, increased markers of alternatively activated macrophages are associated with poor prognosis [6, 48, 49]. It is also believed that activated M2-like macrophages secrete pro-fibrotic cytokines and soluble mediators, which could be essential for cellular differentiation into myofibroblasts [50-52]. Overall, the *in vitro* classifications of M1 and M2 macrophages are simplistic and require more experimental evidence to better define their putative roles *in vivo*. Exploring pathways and signals leading to various macrophage phenotypes could better predict novel pathways that may halt or haste repair processes.

While macrophage polarization towards the M2-like phenotype is anticipated in fibrotic-inducing and Th2-enriched cytokine environment [47, 48], the precise macrophage subtype directly contributing to fibrogenesis remains to be elucidated. In a murine model of silicosis, markers of the AAMs such as arginase-1, Fizz1, Ym1, and

CD206 were shown to be up-regulated [48] [47]. Mice lacking IL-4Rα displayed a reduced M2-macrophage accumulation (via reduction of Ym1), resulting in an abrogated fibrotic response and Th2 immunity during silicosis [53]. In addition, in murine models of pulmonary fibrosis, manipulation of macrophage numbers *in vivo* was shown to result in varying fibrotic outcomes [54]. Of note, one of the early evidence implicating the link between reduced macrophage infiltration with the extent of pulmonary fibrosis stemmed from the elegant work conducted by Okuma et al [55]. In their study, the authors investigated the hypothesis that macrophage infiltration into the lung initiates the fibrotic process using mice deficient in CCR2, which is a key receptor for monocyte/macrophage trafficking into the injured lungs. In response to bleomycin, CCR2 knockout mice exhibited reduced macrophage recruitment into intra-alveolar spaces and diminished macrophage MMP2 and MMP9, thus preserving the structural integrity of the basement membrane and ameliorating the fibrotic outcome. Subsequently, Gibbons et al postulated that the action of macrophages could vary depending on their time of existence during the injury-repair process. It has been shown that depletion of macrophages or circulating monocytes during the inflammatory phase (day 2 to 16) of bleomycin-induced pulmonary fibrosis has no effect on the resultant fibrosis [54]; depletion of macrophages during the fibrotic stage (day 21 to 28) reduced the degree of fibrogenesis in the lungs; in contrast, Gibbons et al. showed that the depletion of macrophages during the resolution phase (day 42 to 46) of the bleomycin model delays the resolution and can promote persistence of disease [54]. These results are consistent with the work done by Atabi et al. which illustrated that macrophages are capable of removing accumulated collagen in murine

lung fibrosis [56]. The presented collection of evidence on the role of macrophages in fibrosis suggests that investigating the mechanisms related to their accumulation, alternative activation and pro-fibrotic function is necessary to uniquely modulate the fibrotic response. One of the key mechanisms that will be explored in this thesis is the ER stress and UPR activation.

ER stress and UPR activation

The endoplasmic reticulum (ER) is an organelle responsible for protein folding, processing and trafficking in the cell. Approximately one third of proteins assembled in the cell processed through the ER [57]. These biochemical mechanisms are critical in producing stable tertiary structures of proteins that are integrated into the cell membrane and processed for secretion. The formation and proper folding of nascent proteins requires the involvement of molecular chaperones such as immunoglobulin heavy chain binding protein (BiP), also known as glucose regulated protein-78 (GRP78) [58, 59]. The accumulation of misfolded proteins in the ER lumen results in ER stress, to which the cells respond by initiating a repair process termed the Unfolded Protein Response (UPR) [60]. The UPR is an intracellular signaling pathway initiated by the dissociation of GRP78 from three ER membrane-bound stress sensors: Inositol-requiring protein 1 (IRE1), activating transcription factor 6 (ATF6) and PKR-like ER kinase (PERK). Dissociation of GRP78 occurs due to its higher affinity for misfolded or unfolded proteins within the ER lumen. To accommodate the enhanced protein folding capacity of the ER, the UPR may also initiate ER membrane biogenesis (the ER expansion program) through

the IRE1-XBP1 pathway or the ATF6 pathway [61, 62]. If protein homeostasis is not restored within the ER, further activation of the UPR can induce programmed cell death (or apoptosis) via C/EBP homologous protein (Chop) mediated program. As such, the UPR is a quality control system aimed to restore proteostasis through the inhibition of protein translation, production of chaperones and/or initiation of the ER-associated protein degradation pathway.

ER stress as a pro-fibrotic stimulant

Growing evidence implicates UPR involvement in various human respiratory conditions, such as fibrotic lung diseases [63-66]. Accumulation of unfolded proteins in the ER is the cellular signature of various human diseases, including infectious, metabolic and malignant diseases. It is intriguing that these seemingly unrelated diseases might share common fundamental molecular principles; thus questions arise whether these pathways can be potentially be manipulated to prevent disease development.

Early postulates of the ER stress as a key component to ILD's pathogenesis became more compelling with findings that the ER stress response is activated in cases of IPF-induced epithelial cell injury [64, 67, 68]. Various factors have been demonstrated to induce ER stress and cause injuries to the alveolar epithelial cells (AECs) including viruses, cigarette smoke, particulate matter and other environment exposures [69-71]. While AECs can maintain homeostasis from a few isolated injuries, it has been suggested that consistent and prolonged injuries disrupt cellular homeostasis via extended or

recurrent ER stress and over-activated UPR response [72]. During this response, various downstream pathways are activated, including ER stress-mediated pro-inflammatory pathways, apoptosis and cellular differentiation events. Dysfunctional AECs may impair the ability to regenerate normal AEC, leading to aberrant injury and fibrosis[64, 68]. Overall, the activated UPR in the pulmonary epithelium is likely involved in disease onset and progression.

Recently, the notion that ER stress and the UPR are involved in the promotion of fibrotic processes in epithelial cells and fibroblasts has caught the attention of biomedical researchers. Previously, it was shown that ER stress is involved in epithelium-to-mesenchymal transition (EMT) during aberrant wound healing – a key process responsible for ECM deposition in pulmonary fibrosis [73]. GRP78, a key molecular chaperone of the ER, and a marker for ER stress and UPR, has been shown to be elevated in an animal model of pulmonary fibrosis as well as in IPF human lung tissues [74]. *In vitro*, the UPR was demonstrated to be involved in transforming growth factor-beta (TGFβ1)-induced myofibroblast differentiation; the level of differentiation was suppressed by administration of 4-phenyl butyric acid (4-PBA), a non-specific chemical chaperone and UPR modulator [74]. The activation of the UPR signalling pathway resulted in the upregulation of other ER resident molecular chaperones that increase cellular protein folding capacity; this response has also been documented in non-pulmonary systems of fibrosis [75]. Conducting research on cell lines derived from IPF patients, Horowitz et al. have shown that UPR and ER stress are strongly associated with

alveolar epithelial cell apoptosis [67]. Furthermore, the expression of L188Q SFTPC (mutated form of surfactant protein C) induced ER stress in type 2 alveolar epithelial cells such as A549 cells. Lawson and colleagues demonstrated that after treating L188Q transgenic mice with intratracheal bleomycin, the mice developed lung fibrosis and had reduced lung compliance – a physiological measurement of lung tissue elastance and stiffness [72]. Moreover, the model showed increased apoptosis of epithelial cells and a greater number of myofibroblasts in the lung. While it is becoming more lucid that ER stress causes apoptosis in type 2 AECs, and thereby potentially promote the development and progression of fibrosis, the underlying mechanisms that cause ER-stress mediated apoptosis are not clear. In short, ER stress may act as a cellular switch that promotes EMT, fibroblasts-to-myofibroblast differentiation and AEC apoptosis, and thus influencing fibrotic disease progression.

Growing evidence suggests that ER stress and UPR activation are important indirect mechanisms through which macrophages influence fibrogenesis. In studies using peripheral macrophages of diabetic patients, the ER stress inhibitor, 4-PBA, suppressed the M2-polarization process and shifted macrophages toward the M1 phenotype, suggesting that ER stress facilitates the polarization of the M2 phenotype [76]. Despite this interesting finding that ER stress and UPR markers are induced during macrophage transition toward the M2 phenotype, the exact UPR pathway contributing to such phenotype, especially in the context of lung injury and fibrosis is still undetermined. Not only was the UPR induced during monocyte to macrophage differentiation [77] but it was

also critical during the differentiation of non-secretory cells to professional secretory cells, such as differentiation of B cells into plasma cells [78]. In this paper, the activation of IRE1-XBP1 arm of UPR was demonstrated to be indispensable in the differentiation of B-cells to antibody-secreting plasma cells [78]. Later evidence showed that B cell activation and differentiation to plasma cells, which is dependent on UPR activation through IRE1-XBP1 splicing, is elicited by IL-4 [79]. Since IL-4-mediated STAT6 activation is a physiologically relevant pathway that also drives M2 macrophage polarization [80], the impact of IL-4 on the UPR and XBP1 splicing requires inspection in macrophages. Collectively, ER stress responds to pro-fibrotic injury by being activated in various cell types within the lung to facilitate pathological wound repair. How ER stress specifically contributes to the pathogenesis of fibrosis is not very clear and which lung cells most importantly require UPR activation to maintain lung homeostasis is still debatable. Better understanding of the contribution of different UPR-axes during pathological wound repair could yield novel cellular mechanisms to prevent the progression of pathological scarring.

IL-6 signaling and lung fibrosis

IL-6 was first discovered in 1986 as a B cell stimulatory factor regulating immunoglobulin G (IgG) production. Later, IL-6 gained further attention as a key regulator of acute phase inflammation through the production of C-reactive protein (CRP) [81] [82]. More recently, IL-6 has been gaining attention for its potential relationship to cancer and fibrotic disease progression. Levels of circulating IL-6 have been found

increased in patients with systemic sclerosis (SSc)-interstitial lung disease [83, 84]. Similarly, circulating level of IL-6 has been shown elevated in IPF patients with acute exacerbations compared to those with stable disease [85], and interestingly was associated with poor prognosis and increased risk of death. These findings suggest an important role of IL-6 in facilitating fibrotic disease progression and necessitate further study to elucidate its plausible function in IPF.

The two ways in which IL-6 is known to activate cells are through *classical* or *trans* signaling. During *classical* signaling, IL-6 can bind to the membrane-bound IL-6 receptor alpha (mIL-6Rα) expressed on the majority of leukocytes and hepatocytes [86], which is then presented to the membrane-bound glycoprotein 130 (gp130). During *trans* signaling, IL-6 can bind to the soluble form of IL-6Rα (sIL-6Rα) in the extracellular space, forming the IL-6/sIL-6Rα complex. This complex then activates cells lacking mIL-6Rα, which cannot respond directly to IL-6 alone [87]. In both pathways, gp130-mediated signaling activates Janus Kinase (JAK) proteins, leading to the phosphorylation of the signal transducer and activator of transcription 3 (STAT3), followed by the dimerization of STAT3. Subsequently, the dimerized form of STAT3 translocates to the nucleus where it mediates the transcription of genes associated with cell migration, angiogenesis, tumour growth and epithelial-to-mesenchymal transition [88]. The protein gp130 exists in a membrane-bound form which enables it to act as a signal transducing β receptor for all IL-6 family cytokines (IL-6, IL-11, IL-27, CNTF, CLC, CT-1, LIF and OSM) [86]. Alternatively, gp130 can also appear as soluble gp130 (sgp130) generated naturally by

differential splicing of the gp130 mRNA. In this form, sgp130 acts to specifically antagonize IL-6 *trans* signaling [86, 89]. This role of sgp130 was acknowledged and later utilized to design the high affinity fusion protein sgp130Fc which selectively binds IL-6/sIL-6Rα complex, and thus inhibiting IL-6 *trans* signaling. Given that gp130 is also a receptor for other gp130 cytokines, the IL-6/sIL-6Rα complex partially emulates the function of these cytokines, which could play an important role in fibrosis [90-93].

Due to the involvement of IL-6 in propagating fibrotic disease pathology, IL-6 signalling has been studied extensively, especially in animal models. In response to the bleomycin challenge, IL-6 knockout mice displayed reduced lung fibrotic changes, accompanied by diminished early influx of macrophages, neutrophils and MIP-1 alpha, which is known to be involved in the recruitment of polymorphonuclear leukocytes primarily responsible for augmenting the responses to lung injury [94]. These findings are not entirely unanticipated given that earlier evidence suggested that IL-6 acts synergistically with bleomycin to increase MIP-1 alpha production in the lung, potentially contributing to fibrosis [95]. Based on these findings, subsequent studies aimed to precisely examine the pathways leading to IL-6 signalling. In one study by Le et Al., it was demonstrated that neutralizing IL-6 *trans* signalling, via sgp130Fc, led to reduced myofibroblast accumulation and ECM deposition, which are key effects relevant in the progression of fibrosis [93]. In their study, the authors showed that bleomycin primes pulmonary macrophages to express ADAM17, and thereby contributes to the shedding of soluble IL-6 receptor and the downstream activation of IL-6 *trans* signalling. Later

published work was aimed to elucidate the importance of IL-6 at different phases (inflammatory phase and fibrotic phase) during the establishment of fibrosis. Since the bleomycin model is a biphasic model comprising of both early inflammatory phase and late fibrotic phase, Kobayashi et Al. rationalized that IL-6 blockade in each of the two phases has opposing outcome on fibrosis [96]. Indeed, neutralizing IL-6 early on increased the epithelial susceptibility to injury by promoting the apoptosis of type II pneumocytes, and accelerated fibrotic remodelling in the lung. In contrast, neutralizing IL-6 beyond the initiation of the fibrotic phase reduced fibrotic outcome in the lung [96]. Although the precise mechanism behind improved fibrotic outcome is not well understood, one plausible mechanism could be linked to the ability of IL-6 to regulate the cell fate of type II pneumocytes – known as alveolar type II epithelial cells with reparative and surfactant producing function [97]. Other than the lung, targeting IL-6 has also been effective in a bleomycin-induced dermal fibrosis model, where IL-6 blockade reduced dermal thickness and fibrosis by possibly reducing pro-collagen 1 production and myofibroblast accumulation [98]. These findings prompted the initiation of clinical trials to test the efficacy of anti-IL-6 antibody, such as Tocilizumab, in patients with diffuse cutaneous systemic sclerosis. Evidence from the phase II trial revealed a reduced rate of percentage-FVC decline in lung function in patients administered with Tociliziumb compared to placebo [99]. Interestingly, these patients had a significantly reduced level of serum CCL18, a key pro-fibrotic M2-like cytokine involved in the progression of fibrotic disease, suggesting that IL-6 may modulate the M2 cytokine milieu in response to chronic tissue injury. A phase III clinical trial is currently underway (ClinicalTrials.gov). Overall,

IL-6 signalling is complex and can exert simultaneous functions that modulate immune cell recruitment and cellular differentiation processes, making it a targetable pathway for many inflammatory-driven fibrotic diseases.

Central Aim and Thesis Objectives

The central hypothesis of this Ph.D. thesis is as follows: Modulating the UPR influences the pathogenesis of pulmonary fibrosis. More specifically, I hypothesize that increased activation of the UPR in the lung would lead to increased epithelial cell death and fibroblasts to myofibroblasts differentiation, resulting in enhanced fibrotic processes. Subsequent objectives or questions were derived from the initial research objective and insights from the initial data. Accordingly, I have developed the following sequence of objectives to test the central hypothesis.

1. To examine the fibrogenic capacity of *Grp78*$^{+/-}$ mice and investigate the potential molecular mechanisms associated with the observed phenotype (Chapter 2).
2. To discuss how targeting the UPR may impact the fibrotic outcome by modulating the survival and polarization of macrophages (Chapter 2).
3. To describe the implication of the endoplasmic reticulum expansion program on the polarization of pro-fibrotic macrophages (Chapter 3).
4. To highlight how targeting the endoplasmic reticulum expansion pathway may suppress a *hyper* pro-fibrotic macrophage phenotype (Chapter 3).
5. To examine how IL-6 may impact the polarization of pro-fibrotic macrophages and the development of the fibrotic process (Chapter 4).

Chapter 2

GRP78 and CHOP modulate macrophage apoptosis and the development of bleomycin-induced pulmonary fibrosis

Summary and Significance

Fibrotic disorders like IPF have been associated with ER stress and activation of the UPR. It is well known that the activation of the UPR regulates cellular proteostasis, and in the case of prolonged activation apoptotic processes may be engaged. In the lung, the specific cellular localization and susceptibility of ER stress and UPR is poorly understood. We have in this manuscript examined the role of GRP78, using Grp78 heterozygous transgenic mice in the experimental animal model of bleomycin-induced fibrosis. We hypothesized that these mice would have an increased fibrotic response due to increased UPR activity in fibroblasts and/or myofibroblasts. To our surprise, the results contradicted our hypothesis in that the mice were well protected against bleomycin-induced fibrosis. Further investigations demonstrated an absence of activated M2 macrophages in lung tissues of the protected Grp78 heterozygous mice. This finding was associated with high TUNEL levels, 7AAD positive cells, Chop and cleaved caspase 3 levels, suggesting GRP78-mediated apoptosis in this population. On the contrary, bleomycin exposure in mice deficient in Chop, a terminal UPR mediator of apoptosis, led to persistence of M2-programmed macrophages in the lungs and increased lung fibrosis and mortality on bleomycin exposure. In conclusion, along with describing macrophages as cells with an activated UPR signal in fibrotic processes, this study indicates that

macrophages are crucial in the fibrotic process, and that modifying their apoptotic death and polarization status may serve as a therapeutic target.

GRP78 and CHOP modulate macrophage apoptosis and the development of bleomycin-induced pulmonary fibrosis.

Ehab A. Ayaub[1,3], Philipp S. Kolb[1], Zahraa Mohammed-ali[2], Victor Tat[1], James Murphy, Pierre-Simon Bellaye[1], Chiko Shimbori[1], Felix J. Boivin[3], Rocky Lai[3], Edward G Lynn[2], Sarka Lhotak[2], Darren Bridgewater[3], Martin R.J. Kolb [1,3], Mark D. Inman[1], Jeffrey G. Dickhout[2],

Richard C Austin[2] and Kjetil Ask[1,3]

1. Department of Medicine, Firestone Institute for Respiratory Health, McMaster University and The Research Institute of St. Joe's Hamilton, Hamilton, ON, Canada
2. Department of Medicine, Hamilton Centre for Kidney Research, McMaster University and The Research Institute of St. Joe's Hamilton, Hamilton, ON, Canada
3. Department of Pathology and Molecular Medicine, McMaster Immunology Research Centre, McMaster University, Hamilton, ON, Canada

Running title: UPR-mediated macrophage apoptosis in pulmonary fibrosis.

Conflict of interest: All authors declared no conflicts of interest

Status of the work: published in "The Journal of Pathology"

Author contributions: Conception and design: EAA, RL, DB, MRJK, MDI, JGD, RCA, KA; Performed experiments: EAA, PSK, ZM, VT, JM, PSB, CS, FJB, RL, EGL, SL; Analysis and interpretations: EAA, PSK, ZM, VT, JM, PSB, CS, FJB, RL, EGL, SL, DB, MRJK, MDI, JGD, RCA, KA; Drafting the manuscript: EAA, PSK, MDI, KA; Edited and revised manuscript: EAA, PSK, MRJK, MDI, JGD, RCA and KA. All authors read and approved the final version.

Corresponding author: Dr. Kjetil Ask, Department of Medicine, McMaster University and The Research Institute of St. Joe's Hamilton, Firestone Institute for Respiratory Health, 50 Charlton Ave East, Room L314-6, Hamilton, Ontario, Canada L8N 4A6, Ph. (905) 522.1155 ext. 33686; Fax (905) 521.6183; E-mail: askkj@mcmaster.ca

ABSTRACT

Endoplasmic Reticulum (ER) stress and the Unfolded Protein Response (UPR) have been associated with fibrotic lung disease, though exactly how they modulate this process remains unclear. Here we investigated the role of GRP78, the main UPR regulator, in an experimental model of lung injury and fibrosis. *Grp78*$^{+/-}$, *Chop*$^{-/-}$ and wild type C57BL6/J mice were exposed to bleomycin by oropharyngeal intubation and lungs were examined at day 7 and 21. We demonstrate here that *Grp78*$^{+/-}$ mice were strongly protected from bleomycin-induced fibrosis, shown by immunohistochemical analysis, collagen content and lung function measurements. In the inflammatory phase of this model, a reduced number of lung macrophages associated with an increased number of TUNEL-positive cells were observed in *Grp78*$^{+/-}$ mice. Dual immunohistochemical and *in situ* hybridization experiments showed that the macrophage population from the protected *Grp78*$^{+/-}$ mice was also strongly positive for cleaved caspase-3 and *Chop* mRNA, respectively. In contrast, the administration of bleomycin to *Chop*$^{-/-}$ mice resulted in increased quasistatic elastance and extracellular matrix deposition associated with an increased number of parenchymal arginase-1-positive macrophages that were negative for cleaved caspase-3. The data presented indicate that the UPR is activated in fibrotic lung tissue and strongly localized to macrophages. GRP78 and CHOP-mediated macrophage apoptosis was found to protect against bleomycin-induced fibrosis. Overall, we demonstrate here that the fibrotic response to bleomycin is dependent on GRP78-mediated events and provides evidence that macrophage polarization and apoptosis may play a role in this process.

Key words: Lung fibrosis, Alternatively Activated Macrophage, GRP78, ER stress, Unfolded Protein Response

INTRODUCTION

Idiopathic pulmonary fibrosis is an irreversible progressive fibrotic disorder with a median survival rate of 2.5-3.5 years post-diagnosis [1]. Though the pathogenesis of pulmonary fibrosis is not fully understood, it is thought that repeated micro-injuries to the epithelium lead to the recruitment of immune cells, which secrete soluble mediators involved in the transdifferentiation process of fibroblasts to myofibroblasts [2-4]. The myofibroblast has been the subject of various investigations [5-8] due to its central role in the deposition of excessive extracellular matrix (ECM) proteins in fibrotic disease [3,9]. It is still poorly understood how these myofibroblasts accumulate in the lung parenchyma and how this process can be halted [9]. Recently, activation of the Unfolded Protein Response (UPR) has been found to be critical in the differentiation of a variety of cell types from a quiescent state to a cell with increased secretory ability [10], including macrophages [11], plasma cells [12], adipocytes [13], myofibroblasts [14-16] and eosinophils [17]. If Endoplasmic Reticulum (ER) protein homeostasis is not restored, the UPR, through prolonged activation, may also initiate apoptotic cell death through the upregulation of C/EBP homologous protein (CHOP), also known as DNA damage-inducible gene 153 (GADD153) [18]. Although initially identified as a protein involved in UPR-associated apoptosis, CHOP is also known to enhance *de novo* protein synthesis, via the dephosphorylation of Eukaryotic Translation Initiation Factor 2α (eIF2α) [19]. Glucose-Regulated Protein 78 kDa (GRP78), also known as Binding Immunoglobulin Protein (BiP) or Heat Shock 70 kDa Protein 5 (HSPA5), is a major chaperone located in the ER [20]. Under homeostatic conditions, GRP78 binds to three UPR sensors activating

transcription factor 6 (ATF6), inositol-requiring kinase 1 (IRE1) and protein kinase RNA-like endoplasmic reticulum kinase (PERK) [20,21]. Upon recognizing misfolded proteins in the lumen of the ER through their exposed hydrophobic regions [22] GRP78 activates the UPR by dissociating from these molecular sensors [23,24]. Although recent investigations have made it possible to understand these regulatory processes at the cellular level, the role of these mechanisms in different cell types composing a complex tissue such as the lung are not well understood. Studies in this area have focused on the role of UPR activation in epithelial cells [25-27] or in the fibroblast-to-myofibroblast differentiation process [16]. Yet, it is still unclear i) how the UPR specifically contributes to the pathogenesis of lung fibrosis; ii) which lung-specific cell types require UPR activation to maintain organ homeostasis; iii) which lung-specific cell types are susceptible to UPR activation and iv) if this is a targetable biochemical process. Initially, we hypothesized that increased activation of the UPR *in vivo* would lead to increased epithelial apoptosis and to the differentiation of fibroblasts to myofibroblasts resulting in an enhanced scarring process and severe fibrotic response. To test this hypothesis, we exposed *Grp78*$^{+/-}$ mice to bleomycin and assessed their response to inflammation and fibrosis. Unlike whole body deletion of *Grp78* which results in embryonic lethality [28] Grp78 haploinsufficiency in mice (*Grp78*$^{+/-}$ mice) leads to mice that are viable; this model has been used to examine the role of GRP78 and UPR in several other systems [29-31]. Contrary to our initial hypothesis, *Grp78*$^{+/-}$ mice were markedly protected against bleomycin-induced pulmonary fibrosis. This protection was associated with a decreased number of pulmonary macrophages in the *Grp78*$^{+/-}$ mice. Further investigation revealed

that these cells were TUNEL-positive and that they expressed GRP78, CHOP and cleaved caspase-3. The exposure of *Chop*$^{-/-}$ mice to bleomycin reversed these observations and resulted in increased quasistatic elastance and extracellular matrix deposition in conjunction with an accumulation of arginase-1-positive pulmonary macrophages in the interstitium. To our knowledge this is the first report to identify that UPR activation is required for the fibrotic response and provides preliminary evidence that the macrophage may play a role in this process.

METHODS

Detailed methods are described in the online supplement.

Animals. *Grp78*$^{+/-}$ mice (C57BL6 background) were a gift from Dr. Amy Lee [28]. *Chop*$^{-/-}$ and wild type mice were commercially obtained.

Administration of bleomycin and collection of mouse specimens. Experimental pulmonary fibrosis was induced using a single intratracheal instillation of bleomycin at 0.04 or 0.06 Unit per mouse.

Measurements of pulmonary function: Lung function was measured using a flexiVent® mechanical respirator.

Collagen assays: Insoluble and soluble collagen from wild type and *Grp78*$^{+/-}$ lung tissues were assessed using hydroxyproline and sircol assays, respectively.

Isolation of mRNA and NanoString gene expression: Total RNA from bone marrow-derived macrophages and from frozen lung tissues were extracted using RNeasy Mini Kit and TRIzol® reagent. Gene expression was either performed by RT-PCR (SYBR green) or by NanoString® nCounter gene expression technology.

Histochemistry and Immunohistochemistry: Tissue slides were generated and subsequent staining was performed for Masson's trichrome, αSMA, F4/80, MAC3, Ki-67, Arginase-I, GRP78 and CHOP.

Immunofluorescence: Immunofluoresecent staining of GRP78, MAC3, E-Cadherin and Cleaved caspase-3 was performed on formalin-fixed lung tissues from wild type, *Grp78*$^{+/-}$ and *Chop*$^{-/-}$ mice.

***In Situ* Hybridization and image quantification:** *In Situ* Hybridization for *Ddit3* (*Chop*) and *F4/80* was performed using the *Affymetrix QuantiGene ViewRNA* assay. Briefly, paraffin blocks were sectioned at a thickness of 5 μm, deparaffinized, boiled in pre-treatment solution (Affymetrix, Santa Clara, CA) and digested with proteinase K. Sections were incubated with *Ddit3* and *F4/80* for 2 hrs at 40°C. Signal was amplified with Pre-Amp and Amp solutions (Affymetrix, Santa Clara, CA) and then developed with Fast-Red and Fast-Blue Substrates. Slides were counter-stained with DAPI, mounted with Fluoromount (Sigma, St. Louis, MO) and scanned on a VS120 Olympus Slide Scanner where CY5 and TRITC channels were used to view *F4/80* and *Chop*, respectively. Dual positive cells were then counted and presented per mm^2 area.

TUNEL Assay: TUNEL was performed on lung tissues derived from wild type and *Grp78*$^{+/-}$ lungs using the *in situ* apoptosis detection kit from Trevigen.

Statistical analysis: Results were expressed as mean ± SEM. When two groups are compared, a two-tailed parametric or non-parametric T-Test was performed. When more than two groups were compared, two-way analysis of variance (two-way ANOVA) followed by Newman-Keuls multiple comparison test was used. All statistical tests were performed using GraphPad Prism 5.0d (GraphPad Software, Inc). A $p<0.05$ was considered statistically significant.

RESULTS

***Grp78* haploinsufficiency protects against bleomycin-induced lung fibrosis.** To examine the role of GRP78 in lung fibrosis, we exposed mice haploinsufficient for *Grp78* (*Grp78*$^{+/-}$) to bleomycin. *Grp78*$^{+/-}$ was verified by genotyping [32] and by western blot analysis in total lung homogenates (Supplementary Figure 1A-C). Figure 1A shows the pressure-driven PV-loops at the fibrotic stage (day 21) in this model. As expected, wild type lungs exposed to 0.04U bleomycin were stiffer as compared to wild type lungs receiving saline only. The associated lung function parameters, quasistatic elastance (Est) and k-value confirmed a statistical difference between bleomycin-exposed wild type mice and respective controls (Figure 1B-C). These findings were in stark contrast to *Grp78*$^{+/-}$ mice exposed to bleomycin, where, no change in elastance could be observed (Figure 1A-C). The quantification of insoluble (Figure 1D) and soluble collagen (Figure 1E) from wild type and *Grp78*$^{+/-}$ mice confirmed the protective phenotype. This was verified by histological examination of fibrosis (Figure 1F) and Ashcroft scoring (Figure 1G) and by □SMA expression (Figure 1H) and quantitation (Figure 1I).

***Grp78*$^{+/-}$ leads to a reduction in macrophage population *in vivo*.** To determine which molecular and cellular factors might have contributed to the protective phenotype observed in *Grp78*$^{+/-}$ mice, we assessed the inflammatory response to bleomycin at day 7 and 21. The total cell number in the broncheoalveolar lavage fluid (BALF) peaked at day 7 and returned towards baseline by day 21 in both genotypes (Supplementary Figure 2A). Further examination of cell differentials indicated a reduced number of macrophages at day 7 in the BALF of *Grp78*$^{+/-}$ mice, compared to wild type (Figure 2A), with no

apparent difference in neutrophils (Supplementary Figure 2B). Cytokine assessment in BALF of TGF-β1 and IL-6 indicated that both were slightly increased in bleomycin-exposed *Grp78*$^{+/-}$ mice compared to saline-exposed mice (Supplementary Figure 2C-D). This was consistent with immunohistochemical examination of phospho-SMAD2 staining (Supplementary Figure 3, 4). The IL-6 findings were replicated in a commercial 32 cytokine and chemokine assay that also indicated that *Grp78*$^{+/-}$ mice had increased levels of six additional cytokines (MCP-1, IP-10, LIF, G-CSF, IL-5 and Eotaxin) at day 7, compared to wild type and *Chop*$^{-/-}$ mice (Supplementary Figure 5, 6). To confirm that the number of macrophages was reduced in lungs of *Grp78*$^{+/-}$ mice, we quantified F4/80 positive cells at days 7 and 21. A drastic reduction of F4/80 positive cells was observed at day 7 in *Grp78*$^{+/-}$ mice compared to wild type mice (Figure 2B-C), suggesting a potential pro-fibrotic role of macrophages in this model. To further characterize the macrophage polarization pattern in this system, we performed immunohistochemical staining of arginase-1 and mannose receptor 1 (MR1) as markers of pro-fibrotic M2 macrophages [33,34]. Both arginase-1 and MR1 positive cells were rarely detected in saline-exposed lungs, both were abundantly increased in fibrotic wild type lungs at days 7 and 21, and strongly reduced at day 21 in the *Grp78*$^{+/-}$ mice (Figure 2D-E, Supplementary Figure 7). A discrepancy between these markers was observed at day 7, where only arginase-1 levels were reduced in *Grp78*$^{+/-}$ mice exposed to bleomycin. To determine the possible cause of the absence of arginase-1-positive macrophages in the *Grp78*$^{+/-}$ mice, we conducted additional experiments to investigate i) the capacity of *Grp78*$^{+/-}$ macrophages to polarize into arginase-1-positive cells and their association with UPR activation, ii) the

pulmonary inflammatory infiltration capacity of macrophages in *Grp78*$^{+/-}$ mice in response to an LPS inflammatory stimulus associated with cytokine release, as well as iii) the proliferative capacity of pulmonary cells in *Grp78*$^{+/-}$ mice in response to bleomycin. These experiments indicated that *Grp78*$^{+/-}$ mice have no defect in their ability to polarize toward the arginase-1-positive cells (Supplementary Figure 8A) and associated with the activation of the UPR, demonstrated by the detection of spliced *Xbp-1* (Supplementary Figure 8B) and increased expression of *Grp78* (Supplementary Figure 8C). Their capacity to infiltrate in response to LPS was not modulated, as a similar number of total cells and macrophages could be found in the BALF (Supplementary Figure 9A-B), along with similar levels of secreted IL-1β (Supplementary Figure 9C). The assessment of Ki67-positive cells and the T-cell marker CD3 also indicated no difference in the total number of cells proliferating and the number of T-cells (Supplementary Figures 10A-B and 11, respectively). We then examined whether the UPR was activated in the macrophage population in response to bleomycin *in vivo*. Dual immunofluorescence staining of MAC3 and GRP78 demonstrated that GRP78 staining could be co-localized in macrophages during bleomycin-induced lung fibrosis (Figure 2F). In addition, immunoblotting analysis of whole lung homogenates revealed that GRP78 protein levels were increased in response to bleomycin in wild type mice (Supplementary Figure 1A-C).

***Grp78*$^{+/-}$ modulates fibrotic transcripts, ER-resident molecular chaperones and *Chop* in response to bleomycin.** To better understand how *Grp78*$^{+/-}$ mice were protected from bleomycin-induced lung fibrosis, we assessed the transcriptional pattern of 67 genes in lung homogenates of all mice examined (See Table I and supplementary Figure 12 in

supplement for a list of all genes investigated and a heat-map of differentially regulated genes). As shown in Figure 3A-C, the expression of extracellular matrix molecules *Col1a1, Col3a1 and Fn1* mRNA was increased in both wild type and *Grp78*$^{+/-}$ mice at day 7, but returned towards baseline only in the less fibrotic *Grp78*$^{+/-}$ mice at day 21. The collagen-folding chaperone *Fkbp10* was also induced at day 21 only in wild type mice (Figure 3D). The UPR and chaperone associated genes *Grp78, Calreticulin and Hsp47* were increased in *Grp78*$^{+/-}$ mice at day 7 (Figure 3E-G). We also detected an increase in the expression of *Chop* in lung homogenates of *Grp78*$^{+/-}$ mice at day 7 (Figure 3H). Based on the above finding that the macrophage population was reduced in both BALF and in the lung tissues of *Grp78*$^{+/-}$ mice upon bleomycin exposure (Figure 2A-C), combined with the finding that GRP78 was co-localized in the macrophage population, we questioned whether the downstream UPR marker *Chop* was expressed in this population of cells and if it could be involved in UPR- and CHOP-mediated apoptosis. To address this question, we conducted *in situ* hybridization studies and determined that *Chop* expression was co-localized in *F4/80* positive macrophages in *Grp78*$^{+/-}$ mice (Figure 3I-J and supplementary Figure 13), suggesting that *Chop*-mediated apoptosis may have occurred in *Grp78*$^{+/-}$ mice exposed to bleomycin.

***Grp78*$^{+/-}$ upregulates apoptotic signals in macrophages upon bleomycin exposure.** To address if CHOP could be involved in macrophage apoptosis in the *Grp78*$^{+/-}$ mice exposed to bleomycin, we examined first the expression of CHOP using immunohistochemical methods. As observed with GRP78 immunohistochemical staining, the expression of CHOP appeared to be localized both in bronchial epithelium and in cells

consistent with a macrophage phenotype (Figure 4A). We then examined if an overall apoptotic signal could be detected in lung homogenates by quantification of cleaved caspase-3, which showed a significant increase (Figure 4B-C). To address the specific cellular localization of this apoptotic signal, we performed TUNEL stain (Figure 4D), revealing that numerous cells were TUNEL-positive in *Grp78*$^{+/-}$ mice at day 7 (Figure 4E). As expected, most TUNEL-positive cells in wild type mice appeared to be of epithelial origin. In contrast, a high number of luminal alveolar cells consistent with a macrophage phenotype were TUNEL positive in lungs of *Grp78*$^{+/-}$ mice 7 days after bleomycin exposure (Figure 4D), suggesting that apoptosis had occurred in the macrophage population. To confirm this observation, we performed dual immunofluorescent staining of a macrophage marker, MAC3, with an epithelial marker, E-Cadherin, in combination with cleaved caspase-3 (Figure 4F-I and supplementary Figure 14). Cleaved caspase-3 expression was strongly co-localized with the macrophage population in the lungs of *Grp78*$^{+/-}$ mice compared to wild type mice, while no difference could be observed in the epithelial cell population, indicating an association between *Chop* mRNA and protein expression with apoptosis in the macrophage population. The examination of whole lung 7AAD and F4/80 positive macrophages by FACS analysis 5 days after bleomycin administration confirmed an increased number of dead macrophages in lungs of *Grp78*$^{+/-}$ mice (Supplementary Figure 15). To determine whether freshly isolated alveolar macrophages from bleomycin-exposed *Grp78*$^{+/-}$ lungs demonstrates an early apoptotic transcriptional signature that precedes the observed apoptotic phenotype at day 5 and 7, we isolated alveolar macrophages by adherence at 3 and 7 post-bleomycin

administration. The results confirmed that *Chop* mRNA level was increased in the *Grp78*$^{+/-}$ isolated alveolar macrophages at day 3 (Supplementary Figure 16A). In addition, the transcriptional level of the apoptotic markers *Bax* and *Bak1* were increased only in *Grp78*$^{+/-}$ isolated alveolar macrophages (Supplementary Figure 16B-C). As observed in total lung homogenates, *Grp78* mRNA expression was slightly increased in isolated alveolar macrophages, suggesting that bleomycin induced an UPR-activation in *Grp78*$^{+/-}$ macrophages (Supplementary Figure 16D). The mRNA expression of the M2 marker *Arginase-1* as well as the fibrotic marker *Fn1* were both decreased in alveolar macrophages isolated from *Grp78*$^{+/-}$ mice exposed to bleomycin, compared to wild type mice (Supplementary Figure 16E-F). Of note, *Col1a1*, *Col3a1*, *Fkbp10*, *Calreticulin* and *Hsp47* previously assessed in the total lung homogenates (Figure 3A-H) were undetected in the ex-vivo isolated macrophage population (data not shown). To exclude the possibility that myofibroblast apoptosis could occur in the protected *Grp78*$^{+/-}$ mice, we examined the percentage of cleaved caspase-3 and αSMA-positive cells by dual IF in both genotypes (Supplementary Figures 17, 18). To further determine if CHOP could be causally involved in the apoptotic process of macrophages *in vivo*, we exposed mice deficient in CHOP to bleomycin.

***Chop* deficiency results in increased bleomycin-induced lung elastance and extracellular matrix deposition associated with the accumulation of arginase-1-positive macrophages in the lung interstitium**. We reasoned that blocking the ability of macrophages to undergo *Chop*-mediated apoptosis would lead to an increase both in lung macrophages and in the fibrotic response to bleomycin. In a first set of experiments,

Chop$^{-/-}$ and wild type mice received 0.06 U of bleomycin per mouse and were followed for 21 days. As shown in Figure 5A, this dose led to a substantial mortality rate in the *Chop*$^{-/-}$ mice (7/9 mice) as compared to wild type mice (2/10), suggesting a potential higher susceptibility to bleomycin in *Chop*-deficient mice. We proceeded to examine the fibrotic response at a lower dose (0.04 U bleomycin per mouse). At this dose, *Chop*$^{-/-}$ mice developed increased quasistatic elastance and extracellular matrix deposition compared to wild type mice (Figure 5B-C and supplementary Figure 19-20) that was associated with an increased number of both F4/80-positive and arginase-1-positive cells (Figure 5D-E and supplement Figure 20). Of note, the assessment of soluble (sircol) and total lung collagen (hydroxyproline) did not result in significant differences between *Chop*$^{-/-}$ and wild-type mice exposed to bleomycin (data not shown). To determine whether the accumulating macrophages were persisting in the tissues due to their inability to undergo programmed cell death, we performed dual immunofluorescence staining of cleaved caspase-3 and MAC3 and demonstrated a significantly reduced amount of cleaved caspase-3 positive macrophages in *Chop*$^{-/-}$ lungs exposed to bleomycin (Figure 5F-H). These data demonstrate that CHOP is involved in regulating the accumulation of non-apoptotic macrophages and extracellular matrix deposition in this model.

DISCUSSION

The data presented in this manuscript shows that modulating the UPR will alter the fibrotic response. The effects of *Grp78* and *Chop* manipulation – with polar effects on fibrosis and macrophage apoptosis – are consistent with the hypothesis that the macrophage plays an important role in fibrosis and that UPR-modulation of the pro-fibrotic macrophage population may be a viable anti-fibrotic target. This finding was admittedly unexpected as we had initially hypothesized that exposing mice with a reduced expression of the UPR regulator GRP78 would result in increased activation of the UPR and enhanced epithelial apoptosis followed by increased fibroblast to myofibroblast differentiation and subsequent lung scarring, as previously suggested [16,25-27,35,36]. By further investigation of this unanticipated finding, we believe we have made significant contributions to the understanding of the mechanisms of fibrosis in the context of the bleomycin model, including the likely profibrotic contribution from activated macrophages and the protective role played by the UPR and *Chop*, in promoting macrophage apoptosis.

The notion that alternatively activated (M2) macrophages may act as regulators of fibrogenesis is not novel and has been described extensively in various reviews [37-39] and in the bleomycin model [40]. This concept supports the idea that skewing the inflammatory response from the M2 toward the M1 phenotype (profibrotic toward inflammatory phenotype) may be reducing fibrogenesis. This was recently suggested in the bleomycin model, where the administration of vaccinia resulted in a shift in macrophage polarization favouring the M1 phenotype and the reduction of lung fibrosis

[41]. Additional studies have shown that enhancing the M2 phenotype with MMP-28 [42] or IL-33 [43] increased bleomycin-induced lung fibrosis, indicating that profibrotic M2 macrophages may be a valid antifibrotic target. Several studies have examined and suggested that alternatively activated M2 macrophages may contribute to the fibrotic process in IPF patients. They are present in the pulmonary interstitium and in fibrotic areas of patients diagnosed with IPF [44,45], acute exacerbations have been shown to promote their polarization [34]. *In vitro*, collagen turnover and breakdown products have been shown to promote their polarization [46], indicating a plausible mechanism by which they could be polarized in scarred tissue. In addition, the notion that corticosteroids have been shown to promote M2 polarization [47] could explain why there is currently no evidence demonstrating a therapeutic benefit in the treatment of IPF [48].

The activation of the UPR is the direct response to increased protein misfolding in the ER and its activation is aimed to restore proteostasis on any insult to the ER; it likely occurs in all cells possessing an ER. The mechanisms of proteostasis restoration are multifactorial, and includes an inhibition of protein translation, an induction of ER chaperone molecules, an activation of the ER associated proteasome degradation (ERAD) pathway. In addition, a well-described molecular mechanism involving IRE1/XBP-1 activation followed by an ER expansion program aimed at reducing protein crowding in the ER can occur. An UPR and *Chop*-mediated cell death program would be initiated if cellular proteostasis is not restored. This could be mediated by GRP78 dissociation and PERK activation [49,50] leading to subsequent phosphorylation of eIF2α that may cause global halt in protein translation and selectively lift the translational repression on ATF4

[51]. This in turn can activate *Chop*, known to repress the anti-apoptotic BSL-2 activity and thus promote apoptosis [52]. According to our initial hypothesis, we expected to see a strong UPR activation pattern in both epithelial cells as well as in fibroblasts, resulting in epithelial apoptosis [26], myofibroblast differentiation and enhanced fibrosis. Although GRP78 staining was expressed in alveolar epithelial cells, we noticed that macrophage-like cells were also highly positive for GRP78, indicating UPR activation in these cells. Cell differential counting indicated that the overall macrophage population was diminished in the protected *Grp78*$^{+/-}$ mouse. Further examination of TUNEL-positive cells by morphology was consistent with macrophage apoptosis, dual staining with cleaved caspase 3/MAC3 or cleaved caspase-3/E-cadherin suggested that it was the macrophage population which was affected by apoptosis, which was confirmed by FACS analysis showing increased F4/80 and 7AAD positive cells at day 5 in the protected *Grp78*$^{+/-}$ mice exposed to bleomycin. In addition to this, we performed an *in situ* hybridization assessment of *Chop* and *F4/80,* which showed that a large fraction of *F4/80* positive cells in the protected *Grp78*$^{+/-}$ mice were also positive for *Chop*. Besides an active UPR-mediated process resulting in macrophage apoptosis, there were several possible alternative explanations that were examined and ruled out. Neither the assessment of an apoptotic event in the myofibroblast population in *Grp78*$^{+/-}$ mice, a proliferative index after bleomycin exposure, the *in vitro* measurement of the ability of bone marrow-derived cells to undergo the macrophage M2 polarization process or the assessment of the capacity of macrophages to infiltrate the lungs after a LPS endotoxin challenge could explain the lower number of F4/80-positive macrophages found in the

protected *Grp78*$^{+/-}$ mice compared to the fibrotic wild type mice. Mice fully deficient in *Chop* are resistant to ER stress-induced cell death [53] and have recently been shown to have increased liver injury and progressive fibrosis associated with an accumulation of macrophages in an experimental model of liver steatosis [54]. Our findings complement this particular model of liver fibrosis as we observed an increase of pulmonary macrophages associated with an increased fibrotic response to bleomycin in the *Chop*-deficient mice, suggesting that *Chop* plays an important role in this model. Of note, it is clear that the modulation of *Chop* expression in different cellular compartments may yield different outcomes depending on the specific context. An attractive hypothesis for *Chop*-deficient mice would be that the alveolar epithelium would be protected against GRP78-mediated apoptosis in response to injury. To fully test this hypothesis, inducible epithelial-specific transgenic mice would need to be generated and tested.

A limitation of our study is the use of *Grp78*$^{+/-}$ and *Chop*$^{-/-}$ mice, as these animals have a global reduction in gene expression in all cell types. In addition, the biochemical signature of UPR activation is the detection of increased *Grp78* at the mRNA level as well as at the protein level, likely through the activation of the IRE1/XBP-1 pathway [55,56]. In line with these observations, we show here that *Grp78* gene expression was not reduced in the *Grp78*$^{+/-}$ mice, although at the protein level, a substantial reduction of GRP78 expression was detected, suggesting a true haploinsufficency. Using siRNA-mediated knockdown of *Grp78*, it was shown that a compensatory activation of the *Grp78* promoter was induced [57]. We confirmed this further in isolated BMDMs derived from *Grp78*$^{+/-}$ and wild type mice, displaying an increased level of spliced *Xbp-1* and

Grp78 in the haploinsufficient cells, both of which are characteristic of UPR activation. In addition, Amy Lee and colleagues [58] demonstrated that GRP78 haploinsufficency promoted an adaptive UPR in mice exposed to high fat diet. This group showed that there was an increase in spliced *Xbp-1* and other ER-resident molecular chaperones in these animals. Examination of gene expression using NanoString nCounter technology showed that fibrotic markers were induced to the same extent in both the wild type and haploinsufficient mice at day 7, but only the haploinsufficient mice were able to recover and suppress the expression of these ECM genes at day 21 suggesting an important role for the UPR in the context of fibrogenesis. This analysis also indicated signs of an adaptive UPR as described previously. Both UPR-associated markers *Calreticulin* and *Hsp47* were increased in the haploinsufficient mice at day 7, consistent with findings from Ye *et al.* [58] who showed that *Grp78*$^{+/-}$ mice were protected against diet-induced obesity and insulin resistance through an adaptive UPR. Although we have not yet fully characterized and outlined the exact mechanisms of UPR-activated macrophage death *in vivo,* our data suggest that a better understanding of the molecular and cellular mechanisms involved in the profibrotic polarization process of macrophages and the role of UPR-mediated macrophage apoptosis are needed. This may result in therapies either preventing the recruitment of, or targeting pro-fibrotic macrophages as they appear to be critical for the fibrogenic response.

In summary, our data suggest that bleomycin triggers *Chop*-mediated apoptosis in the pulmonary macrophage population in *Grp78*$^{+/-}$ mice and that the reduction of activated macrophages is associated with a markedly reduced fibrotic response. The data presented

are consistent with the hypothesis that the alteration of macrophage polarization prevented the fibrotic response, although additional experimentation is required to establish a causal link (please see Figure 6 for an illustration describing the key findings of this paper). A better understanding of the molecular mechanisms involved in macrophage polarization and the exact involvement of the UPR in the apoptotic process may help us to better understand how current treatment options are beneficial in fibrotic lung disease and help us in developing novel antifibrotic therapies.

ACKNOWLEDGEMENTS

We sincerely thank Dr. Amy Lee for the kind gift of GRP78 haploinsufficient mice. We thank Jane Ann Smith (McMaster University, ON, Canada) for her exceptional technical assistance with the experimental animal work. We thank Mary Jo Smith, Mary Bruni and Matthew Gravina (McMaster University, ON, Canada) for their efficient technical help in immunohistochemistry and for developing immunohistochemical methods to detect GRP78 in lung tissues. We thank Jennifer Wattie for technical help performing lung function assessments (St. Joseph's Healthcare Hamilton, ON, Canada). We thank Mike Anderson (NanoString Technologies®) and Christine King (Farncombe Metagenomics Facility, McMaster University, ON, Canada) for help with NanoString experiments. We also thank *Sohail Mahmood, Pavithra Parthasarathy, Karun Tandon and* Drs. Carl Richards, Martin Stämpfli and *Jack Gauldie for their helpful support and constructive discussions. This work was performed with funding from the Ontario Thoracic Society (Canadian Lung Association). EAA is funded by the Canadian Institute of Health Research (#140358). RCA* is a Career Investigator of the Heart and Stroke Foundation of Ontario and holds the Amgen Canada Research Chair in the Division of Nephrology at St. Joseph's Healthcare and McMaster University.

FIGURE LEGENDS.

Figure 1. *Grp78*$^{+/-}$ lungs are resistant against bleomycin-induced changes in lung function and bleomycin-induced fibrotic changes. Mice were intubated with bleomycin (0.04 U/mouse). Fibrosis was assessed after 21 days. (A) Pressure-driven pressure-volume (PV) loops was performed with flexiVent®, and graphed as an average value of all the animals per group. The derived functional parameters (B) K_{value} and (C) quasistatic elastance (Est) are shown. (D) Insoluble collagen and (E) soluble collagen were determined using the hydroxyproline and the Sircol collagen assay, respectively. (F) Representative Masson's trichrome stained lung images, and (G) Ashcroft score were presented from lung tissues of control (sterile saline) and bleomycin-exposed animals. Myofibroblast accumulation is shown by (H) representative αSMA-stained lung images and (I) quantification from saline- and bleomycin-exposed lung tissues. Bars represent mean ± SEM from 5-8 mice per group. This figure shows one of two representative experiments. *:P<0.05; **:P<0.01; ***:P<0.001; #:P<0.05; ##:P<0.01; ###:P<0.001; * represent a difference between bleomycin-exposed groups and their littermate controls; # represent a difference between genotypes. Significance was established using GraphPad, Prism 5.0 with two-way ANOVA using Newman-Keuls Multiple Comparison test.

Figure 2. *Grp78*$^{+/-}$ leads to a reduction in the number of BALF and tissue infiltrated macrophages as well as arginase-positive macrophages in response to bleomycin. Mice were intubated with bleomycin (0.04 U/mouse) and examined after 7 and 21 days. Control animals were exposed to vehicle only (sterile saline). (A) Differential BALF macrophage counts shown at 7 and 21 days post-bleomycin administration. (B-C)

Immunohistochemical detection of the macrophage receptor F4/80 and quantification per mm^2 of area as assessed in both saline and bleomycin-exposed lungs. (D-E) Arginase-1 immunostaining and quantification on lung tissue sections showing positive cells (see boxes) in wild type and *Grp78*$^{+/-}$ mice exposed to bleomycin at day 7 and 21. (F) Immunofluorescence dual staining of GRP78 (red) and MAC3 (green) in lung sections of bleomycin-exposed wild type and *Grp78*$^{+/-}$ mice. Bars represent mean ± SEM from 5-8 mice per group and graph shows one of two representative experiments; *:P<0.05; **:P<0.01; ***:P<0.001; #:P<0.05; ##:P<0.01; ###:P<0.001; * represent a difference between bleomycin-exposed groups and their littermate controls; # represent a difference between genotypes. Significance was established using GraphPad, Prism 5.0 with two-way ANOVA using Newman-Keuls Multiple Comparison test.

Figure 3. *Grp78*$^{+/-}$ leads to a reduction in fibrotic transcripts and an enhancement in the UPR response following bleomycin administration. NanoString nCounter technology was used to measure the expression of 67 genes in the lungs of wild type and *Grp78*$^{+/-}$ mice at 7 and 21 days following exposure to bleomycin or vehicle. Saline-exposed mice were examined at day 21. The relative mRNA counts of (A) *Col1a1* (B) *Col3a1* (C) *Fn1* (D) *Fkbp10* (E) *Grp78* (F) *Calreticulin* (G) *Hsp47* and (H) *Chop* are shown. (I-J) *In situ* hybridization representative images and quantification showing the co-localization of *Chop* mRNA by cells expressing *F4/80* in bleomycin-exposed lung tissues (Scale bar = 20µm). The arrows point towards a single stain (either *F4/80 or Chop*) and the arrowheads point towards cells positive for both *F4/80* and *Chop*. Each bar represents mean ± SEM, n = 4–7 per group. *:P<0.05; **:P<0.01; ***:P<0.001;

#:P<0.05; ##:P<0.01; ###:P<0.001, * represent a difference between *Grp78*$^{+/-}$ and their littermate controls, # represent a difference between genotypes. Significance was established using GraphPad, Prism 5.0 with Two-way ANOVA using Newman-Keuls Multiple Comparison test. Please see supplement Figure 10 for a heat-map of genes regulated and Supplement Table I for detailed information of all genes investigated. Please see supplementary Figure 14 for the saline control images of Figure 3I.

Figure 4. Macrophage apoptosis is prominent in *Grp78*$^{+/-}$ lungs seven days post bleomycin administration. Animals were intubated with bleomycin (0.04 U/mouse) and examined at day 7 and 21. Control animals were exposed to vehicle only (sterile saline). (A) Representative images from CHOP-stained lung tissues from control saline and 7-day post bleomycin administration. (B-C) Representative immunoblot and densitometry analyses of cleaved caspase-3 from lung homogenates of wild type and *Grp78*$^{+/-}$ mice 7 or 21 days after bleomycin administration. Tunicamycin treatment (1 µg/mL for 18 hours) of A549 cells was used as a positive control for cleaved caspase 3. The actin bands panel is the same used in supplementary figure 1A. (D) TUNEL stained representative images are shown from both wild type and *Grp78*$^{+/-}$ lungs in both saline and at day 7. (E) Graph showing semi-quantitative analysis of TUNEL-positive cells expressed per mm^2 tissue. (F-G) Representative images and quantification of fluorescent MAC3 signal co-localizing with cleaved caspase-3 in bleomycin exposed lung tissues. (H-I) Representative images and quantification of fluorescent E-Cadherin signal co-localizing with cleaved caspase-3 in bleomycin exposed lung tissues. For the saline control images, please see supplementary Figure 13A-B. Data represent mean ± SEM, n=5 in each group, *:P<0.05;

**:P<0.01; ***:P<0.001; #:P<0.05; ##:P<0.01; ###:P<0.001; * represent a difference between bleomycin-exposed groups and vehicle; # represents a difference between genotypes. Significance was established using GraphPad, Prism 5.0 with unpaired T-test and Two-way ANOVA using Newman-Keuls Multiple Comparison test.

Figure 5. Bleomycin-exposed *Chop*$^{-/-}$ mice have increased mortality and an exacerbated fibrotic phenotype associated with the accumulation of non-apoptotic macrophages. Both wild type and *Chop*$^{-/-}$ mice were given bleomycin by intratracheal intubation. Lung function and fibrotic measurements were assessed 21 days following bleomycin administration. Lung tissue sections were stained for arginase-1 as well as a dual fluorescent macrophage (MAC3) and apoptosis (cleaved caspase-3) markers. (A) Kaplan-Meier survival curves showing percent survival of wild type and *Chop*$^{-/-}$ mice in response to 0.06 U of bleomycin by log-rank test († P<0.05; ††<0.01), n=8-10 animals per group. (B) Lung tissue stiffness (Est) was assessed by flexiVent® in response to 0.04 U of bleomycin in wild type and *Chop*$^{-/-}$ mice, n = 8-10 per group. (C) Representative Masson's trichrome stained images and assessment of the grade of fibrosis by ashcroft score in saline- and bleomycin-exposed (0.04U per mouse) wild type and *Chop*$^{-/-}$ lungs. Additional images with high and low magnification are shown in supplementary Figure 19. D) Representative images and quantification of F4/80 positive cells in bleomycin-exposed lung tissues (Day 21). F4/80 quantification per mm^2 of area from wild type and *Chop*$^{-/-}$ mice 21 days post bleomycin administration. For the saline control images, please see supplementary Figure 20. (E) Representative images and quantification of arginase-1 positive cells in bleomycin-exposed lung tissues (Day 21). For the saline control images,

please see supplementary Figure 20. (F-H) Representative images and quantification of fluorescent MAC3 signal co-localizing with cleaved caspase-3 in the lungs of bleomycin-exposed lung tissues at day 7 and day 21. For the saline control images, please see supplementary Figure 14C. Data represent mean ± SEM, n=8-10 in each group, *:P<0.05; **:P<0.01; ***:P<0.001; #:P<0.05; ##:P<0.01; ###:P<0.001; * represent a difference between bleomycin-exposed groups and their controls; # represents a difference between genotypes. Significance was established using GraphPad, Prism 5.0 with log-rank (Mantel-Cox) test and two-way ANOVA using Newman-Keuls Multiple Comparison test.

Figure 6. An illustration of the findings showing that interfering with *Grp78* protects against bleomycin–induced lung fibrosis while upregulating *Chop* and promoting apoptosis in macrophages. Conversely, inhibition of *Chop* promotes accumulation and survival of macrophages while exacerbating lung fibrosis.

It is understood that bleomycin can cause injury to the epithelium through the generation of reactive oxygen species (ROS) [26,59-62]. T-cells are then recruited and release factors responsible for monocyte/macrophage differentiation and recruitment [63-65], leading to the polarization of macrophages toward the M2 phenotype [11,66]. This may facilitate the transition of fibroblasts to myofibroblasts [40,67,68], which are ultimately responsible for the secretion of ECM proteins involved in the scarring process. Our data indicate that manipulation of the UPR is a potential therapeutic avenue in pulmonary fibrosis, and suggest a relationship between the extent of fibrosis and the polarization/survival of lung macrophages. Further experimentation is needed to determine the precise nature of this relationship and whether this might encompass more

precise targets for intervention. In this cartoon, we have specifically distinguished the work of others from our findings by adding a shaded overlay onto previously published work.

REFERENCES

1. King TE, Jr., Pardo A, Selman M. Idiopathic pulmonary fibrosis. *Lancet* 2011; **378**: 1949-1961.
2. Selman M, King TE, Pardo A, *et al.* Idiopathic pulmonary fibrosis: prevailing and evolving hypotheses about its pathogenesis and implications for therapy. *Ann Intern Med* 2001; **134**: 136-151.
3. Phan SH. The myofibroblast in pulmonary fibrosis. *Chest* 2002; **122**: 286S-289S.
4. Rosenbloom J, Mendoza FA, Jimenez SA. Strategies for anti-fibrotic therapies. *Biochim Biophys Acta* 2013; **1832**: 1088-1103.
5. Hirschel BJ, Gabbiani G, Ryan GB, *et al.* Fibroblasts of granulation tissue: immunofluorescent staining with antismooth muscle serum. *Proc Soc Exp Biol Med* 1971; **138**: 466-469.
6. Majno G, Gabbiani G, Hirschel BJ, *et al.* Contraction of granulation tissue in vitro: similarity to smooth muscle. *Science* 1971; **173**: 548-550.
7. Gabbiani G, Ryan GB, Majne G. Presence of modified fibroblasts in granulation tissue and their possible role in wound contraction. *Experientia* 1971; **27**: 549-550.
8. Majno G, Shea SM, Leventhal M. Endothelial contraction induced by histamine-type mediators: an electron microscopic study. *J Cell Biol* 1969; **42**: 647-672.
9. Scotton CJ, Chambers RC. Molecular targets in pulmonary fibrosis: the myofibroblast in focus. *Chest* 2007; **132**: 1311-1321.
10. Schroder M, Kaufman RJ. The mammalian unfolded protein response. *Annu Rev Biochem* 2005; **74**: 739-789.
11. Dickhout JG, Lhotak S, Hilditch BA, *et al.* Induction of the unfolded protein response after monocyte to macrophage differentiation augments cell survival in early atherosclerotic lesions. *FASEB J* 2011; **25**: 576-589.
12. Iwakoshi NN, Lee AH, Vallabhajosyula P, *et al.* Plasma cell differentiation and the unfolded protein response intersect at the transcription factor XBP-1. *Nat Immunol* 2003; **4**: 321-329.
13. Basseri S, Lhotak S, Sharma AM, *et al.* The chemical chaperone 4-phenylbutyrate inhibits adipogenesis by modulating the unfolded protein response. *J Lipid Res* 2009; **50**: 2486-2501.
14. Pallet N, Bouvier N, Bendjallabah A, *et al.* Cyclosporine-induced endoplasmic reticulum stress triggers tubular phenotypic changes and death. *American Journal of Transplantation* 2008; **8**: 2283-2296.
15. Carlisle RE, Heffernan A, Brimble E, *et al.* TDAG51 mediates epithelial-to-mesenchymal transition in human proximal tubular epithelium. *Am J Physiol Renal Physiol* 2012; **303**: F467-481.
16. Baek HA, Kim do S, Park HS, *et al.* Involvement of endoplasmic reticulum stress in myofibroblastic differentiation of lung fibroblasts. *American journal of respiratory cell and molecular biology* 2012; **46**: 731-739.

17. Bettigole SE, Lis R, Adoro S, *et al.* The transcription factor XBP1 is selectively required for eosinophil differentiation. *Nat Immunol* 2015, 16:829-837.
18. Oyadomari S, Mori M. Roles of CHOP/GADD153 in endoplasmic reticulum stress. *Cell Death Differ* 2004; **11**: 381-389.
19. Han J, Back SH, Hur J, *et al.* ER-stress-induced transcriptional regulation increases protein synthesis leading to cell death. *Nat Cell Biol* 2013; **15**: 481-490.
20. Haas IG. BiP (GRP78), an essential hsp70 resident protein in the endoplasmic reticulum. *Experientia* 1994; **50**: 1012-1020.
21. Kaufman RJ. Orchestrating the unfolded protein response in health and disease. *J Clin Invest* 2002; **110**: 1389-1398.
22. Kuznetsov G, Chen LB, Nigam SK. Multiple molecular chaperones complex with misfolded large oligomeric glycoproteins in the endoplasmic reticulum. *The Journal of biological chemistry* 1997; **272**: 3057-3063.
23. Hendershot L, Wei J, Gaut J, *et al.* Inhibition of immunoglobulin folding and secretion by dominant negative BiP ATPase mutants. *Proc Natl Acad Sci U S A* 1996; **93**: 5269-5274.
24. Gorbatyuk MS, Gorbatyuk OS. The Molecular Chaperone GRP78/BiP as a Therapeutic Target for Neurodegenerative Disorders: A Mini Review. *J Genet Syndr Gene Ther* 2013; 4(2): 128.
25. Tanjore H, Lawson WE, Blackwell TS. Endoplasmic reticulum stress as a pro-fibrotic stimulus. *Biochim Biophys Acta* 2013; **1832**: 940-947.
26. Tanjore H, Blackwell TS, Lawson WE. Emerging evidence for endoplasmic reticulum stress in the pathogenesis of idiopathic pulmonary fibrosis. *American journal of physiology Lung cellular and molecular physiology* 2012.
27. Lawson WE, Crossno PF, Polosukhin VV, *et al.* Endoplasmic reticulum stress in alveolar epithelial cells is prominent in IPF: association with altered surfactant protein processing and herpesvirus infection. *American journal of physiology Lung cellular and molecular physiology* 2008; **294**: L1119-1126.
28. Luo S, Mao C, Lee B, *et al.* GRP78/BiP is required for cell proliferation and protecting the inner cell mass from apoptosis during early mouse embryonic development. *Mol Cell Biol* 2006; **26**: 5688-5697.
29. Lee AS. GRP78 induction in cancer: therapeutic and prognostic implications. *Cancer Res* 2007; **67**: 3496-3499.
30. Luo B, Lee AS. The critical roles of endoplasmic reticulum chaperones and unfolded protein response in tumorigenesis and anticancer therapies. *Oncogene* 2013; **32**: 805-818.
31. Wang M, Wey S, Zhang Y, *et al.* Role of the unfolded protein response regulator GRP78/BiP in development, cancer, and neurological disorders. *Antioxid Redox Signal* 2009; **11**: 2307-2316.
32. Luo S, Baumeister P, Yang S, *et al.* Induction of Grp78/BiP by translational block: activation of the Grp78 promoter by ATF4 through and upstream ATF/CRE site independent of the endoplasmic reticulum stress elements. *J Biol Chem* 2003; **278**: 37375-37385.

33. Novak ML, Koh TJ. Macrophage phenotypes during tissue repair. *J Leukoc Biol* 2013; **93**: 875-881.
34. Schupp JC, Binder H, Jager B, *et al.* Macrophage activation in acute exacerbation of idiopathic pulmonary fibrosis. *PLoS One* 2015; **10**: e0116775.
35. Lenna S, Trojanowska M. The role of endoplasmic reticulum stress and the unfolded protein response in fibrosis. *Curr Opin Rheumatol* 2012; **24**: 663-668.
36. Wei J, Rahman S, Ayaub EA, *et al.* Protein misfolding and endoplasmic reticulum stress in chronic lung disease. *Chest* 2013; **143**: 1098-1105.
37. Wynn TA. Integrating mechanisms of pulmonary fibrosis. *J Exp Med* 2011; **208**: 1339-1350.
38. Wynn TA, Barron L. Macrophages: master regulators of inflammation and fibrosis. *Semin Liver Dis* 2010; **30**: 245-257.
39. Wynn TA, Chawla A, Pollard JW. Macrophage biology in development, homeostasis and disease. *Nature* 2013; **496**: 445-455.
40. Gibbons MA, MacKinnon AC, Ramachandran P, *et al.* Ly6Chi monocytes direct alternatively activated profibrotic macrophage regulation of lung fibrosis. *Am J Respir Crit Care Med* 2011; **184**: 569-581.
41. Collins SL, Chan-Li Y, Hallowell RW, *et al.* Pulmonary vaccination as a novel treatment for lung fibrosis. *PLoS One* 2012; **7**: e31299.
42. Gharib SA, Johnston LK, Huizar I, *et al.* MMP28 promotes macrophage polarization toward M2 cells and augments pulmonary fibrosis. *J Leukoc Biol* 2014; **95**: 9-18.
43. Li D, Guabiraba R, Besnard AG, *et al.* IL-33 promotes ST2-dependent lung fibrosis by the induction of alternatively activated macrophages and innate lymphoid cells in mice. *J Allergy Clin Immunol* 2014; **134**: 1422-1432 e1411.
44. Prasse A, Pechkovsky DV, Toews GB, *et al.* A vicious circle of alveolar macrophages and fibroblasts perpetuates pulmonary fibrosis via CCL18. *Am J Respir Crit Care Med* 2006; **173**: 781-792.
45. Pechkovsky DV, Prasse A, Kollert F, *et al.* Alternatively activated alveolar macrophages in pulmonary fibrosis-mediator production and intracellular signal transduction. *Clin Immunol* 2010; **137**: 89-101.
46. Stahl M, Schupp J, Jager B, *et al.* Lung collagens perpetuate pulmonary fibrosis via CD204 and M2 macrophage activation. *PLoS One* 2013; **8**: e81382.
47. Solinas G, Germano G, Mantovani A, *et al.* Tumor-associated macrophages (TAM) as major players of the cancer-related inflammation. *J Leukoc Biol* 2009; **86**: 1065-1073.
48. Richeldi L. Clinical trials of investigational agents for IPF: a review of a Cochrane report. *Respir Res* 2013; **14 Suppl 1**: S4.
49. Harding HP, Zhang Y, Ron D. Protein translation and folding are coupled by an endoplasmic-reticulum-resident kinase. *Nature* 1999; **397**: 271-274.
50. Bertolotti A, Zhang Y, Hendershot LM, *et al.* Dynamic interaction of BiP and ER stress transducers in the unfolded-protein response. *Nature cell biology* 2000; **2**: 326-332.

51. Vattem KM, Wek RC. Reinitiation involving upstream ORFs regulates ATF4 mRNA translation in mammalian cells. *Proc Natl Acad Sci U S A* 2004; **101**: 11269-11274.
52. Harding HP, Novoa I, Zhang Y, *et al.* Regulated translation initiation controls stress-induced gene expression in mammalian cells. *Molecular cell* 2000; **6**: 1099-1108.
53. Zinszner H, Kuroda M, Wang X, *et al.* CHOP is implicated in programmed cell death in response to impaired function of the endoplasmic reticulum. *Genes Dev* 1998; **12**: 982-995.
54. Malhi H, Kropp EM, Clavo VF, *et al.* C/EBP homologous protein-induced macrophage apoptosis protects mice from steatohepatitis. *J Biol Chem* 2013; **288**: 18624-18642.
55. Hirota M, Kitagaki M, Itagaki H, *et al.* Quantitative measurement of spliced XBP1 mRNA as an indicator of endoplasmic reticulum stress. *The Journal of toxicological sciences* 2006; **31**: 149-156.
56. Sriburi R, Bommiasamy H, Buldak GL, *et al.* Coordinate regulation of phospholipid biosynthesis and secretory pathway gene expression in XBP-1(S)-induced endoplasmic reticulum biogenesis. *J Biol Chem* 2007; **282**: 7024-7034.
57. Baumeister P, Luo S, Skarnes WC, *et al.* Endoplasmic reticulum stress induction of the Grp78/BiP promoter: activating mechanisms mediated by YY1 and its interactive chromatin modifiers. *Mol Cell Biol* 2005; **25**: 4529-4540.
58. Ye R, Jung DY, Jun JY, *et al.* Grp78 heterozygosity promotes adaptive unfolded protein response and attenuates diet-induced obesity and insulin resistance. *Diabetes* 2010; **59**: 6-16.
59. Suwara MI, Green NJ, Borthwick LA, *et al.* IL-1alpha released from damaged epithelial cells is sufficient and essential to trigger inflammatory responses in human lung fibroblasts. *Mucosal Immunol* 2014; **7**: 684-693.
60. Nakatani-Okuda A, Ueda H, Kashiwamura S, *et al.* Protection against bleomycin-induced lung injury by IL-18 in mice. *Am J Physiol Lung Cell Mol Physiol* 2005; **289**: L280-287.
61. Barth K, Reh J, Sturrock A, *et al.* Epithelial vs myofibroblast differentiation in immortal rat lung cell lines--modulating effects of bleomycin. *Histochem Cell Biol* 2005; **124**: 453-464.
62. Kuwano K, Kunitake R, Maeyama T, *et al.* Attenuation of bleomycin-induced pneumopathy in mice by a caspase inhibitor. *Am J Physiol Lung Cell Mol Physiol* 2001; **280**: L316-325.
63. Phan SH, Kunkel SL. Inhibition of bleomycin-induced pulmonary fibrosis by nordihydroguaiaretic acid. The role of alveolar macrophage activation and mediator production. *Am J Pathol* 1986; **124**: 343-352.
64. Gharaee-Kermani M, Nozaki Y, Hatano K, *et al.* Lung interleukin-4 gene expression in a murine model of bleomycin-induced pulmonary fibrosis. *Cytokine* 2001; **15**: 138-147.

65. Khalil N, Bereznay O, Sporn M, *et al.* Macrophage production of transforming growth factor beta and fibroblast collagen synthesis in chronic pulmonary inflammation. *J Exp Med* 1989; **170**: 727-737.
66. Oh J, Riek AE, Weng S, *et al.* Endoplasmic reticulum stress controls M2 macrophage differentiation and foam cell formation. *J Biol Chem* 2012; **287**: 11629-11641.
67. Murray LA, Chen Q, Kramer MS, *et al.* TGF-beta driven lung fibrosis is macrophage dependent and blocked by Serum amyloid P. *Int J Biochem Cell Biol* 2011; **43**: 154-162.
68. Kim JH, Oh SH, Kim EJ, *et al.* The role of myofibroblasts in upregulation of S100A8 and S100A9 and the differentiation of myeloid cells in the colorectal cancer microenvironment. *Biochem Biophys Res Commun* 2012; **423**: 60-66.
69. Zhang X, Goncalves R, Mosser DM. The isolation and characterization of murine macrophages. *Current protocols in immunology / edited by John E Coligan [et al]*. John Wiley and Sons, Inc, Hoboken, New Jersey, USA, 2008; **Chapter 14**: Unit 14 11.
70. Lauber S, Wong S, Cutz JC, *et al.* Novel function of Oncostatin M as a potent tumour-promoting agent in lung. *International journal of cancer Journal international du cancer* 2014, 136:831-843.
71. Tuominen VJ, Ruotoistenmaki S, Viitanen A, *et al.* ImmunoRatio: a publicly available web application for quantitative image analysis of estrogen receptor (ER), progesterone receptor (PR), and Ki-67. *Breast cancer research : BCR* 2010; **12**: R56.
72. Ask K, Bonniaud P, Maass K, *et al.* Progressive pulmonary fibrosis is mediated by TGF-beta isoform 1 but not TGF-beta3. *The international journal of biochemistry & cell biology* 2008; **40**: 484-495.

Figure 1

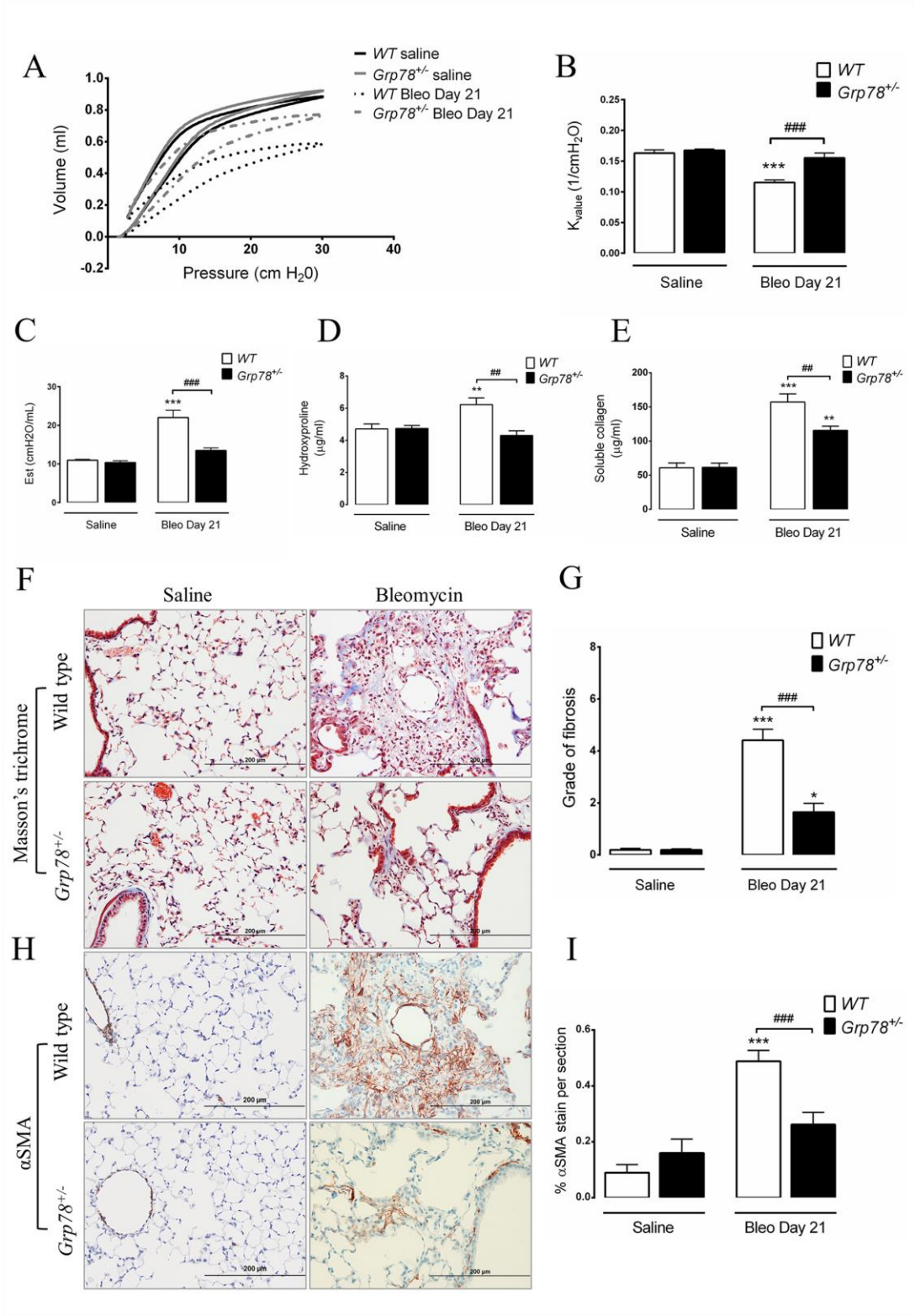
A
WT saline
Grp78+/- saline
WT Bleo Day 21
Grp78+/- Bleo Day 21
Volume (ml)
Pressure (cm H20)
B
WT
Grp78+/-
Kvalue (1/cmH2O)
###
***
Saline
Bleo Day 21
C
Est (cmH2O/mL)
D
Hydroxyproline (µg/ml)
E
Soluble collagen (µg/ml)
F
Saline
Bleomycin
Masson's trichrome
Wild type
Grp78+/-
G
Grade of fibrosis
H
αSMA
I
% αSMA stain per section

Figure 2

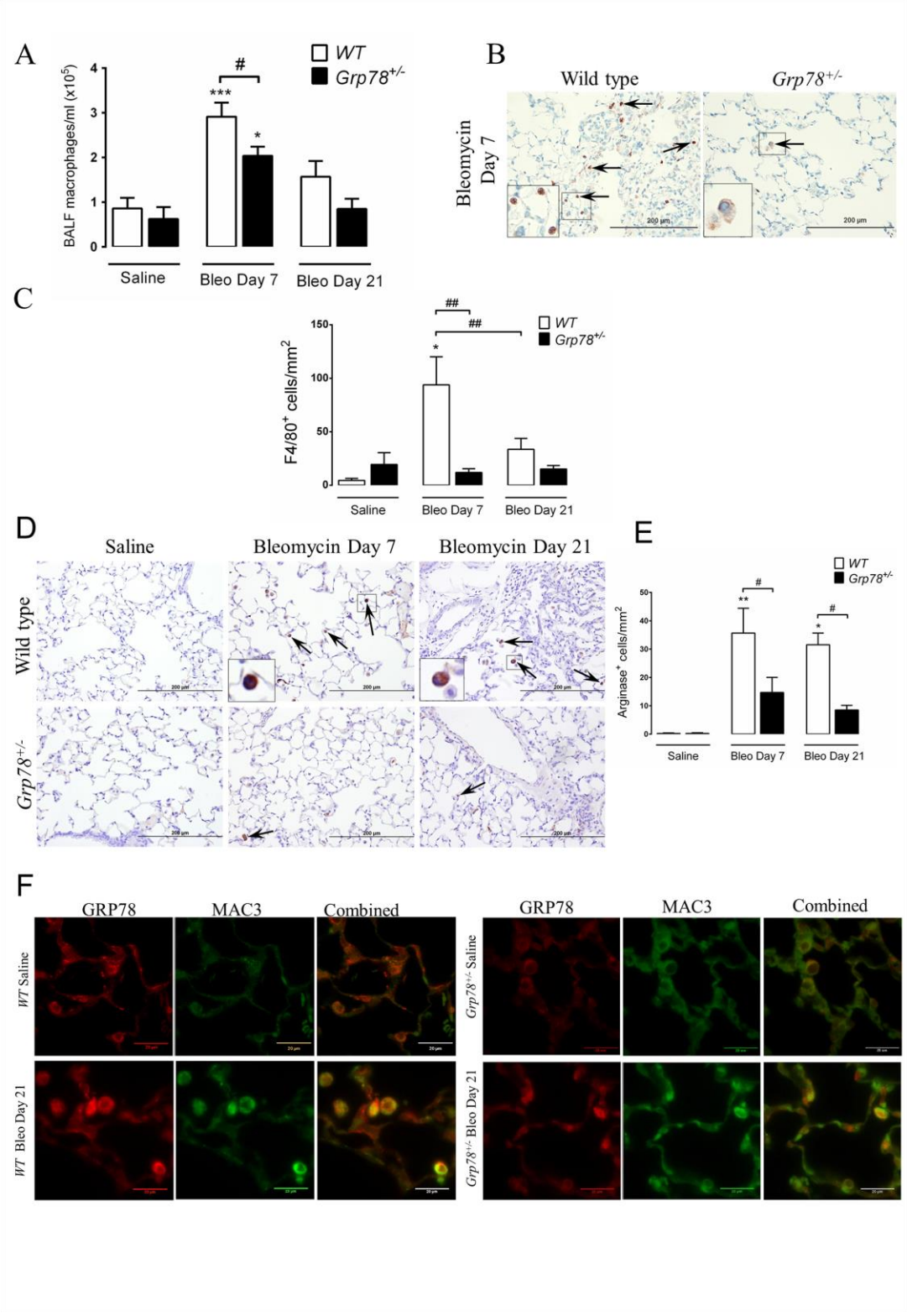
A
WT
Grp78+/-
BALF macrophages/ml (x10^5)
Saline
Bleo Day 7
Bleo Day 21
B
Wild type
Grp78+/-
Bleomycin Day 7
C
F4/80+ cells/mm2
D
Saline
Bleomycin Day 7
Bleomycin Day 21
Wild type
Grp78+/-
E
Arginase+ cells/mm2
F
GRP78
MAC3
Combined
WT Saline
Grp78+/- Saline
WT Bleo Day 21
Grp78+/- Bleo Day 21

Figure 3

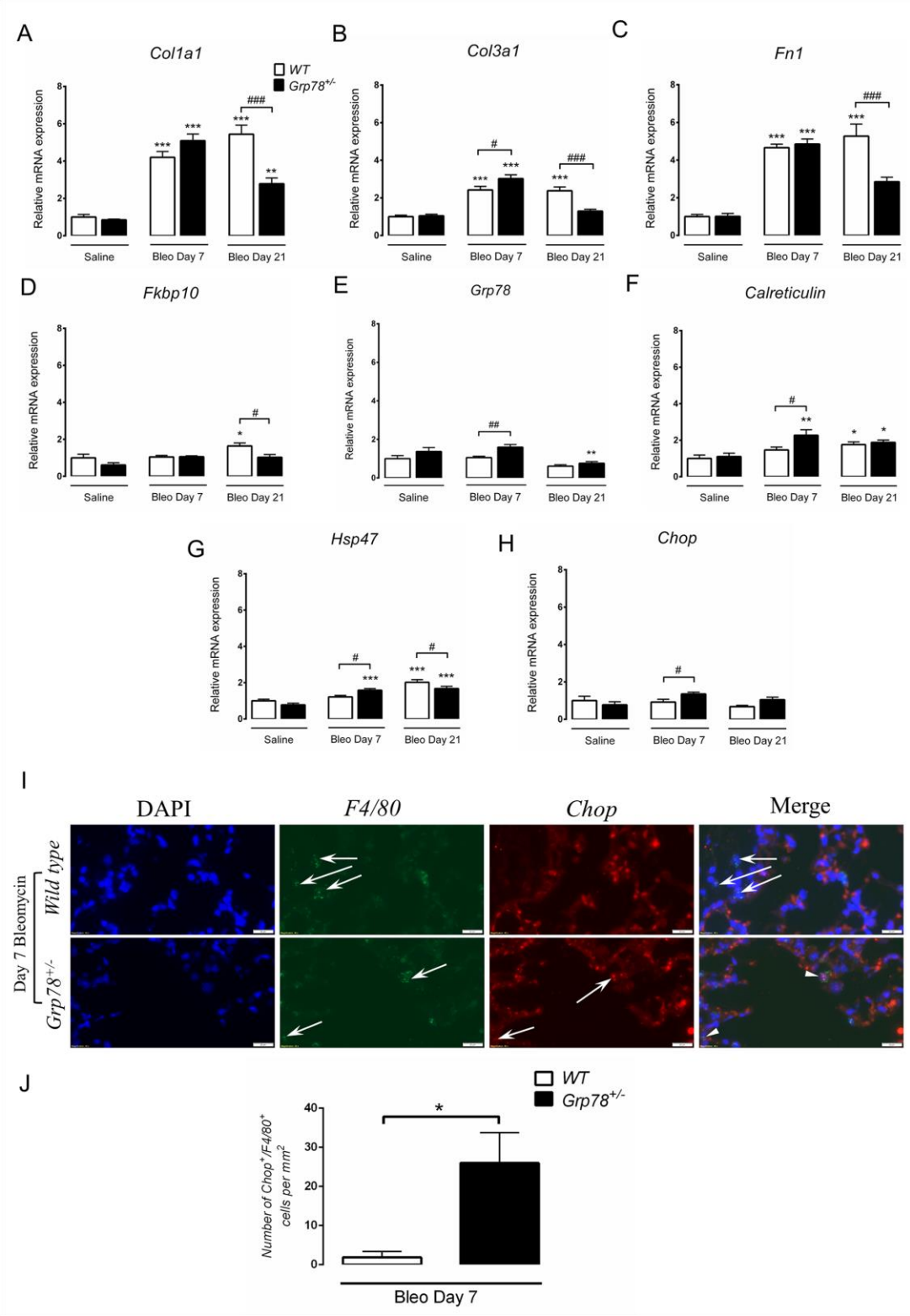
A
Col1a1
WT
Grp78+/-
Relative mRNA expression
Saline
Bleo Day 7
Bleo Day 21
B
Col3a1
C
Fn1
D
Fkbp10
E
Grp78
F
Calreticulin
G
Hsp47
H
Chop
I
DAPI
F4/80
Chop
Merge
Day 7 Bleomycin
Wild type
Grp78+/-
J
Number of Chop+/F4/80+ cells per mm2

Figure 4

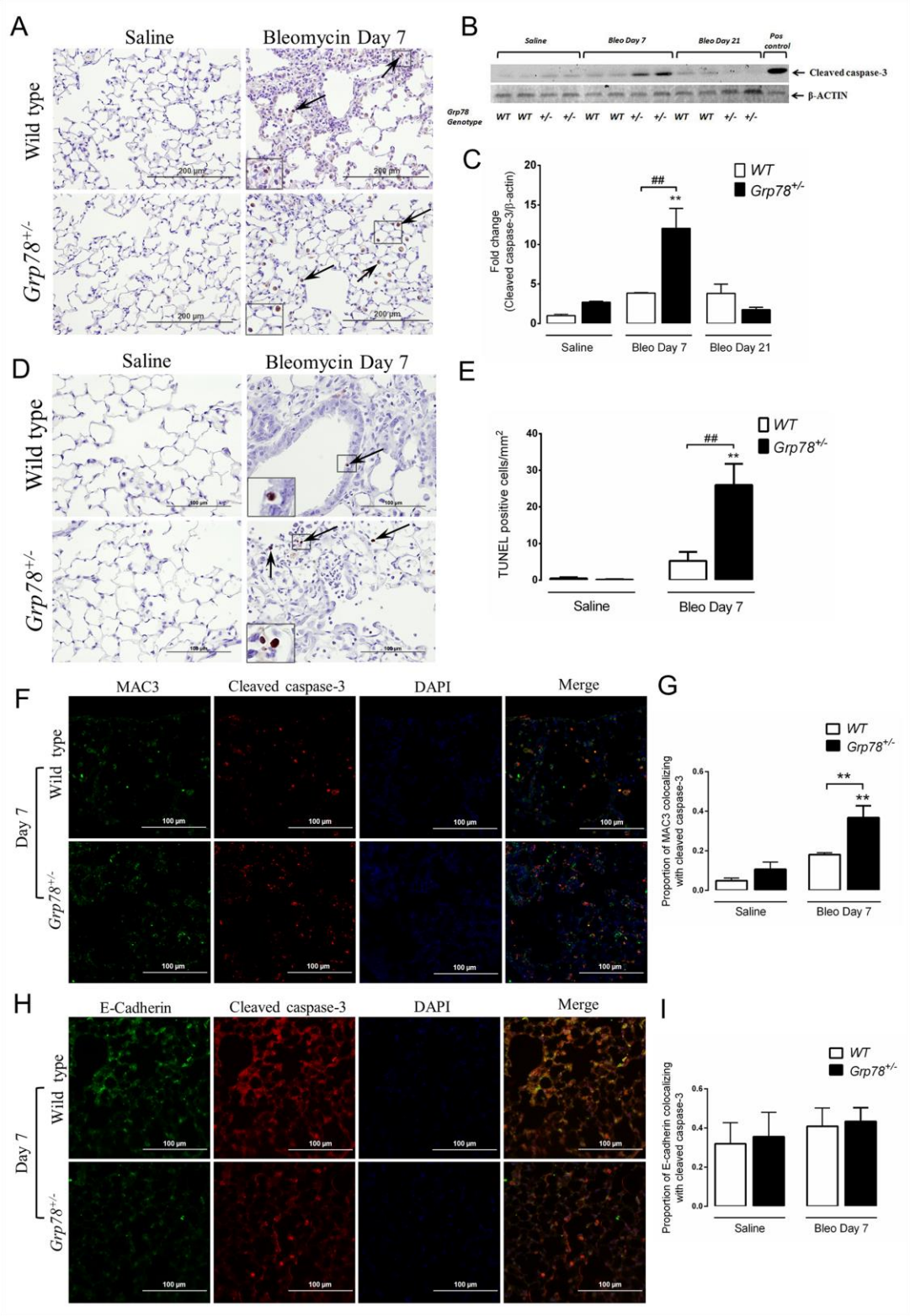
A
Saline
Bleomycin Day 7
Wild type
Grp78+/-
200 μm
B
Saline
Bleo Day 7
Bleo Day 21
Pos control
Cleaved caspase-3
β-ACTIN
Grp78 Genotype
WT WT +/- +/- WT WT +/- +/- WT WT +/- +/-
C
WT
Grp78+/-
Fold change (Cleaved caspase-3/β-actin)
##
**
Saline
Bleo Day 7
Bleo Day 21
D
Saline
Bleomycin Day 7
Wild type
Grp78+/-
100 μm
E
WT
Grp78+/-
TUNEL positive cells/mm2
##
**
Saline
Bleo Day 7
F
MAC3
Cleaved caspase-3
DAPI
Merge
Day 7
Wild type
Grp78+/-
100 μm
G
WT
Grp78+/-
Proportion of MAC3 colocalizing with cleaved caspase-3
**
**
Saline
Bleo Day 7
H
E-Cadherin
Cleaved caspase-3
DAPI
Merge
Day 7
Wild type
Grp78+/-
100 μm
I
WT
Grp78+/-
Proportion of E-cadherin colocalizing with cleaved caspase-3
Saline
Bleo Day 7

Figure 5

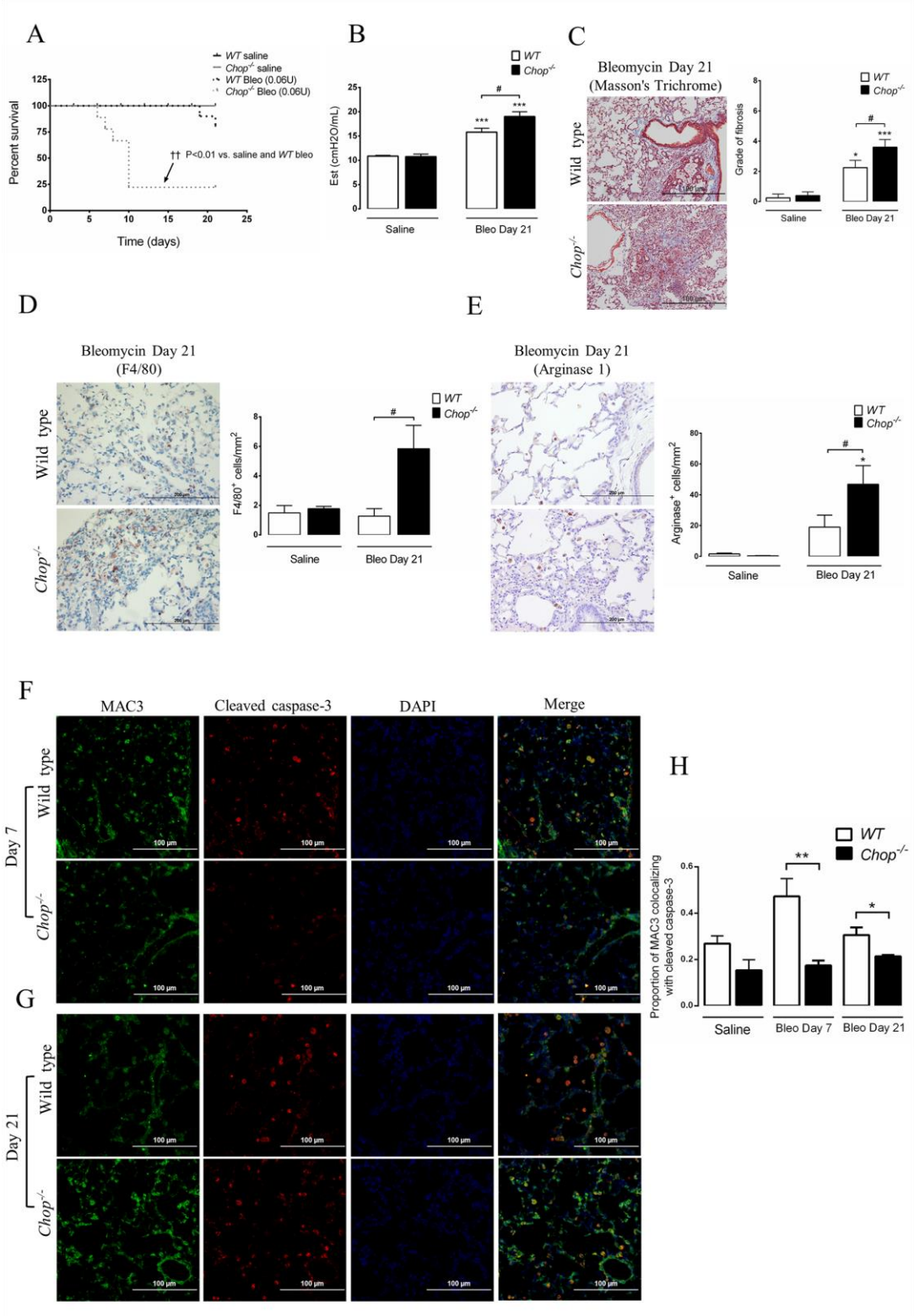
A
WT saline
Chop-/- saline
WT Bleo (0.06U)
Chop-/- Bleo (0.06U)
†† P<0.01 vs. saline and WT bleo
Percent survival
Time (days)
B
WT
Chop-/-
Est (cmH2O/mL)
Saline
Bleo Day 21
C
Bleomycin Day 21
(Masson's Trichrome)
Wild type
Chop-/-
Grade of fibrosis
Saline
Bleo Day 21
D
Bleomycin Day 21
(F4/80)
Wild type
Chop-/-
F4/80+ cells/mm2
Saline
Bleo Day 21
E
Bleomycin Day 21
(Arginase 1)
Arginase+ cells/mm2
Saline
Bleo Day 21
F
MAC3
Cleaved caspase-3
DAPI
Merge
Day 7
Wild type
Chop-/-
100 µm
G
Day 21
Wild type
Chop-/-
H
Proportion of MAC3 colocalizing with cleaved caspase-3
Saline
Bleo Day 7
Bleo Day 21

Figure 6

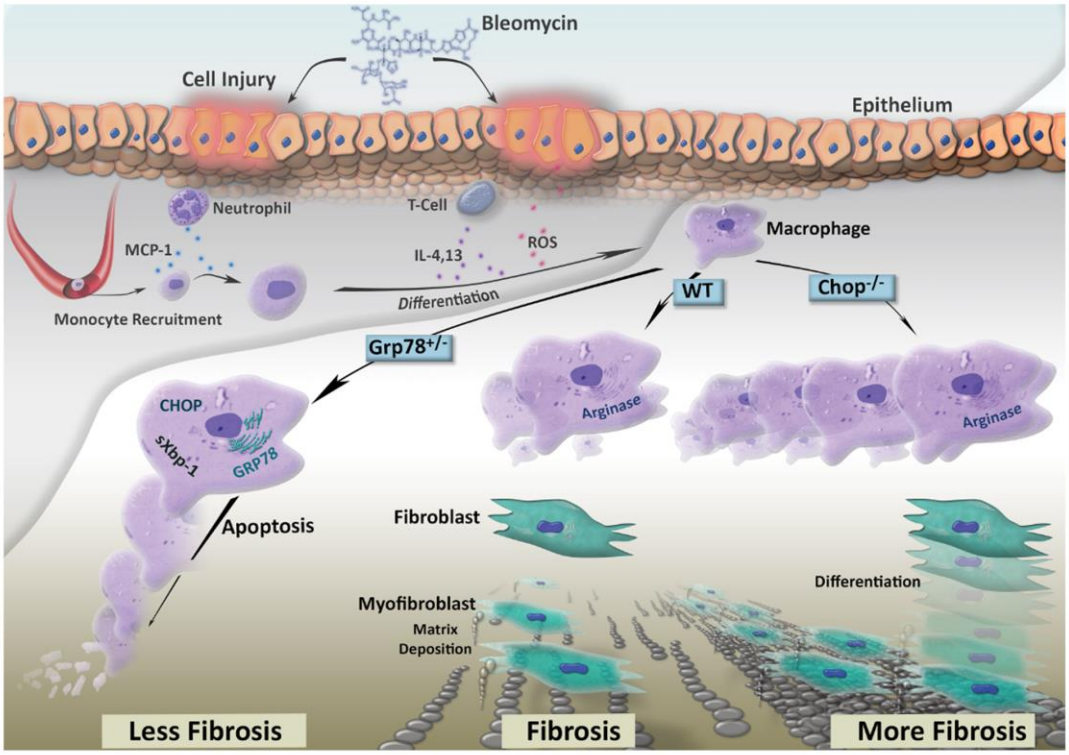
Bleomycin
Cell Injury
Epithelium
Neutrophil
T-Cell
MCP-1
IL-4,13
ROS
Macrophage
Monocyte Recruitment
Differentiation
WT
Chop-/-
Grp78+/-
CHOP
sXbp-1
GRP78
Arginase
Arginase
Apoptosis
Fibroblast
Differentiation
Myofibroblast
Matrix
Deposition
Less Fibrosis
Fibrosis
More Fibrosis

<Supplementary material>

+A: **Supplementary materials and methods**

+B: Animals

Grp78$^{+/-}$ mice (C57BL6 background) were a kind gift from Dr Amy Lee [28]. Wild type female C57BL6/J mice were purchased from Charles River Laboratories International (Wilmington, MA, USA) and *Chop*$^{-/-}$ mice (C57BL6 background) were obtained from Jackson Laboratories (cat. no. 005530). Both strains of mice were bred in-house and experiments conducted with appropriate littermate controls for *Grp78*$^{+/-}$ or corresponding wild type breeding colony for *Chop*$^{-/-}$ mice. All mice were used at age 8–12 weeks and housed at McMaster University (Hamilton, ON, Canada). The animals were kept on a 12 h light/12 h dark cycle at a controlled temperature of 20–25°C, ambient humidity of ~50% and fed *ad libitum*. All work was conducted under the guidelines of the Canadian Council on Animal Care and approved by the Animal Research Ethics Board of McMaster University under Protocol No. 12.02.06.

+B: Administration of bleomycin

Mice were kept under gaseous isoflurane anaesthesia (MTC Pharmaceuticals, Cambridge, ON, Canada) throughout the procedure. Experimental pulmonary fibrosis was induced using intratracheal intubation of bleomycin at 0.04 or 0.06 U/mouse in a volume of 50 µl sterile saline (Hospira Healthcare Corp., NDC

61703-332-18). Control animals received sterile saline alone. Animal groups were sacrificed after 3, 5, 7 or 21 days.

+B: Administration of LPS

LPS was administered intratracheally to *Grp78*$^{+/-}$ or wild type C57BL6/J female mice (50 µg/mouse in a volume of 50 µl sterile saline; Sigma-Aldrich, cat. no. L6511 61703-332-18) and sacrificed after 42 h. BALF was then collected and total cellular differentials and cytokine assessment conducted as described below.

+B: Collection of mouse specimens

Mice were anesthetized with isoflurane and sacrificed by exsanguination by severing the descending aorta. After exsanguination, the lungs were cannulated, excised and washed with phosphate-buffered saline (PBS; 600 µl) for broncheoalveolar lavage fluid (BALF) collection and analysis. The four lobes of the right lung were rinsed with PBS, tied up with a surgical thread, excised and immediately frozen in liquid nitrogen. These were later stored at –80°C for further protein and RNA isolation assays. The left lung was removed and inflated to 30 cmH_2O for 3–5 min in 10% formalin solution and fixed for 48–72 h before embedding and subsequent histological analysis.

+B: Bronchoalveolar lavage – cell counts and cytospin preparation

Following BALF collection, tubes were placed immediately on ice. Total cell count was performed using a haemocytometer from an aliquot of 50 µl from each sample. Trypan blue solution (Sigma-Aldrich, cat. no. T8154) was added to these tubes to test for cellular viability. The original BALF samples were then spun down at 12

000 rpm (Eppendorf centrifuge 5417C) for 10 min. The supernatant was stored at –80°C for later analysis. Cell pellets were resuspended in PBS and smears were prepared by cytocentrifugation (Shandon, Pittsburgh, PA, USA) at a speed of 1000 rpm for 3 min. The developed cytospin slides were stained with Wright–Giemsa stain (Sigma-Aldrich, Oakville, ON, Canada) according to the manufacturer's protocol. Differential cell counts were determined from approximately 300 random leukocytes using haemocytological procedures to classify the cells as neutrophils, macrophages, eosinophils or lymphocytes. Each cell type is presented as total numbers, based on the corresponding total cell count calculated from each sample.

+B: Homogenization of lung tissues

Before homogenization, the originally snap-frozen right lobes of the extracted lungs were removed from the –80°C freezer and transferred back into liquid nitrogen. A metal chamber fitted with a cylindrical piston was submerged in liquid nitrogen until equilibrium was reached. Lung tissues were placed in the metal chamber and crushed into a fine powder. Approximately one-third of each finely ground tissue was placed in 1 ml TRIzol (Invitrogen, Burlington, ON, Canada, cat. no. 15596-026), with two-thirds placed into 1 ml RIPA buffer with freshly added protease inhibitors (1× PBS, 1% IGEPAL CA-130, 0.5% Na-deoxycholate, 0.1% SDS and 1 mM Na-orthovanadate, 5 µg/ml aprotinin, 1 mM phenylmethylsulphonylfluoride and 1 mM dithiothreitol). The powdered lobes contained both RIPA buffer and TRIzol reagent were then briefly homogenized using a mechanical homogenizer (Ultra-Turrax® T25) for protein and RNA work.

+B: Western blot

Immediately following lung homogenization in RIPA buffer, tissue lysates were incubated on ice for 30 min and then centrifuged at a speed of 12 000 rpm (Eppendorf centrifuge 5417C) for 20 min at 4^{o}C. The supernatant was collected and protein concentration assessed using a detergent-compatible protein assay (Bio-Rad Laboratories, cat. no. 500-0112). For western blotting, 40 µg total protein was separated on 10% SDS polyacrylamide electrophoresis gel. Proteins were transferred to a pure nitrocellulose membrane (pore size 0.2 µm; Bio-Rad, Hercules, CA, USA) using a wet transfer apparatus (Bio-Rad) and blocked at room temperature for 1 h using Odyssey Blocking Buffer (LI-COR Biosciences, cat. no. LIC92740003). Membranes were probed using anti-GRP78 (N-20; Santa Cruz Biotechnology, cat. no. sc1050) and anti-cleaved Caspase-3 (Asp175; Cell Signaling, cat. no. 9661S) in Odyssey blocking buffer with 0.15% Tween 20 overnight at 4°C. Anti-actin (Santa Cruz Biotechnology, cat. no. sc1616) antibody was used in all western blots to measure housekeeping protein concentration. Anti-goat (cat. no. LIC92632214) and anti-rabbit (cat. no. LIC92632211) conjugated secondary antibodies (LI-COR Biosciences) were used to detect binding of antibodies in Odyssey blocking buffer with 0.15% Tween 20. A two-colour western blot infrared fluorescent detection method was employed for the detection process and an Odyssey® imager (LI-COR Biosciences) was used to visualize protein bands. Images were subsequently quantified through densitometry analysis using ImageJ software v. 1.46r (National Institutes of Health, USA).

+B: ELISA

IL-6, total and active TGFβ1 and IL-1β concentrations were measured in the BALF samples using commercially available ELISA kits (DY406, DY1679 and DY401), according to the manufacturer's protocol (R&D Systems, Minneapolis, MN, USA). All samples were measured in duplicate.

+B: Multiplex analysis of cytokines

We quantified 32 different cytokines, chemokines and growth factors simultaneously using a Discovery Assay® (Mouse Cytokine and Chemokine Array 32-Plex, Eve Technologies Corp., Calgary, AB, Canada). These 32 different mediators were assessed in the BALF of *Grp78*$^{+/-}$ and littermate control wild type as well as in C*hop*$^{-/-}$ mice and wild type, at both 7 and 21 days after bleomycin administration. The multiplex assay was performed at Eve Technologies using the Bio-Plex™ 200 system (Bio-Rad Laboratories) and a Milliplex Mouse Cytokine/Chemokine Kit (Millipore, St. Charles, MO, USA), according to their protocol. The 32-plex consisted of Eotaxin, G-CSF, GM-CSF, IFNγ, IL-1α, IL-1β, IL-2, IL-3, IL-4, IL-5, IL-6, IL-7, IL-9, IL-10, IL-12 (p40), IL-12 (p70), IL-13, IL-15, IL-17, IP-10, KC, LIF, LIX, MCP-1, M-CSF, MIG, MIP-1α, MIP-1β, MIP-2, RANTES, TNFα and VEGF. The assay sensitivities of these markers are in the range 0.1–33.3 pg/ml. Individual analyte values and other assay details are available on the Eve Technologies website or in the Milliplex protocol.

+B: Isolation of murine alveolar macrophages

In brief, following intratracheal instillation of saline or bleomcyin (days 3 and 7) into the lungs of wild type and *Grp78*$^{+/-}$ mice, lungs were harvested as described above and BALF was performed several times with ice-cold PBS. Collected cells were pelleted at 4°C at 1500 rpm for 5 min. The cells were then seeded in 96-well tissue culture plates using Dulbecco's modified Eagle's medium (DMEM)-F12 containing 10% fetal bovine serum (FBS; Sigma-Aldrich). After 40 min of incubation at 37°C, adherent cells were selected by washing all wells with PBS. Cell morphology was observed under an inverted microscope, confirming the

successful alveolar macrophage adherence, as well as ensuring the exclusion of other cell types. The cells were then lysed and subjected to RNA isolation, as described below.

+B: Isolation and M2 polarization of bone marrow-derived macrophages

Bone marrow-derived macrophages (BMDMs) were isolated and cultured as described previously [69]. Briefly, bone marrow cells from wild type and *Grp78*$^{+/-}$ were isolated and treated with 20 ng/ml M-CSF (PeproTech Canada) for 7 days. Following 7 days in culture, macrophages were treated for 6 and 24 h with recombinant IL-4 (20 ng/ml) and IL-13 (50 ng/ml) (PeproTech Canada) to induce alternative programming. Polarization to the M2 phenotype was assessed by arginase activity in cell lysates, as described previously [70].

+B: Extraction of RNA and assessment of RNA quality

Total RNA from frozen lung tissues was extracted using TRizol® reagent (Life Technologies, Burlington, ON, Canada). RNA from freshly isolated and adhered alveolar macrophages (AMs) and BMDMs were isolated using the RNAeasy mini kit (Qiagen, Valencia, CA, USA, cat. no. 74106). Concentrations were measured using a NanoDrop spectrophotometer and 3.3.0 software (NanoDrop Technologies, Wilmington, DE, USA). The integrity and the quantity of the RNA were examined using the Bioanalyser 2100 (Agilent Technologies, Santa Clara, CA, USA) before NanoString analysis.

+B: Reverse transcription–polymerase chain reaction (RT–PCR)

mRNA isolated from BMDMs was reversed-transcribed using Superscript II RT (Invitrogen, Carlsbad, CA, USA) to obtain cDNA for gene expression analysis. A 7500 Real-Time PCR Machine (Applied Biosystems, Foster City, CA, USA) with fast SYBR green mix (Applied Biosystems, cat. no. 4385612) were used. The PCR protocol used was a 20 s initiation at 50°C, followed by 10 min at 95°C; 40 cycles of 15 s amplification at 95°C and 1 min at 60°C. SYBR green primers, including: spliced *Xbp1*, forward 5′-TCCGCAGCAGGTGCAGG-3′, reverse 5′-GCCCAAAAGGATATCAGACTCAGA-3′; and *18S*, forward 5′-AGTCCCTGCCCTTTGTACACA-3′, reverse 5′CGATCCGAGGGCCTCACT-3′ were prepared by Integrated DNA Technologies. *18s* was used as the reference gene to assess transcriptional patterns of spliced *Xbp-1* and *Grp78*. Candidate gene mRNA levels were analysed using semi-quantitative gene expression analysis ($\Delta\Delta C_T$ method) and expressed as fold-change relative to the specified control.

+B: NanoString gene expression

NanoString gene expression technology was employed on RNA purified from murine lung homogenates and from freshly isolated and adhered murine AMs. The nCounter system (Nanostring Technologies, Seattle, WA, USA) was used to quantify the expression levels of 67 mouse genes in the mRNA derived from the whole lung homogenates (Table 1). Each hybridization reaction contained 100 ng (murine) total RNA in a 5 µl aliquot, reporter and capture probes, six pairs of positive spike-in RNA hybridization controls and six pairs of negative control probes. The hybridization reaction proceeded for 21 h at 65°C. Isolated alveolar

macrophages from bleomycin-exposed mice were assessed for *Col1a1*, *Col3a1*, *Fn1*, *Fkbp10*, *Grp78*, *Calreticulin*, *Hsp47*, *Chop*, *Bax*, *Bak1* and *Arginase-1*. For the statistical analysis of Nanostring data, nSolver Analysis Software v. 1.1 (Nanostring Technologies) was used to normalize the raw gene expression data to the positive controls and six reference genes, *Actb*, *B2m*, *Hprt1*, *Ipo8*, *Pgk1*, *Ppia* and *Ubc*, and data are expressed as fold change relative to the specified control. Two-way ANOVA was conducted using GraphPad Prism v. 5.0 (GraphPad Software Inc.). Unsupervised hierarchical clustering was performed with Multiexperiment Viewer v. 4.9. using Euclidian distance with average linkage clustering.

+B: Immunohistochemistry

The left lung was inflated and fixed by intratracheal instillation of 10% neutral-buffered formalin at a constant pressure of 30 cmH_2O for 3–5 min. The whole left lung was then placed in 10% formalin-filled Falcon tubes and after 48–72 h each left lung was cut and placed into histology cassettes. All tissue-containing cassettes were stored in 70% ethanol and were then sent to McMaster's in-house Histology Core Facility to be processed and embedded in paraffin wax; 5 µm sections were cut and washed multiple times with xylene to remove the wax. The sections were treated with ethanol and hydrogen peroxide. Sections were stained with haematoxylin and eosin (H&E) for cellular/tissue architectural analysis, PicroSirius red (PSR) and Masson's trichrome for collagen analysis and anti-αSMA (Dako, Mississauga, ON, Canada, cat. no. M0851) for the identification of αSMA-positive myofibroblasts. Lung paraffin-embedded tissues were also stained with anti-F4/80 (AbD Serotec, cat. no. MCA497) for the identification of lung murine macrophages as well as anti-GRP78 (N-20), anti-GADD 153 (F-168) (Santa Cruz Biotechnology, cat. no. sc575), anti-iNOS (Abcam, cat. no. ab15323), anti-mannose receptor 1

(Abcam, cat. no. ab64693), anti-arginase-1 (BD Biosciences, cat. no. 610708), anti-CD3 (SP7) (Abcam, cat. no. ab16667), anti-Phospho-Smad2 (Cell Signaling, cat. no. 3101) and anti-Ki67 (Abcam, cat. no. ab16667). For IHC that involved mouse primary antibodies on mouse tissues, we used the Dako ARK^{TM} (Animal Research Kit) Peroxidase (cat. no. K3954). As for tissues that contain endogenous biotin (such as liver and kidney), an avidin/biotin block (Vector Laboratories, cat. no. SP2001) was performed prior to immunostaining mouse lung tissues. Diluent and IgG negative controls as well as tissue controls were employed to ensure accuracy of the staining protocol and optimal antibody concentrations.

+B: Image analysis and quantification of Arginase-1- and CD3-positive cells

Slides were stained for Arginase-1 and CD3 as described above. Images were subsequently digitalized using an Olympus VS120-L100-W slide scanner at a resolution of ×400. VSI Desktop Software (Olympus Soft Imaging Solution GmbH) was used to measure the area of each individual lung and to export each whole lung as a .tiff file at ×10 resolution. Subsequent image analysis was performed using ImageJ v. 1.49 (National Institutes of Health, Bethesda, MD, USA) bundled with a Java 1.8.0_60 engine. After background subtraction, the threshold was adjusted using the B&W filter. This threshold was selected based on the stain and how the threshold value compared to a manual cell count. Next, the particles (stained cells) were analysed with a particle size threshold of 35^2 pixels and a circularity of 0.0–infinity. Outlines of counted cells were superimposed onto the original image to ensure accurate counting methodology. Total cell count was divided by the lung area in order to describe positively stained cells/mm^2. A macro was created to ensure consistency across groups. Arginase 1-positive cells were also initially quantified manually by counting the number of positive cells. The process was

subsequently performed using the automated digital protocol mentioned above. Consistent results were obtained using the two methods.

+B: Immunofluorescence staining and quantification

Immunostaining of antibodies including MAC3, GRP78, E-Cadherin, αSMA and cleaved Caspase-3 was performed on formalin-fixed lung tissue sections. Briefly, following deparaffinization and antigen retrieval with citric acid buffer, tissues were blocked with normal donkey serum and then then incubated with the primary antibodies, anti-MAC3 (BD Biosciences, cat. no. 553322), anti-GRP78, anti-E-Cadherin (Santa Cruz Biotechnology, cat. nos sc59778 and sc31020), anti-αSMA (Abcam, cat. no. ab7817) or anti-cleaved-caspase-3 for 1 h. All primary antibodies were used at 1:50 dilution. Secondary antibodies for the respective primary antibodies were then applied for 30 min before imaging (donkey anti-rat Alexa 488; Abcam, cat. no. Ab150155) to stain for MAC-3 and E-Cad, donkey anti-mouse Alexa 488 for αSMA (Abcam, cat. no. Ab150105) and donkey anti-goat Alexa 594 (Abcam, cat. no. Ab150129) to stain for GRP78 and cleaved caspase-3). All secondary antibodies were applied at 1:500 dilutions. Slides were mounted in Prolong-gold with DAPI. Pictures were taken with an epifluorescence microscope (Olympus) with the same setting and exposure time for all pictures. The analyses of MAC3/cleaved caspase-3, E-Cad/cleaved caspase-3 and αSMA/cleaved caspase-3 dual stains were performed using the plugin (JACoP) for ImageJ. Picture threshold and co-localization measurements used for the analyses were identical for all images and were performed on non-modified images. Analyses show the proportion of green pixels (E-Cad/MAC3) colocalizing with red pixels (cleaved caspase-3) and/or the percentage of αSMA/cleaved caspase-3-positive cells. For presentation purposes, image quality has been improved in the same way (brightness only).

+B: Quantification of immunohistochemical αSMA staining

Images from αSMA-stained slides were captured on a microscope (Leica DM R, Leica Imaging Systems, Cambridge, UK) equipped with Openlab software v. 5.5.0 (Perkin-Elmer, MA, USA). Twenty to thirty randomly taken pictures from two transverse lung sections was captured using a ×10 objective. The quantification of αSMA stain was digitally performed using ImageJ software v.1, 46r (National Institutes of Health, USA; http://rsb.info.nih.gov/ij/). All images were threshold-adjusted into a black/white background, where total and stained areas were differentiated. The total area of each image was initially calculated by measuring aggregates of cells and tissues with the exclusion of empty space, including airways. The area that was positive for the stain was calculated by adjusting the hue of the image until the stained areas were the only highlighted areas. In order to address imager intergroup bias, a macro was created to execute the preselected parameters and calculate the percentage of the tissue area that was positive for the stain. Each of the 20–30 calculated sets of percentage tissue area stain was compiled and an average was established in order to represent each sample.

+B: Quantification of immunohistochemical Ki67 and F4/80 staining

Ki67 staining was quantified using the ImageJ ImmunoRatio plugin (available at: http:\\imtmicroscope.uta.fi/immunoratio/). This software expresses the area of Ki67-positive nuclei as a percentage of the total nuclear area present in each image. The colour thresholds for the nuclear stains were adjusted so that only nuclei were analysed and a blank field correction image was used to standardize brightness between images, as described previously [71]. F4/80-stained sections were processed using the cell count tool in ImageJ software and expressed as F4/80-positive cells/mm^2.

+B: Histological analysis of pulmonary fibrosis

Two transverse sections were taken from random positions in the left lung, which had been previously stained with Masson's trichrome; 20–30 Masson's trichrome images, encompassing the whole tissue field, were acquired with OpenLab software (×20 Objective, Perkin-Elmer) using a Leica DM R microscope (Leica Imaging Systems, Cambridge, UK). A semi-quantitative assessment of the lung fibrosis was established using the Ashcroft grading procedure, as previously described [72]. This numerical scale was implemented to measure the extent of fibrotic remodelling events in both naïve and experimental subjects at day 21. Six scorers, who had no prior knowledge of the identity of the samples, graded each image using a 0–8 range: a score of 0 represented a normal lung tissue; a score of 4 indicated that 50% of the field was covered with fibrotic lesions while the other half displayed normal lung characteristics; a score of 8 represented total fibrous obliteration of the entire field. The final score for each specimen was calculated as an average of all fields, and the mean score across the six scorers was established. Each sample grade was later rounded to two decimal places.

+B: TUNEL assay

To assess apoptosis, lung sections were stained using the protocol and reagents provided by the TACS 2 TdT-Fluor *In Situ* Apoptosis Detection Kit (Trevigen, cat. no. 4812-30-K). Immunohistochemistry sections were imaged using a Leica DM R microscope (Leica Imaging Systems) with a ×60 objective lens. TUNEL-stained

sections were processed using the cell count tool in ImageJ and expressed as TUNEL-positive cells/mm^2.

+B: Lung mononuclear cell isolation and purification for flow cytometry

Following the sacrifice of wild type and *Grp78*$^{+/-}$ mice 5 days after bleomycin administration, the lungs were isolated, cut into small pieces and digested with 150 U collagenase type I (Gibco, Grand Island, NY, USA) in Hanks' buffer for 1 h at 37°C with agitation. The digested lungs were then crushed through a 100 µm filter (BD Falcon, Franklin Lakes, NJ, USA) and the lungs were treated with ACK lysis buffer for 2 min to remove all erythrocytes. The cells were resuspended in PBS.

+B: Cell surface and viability staining for flow cytometry

Immunoprofiling of innate immune cells from wild type and *Grp78*$^{+/-}$ lungs was performed by staining for cell surface markers. Two million lung mononuclear cells from each mouse were pelleted and resuspended in an antibody master mix containing the following antibodies: CD45-APC-Cy7 (1:200), Ly6G-PE (1:200) from BD Biosciences (San Jose, CA, USA); F4/80-Pacific Blue (1:100) from eBiosciences (San Diego, CA, USA); Streptavidin–Qdot800 (1:500) from Invitrogen (Burlington, ON, Canada); Ly6C-Biotin (1:100) from Biolegend (San Diego, CA, USA). Cell viability was determined by applying 5 µl 7-AAD (BD Biosciences, San Jose, CA, USA) 10 min prior to the assay. Data were collected using LSRII and FACSDiva software (BD Biosciences) and analysed using FlowJo software (Treestar, Ashland, OR, USA).

+B: Measurements of pulmonary function

Lung function was measured using a flexiVent® mechanical respirator (flexiVent®, SCIREQ, Montreal, PQ, Canada). Mice were sedated via an intraperitoneal (i.p.) injection of xylazine (Bayer Healthcare, 10 mg/kg) and pentobarbital (30 mg/kg). After exposing a section of the anterior side of the neck and opening a portion of the trachea, an 18-gauge needle was inserted into the trachea and fitted to the mechanical ventilator controlled by the SCIREQ software (v. 5.1). The mice were paralysed by administration of pancuronium bromide (20 mg/kg i.p.). Baseline conditions for each animal were attained by starting with total lung capacity (TLC) to hyperinflate the lung. A script was then run by the program and lung perturbations (prime-8, snapshot-150, PVs-V and PVr-P) were measured in the anaesthetized animals. All mice were ventilated to a volume of 10 ml/kg/breath. Quasi-static elastance and curvature of the deflating PV loop were derived from the PVrP perturbations. All measurements were repeated twice.

+B: Hydroxyproline assay

Hydroxyproline concentrations were measured by a colorimetric assay, as described previously [72]. Briefly, after sacrifice, the right four lobes of the lung were removed, snap-frozen and stored at –80°C. As described above in the homogenization protocol, the right four lobes were turned into a finely ground powder and immediately homogenized in RIPA buffer. The total pellet formed from the centrifugation of the RIPA-homogenized lung tissues was resuspended in PBS and allowed to freeze at –80°C. The pellet was subsequently lyophilized for at least

24 h using a freezer-dryer apparatus (Modulyod Freezer Dryer, Thermo Electron Corp.). Following the addition of 10% TCA solution and subsequent centrifugation, 5 ml 6 M HCL was added to each tube for pellet hydrolysis at 110°C in dry bath incubator. The samples were later brought to pH 7 by the addition of NaOH and were incubated for 20 min after the addition of 0.05 M Chloramine T reagent. Chloramine T reagent was destroyed by adding 70% perchloric acid and the samples were ultimately incubated for 20 min in a 55–65°C water bath shortly after adding Ehrlich's reagent solution. The final reaction absorbance was read at 550 nm and sample concentrations were determined from the hydroxyproline standard curve. Hydroxyproline concentrations were finally calculated and expressed as µg hydroxyproline/ml solution.

+B: Sircol collagen assay

The supernatant from the RIPA-homogenized lung tissues, free from cell debris and insoluble ECM fragments, was used to assess Sircol soluble collagen, according to the manufacturer's instructions (Sircol^{TM} Soluble Collagen Assay, Biocolor, Carrickfergus, UK). Absorbance readings were measured at 550 nm and test sample collagen concentrations were determined from the standard curve's collagen concentrations. Results were expressed as µg soluble collagen/ml solution.

+B: Statistical analysis

Results were expressed as mean ± SE. When two groups were compared, a normality test was performed before the appropriate two-tailed parametric or non-parametric *t*-test was performed. When more than two groups and/or conditions

were compared, two-way analysis of variance (ANOVA) followed by Newman–Keuls multiple comparison test was used. All statistical tests were performed using GraphPad Prism v. 5.0d (GraphPad Software Inc.); $p < 0.05$ was considered statistically significant.

Supplementary Figure Legends:

Figure S1. GRP78 level is reduced in naïve *Grp78*$^{+/-}$ lungs and in bleomycin exposed *Grp78*$^{+/-}$ lungs 21 days post-bleomycin administration. Both wild type and *Grp78*$^{+/-}$ mice were exposed to bleomycin (0.04U/mouse) and sacrificed after 7 and 21 d. (A) 40 µg of protein homogenate from both wild type and *Grp78*$^{+/-}$ lungs were immunoblotted against β-actin and the UPR marker GRP78. (B) Blots were quantified by densitometry using ImageJ. (C) Representative GRP78 images of wild type and *Grp78*$^{+/-}$ lungs from both saline and bleomycin-exposed mice at day 21. The actin bands panel is the same used in Figure 4B. Data are presented as mean ± SEM, n = 5 mice per group. *:P<0.05; **:P<0.01; ***:P<0.001; #:P<0.05; ##:P<0.01; ###:P<0.001, * represent a difference between bleomycin-exposed groups and their littermate saline controls, and # represent a difference between genotypes. Significance was established using GraphPad, Prism 5.0 with two-way ANOVA using Newman-Keuls Multiple Comparison test.

Figure S2. *Grp78*$^{+/-}$ mice displays comparable amount of neutrophilia in the lung and have an enhanced IL-6 response following bleomycin administration. Mice were given bleomycin (0.04 U/mouse) intra-tracheally at day 0 and animals were sacrificed after 7 and 21 d. (A) Total cell number and (B) differential neutrophil count are shown. (C) BALF total TGF-β1 and (D) IL-6 protein level as assessed 7 days post-bleomycin administration. Both BALF TGF-β1 and IL-6 were below the level of detection 21 days post-bleomycin administration (data not shown). Data are presented as mean ± SEM,

n=5-8 mice per group, * $p<0.05$; ** $p<0.01$; *** $p<0.001$; # $p<0.05$; ## $p<0.01$; ### $p<0.001$, * represent a difference between bleomycin-exposed groups and their littermate saline controls, # represent a difference between genotypes. Significance was established using GraphPad, Prism 5.0 with two-way ANOVA using Newman-Keuls Multiple Comparison test.

Figure S3. Immunohistochemical staining of phospho-Smad2 in the lungs of saline-exposed wild type and *Grp78*$^{+/-}$ mice. Following intra-tracheal intubation of saline, mice were sacrificed and immunohistochemical staining of phosph-smad2 was performed on formalin-fixed tissues. Representative images of whole tissue sections and high magnification images are shown.

Figure S4. Immunohistochemical staining of phospho-smad2 in the lungs of bleomycin-exposed wild type and *Grp78*$^{+/-}$ mice. Following intra-tracheal intubation of bleomycin (0.04U per mouse) mice were sacrificed after 7 and 21 d, and immunohistochemical staining of phosph-smad2 was performed on formalin-fixed tissues. Representative images of whole tissue sections and high magnification images are shown.

Figure S5. Assessment of cytokine and chemokine mediators in the BALF of wild type and *Grp78*$^{+/-}$ mice upon bleomycin administration. Following intra-tracheal intubation of bleomycin (0.04U per mouse) mice were sacrificed after 7 and 21 d. A total of 32 different cytokines and chemokines were assessed in the BALF. Seven analytes were detected, including (A) MCP-1 (B) KC (C) IP-10 (D) G-CSF (E) LIF (F) IL-5 (G) Eotaxin and (H) IL-6. Data is presented as mean ± SEM, n=4-6 mice per group, * $p<0.05$; ** $p<0.01$; *** $p<0.001$; # $p<0.05$; ## $p<0.01$; ### $p<0.001$, * represent a difference between *Grp78*$^{+/-}$ and their littermate saline controls, # represent a difference between genotypes. Significance was established using GraphPad, Prism 5.0 with two-way ANOVA using Newman-Keuls Multiple Comparison test.

Figure S6. Assessment of cytokine and chemokine mediators in the BALF of wild type and *Chop*$^{-/-}$ mice upon bleomycin administration. Following intra-tracheal intubation of bleomycin (0.04U per mouse) mice were sacrificed after 7 and 21 d. A total of 32 different cytokines and chemokines were assessed in the BALF. Seven analytes were detected, including (A) MCP-1 (B) KC (C) IP-10 (D) G-CSF (E) LIF (F) IL-5 and (G) Eotaxin (H) IL-6. Data is presented as mean ± SEM, n=4-6 mice per group, * $p<0.05$; ** $p<0.01$; *** $p<0.001$; # $p<0.05$; ## $p<0.01$; ### $p<0.001$, * represent a difference between *Chop*$^{-/-}$ mice and their corresponding saline controls, # represent a difference between genotypes. Significance was established using GraphPad, Prism 5.0 with two-way ANOVA using Newman-Keuls Multiple Comparison test.

Figure S7. Characterization of the M2 macrophage marker, mannose receptor 1, and the M1 macrophage marker, iNOS2 in wild type and *Grp78*$^{+/-}$ lungs upon bleomycin administration. Following intra-tracheal intubation of saline and bleomycin (0.04U per mouse) mice were sacrificed after 7 and 21 d and MR1/iNOS2 immunohistochemical staining was performed on formalin-fixed tissues. Representative images showing (A) MR1 and (B) iNOS2 staining in both saline- and bleomycin-exposed lungs.

Figure S8. *Grp78* haploinsufficiency upregulates arginase and UPR activity in bone-marrow derived macrophages. (A) Bone-marrow derived macrophages from *Grp78*$^{+/-}$ and wild type littermate mice were derived and exposed to the M2 differentiation cocktail IL-4/IL-13 for 24 h and assessed for total arginase activity. (B-C) UPR activation as transcriptionally measured by *spliced Xbp-1* and *Grp78* in mouse WT and *Grp78*$^{+/-}$ BMDMs at baseline and following 6 h of treatment with IL-4/IL-13. Data is presented as mean ± SEM, n=4 per group, * $p<0.05$; ** $p<0.01$; *** $p<0.001$; # $p<0.05$; ## $p<0.01$; ### $p<0.001$, * represent a difference between wild type or *Grp78*$^{+/-}$ BMDMs and their corresponding controls, # represent a difference between genotypes. Significance was established using GraphPad, Prism 5.0 with two-way ANOVA using Newman-Keuls Multiple Comparison test.

Figure S9. Recruitment of macrophages is not altered in lungs of *Grp78*$^{+/-}$ mice in response to LPS or bleomycin. (A) Total cell, (B) macrophage number and (C) secreted IL-1β in the BALF of wild type and *Grp78*$^{+/-}$ mice exposed to saline and LPS for 42 h. Data is presented as mean ± SEM, n=4-5 per group, * $p<0.05$; ** $p<0.01$; *** $p<0.001$; # $p<0.05$; ## $p<0.01$; ### $p<0.001$, * represent a difference between wild type or *Grp78*$^{+/-}$ mice and their corresponding controls, # represent a difference between genotypes. Significance was established using GraphPad, Prism 5.0 with two-way ANOVA using Newman-Keuls Multiple Comparison test.

Figure S10. GRP78 haploinsufficiency does not influence cellular proliferation in response to bleomycin. Both wild type and *Grp78*$^{+/-}$ mice were exposed to saline and bleomycin (0.04U/mouse) and sacrificed after 7 and 21 d. Cell proliferation was assessed by immunohistochemical staining of the proliferation marker, Ki67. (A) Representative images from Ki67 stained wild type and *Grp78*$^{+/-}$ mice exposed to bleomycin at day 7 and 21. (B) A proliferation index (% Ki67^{+} cells) was created based on Ki67 positive nuclei. Data represents mean ± SEM, n=4-5 in each group, *:$P<0.05$; **:$P<0.01$; ***:$P<0.001$; #:$P<0.05$; ##:$P<0.01$; ###:$P<0.001$; * represent a difference between bleomycin-exposed groups and vehicle (saline); # represents a difference between genotypes. Significance was established using GraphPad, Prism 5.0 with two-way ANOVA using Newman-Keuls Multiple Comparison test.

Figure S11. Assessment of CD3 positive cells in the lungs of wild type, *Grp78*$^{+/-}$ and *Chop*$^{-/-}$ mice following bleomycin administration. Following intratracheal intubation of bleomycin (0.04U per mouse) mice were sacrificed after 7 and 21 d. CD3 staining was performed on formalin-fixed tissues. (A) Quantification of CD3 positive cells per mm^2 area in wild type and *Grp78*$^{+/-}$, (B) representative images of wild type and *Grp78*$^{+/-}$ lungs at day 21, (C) quantification of CD3 positive cells per mm^2 area in wild type and *Chop*$^{-/-}$ mice, (D) representative images of wild type and *Chop*$^{-/-}$ lungs at day 21. Quantification was performed on whole tissue sections. Black arrowheads on the representative images are pointing towards some of the CD3 positive cells. Data represents mean ± SEM, n=5-8 in each group, *:P<0.05; **:P<0.01; ***:P<0.001; #:P<0.05; ##:P<0.01; ###:P<0.001; * represent a difference between bleomycin-exposed groups and vehicle (saline); # represents a difference between genotypes. Significance was established using GraphPad, Prism 5.0 with two-way ANOVA using Newman-Keuls Multiple Comparison test.

Figure S12. NanoString® gene expression profiling of lungs of *Grp78*$^{+/-}$ mice exposed to bleomycin. RNA was isolated from from frozen wild type C57BL6/J and *Grp78*$^{+/-}$ murine lungs at 7 and 21 d post bleomycin administration. NanoString nCounter technology was used to measure the levels of fibrotic, inflammatory and UPR mRNAs in mouse specimens. A Heatmap was then generated based on the normalized gene expression counts and expressed as fold-change relative to control (saline-exposed) samples. Hierarchical clustering analysis using Euclidean distance and average linkage was performed. Heatmaps were generated using Multi-experiment viewer 4.9 and

significance was established based on Welch's t-test (for human specimens; $p<0.05$) and one-way ANOVA (for mouse specimens; $p<0.05$). Only significant genes are shown. A complete list of genes investigated is listed in Table 1.

Figure S13. Panels showing images from saline-exposed lungs co-stained with MAC3/Cleaved caspase-3 and E-Cadherin/Cleaved caspase-3. Sections from saline-exposed wild type, *Grp78*$^{+/-}$, *Chop*$^{-/-}$ lungs were fixed in formalin. Dual immunofluorescence staining was later performed on these lungs**.** (A) Representative images of MAC3 and cleaved caspase-3 in saline-exposed wild type and *Grp78*$^{+/-}$ lung tissues. (B) Representative images of E-Cadherin and cleaved caspase-3 in saline-exposed wild type and *Grp78*$^{+/-}$ lung tissues. (C) Representative images of MAC3 and cleaved caspase-3 in saline-exposed wild type and *Chop*$^{-/-}$ lung tissues. Panel (A) and (B) represents the corresponding saline control images for Figure 4F-I in the original manuscript. (C) Represents the corresponding saline control images for Figure 5F-H.

Figure S14. *In situ* hybridization of *F4/80* and *Chop* mRNA in saline exposed wild type and *Grp78*$^{+/-}$ lungs. Representative ISH images showing *F4/80* (green) and *Chop* (red) signals mounted with DAPI (blue). The images from this figure represent the corresponding saline control images for Figure 3I (Scale bar = 100µm).

Figure S15. Immunoprofiling and assessment of lung macrophage death in wild type and *Grp78*$^{+/-}$ mice exposed to bleomycin. Following intra-tracheal intubation of bleomycin (0.04U per mouse) mice were sacrificed after 5 days and lungs were isolated and subjected for mononuclear cell isolation and purification. Immunoprofiling of innate immune cells was then established by flow cytometry through multiple antibody staining (CD45, Ly6c, Ly6G and F4/80). The viable vs. non-viable cell population was differentiated by performing 7-AAD staining. Flow cytometry plots were analysed by flowJo, the bar graph indicates $CD45^{+}$, $Ly6G^{-}$, $Ly6G^{-}$, $F4/80^{+}$ and $7\text{-}AAD^{+}$ cells. Data represents mean ± SEM, n=4-5 animals in each group, *:$P<0.05$ where * represent a difference between the indicated groups. Significance was established using GraphPad, Prism 5.0 with unpaired *t*-test.

Figure S16. NanoString transcript counts demonstrating relative abundance of selected apoptotic and pro-fibrotic related genes in freshly adhered wild type and *Grp78*$^{+/-}$ alveolar macrophages (AMs) upon bleomycin administration. Following the intra-tracheal intubation of wild type and *Grp78*$^{+/-}$ mice with saline and bleomycin (0.04U/mouse) mice were sacrificed at day 3 and 7 and bronchoalveolar lavage fluid (BALF) was performed on the whole lung. The viable cells were isolated by allowing BALF immune infiltrates to adhere for 40 minutes and then subsequently subjected for RNA isolation and analysis. The relative mRNA counts of (A) *Chop* (B) *Bax* (C) *Bak1* (D) *Grp78* (E) *Arginase-1* and (F) *Fn1* are shown. Nanostring gene counts were normalized to multiple reference housekeeping genes (*Actb, B2m, Hprt1, Ipo8, Pgk1,*

Ppia and Ubc) and are here expressed as fold-change relative to the counts from saline-exposed AMs. Data represent mean ± SEM, n=3 in each group, * P<0.05; ** P<0.01; *** P<0.001; # P<0.05; ## P<0.01; ### P<0.001; * represent a difference between bleomycin-exposed groups and saline; # represents a difference between genotypes. Significance was established using GraphPad, Prism 5.0 with two-way ANOVA using Newman-Keuls Multiple Comparison test.

Figure S17. Characterization of αSMA/cleaved caspase-3 positive cells in the lungs of wild type and *Grp78*$^{+/-}$ mice upon bleomycin administration. Following intra-tracheal intubation of bleomycin (0.04U per mouse) mice were sacrificed after 7 and 21 d. Dual immunofluorescent staining was performed on formalin-fixed lung tissues in order to examine the percentage of αSMA^{+}/cleaved caspase-3^{+} cells, indicating the presence of apoptotic myofibroblasts. (A) Representative lung IF images showing αSMA (green pixels), cleaved caspase-3 (red pixels), DAPI (blue pixels) and merged images from control (saline-exposed lungs) and bleomycin-exposed lungs (Day 7 and Day 21). (B) Bar graph showing quantification of the percentage of αSMA/cleaved caspase-3 positive cells. Quantification was performed from multiple images covering lung tissue sections. Data represents mean ± SEM, n=4 in each group, * P<0.05; ** P<0.01; *** P<0.001; # P<0.05; ## P<0.01; ### P<0.001; * represent a difference between bleomycin-exposed groups and vehicle (saline); # represents a difference between genotypes. Significance was established using GraphPad, Prism 5.0 with two-way ANOVA using Newman-Keuls Multiple Comparison test.

Figure S18. Characterization of αSMA/cleaved caspase-3 positive cells in the lungs of wild type and *Chop*$^{-/-}$ mice upon bleomycin administration. Following intra-tracheal intubation of bleomycin (0.04U per mouse) mice were sacrificed after 7 and 21 d. Dual immunofluorescence staining was performed on formalin-fixed lung tissues in order to examine the percentage of αSMA^{+}/cleaved caspase-3^{+} cells, indicating the presence of apoptotic myofibroblasts. (A) Representative lung IF images showing αSMA (green pixels), cleaved caspase-3 (red pixels), DAPI (blue pixels) and merged images from control (saline-exposed lungs) and bleomycin-exposed lungs (Day 7 and Day 21). (B) Bar graph showing quantification of αSMA/cleaved caspase-3 positive cells. Quantification was performed from multiple images covering lung tissue sections. Data represents mean ± SEM, n=4 in each group, * P<0.05; ** P<0.01; *** P<0.001; # P<0.05; ## P<0.01; ### P<0.001; * represent a difference between bleomycin-exposed groups and vehicle (saline); # represents a difference between genotypes. Significance was established using GraphPad, Prism 5.0 with two-way ANOVA using Newman-Keuls Multiple Comparison test.

Figure S19. High and low magnification images of Masson's trichrome stained lung sections of wild type and *Chop*$^{-/-}$ mice upon bleomycin administration. Following intra-tracheal intubation of bleomycin (0.04U per mouse) mice were sacrificed after 21 d. Masson's trichrome staining was performed on formalin-fixed lung tissues. Representative images showing whole tissue sections and high magnification images are shown.

Figure S20. Panels showing images from saline-exposed lungs stained with Masson's trichrome, F4/80 and arginase-1. Sections from saline-exposed wild type and *Chop*$^{-/-}$ lungs that were fixed in formalin. Representative images shows Masson's trichrome-stained lung tissues and immunohistochemical staining of F4/80 and arginase-1. The images from this figure represent the corresponding saline control images for Figure 5C-E.

Table S1. Gene symbols and reference sequence details

HUGO Gene	Accession 2
Actb	NM_007393.3
B2m	NM_009735.3
Gapdh	NM_001001303.1
Gusb	NM_010368.1
Hprt	NM_013556.2
Ipo8	NM_001081113.1
Pgk1	NM_008828.2
Polr2a	NM_009089.2
Ppia	NM_008907.1
Rplp2	NM_026020.6
Tbp	NM_013684.3
Tuba1a	NM_011653.2
Ubc	NM_019639.4
Ywhaz	NM_011740.2
Xbp1	NM_013842.2
Atf6	NM_001081304.1
Ddit3	NM_007837.3
Hspa5	NM_022310.2
Canx	NM_007597.3
Calr	NM_007591.3
P4hb	NM_011032.2

Edem1	NM_138677.2
Fkbp2	NM_008020.3
Taok3	NM_001081308.2
Map3k5	NM_008580.4
Atf4	NM_009716.2
C1qc	NM_007574.2
Tnf	NM_013693.1
Nfkb1	NM_008689.2
Il6	NM_031168.1
Osm	NM_001013365.2
Ccl12	NM_011331.2
Cxcl3	NM_203320.2
Il1b	NM_008361.3
Il1a	NM_010554.4
Il10	NM_010548.1
Tgfb1	NM_011577.1
Acta2	NM_007392.2
Fn1	NM_010233.1
Col1a1	NM_007742.3
Col3a1	NM_009930.1
Serpinh1	NM_009825.2
Hspb1	NM_013560.2
Fkbp10	NM_010221.2

Loxl2	NM_033325.2
Cxcl10	NM_021274.1
Cd44	NM_009851.2
Jun	NM_010591.2
Il2	NM_008366.2
Il4	NM_021283.1
Ifng	NM_008337.1
Csf2	NM_009969.4
Tlr4	NM_021297.2
Tlr2	NM_011905.2
Il17a	NM_010552.3
Cd4	NM_013488.2
Cd8a	NM_001081110.2
Il2ra	NM_008367.2
Foxp3	NM_054039.1
Cxcr3	NM_009910.2
Ccr5	NM_009917.5
Cxcr6	NM_030712.4
Ccr3	NM_009914.4
Ccr4	NM_009916.2
Ccr8	NM_007720.2
Ccl20	NM_016960.1
Itgae	NM_008399.2

Figure S1

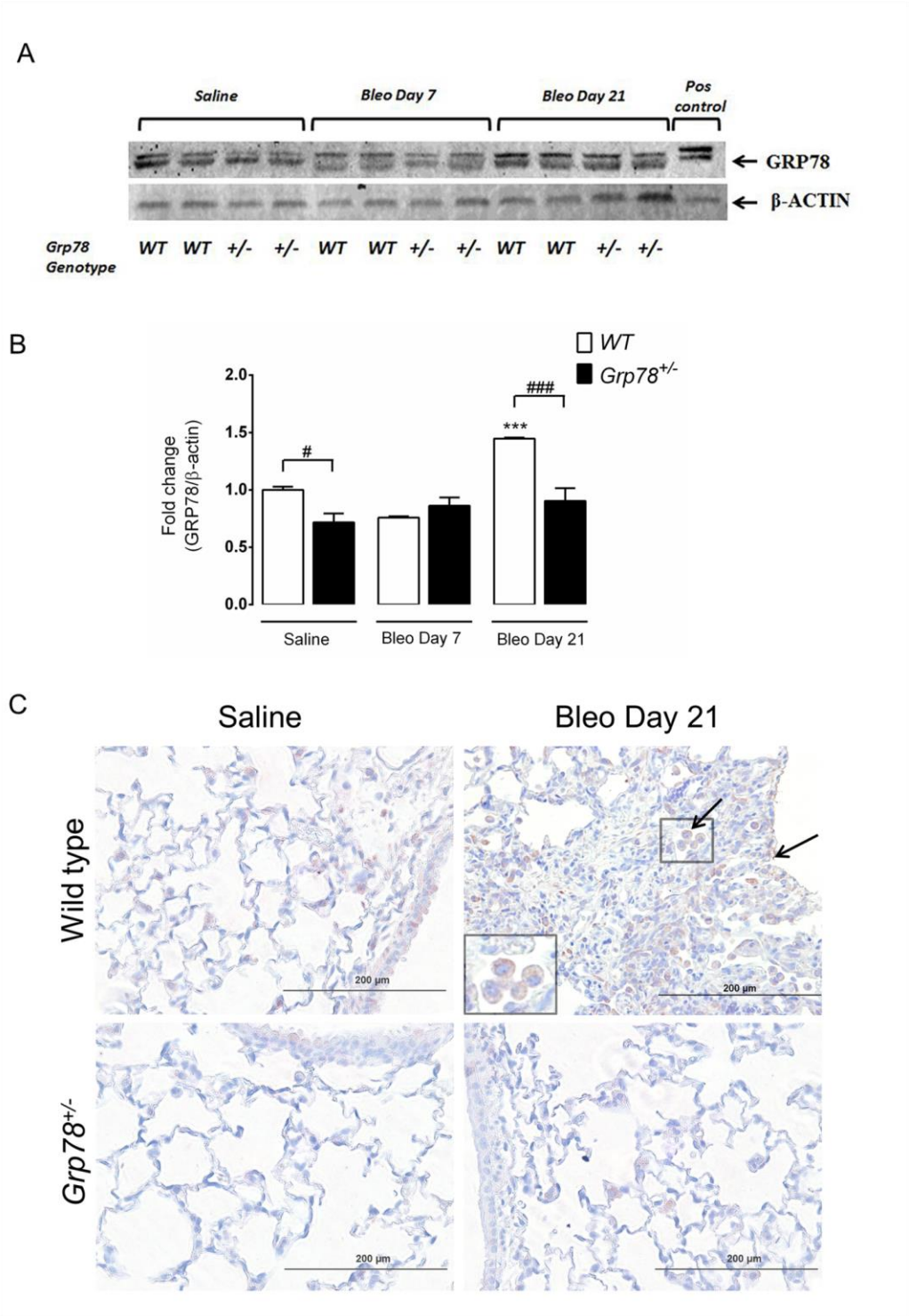
A
Saline
Bleo Day 7
Bleo Day 21
Pos control
GRP78
β-ACTIN
Grp78 Genotype
WT WT +/- +/- WT WT +/- +/- WT WT +/- +/-
B
WT
Grp78+/-
Fold change (GRP78/β-actin)
2.0
1.5
1.0
0.5
0.0
#
###
***
Saline
Bleo Day 7
Bleo Day 21
C
Saline
Bleo Day 21
Wild type
Grp78+/-
200 µm

Figure S2

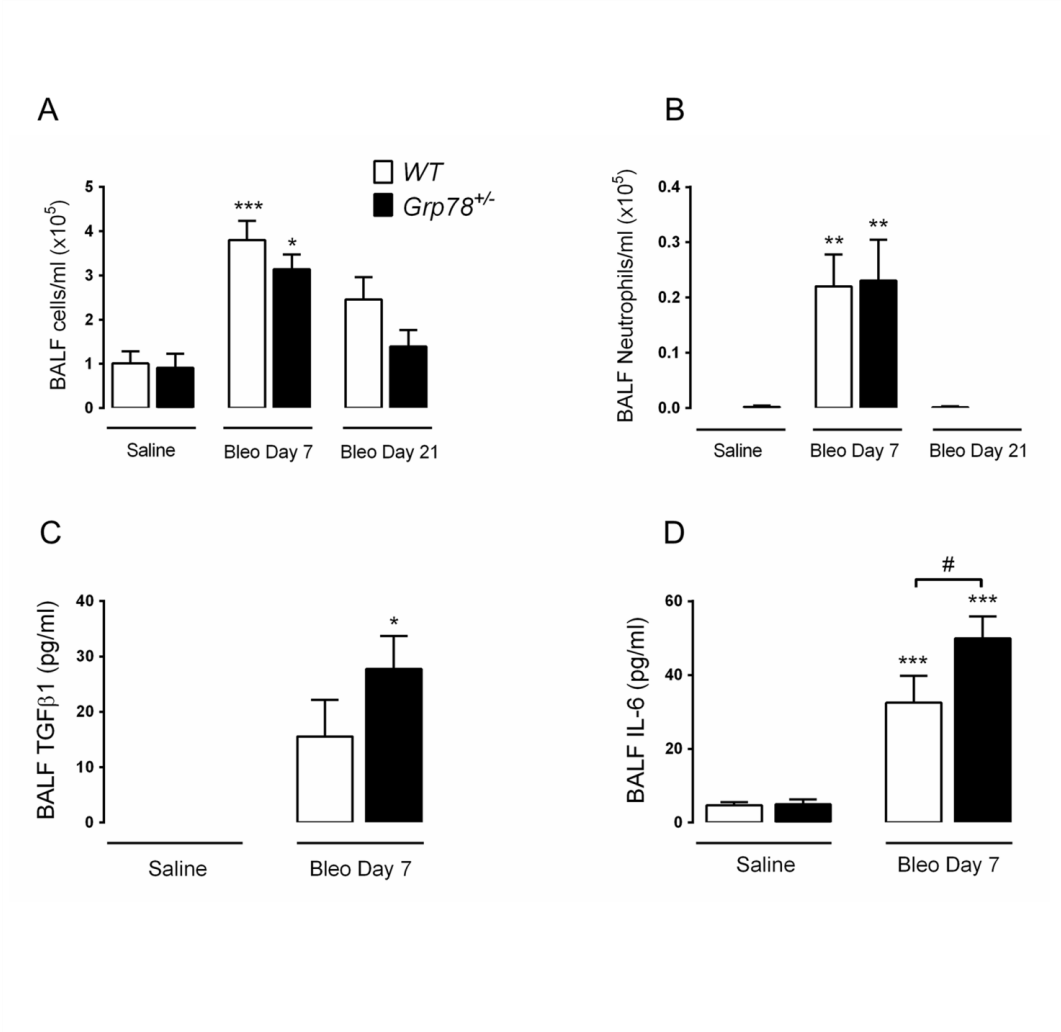
A
WT
Grp78+/-
BALF cells/ml (x10^5)
Saline
Bleo Day 7
Bleo Day 21
B
BALF Neutrophils/ml (x10^5)
C
BALF TGFβ1 (pg/ml)
D
BALF IL-6 (pg/ml)

Figure S3

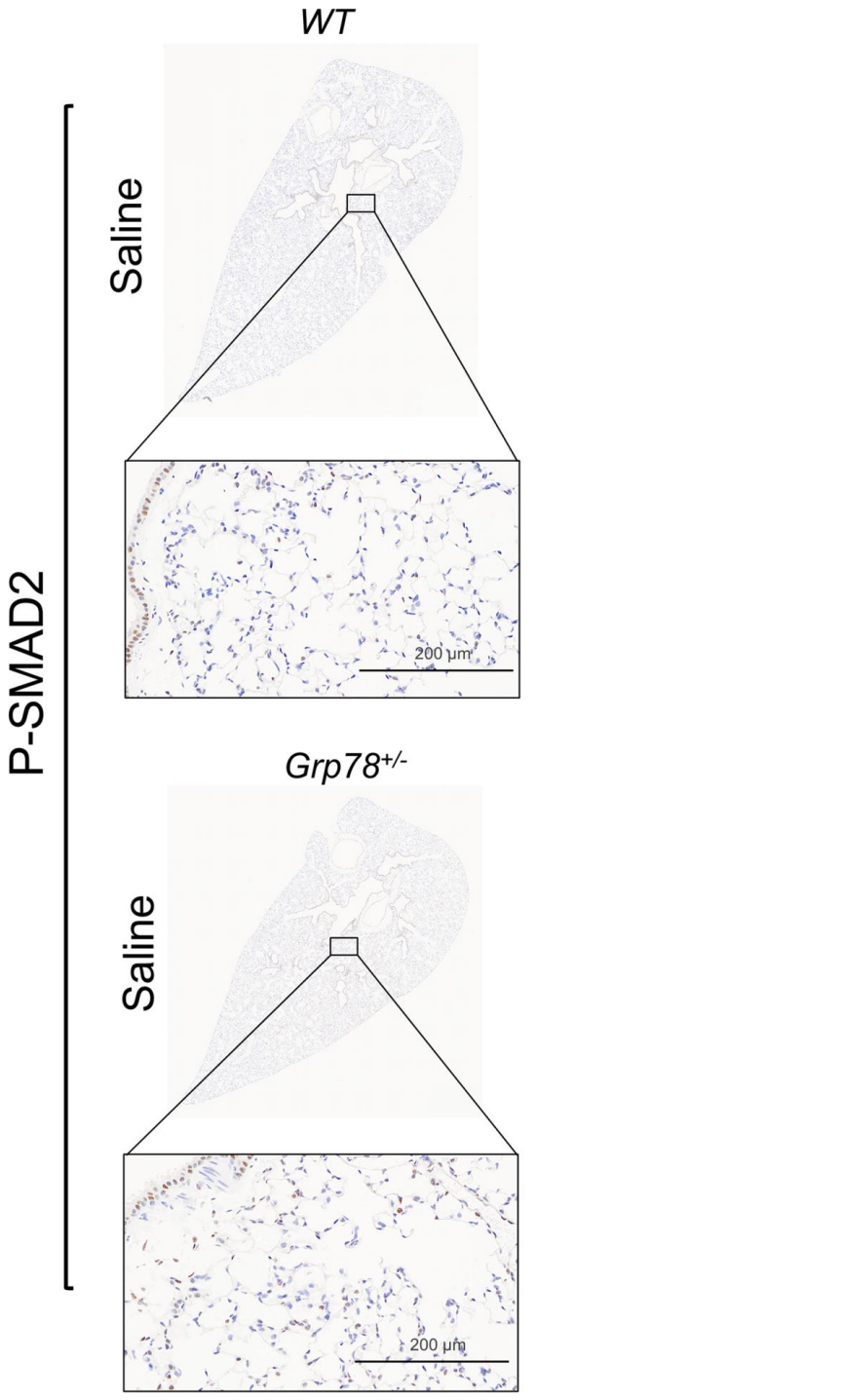

Figure S4

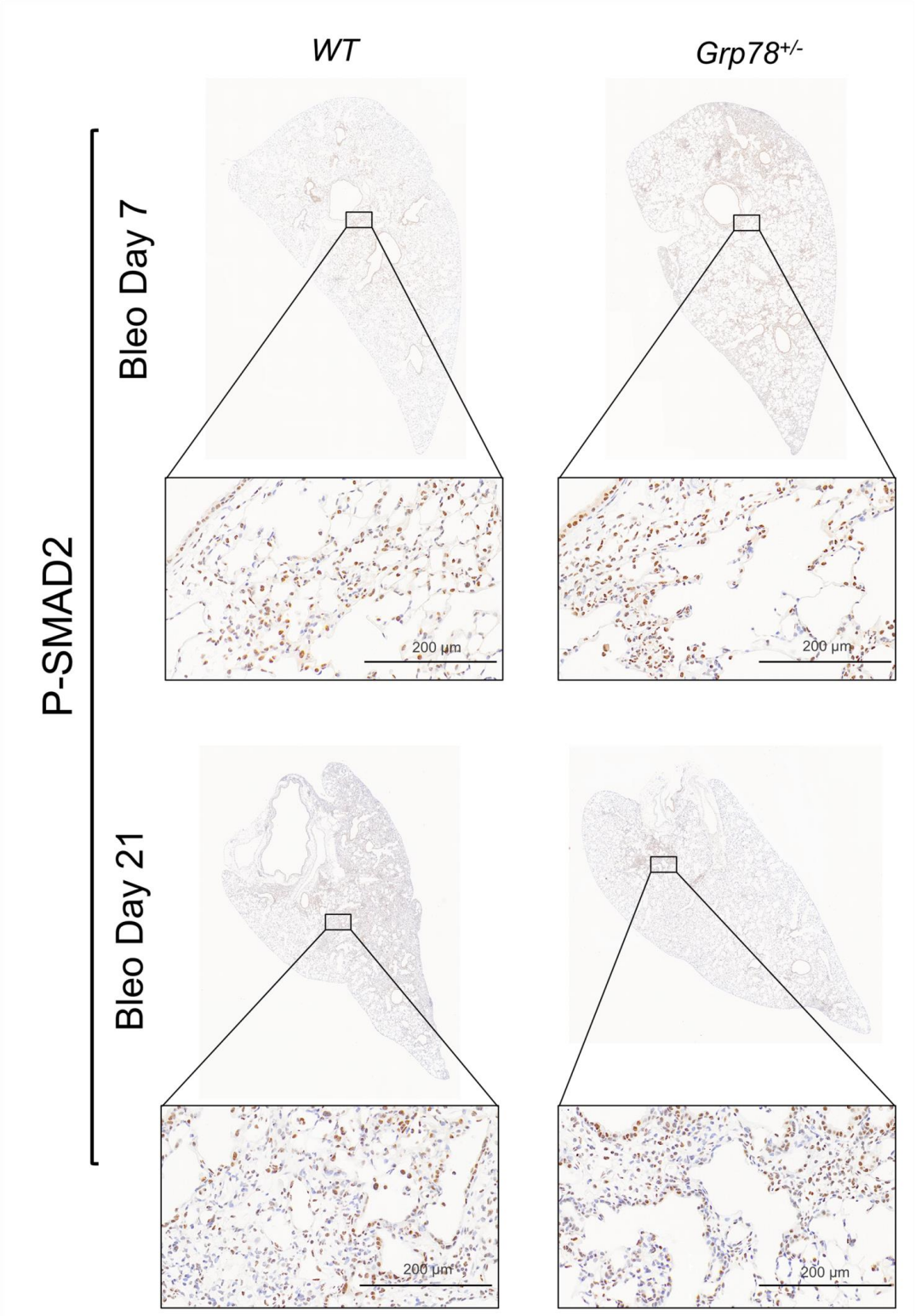
WT
Grp78+/-
P-SMAD2
Bleo Day 7
Bleo Day 21
200 µm
200 µm
200 µm
200 µm

Figure S5

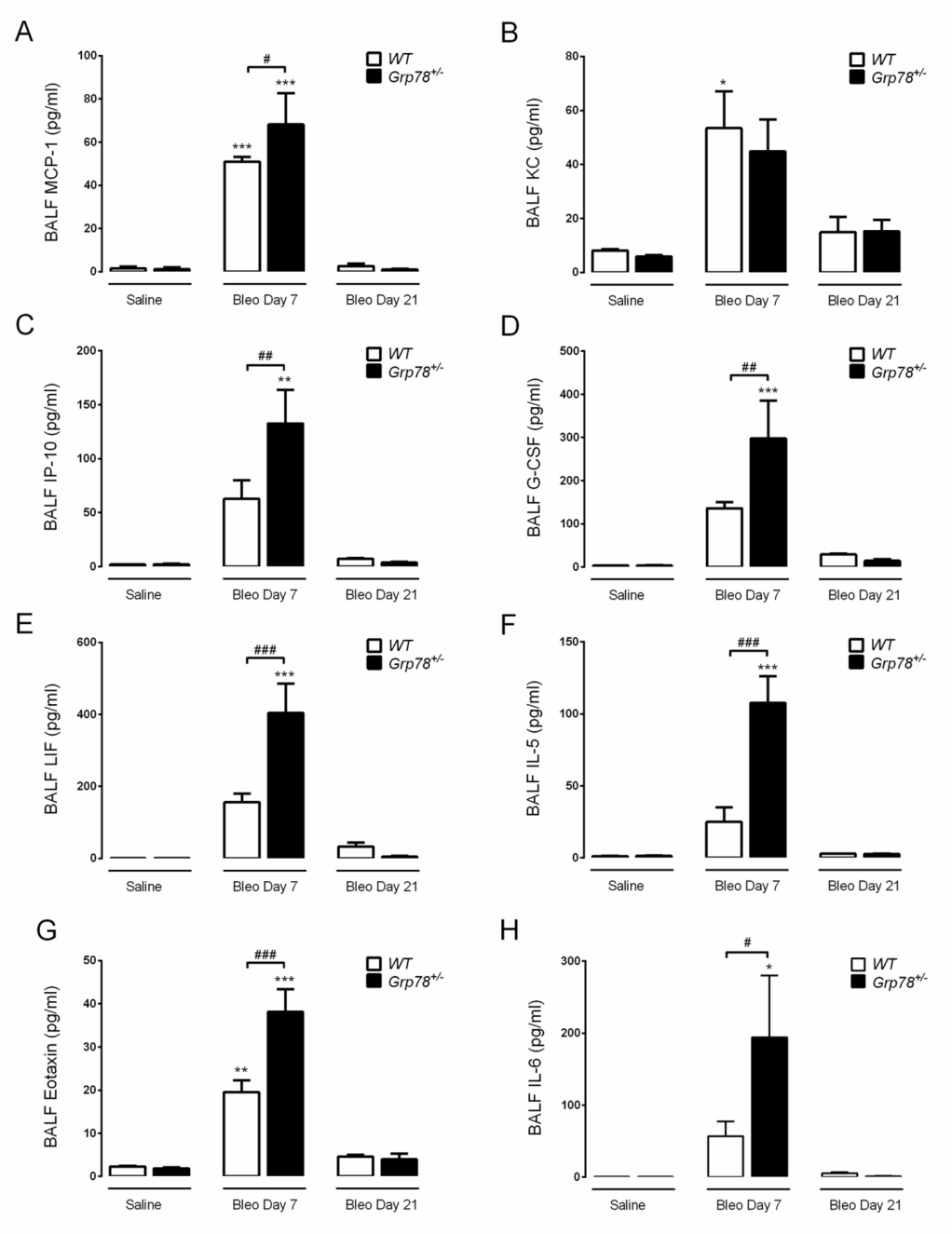
A
BALF MCP-1 (pg/ml)
B
BALF KC (pg/ml)
C
BALF IP-10 (pg/ml)
D
BALF G-CSF (pg/ml)
E
BALF LIF (pg/ml)
F
BALF IL-5 (pg/ml)
G
BALF Eotaxin (pg/ml)
H
BALF IL-6 (pg/ml)
WT
Grp78+/-
Saline
Bleo Day 7
Bleo Day 21

Figure S6

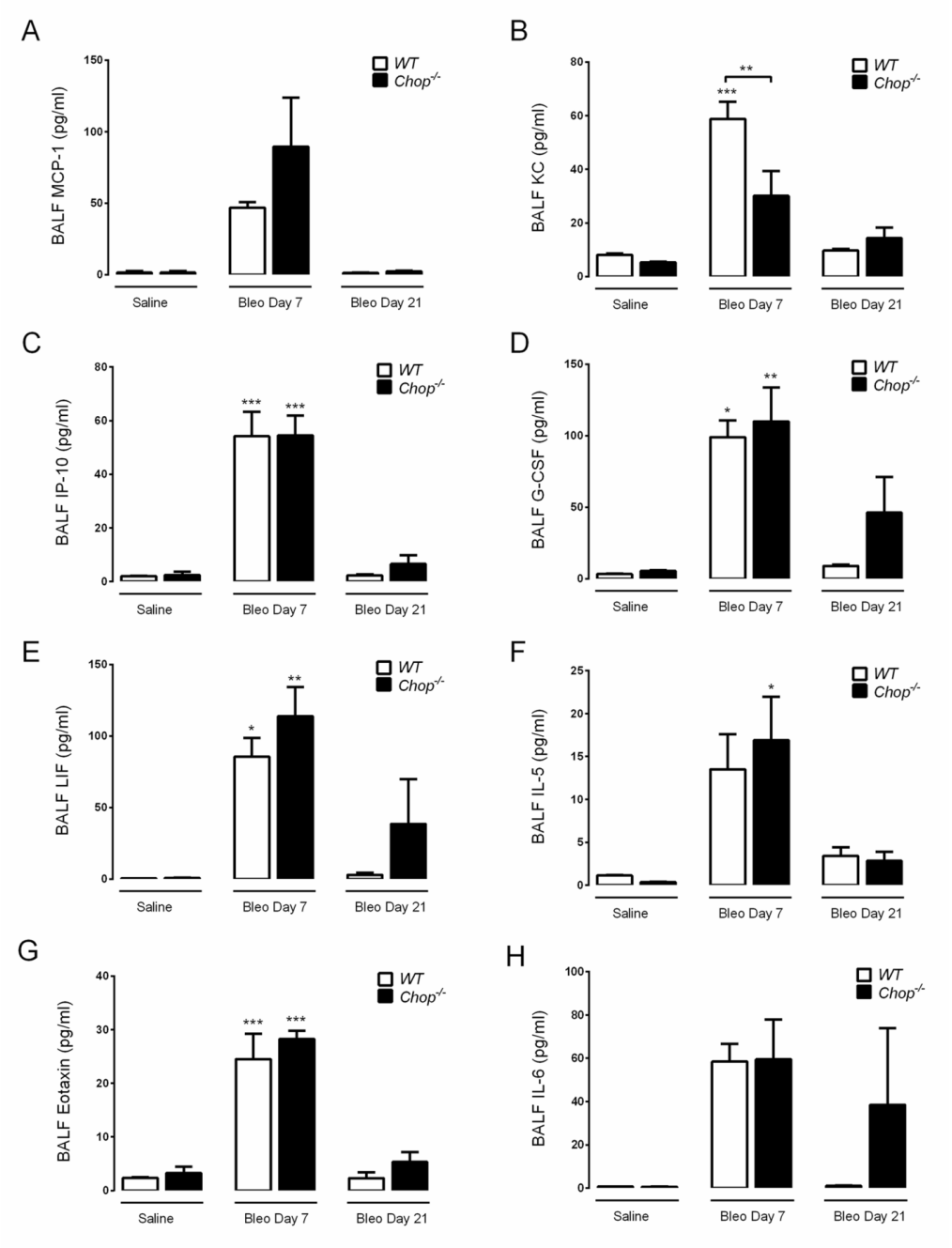
A
BALF MCP-1 (pg/ml)
150
100
50
0
WT
Chop-/-
Saline
Bleo Day 7
Bleo Day 21
B
BALF KC (pg/ml)
80
60
40
20
0
**
***
C
BALF IP-10 (pg/ml)
***
***
D
BALF G-CSF (pg/ml)
*
**
E
BALF LIF (pg/ml)
*
**
F
BALF IL-5 (pg/ml)
25
20
15
10
5
G
BALF Eotaxin (pg/ml)
40
30
H
BALF IL-6 (pg/ml)

Figure S7

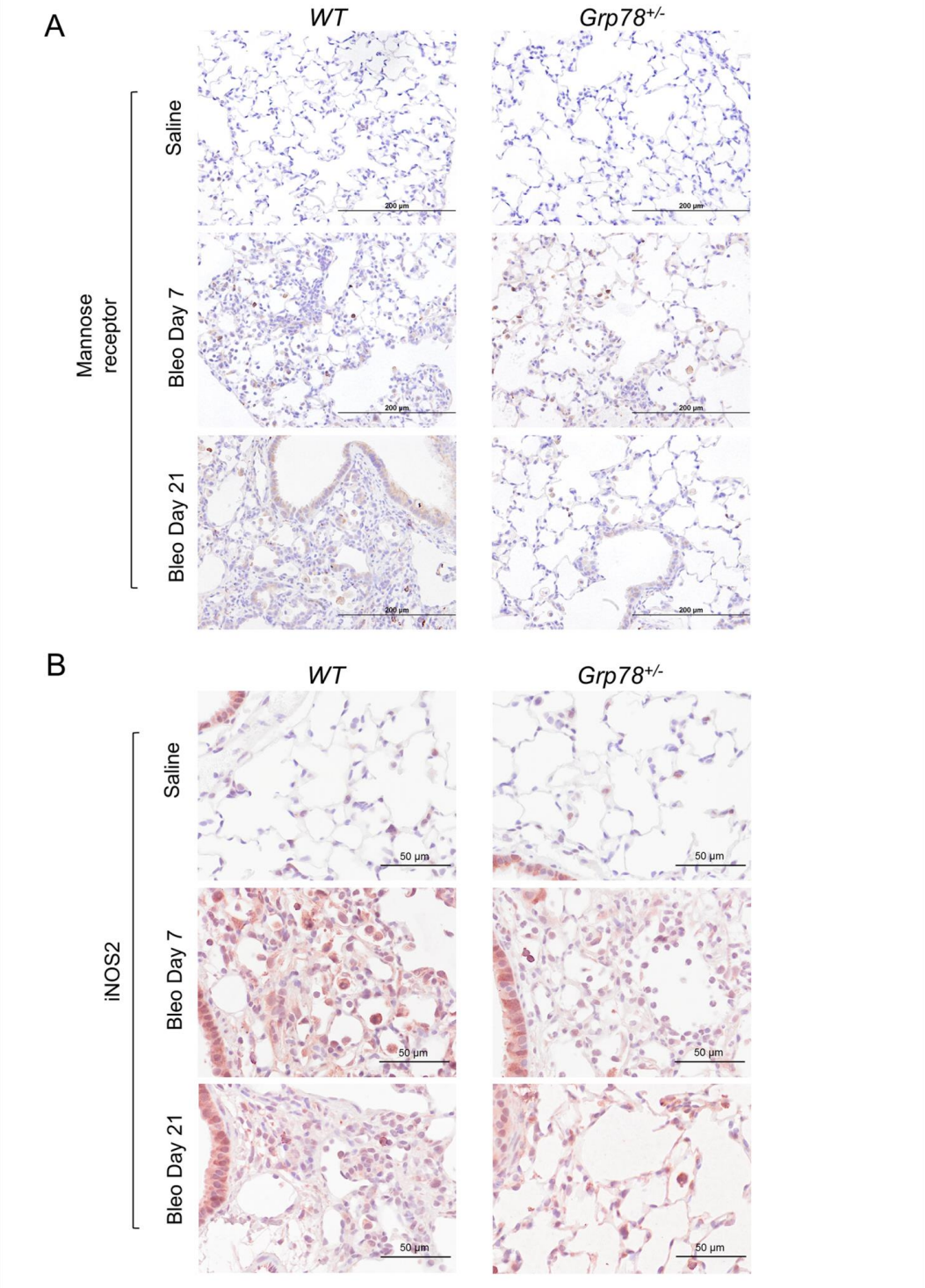
A
WT
Grp78+/-
Saline
Bleo Day 7
Bleo Day 21
Mannose receptor
200 µm
B
WT
Grp78+/-
Saline
Bleo Day 7
Bleo Day 21
iNOS2
50 µm

Figure S8

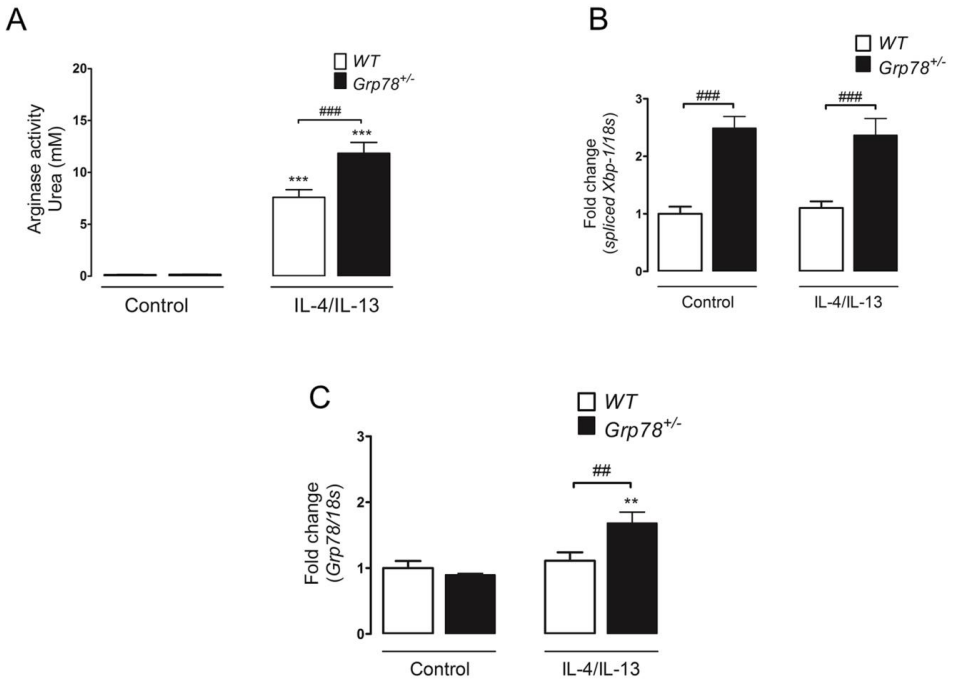
A
WT
Grp78+/-
Arginase activity
Urea (mM)
20
15
10
5
0
###
***
***
Control
IL-4/IL-13
B
WT
Grp78+/-
Fold change
(spliced Xbp-1/18s)
3
2
1
0
###
###
Control
IL-4/IL-13
C
WT
Grp78+/-
Fold change
(Grp78/18s)
3
2
1
0
##
**
Control
IL-4/IL-13

Figure S9

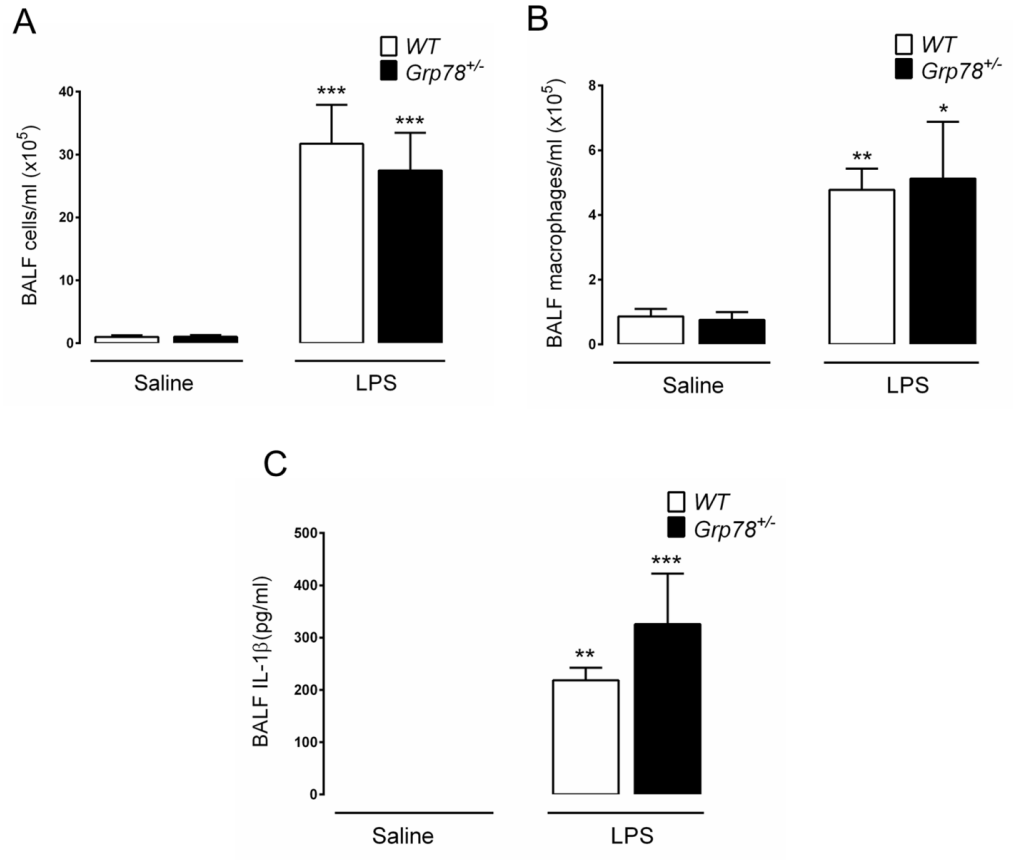
A
WT
Grp78+/-
BALF cells/ml (x10^5)
40
30
20
10
0
***
***
Saline
LPS
B
WT
Grp78+/-
BALF macrophages/ml (x10^5)
8
6
4
2
0
**
*
Saline
LPS
C
WT
Grp78+/-
BALF IL-1β(pg/ml)
500
400
300
200
100
0
**
***
Saline
LPS

Figure S10

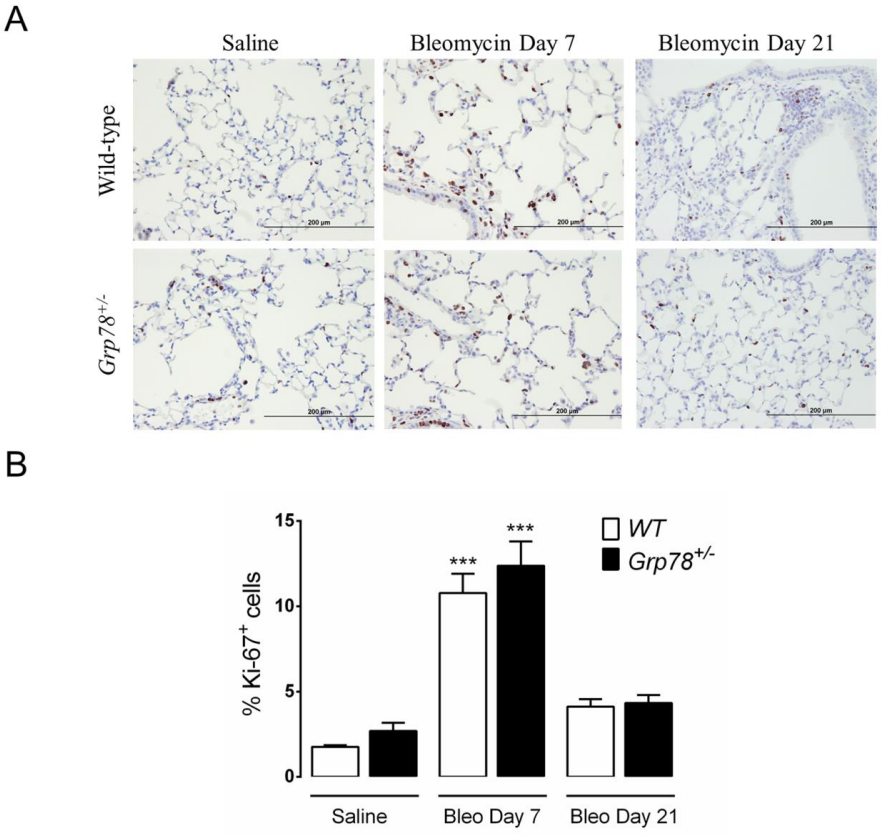
A
Saline
Bleomycin Day 7
Bleomycin Day 21
Wild-type
Grp78+/-
B
% Ki-67+ cells
15
10
5
0
***
***
WT
Grp78+/-
Saline
Bleo Day 7
Bleo Day 21

Figure S11

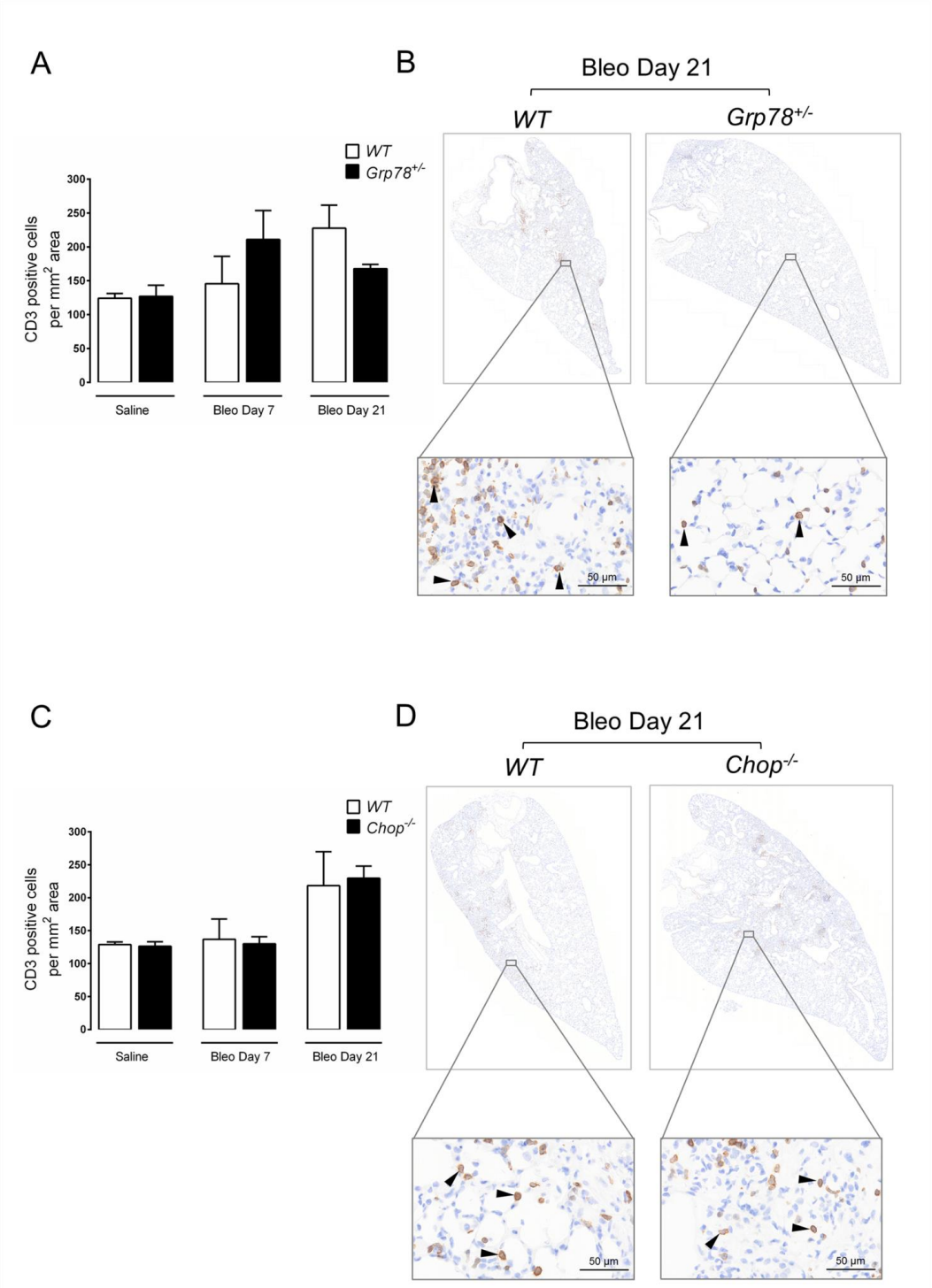
A
B
Bleo Day 21
WT
Grp78+/-
WT
Grp78+/-
CD3 positive cells per mm2 area
300
250
200
150
100
50
0
Saline
Bleo Day 7
Bleo Day 21
50 µm
50 µm
C
D
Bleo Day 21
WT
Chop-/-
WT
Chop-/-
CD3 positive cells per mm2 area
300
250
200
150
100
50
0
Saline
Bleo Day 7
Bleo Day 21
50 µm
50 µm

Figure S12

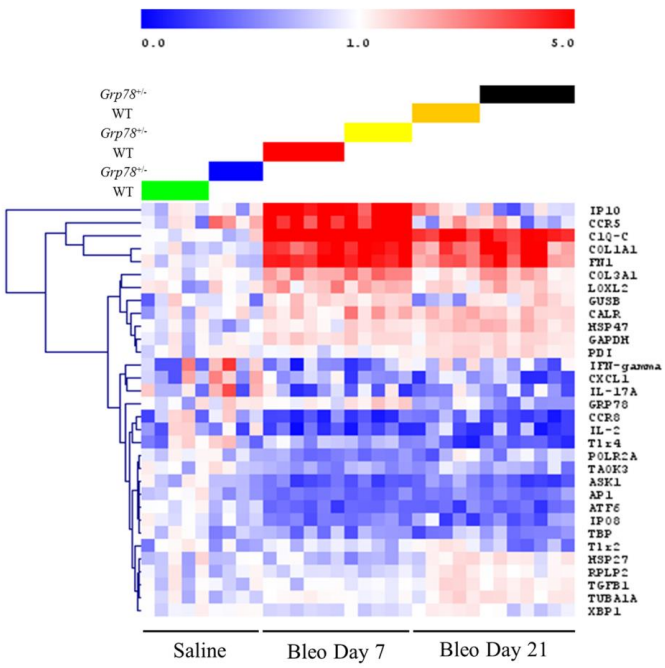
0.0
1.0
5.0
Grp78+/-
WT
Grp78+/-
WT
Grp78+/-
WT
IP10
CCR5
C1Q-C
COL1A1
FN1
COL3A1
LOXL2
GUSB
CALR
HSP47
GAPDH
PDI
IFN-gamma
CXCL1
IL-17A
GRP78
CCR6
IL-2
Tlr4
POLR2A
TAOK3
ASK1
AP1
ATF6
IP06
TBP
Tlr2
HSP27
RPLP2
TGFB1
TUBA1A
XBP1
Saline
Bleo Day 7
Bleo Day 21

Figure S13

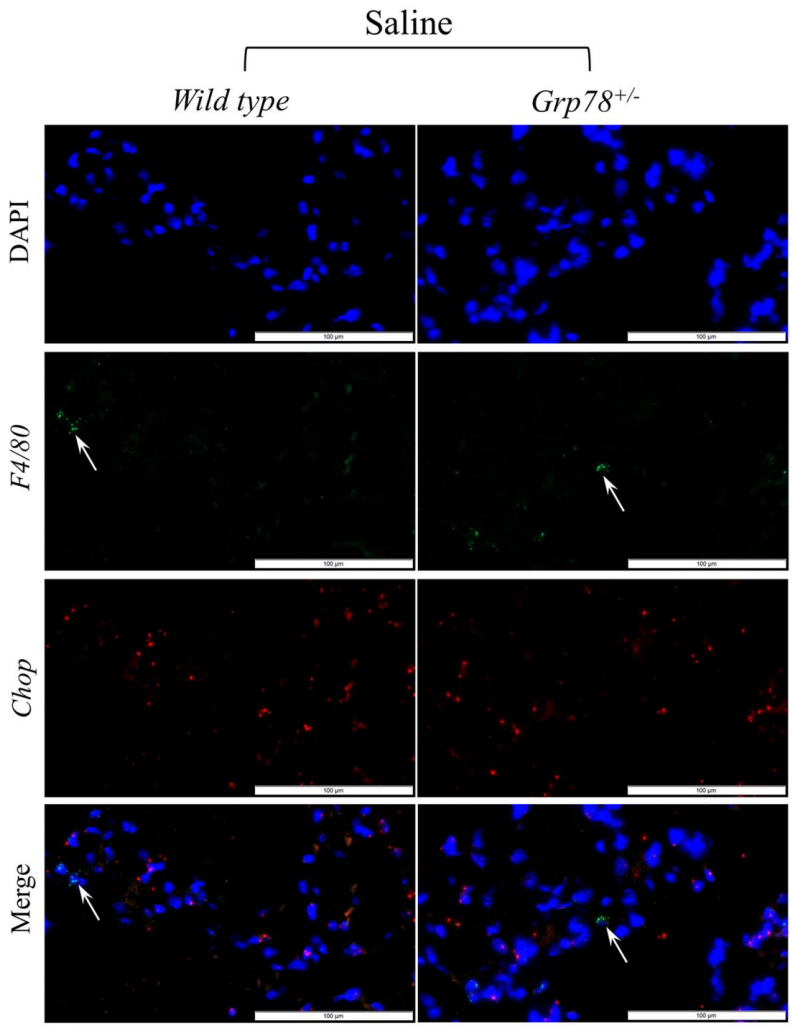

Figure S14

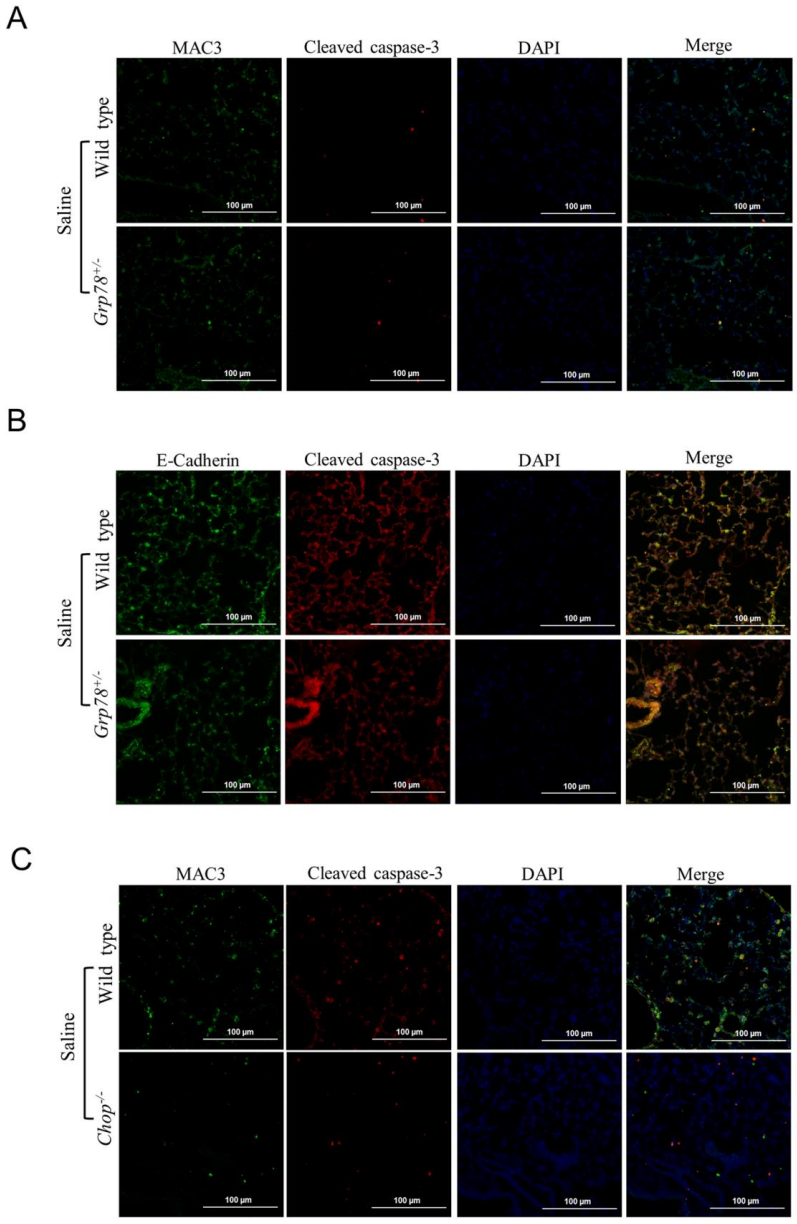
A
MAC3
Cleaved caspase-3
DAPI
Merge
Saline
Wild type
Grp78+/-
100 µm
B
E-Cadherin
Cleaved caspase-3
DAPI
Merge
Saline
Wild type
Grp78+/-
100 µm
C
MAC3
Cleaved caspase-3
DAPI
Merge
Saline
Wild type
Chop-/-
100 µm

Figure S15

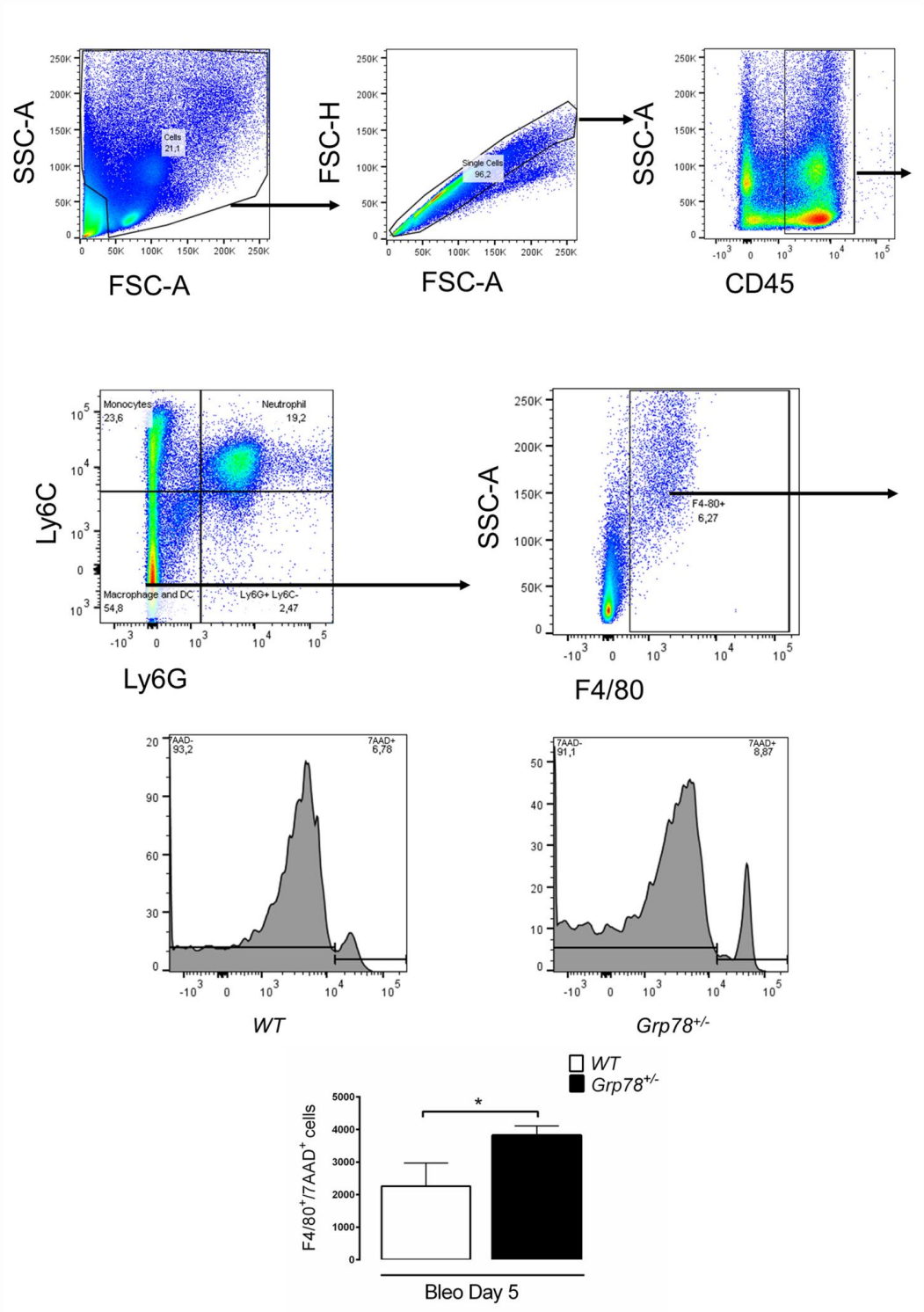
SSC-A
FSC-A
Cells
21,1
FSC-H
FSC-A
Single Cells
96,2
SSC-A
CD45
Ly6C
Ly6G
Monocytes
23,6
Neutrophil
19,2
Macrophage and DC
54,8
Ly6G+ Ly6C-
2,47
SSC-A
F4/80
F4-80+
6,27
7AAD-
93,2
7AAD+
6,78
WT
7AAD-
91,1
7AAD+
8,87
Grp78+/-
WT
Grp78+/-
F4/80+/7AAD+ cells
*
Bleo Day 5

Figure S16

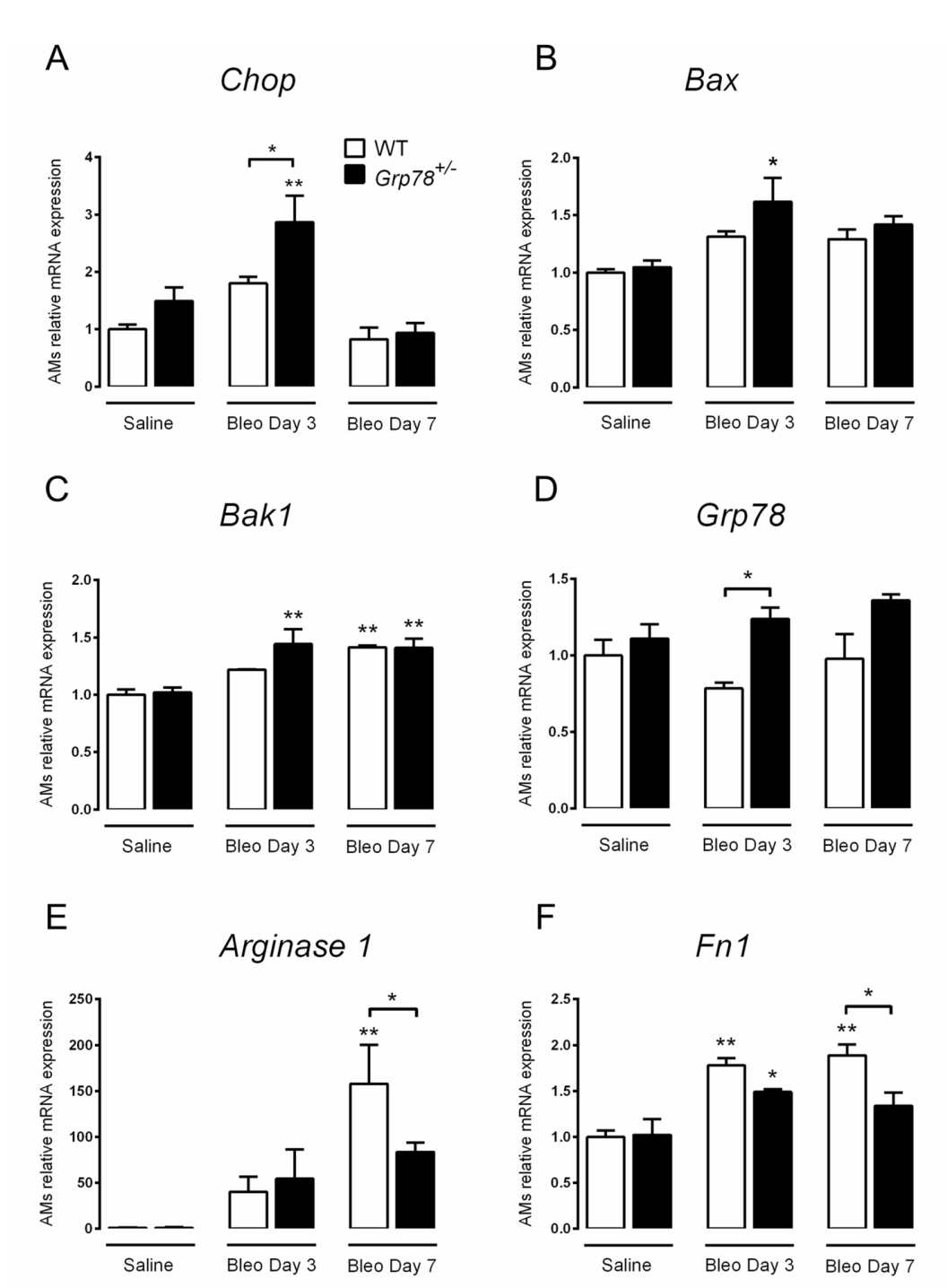
A
Chop
B
Bax
C
Bak1
D
Grp78
E
Arginase 1
F
Fn1
WT
Grp78+/-
AMs relative mRNA expression
Saline
Bleo Day 3
Bleo Day 7

Figure S17

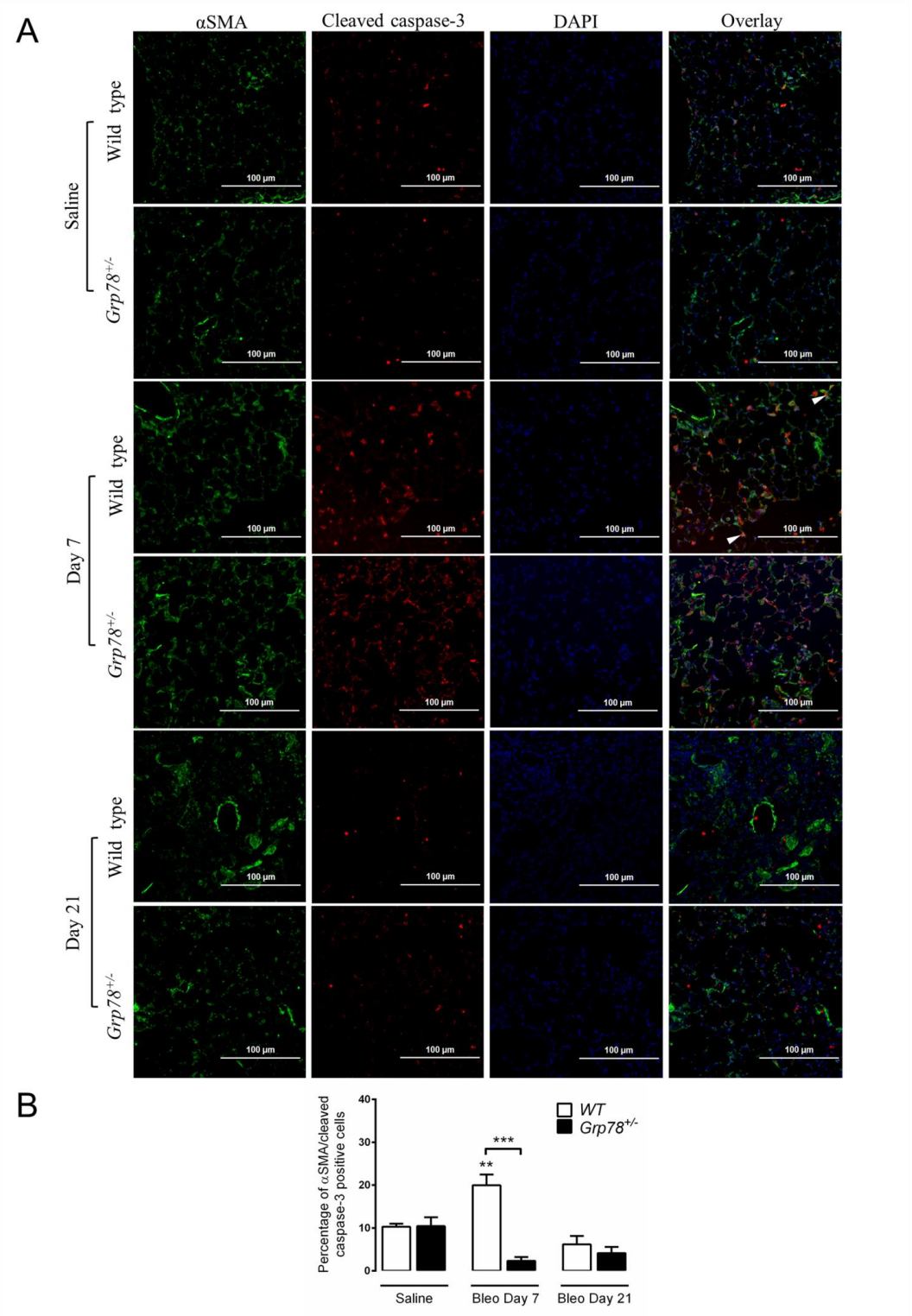
A
αSMA
Cleaved caspase-3
DAPI
Overlay
Saline
Day 7
Day 21
Wild type
Grp78+/-
100 μm
B
Percentage of αSMA/cleaved caspase-3 positive cells
WT
Grp78+/-
***
**
Saline
Bleo Day 7
Bleo Day 21

Figure S18

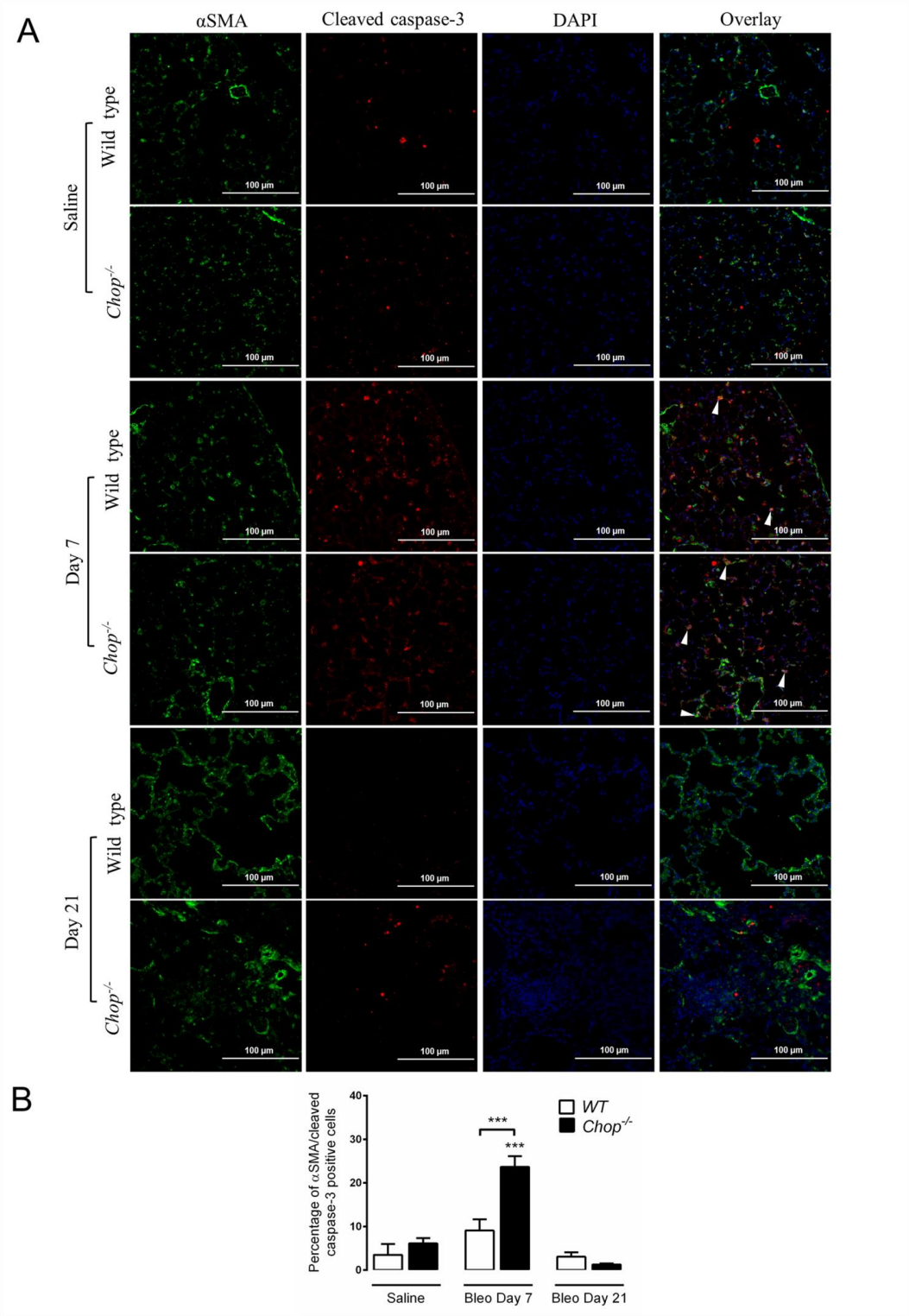
A
αSMA
Cleaved caspase-3
DAPI
Overlay
Saline
Wild type
Chop-/-
Day 7
Day 21
100 μm
B
Percentage of αSMA/cleaved caspase-3 positive cells
WT
Chop-/-
***
***
Saline
Bleo Day 7
Bleo Day 21

Figure S19

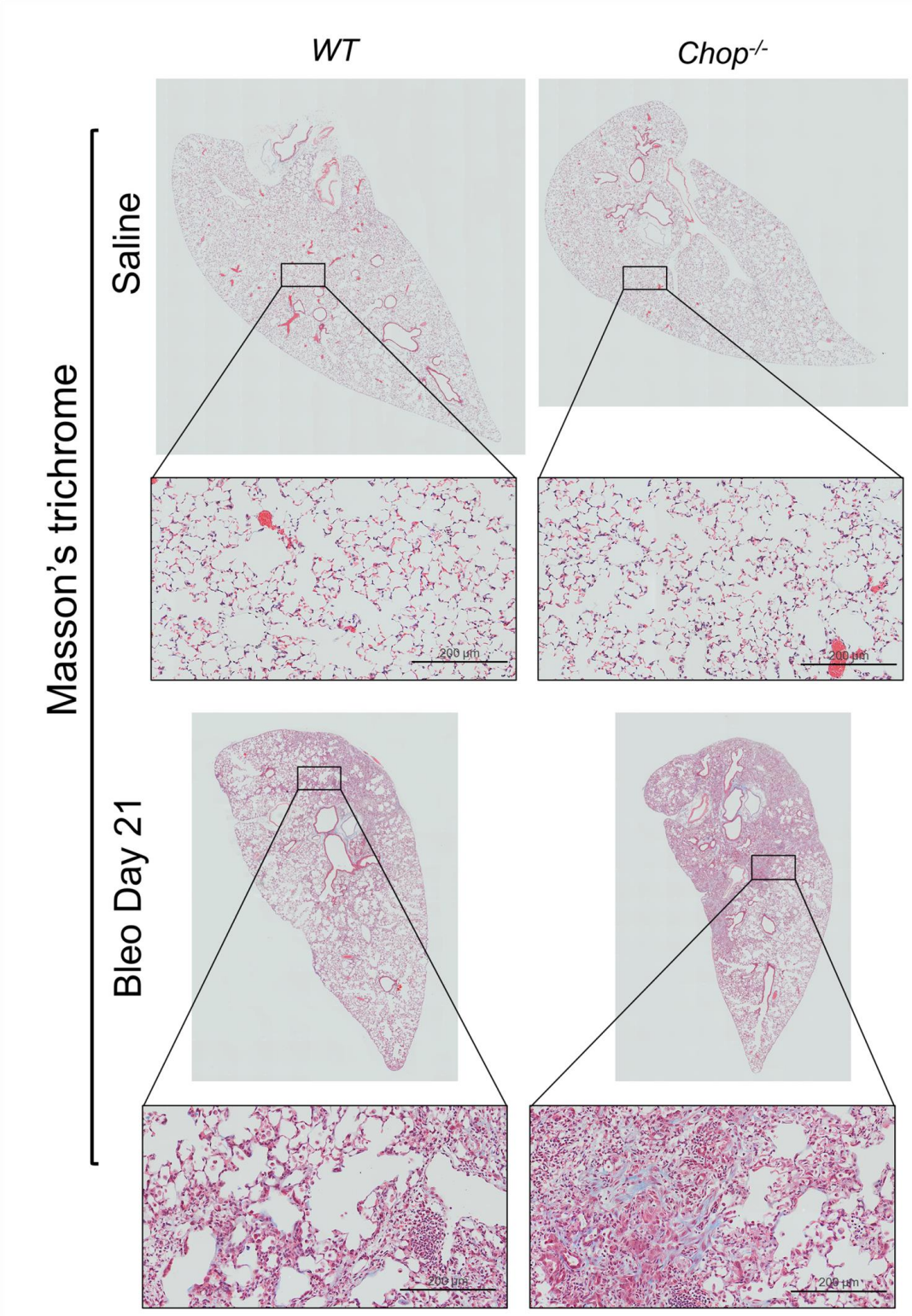
WT
Chop-/-
Masson's trichrome
Saline
Bleo Day 21
200 µm
200 µm
200 µm
200 µm

Figure S20

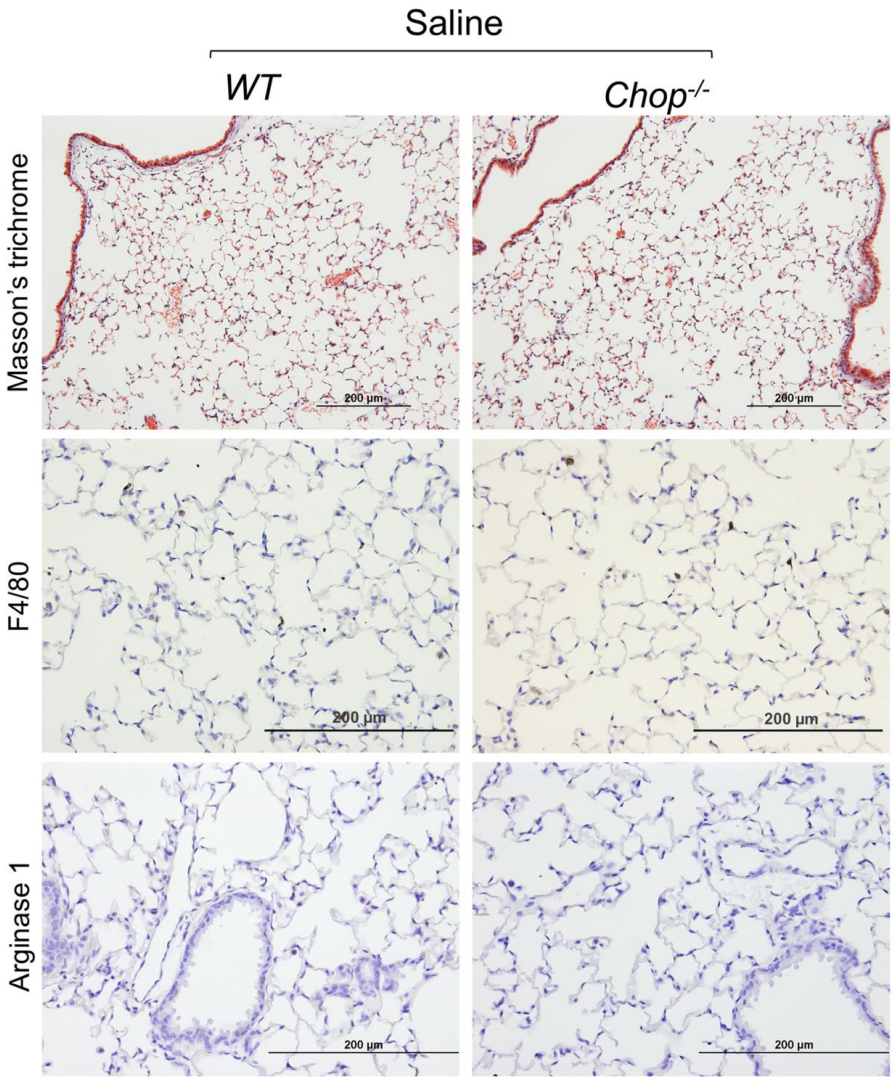

Chapter 3

IL-6 mediates ER expansion and hyperpolarization of alternatively activated macrophages

Summary and Significance

Alternatively activated (M2) macrophages are known to accumulate in the tissues and drive the progression of many fibrotic diseases and various cancers. While IL-4 and IL-13 are the primary Th2 cytokines leading to M2 macrophage programming, it has been recently demonstrated that IL-6 can act synergistically with IL-4, thereby potentiating the M2 macrophage phenotype. The involvement of IL-6 provides a compelling model by which to study possible M2 polarization mechanisms and functional pro-fibrotic effects. In B cell biology, IL-4 has been known as a key promoter of B cell differentiation into plasma cell. During this differentiation process, IL-4 augments ER expansion through one of key arms of the UPR called IRE1-XBP1. The enlarged ER is thought to be needed to accommodate the presence of antibodies. While antibody production is not a function of M2 macrophages, their stimulation with IL-4 facilitates their remodelling capacity through the production of anti-inflammatory/pro-fibrotic mediators (which likely necessitates an enlarged ER, similar to B cells/plasma cells). Thus, here we have explored the ER expansion mechanism in IL-4/IL-13/IL-6-stimulated macrophages and provided experimental evidence that both IL-6 and the IRE1-XBP1 arm of the UPR are involved in the generation of a hyper-pro-fibrotic macrophage phenotype. We showed that IL-6 promoted macrophage alternative programming, spliced XBP1 induction, and expansion of the ER and mitochondrial membranes. By pharmacologically inhibiting XBP1 splicing by STF-083010, the hyper M2 macrophage phenotype was abrogated (as assessed by

arginase activity, RT-PCR, flow cytometry analysis of arg1 and CD206, and NanoString gene expression). Interestingly, the addition of IL-6 to IL-4/IL-13 augmented pro-fibrotic gene signature in macrophages; when these macrophages were co-cultured with fibroblasts, fibroblast-to-myofibroblast differentiation occurred (as assessed by αSMA staining). These findings implicate IL-6 and XBP1/ER expansion program in the polarization of M2 macrophages and identifies their novel functional pro-fibrotic role. Based on these results, it is possible that UPR-mediated ER expansion may be a viable therapeutic target during pathological wound repair processes.

IL-6 mediates ER expansion and hyperpolarization of alternatively activated macrophages

Ehab E Ayaub [1,3], Karun Tandon [1,3], Pavithra Parthasarathy [1,3], Anisha Dubey[3], Anna Dvorkin-Gheva[3], James Murphy[1,3], Philipp S Kolb [1,3], Sarka Lhotak[2], Jeffrey G Dickhout[2], Rick C Austin[2], Martin RJ Kolb[1], Carl D Richards[3] and Kjetil Ask*[1,3].

1. *Department of Medicine, Firestone Institute for Respiratory Health, McMaster University and The Research Institute of St. Joe's Hamilton, Hamilton, ON, Canada*
2. *Department of Medicine, Hamilton Centre for Kidney Research, McMaster University, Hamilton, ON, Canada*
3. *Department of Pathology and Molecular Medicine, McMaster Immunology Research Centre, McMaster University, Hamilton, ON, Canada*

Corresponding author: Dr. Kjetil Ask, Department of Medicine, McMaster University and The Research Institute of St. Joe's Hamilton, Firestone Institute for Respiratory Health, Luke Wing, Rm L314-5, 50 Charlton Ave East, Hamilton, Ontario, Canada L8N 4A6, Ph. (905) 522 1155 ext. 33683; Fax (905) 521 6183; E-mail: askkj@mcmaster.ca

Running title: The role of IL-6 in ER expansion and macrophage polarization

Status of the work: to be submitted

This work was funded partly by the Canadian Institute of Health Research (CIHR; Grant No. 137013) and the Ontario Thoracic Society (Canadian Lung Association) awarded to KA and CDR. EAA is funded by the Canadian Institute of Health Research (CIHR; Grant No. 140358). AA is funded by Ontario Graduate Scholarships (OGS) and by Eva Eugenia Lillian Cope Graduate scholarship.

ABSTRACT

Although recent evidence has shown that IL-6 is involved in enhanced alternative activation of macrophages toward a pro-fibrotic phenotype, the mechanisms leading to the increased secretory capacity is not fully understood. Here, we investigated the effect of IL-6 on endoplasmic reticulum (ER) expansion and alternative activation of macrophages *in vitro*. IL-4/IL-13 and IL-4/IL-13/IL-6 -mediated alternative programming of murine bone marrow derived macrophages and human THP1 macrophages was assessed by arginase activity in cell lysates and by CD206 and arginase-1 expression by flow cytometry. Ultrastructural intracellular morphology and ER biogenesis was examined by transmission electron microscopy. Secreted cytokine and chemokine secretion was examined by multiplex assay and gene transcription profile of 128 genes by nanoString. CCL18 was used to assess human macrophage alternative activation. Pharmacological inhibition of the IRE1-XBP1 arm was achieved using STF-083010 and was verified by RT-PCR. The addition of IL-6 to the conventional alternative programming cocktail IL-4/IL-13 resulted in increased ER expansion and pro-fibrotic profiles. IRE1-XBP1 inhibition substantially reduced the IL-6-mediated hyperpolarization. In conclusion, the addition of IL-6 enhances ER expansion and the pro-fibrotic capacity of IL-4/IL-13-mediated activation of macrophages. Therapeutic strategies targeting IL-6 or the IRE1-XBP1 axis may be beneficial to prevent the pro-fibrotic capacity of macrophages.

Key words: macrophage polarization, ER Expansion

INTRODUCTION

Since the discovery of macrophages by Metchnikov over 100 years ago, the overall understanding of the various roles they have on host defense, wound healing or as structural cells are not well understood. Macrophages are found in virtually all tissues, either derived from the yolk sac or from the bone marrow. Depending on their localization and activation status, they may act as silent surveillance cells and in response to danger signals they can differentiate into cytokine-producing factories that participate in immune functions and wound healing. Based on *in vitro* studies, their capacity of polarization was mimicked by T-cell biology and the well-defined Th1 and Th2 phenotype, where the stimulation by INFg/LPS was shown to promote an immune phenotype (named classical or "M1" polarized) as opposed to macrophages exposed to the Th2-cocktail (IL-4/IL-13) promoting a wound-healing phenotype (named alternative activation or "M2" polarized macrophages) [1,2]. The identification of biological markers selectively expressed on *in vitro* polarized "M1" or "M2" macrophages, has been helpful in identifying macrophages *in vivo* that share phenotypic in vitro-established markers. This has allowed scientists to label activated macrophages found in animal tissues either "M1- or M2-like" as the initial triggers, exposure time and specific *in vivo* context is different from the standard *in vitro* assays that led to their initial nomenclature. Recently, the addition of the pro-inflammatory cytokine IL-6 was shown to enhance the M2-like macrophage *in vitro* phenotype, through the induction of IL-4-receptor expression enhancing the response to IL-4[3]. The differentiation of various cell types is thought to involve the IRE1/XBP-1 arm of the unfolded protein response, and this is thought to

include monocyte to macrophage transition[4], eosinophil maturation[5] and B-cell to plasma cell differentiation[6]. Plasma cell differentiation process was dependent on IL-6 mediated activation of the IRE1 pathway and expansion of the endoplasmic reticulum (ER), required for antibody generation[6]. The highly conserved IRE1 kinase activity performs the intracellular splicing of X box binding protein 1 (XBP-1) mRNA, critical in determining cell fate in response to ER stress in plasma cells[6], dendritic cells[7] and eosinophils[5]. Thus, ER expansion may be IRE1-XBP1 dependent pathway that is conserved in the transformation and activation of specific cell types such as the wound-healing macrophage. The availability of IRE1 inhibitors would potentially prevent ER-expansion and activation in these systems. Here we hypothesized that the addition of IL-6 to macrophages exposed to the *in vitro* M2 activation cocktail IL-4 and IL-13 would lead to increased IL-4 receptor expression and IRE1 activation, leading to abundant macrophage ER expansion, associated with increased secretory capacity that could be prevented by the specific IRE1 inhibitors. Collectively, our data suggested that alternative macrophage polarization (achieved with IL-4/IL-13 stimulation) supplemented the addition of IL-6 results in a much-enhanced ER expansion associated with a dramatic increase in ER stress-associated gene expression and cytokine secretion. Furthermore, inhibition of the IRE1 pathway prevented ER expansion and suppressed the M2 macrophage phenotype observed *in vitro*. Combined, the data presented suggests that therapeutic targeting of the IRE1 pathway or IL-6 signalling may prevent the pro-fibrotic activity of M2-like macrophages *in vivo*.

RESULTS.

IL-6 mediates IL-4/IL-13 induced alternative programming and IRE1-XBP1 activation of macrophages. To address the hypothesis that IL-6 addition to the standard alternative polarization cocktail IL-4/IL-13 mediates enhanced polarization and increased IRE1-XBP1 activation, we developed a 96-well assay wherein BMDMs were seeded and exposed to the different treatments and later assessed for arginase activity, arginase protein expression or spliced XBP1 gene expression in the cell lysates. The conventional cytokine cocktail IL-4/IL-13 or IL-4/IL-13/IL-6 were administered to M-CSF exposed BMDM's and assessed at 2, 4, 7, 15, 24 and 30 hours. While the standard IL-4/IL-13 polarization cocktail alone resulted in a 2.9-fold increase of arginase activity at 30 hours (from 1.8 ± 0.36 mM urea per well at 2 hours to 5.2 ± 4.85 at 30 hours), the addition of IL-6 resulted in a 4.6-fold increase at 24 hours and a 12.0-fold increase at 30 hours (from 1.5 ± 0.11 mM urea per well at 2 hours to 17.6 ± 4 at 30 hours) **(Figure 1A)**. Control macrophages or IL-6 stimulated macrophages demonstrated no increase in arginase activity at any of the indicated time points (data not shown). The increased arginase activity was associated with increased arginase-1 protein expression by western blotting **(Figure 1B)**. When co-cultured with murine fibroblasts, IL-4/IL-13/IL-6 exposed macrophages and not their conditioned growth medium, led to fibroblast-to-myofibroblast differentiation as shown by increased αSMA positivity (Supplementary figure 1). We next assessed the activation of the IRE1-XBP1 axis by RT-PCR in BMDMs exposed to the IL-4/IL-13 or the IL-4/IL-13/IL-6-polarizing cocktails. Here, spliced XBP1 was modestly increased at 4 hours (2-fold), and maintained at the later time-points

investigated (**Figure 1C**). The addition of IL-6 led to increased levels of spliced XBP1 that reached a 3.5-fold increase at 30 hours **(Figure 1C)**. This data suggests that the addition of IL-6 leads to increased polarization and activation of the IRE1-XBP1 pathway. As the IRE1-XBP1 pathway have been shown to be required to induce ER membrane biogenesis programs in various cell types activated towards a secretory phenotype[5,8,9], we investigated next if the addition of IL-6 influenced ER expansion in alternatively activated macrophages.

IL-6 enhances ER expansion in alternatively activated macrophages. Bone marrow derived murine macrophages were polarized as described above and examined by transmission electron microscopy (TEM). As expected, the addition of IL-6 to the standard IL-4/IL-13 cocktail led to a marked increase of both mitochondria and rough ER **(Figure 2)**. The presented data in **Figure 1 and 2** suggest a key role of IL-6 in enhancing alternatively activation of macrophages, associated with IRE1-XBP1 activation and increased ER expansion. Based on these observations, we then examined if pharmacological inhibition of the IRE1-XBP1 pathway affected IL-6-mediated polarization of alternatively activated macrophages.

IRE1-XBP1 inhibition prevents IL-6-mediated alternative activation of macrophages. The potent IRE1 inhibitor STF-083010, known to inhibit IRE1 endonuclease activity and mRNA splicing of XBP1 was added to the conventional IL-4/IL-13 polarization cocktail and to IL-4/IL-13/IL-6-mediated hyperpolarizing cocktail described above. Arginase activity and spliced XBP1 mRNA was measured in cell lysates after incubation with STF-083010. Shown in **Figure 3A**, IL-4/IL-13 mediated

polarization of murine BMDM's for 30 hours led to an increase in arginase activity, that was reduced by the addition of STF-083010 at a concentration of 60µM. The prevention of arginase activity was associated with a decrease in spliced XBP1 mRNA (**Figure 3B**), suggesting that the IRE1-XBP1 axis is involved in alternative programming of macrophages. As shown above, the addition of IL-6 to the standard IL-4/IL-13 polarization cocktail resulted in a 5.4-fold increase of arginase activity (from 2.0 ± 0.88 mM Urea per well to 10.7 ± 2.44, expressed as mean ± SEM). The addition of IRE1-XBP1 inhibitor led to a 55% decrease of arginase activity as well as a robust inhibition of spliced XBP1 at 60µM STF-083010, confirming the likely involvement of the IRE1-XBP1 pathway in IL-6-mediated hyperpolarization of macrophages. Of note, STF-083010 administration at the concentrations shown in **Figure 3** did not lead increased cellular toxicity as measured by the MTS 3-(4,5-dimethylthiazol-2-yl)-5-(3-carboxymethoxyphenyl)-2-(4-sulfophenyl)-2H-tetrazolium) assay (supplementary figure 1). To further consolidate the finding that XBP1 inhibition prevents both conventional IL-4/IL-13-mediated alternative programming of macrophages and IL-6-mediated hyperpolarization, we performed flow cytometric analysis of the well-established alternative macrophage flow markers arginase-1 and CD206 to the different cocktails and treatments shown above. Arginase-1/CD206 levels were increased from less than 20% to 52.8% after IL-4/IL-13 exposure and further increased to 73.6% when IL-6 was added (**Figure 3C**). The addition of the IRE1-XBP1 inhibitor STF-083010 prevented both IL-4/IL-13 and IL-4/IL-13/IL-6 mediated polarizations with less than 10% Arginase-1/CD206 positive macrophages detected (**Figure 3C**). These findings collectively suggest

that XBP1 blockade markedly inhibit both conventional IL-4/IL-13 mediated alternative programming as well as IL-6 mediated hyperpolarization of macrophages. To better understand the functional effect of IL-6-mediated hyperpolarization of alternatively activated macrophages and the effect of IRE1 inhibition, we next examined more broadly the gene expression pattern as well as the cytokine production of the different polarization cocktails described above.

IRE1-XBP1 inhibition prevents IL-6-mediated gene expression and cytokine production of alternative activation of macrophages. Murine bone marrow-derived macrophages were exposed to IL-4/IL-13 and IL-4/IL-13/IL-6 and STF-083010 for 30 hours as described above. RNA was extracted from the cell lysates and subjected for NanoString(R) assessment of 128 inflammatory, UPR and fibrotic related genes (please see supplementary table 1 for information about all genes investigated). While cell supernatants were analyzed using a luminex assay composed of 32 cytokines and chemokines. Principal component analysis and hierarchical clustering of the samples demonstrated a unique transcriptional signature of IL-4/IL-13/IL-6 stimulated macrophages compared to other treatment conditions **(Figure 4A)**. Upon examination of the plots of the assessed samples as evidenced by the cluster dendrogram, the data shows that samples treated with STF-083010 plus the IL-4/IL-13/IL-6 cocktail cluster in a similar fashion to IL-4/IL-13 exposed samples, suggesting that STF-083010 might have normalized the transcriptional signature of IL-4/IL-13/IL-6-exposed macrophages to IL-4/IL-13-exposed macrophages **(Figure 4B)**. To quantitatively and qualitatively understand the meaning of the assessed transcriptional signature, differentially regulated

genes were presented as a table showing pair-wise comparisons of interest **(Figure 5A)** demonstrating the number of up-regulated and down-regulated genes within the specified groups. Functional networks were then established based on the assessed gene signature, and processes were illustrated by ellipses, with multiples genes of interest comprising 8 modules **(Figure 5B-C)**. Regarding pro-fibrotic related genes, the data indicates that some of these genes were undetected in the IL-4/IL-13 with/without IL-6 condition (such as *Col1a1* and *Col3a1*). The ones that were upregulated in the IL-4/IL-13 treatment condition was further elevated upon their stimulation alongside IL-6 and these genes included *Fn1*, *Timp1* and *Mcp1*. The addition of STF-083010 reduced markedly the IL-6-mediated upregulation of the pro-fibrotic related genes mentioned above **(Figure 5D)**. Overall, these findings suggest that STF-083010 reduces the "hyper" M2 macrophage phenotype elicited by IL-4/IL-13/IL-6.

STF-083010 prevents IL-4/IL-13/IL-6 mediated CCL18 secretion and hyperpolarization of human macrophages. To examine whether our findings in murine bone marrow derived M-CSF activated macrophages could be replicated in a human setting, we investigated the effect of IL-4/IL-13 + IL-6 polarization in the well-characterized PMA-activated THP-1 macrophage cell line. During macrophage polarization, the endoplasmic reticulum was quantitatively visualized and tracked using the ER tracker dye and transmission electron microscopy, respectively. In the living cells, ER distension was observed during IL-4/IL-13/IL-6-mediated polarization **(Figure 6A).** These findings were further supported by transmission electron microscopy, which showed enhanced ultrastructural changes of the ER **(Figure 6B)**. Alternative activation

was assessed by measuring the M2 marker CCL18 secretion in supernatants by ELISA as described earlier[10]. The addition of the IL-4/IL-13 polarizing cocktail resulted in a significant increase in CCL-18 (from 5 ± 0.5 to 181.6 ± 15.6 pg/ml), consistent with previously published data[11], while the addition of IL-6 resulted in a 7-fold further increase of CCL-18 (1283.0 ± 72.6 pg/ml) **(Figure 6B)**. The addition of STF-083010 at 6μM resulted normalized the effect IL-6 and reduced the amount of CCL-18 release to levels comparable to IL-4/IL-13 mediated polarization cocktail (208.3 ± 12.6 pg/mL) **(Figure 6B)**. Gene expression analysis indicated that CCL-18 mRNA expression was increased in a similar manner, mimicking the protein observations by IL-4/IL-13 exposure and highly upregulated by the addition of IL-6 **(Figure 6C)**. Additionally, *Fn1* was quantitated to reflect the pro-fibrotic macrophage phenotype. Consistent with our findings in murine-derived alternatively activated macrophages, STF-083010 also reduced the levels of secreted CCL18 as well as *Fn1* secretion, reflecting its ability to prevent the "hyper" polarization mediated by IL-6 **(Figure 6B-6D)**. Overall, our findings show that IL-6 is responsible for increased ER expansion and a "hyper" pro-fibrotic phenotype in alternatively activated macrophages both in murine and human systems. It suggests further that the therapeutic targeting of IRE1 and IL-6 may lead to the prevention of the pro-fibrotic activity of alternatively activated macrophages and thus contribute to prevent progression of fibrosis *in vivo*.

DISCUSSION

Pro-fibrotic, alternatively activated "M2" macrophages have been implicated in the pathogenesis of many fibrotic diseases and in many different types of cancer [2]. Their close interaction with fibroblasts and their mediation of the fibrotic process has been extensively documented in the literature[12]. The "M2" phenotype can be induced by the binding of the pleiotropic cytokine IL-4 to its receptor, IL-4Rα, which induces rapid tyrosine phosphorylation of STAT6, leading to the upregulation of the pro-fibrotic M2-related phenotype[13]. Similar to *ex-vivo* isolated macrophages, which are involved in pathological wound repair, IL-4/IL-13 stimulated macrophages may also share many of the factors involved in tissue repair. Therefore, to learn more about the behaviour and phenotypic pro-fibrotic functions of these macrophages, it is important to understand: 1) the cellular organelles/mechanisms underlying macrophage polarization (IL-4/IL-13-mediated) and hyperpolarization (IL-4/IL-13/IL-6-mediated); 2) the pro-fibrotic phenotype associated with these polarization states; and 3) whether the pro-fibrotic phenotype of M2 macrophages can be attenuated.

It has been proposed that the IRE1-XBP1 axis is involved in the differentiation of many cell types that possess high secretory capacity through the activation of ER expansion programs [9,14]. For instance, UPR-mediated XBP1 production and splicing has been implicated in B-cell-to-plasma-cell differentiation[6] as well as the differentiation of eosinophils[5]. Further, IL-4 is one of the main Th2 cytokines that drives B cell differentiation into antibody-secreting plasma cells via an XBP1 dependent mechanism[15]. This led to the logical speculation that IL-4 and XBP1 might also be involved in ER

membrane biogenesis and in the polarization of macrophages to the pro-fibrotic M2 phenotype.

Interestingly, recent data has implicated IL-6 in augmenting the responses of macrophages to IL-4, and in subsequently enhancing the alternatively activated macrophage phenotype[3]. The inclusion of IL-6 with IL-4/IL-13 therefore provided a compelling model to study the hyper-polarization process of macrophages in relation to XBP1 induction and pro-fibrotic signature. Overall our data strongly supported the hypothesis that IL-6 can act synergistically with IL-4/IL-13 to augment spliced XBP1, leading to ER membrane expansion and the generation of a hyper pro-fibrotic macrophage phenotype. With the use of bioinformatics analysis, we have been able to demonstrate the distinct transcriptional signatures induced by UPR-dependent macrophage polarization. This data has provided substantial evidence in proposing that the IL-4/IL-13+IL-6 macrophage signature can be mediated by ER-related pathways. Additionally, our study suggests that targeting IRE1-endonuclease activity prevents the IL-6 dependent "hyper" pro-fibrotic phenotype observed. Although we cannot exclude off-target effects of STF-080310, our data strongly suggest the involvement of the IRE1-XBP1 pathway in IL-6-mediated hyperpolarization of alternatively activated macrophages, which warrants further investigations to elucidate the specific role of the IRE1 pathway in this polarization process. Other molecular alternatives have been suggested previously[16] . Here, Bommiasamy *et al*, reported that UPR-mediated ATF6α activation could also promote ER expansion and phospholipid biosynthesis, independent of XBP1-splicing[16]. The mechanisms acted by ATF6α could be distinct from those

previously shown by XBP1, suggesting a redundant pathway executing a vital cellular task. While this process was investigated in stromal cells like NIH-3T3 and CHO, it remains unclear whether it applies to the myeloid compartment – or if activated ATF6α is also involved to promote macrophage pro-fibrotic activation. Overall, multiple UPR arms could devote a concerted effort into activating macrophage-ER expansion program, leading to enhanced pro-fibrotic capacity.

Overall, our data show that the induction of spliced XBP1 correlated with the production of macrophage arginase activity during their polarization with IL-4/IL-13/IL-6. We did not find evidence for IL-6 alone to upregulate sXBP1 transcript counts, nor did we find evidence for IL-6 alone to modulate macrophage arginase activity, suggesting a true synergistic effect of IL-6 with IL-4/IL-13. As IL-6 is increased during chronic tissue injury and some infections, the findings suggest that IL-6 may enhance the fibrotic process, possibly by priming macrophages to be more pro-fibrotic. Furthermore, given the observation that spliced XBP1 was not robustly increased during the first 10 hours of polarization suggests that it may not be essential for initiation the M2-like phenotype but rather propagating the phenotype. It has been previously determined that IL-4/STAT6 axis is indispensable for the induction of alternative macrophage activation both *in vivo* and *in vitro*[17]. Thus, the precise mechanism by which XBP1 influences IL-4 dependent pathway activation and whether XBP1 selective inhibition is sufficient to ablate the macrophage pro-fibrotic phenotype *in vivo* are valid approaches that remain under investigation.

In conclusion, the data presented suggest that the addition of IL-6 to the alternatively activation of phenotype, the UPR is activated and the ER is expanded to accommodate the production, expression and secretion of pro-fibrotic products. During this process, XBP1 splicing occurs to promote the expansion process and further enhance UPR activation to support the protein folding load within the ER. When IL-6 is present, it acts concurrently with IL-4 to synergize the above effects, thus further augmenting the UPR, ER expansion and pro-fibrotic potential of the macrophage. Targeting ER expansion and IL-6 signalling in alternatively activated macrophages could be a valid strategy to lower the pro-fibrotic cellular activity in fibrotic diseases where M2-macrophages are known as primary cellular contributors.

REFERENCES

1 Murray, P. J. *et al.* Macrophage activation and polarization: nomenclature and experimental guidelines. *Immunity* **41**, 14-20, doi:10.1016/j.immuni.2014.06.008 (2014).

2 Wynn, T. A. & Vannella, K. M. Macrophages in Tissue Repair, Regeneration, and Fibrosis. *Immunity* **44**, 450-462, doi:10.1016/j.immuni.2016.02.015 (2016).

3 Mauer, J. *et al.* Signaling by IL-6 promotes alternative activation of macrophages to limit endotoxemia and obesity-associated resistance to insulin. *Nat Immunol* **15**, 423-430, doi:10.1038/ni.2865 (2014).

4 Dickhout, J. G. *et al.* Induction of the unfolded protein response after monocyte to macrophage differentiation augments cell survival in early atherosclerotic lesions. *Faseb J* **25**, 576-589, doi:10.1096/fj.10-159319 (2010).

5 Bettigole, S. E. *et al.* The transcription factor XBP1 is selectively required for eosinophil differentiation. *Nature immunology* **16**, 829-837, doi:10.1038/ni.3225 (2015).

6 Reimold, A. M. *et al.* Plasma cell differentiation requires the transcription factor XBP-1. *Nature* **412**, 300-307, doi:10.1038/35085509 (2001).

7 Iwakoshi, N. N., Pypaert, M. & Glimcher, L. H. The transcription factor XBP-1 is essential for the development and survival of dendritic cells. *J Exp Med* **204**, 2267-2275, doi:10.1084/jem.20070525 (2007).

8 Bettigole, S. E. & Glimcher, L. H. Novel roles for XBP1 in hematopoietic development. *Cell Cycle* **15**, 1653-1654, doi:10.1080/15384101.2016.1172470 (2016).

9 Shaffer, A. L. *et al.* XBP1, downstream of Blimp-1, expands the secretory apparatus and other organelles, and increases protein synthesis in plasma cell differentiation. *Immunity* **21**, 81-93, doi:10.1016/j.immuni.2004.06.010 (2004).

10 Schutyser, E., Richmond, A. & Van Damme, J. Involvement of CC chemokine ligand 18 (CCL18) in normal and pathological processes. *J Leukoc Biol* **78**, 14-26, doi:10.1189/jlb.1204712 (2005).

11 Schupp, J. C. *et al.* Macrophage activation in acute exacerbation of idiopathic pulmonary fibrosis. *PloS one* **10**, e0116775, doi:10.1371/journal.pone.0116775 (2015).

12 Ploeger, D. T. *et al.* Cell plasticity in wound healing: paracrine factors of M1/ M2 polarized macrophages influence the phenotypical state of dermal fibroblasts. *Cell communication and signaling : CCS* **11**, 29, doi:10.1186/1478-811X-11-29 (2013).

13 Wang, N., Liang, H. & Zen, K. Molecular mechanisms that influence the macrophage m1-m2 polarization balance. *Frontiers in immunology* **5**, 614, doi:10.3389/fimmu.2014.00614 (2014).

14 Niederreiter, L. *et al.* ER stress transcription factor Xbp1 suppresses intestinal tumorigenesis and directs intestinal stem cells. *J Exp Med* **210**, 2041-2056, doi:10.1084/jem.20122341 (2013).

15 Iwakoshi, N. N. *et al.* Plasma cell differentiation and the unfolded protein response intersect at the transcription factor XBP-1. *Nat Immunol* **4**, 321-329, doi:10.1038/ni907 (2003).

16 Bommiasamy, H. *et al.* ATF6alpha induces XBP1-independent expansion of the endoplasmic reticulum. *Journal of cell science* **122**, 1626-1636, doi:10.1242/jcs.045625 (2009).

17 Ohmori, Y. & Hamilton, T. A. STAT6 is required for the anti-inflammatory activity of interleukin-4 in mouse peritoneal macrophages. *The Journal of biological chemistry* **273**, 29202-29209 (1998).

18 Lauber, S. *et al.* Novel function of Oncostatin M as a potent tumour-promoting agent in lung. *International journal of cancer* **136**, 831-843, doi:10.1002/ijc.29055 (2015).

19 Shannon, P. *et al.* Cytoscape: a software environment for integrated models of biomolecular interaction networks. *Genome research* **13**, 2498-2504, doi:10.1101/gr.1239303 (2003).

20 Wu, G. & Stein, L. A network module-based method for identifying cancer prognostic signatures. *Genome biology* **13**, R112, doi:10.1186/gb-2012-13-12-r112 (2012).

METHODS

Isolation and polarization of bone marrow-derived macrophages. Bone marrow-derived macrophages were isolated and cultured as described previously (25). Briefly, bone marrow cells from C57BL/6 mice were isolated and treated with 20 ng/ml M-CSF for 7 days. Following 7 days in culture, macrophages were exposed to recombinant IL-4 (20 ng/ml), IL-13 (50 ng/ml) and where applicable, IL-6 (5 ng/mL), for 24-120 hours to induce alternative programming. Polarization to the M2-like phenotypes was assessed by arginase activity in cell lysates and by Arg1 and CD206 protein expression by flow cytometry. STF-083010 drug (Axon Medchem) was solubilized in DMSO and used at 6 and 60μM).

Arginase assay. The arginase assay was adapted and optimized from a previously established protocol[18]. Following the seeding of BMDMs (80,000 cells/per well of a 96-well plate) and their subsequent stimulation with the above cytokine cocktails, supernatant was collected and cells were washed twice with ice-cold PBS. Next, cells were lysed in 25-100 µl of 0.1% Triton X-100 supplemented with protease inhibitors (200 mM sodium orthovanadate, 0.1 M PMSF, 1 M DTT and 5 µg/ml and bovine lung aprotinin). A 1:1 dilution with 25 mM of Tris-HCl (pH 7.5) was later performed. 25 µl of this mixture was transferred to a 96-well PCR plate, with the addition of 2.5 µl of 10 mM manganese chloride. The PCR plate was then placed in a thermal cycler programmed to heat at 56 degrees Celsius for 10 minutes. Afterwards, 25 µl of 0.5 M L-arginine was mixed with the pre-heated mixture and the entire plate was then re-incubated at 37 degrees Celsius for 30 minutes. An eight-point urea standard curve was then established

(0 to 15 mM). 200 µl of acid solution (63.6% water, 9.1% concentrated sulphuric acid and 27.3% concentrated phosphoric acid), followed by 10 µl of 9% alpha-isonitrosopropiophenone, were added to both samples and the urea solutions. The contents of each well were mixed thoroughly and the plate was incubated at 95 degrees Celsius for 30 minutes, followed by 10 minutes of cooling at 20 degrees Celsius. 150-200 µl of each sample was removed and placed in a new, clear, flat bottom, 96-well plate for absorbance reading at 550 nm.

Multiplex analysis of mediators. We quantified 32 different cytokines, chemokines, and growth factors simultaneously by using a Discovery Assay® (Mouse Cytokine and Chemokine Array 32-Plex, Eve Technologies Corp, Calgary, AB, Canada). These 32 different mediators were assessed in the cell culture supernatant of BMDMs. The multiplex assay was performed at Eve Technologies using the Bio-Plex™ 200 system (Bio-Rad Laboratories, Inc., Hercules, CA, USA) and a Milliplex Mouse Cytokine/Chemokine kit (Millipore, St. Charles, MO, USA) according to Evetech protocol. The 32-plex consisted of eotaxin, G-CSF, GM-CSF, IFN-γ, IL-1α, IL-1β, IL-2, IL-13, IL-4, IL-5, IL-6, IL-7, IL-9, IL-10, IL-12 (p40), IL-12 (p70), IL-13, IL-15, IL-17, IP-10, KC, LIF, LIX, MCP-1, M-CSF, MIG, MIP-1α, MIP-1β, MIP-2, RANTES, TNFα, and VEGF. The assay sensitivities of these markers range from 0.1 pg/ml to 33.3 pg/ml. Individual analytes' values and other assay details are available on Eve Technologies' website and in the Milliplex protocol.

ELISA. Human CCL18/PARC protein was assessed in the cell culture supernatant using the commercially available CCL18 ELISA, according to the manufacturer's protocol (R&D systems, Cat# DCL180B).

Flow cytometry. Following polarization of BMDMs, ~$2x10^6$ cells were subjected to FACS surface and intracellular staining protocol. Briefly, cells were initially suspended in FACS buffer solution (0.3% BSA in PBS). Non-antigen-specific binding of immunoglobulins to Fcγ II/III receptor on BMDMs was blocked using purified rat anti-mouse CD16 (Mouse FC Block) (BD Pharmingen, Cat#553142). Next, cells were subjected to surface antibody staining solution, containing a mix of anti-mouse F4/80 and anti-mouse CD206 (MMR) (BioLegend, Cat#123133 and 141723). Cells were then fixed and permeabilized using BD Cytofix/Cytoperm solution (BD Biosciences, Cat#554722) prior to performing intracellular staining with anti-mouse/human arginase-1 (1:5) (R&D Systems, Cat#IC5868A). Intracellular staining antibody solution was made up in 1x BD Perm/Wash buffer solution (BD Biosciences, Cat#554723). Cells were finally resuspended in FACS buffer for FACS and data was collected using BD LSRFortessa™ and FACSDiva software from BD Biosciences. Data were analyzed using FlowJo Software from Treestar.

Transmission electron microscopy. BMDMs were seeded onto a 6-well plate and polarized towards the macrophage phenotypes using the cytokine concentrations mentioned above. Following their polarization, the supernatant was collected and cells were washed twice with ice-cold PBS. Cells were then fixed in 2% glutaraldehyde in sodium cacodylate for 24 hours. Cells were then post-fixed in osmium tetroxide,

dehydrated in alcohol, lifted off the plate by propylene oxide, spun down into pellets and further processed for pellet embedding in epoxy resin. After polymerization, sections were stained with uranyl acetate and lead citrate and observed under a transmission electron microscope (Jeol TEMSCAN, Tokyo, Japan) by trained personnel in the Faculty of Health Sciences Electron Microscopy Core Facility at McMaster University.

RNA extraction and assessment of RNA quality. Total RNA from BMDMs was isolated using Nucleospin RNA plus (D-Mark BioSciences, Toronto, Canada [Catalog No. MN-740984.250]). Concentrations and RNA purity were measured using a NanoVue spectrophotometer (V1.7.3). The integrity and quantity of the RNA were examined using the Agilent Bioanalyzer 2100 (Agilent Technologies, Santa Clara, USA) before NanoString gene expression analysis.

Real-time polymerase chain reaction (RT-PCR). mRNA isolated from BMDMs reverse-transcribed using Superscript II RT (Invitrogen, Carlsbad, California, USA) to obtain cDNA for gene expression analysis. A 7500 Real-Time PCR Machine (Applied Biosystems, Foster City, CA) with fast SYBR green mix (Applied Biosystems, Catalog No. 4385612) were employed. The PCR protocol used was a 20-second initiation at 50°C, followed by 10 minutes at 95° C, 40 cycles of 15s amplification at 95°C and 1 minute at 60°C. SYBR green primers, including *spliced Xbp1*, forward, 5'-TCCGCAGCAGGTGCAGG- 3', and reverse, 5'-GCCCAAAAGGATATCAGACTCAGA- 3' and for *18S*, forward, 5'-AGTCCCTGCCCTTTGTACACA- 3', and reverse, 5'CGATCCGAGGGCCTCACT- 3' were produced by the DNA Sequencing and Oligo Synthesis Facility at McMaster

University (MOBIX Lab). *18s* was used as reference gene to assess *spliced Xbp-1* mRNA gene expression. Candidate genes were analyzed using semi-quantitative gene expression analysis (ΔΔCT method) and expressed as fold change relative to the gene expression of the control untreated BMDMs.

Nanostring analysis. Nanostring gene expression was performed on both murine (BMDM-derived) and human (THP-1) macrophages. We performed multiplexed target profiling of inflammation- and immune-related transcripts on Control, IL-4/IL-13, IL-4/IL-13+IL-6 and IL-4/IL-13+IL-6+STF-083010 samples. Pre-processing and normalization was performed with nSolver 2.5 software (www.nanostring.com) by using 6 negative controls for background subtraction and 6 positive controls for normalization. Next total counts normalization was performed. All genes were used to perform PCA and visualize the first 3 components (Bioconductor, rgl package; https://cran.r-project.org/web/packages/rgl/index.html), and to perform hierarchical clustering (using euclidean distance and average linkage). The "limma" package and differential expression in microarray experiments were performed as described previously.

Network analysis of Nanostring data. Networks were constructed using Cytoscape software [19]. Reactome FI plugin was used to build functional networks, which were then were then analyzed for presence of significant modules (gene clusters) [20]. These modules were further examined with Pathway enrichment and Gene Ontology (GO) tools in Cytoscape. Functional networks contain the differentially regulated genes within the indicated biological process and do not necessarily include all other significantly regulated genes.

Macrophage-fibroblast co-culture assay. Murine BMDMs were stimulated with IL-4/IL-13/IL-6 for 30 hours to polarize them towards the alternatively activated macrophage phenotype. Macrophages were then lifted off the plates and co-cultured with 15,000 fibroblasts (NIH-3T3 cell line) for 48 hours. The seeding ratio of macrophages:fibroblasts was approximately 5:1. During the co-culture process, fibroblasts were cultured on black collagen coated 96-well plates (Corning™ Biocoat™ Collagen 1 coated plates). To assess the process of fibroblasts-to-myofibroblasts differentiation, fibroblasts were treated with recombinant TGFβ1 (2ng/ml) (R&D biosystems, Cat# 7666-MB-005). Following the duration of co-culture, the supernatant was saved and cells were fixed and permeabilized using 4% paraformaldehyde and 0.1% triton-X in PBS, respectively. Blocking of non-specific sites was achieved using 1% BSA in PBS, followed subsequently with anti-αSMA conjugated to AF488 (eBioscience, anti-alpha-smooth muscle actin Alexa Fluor® 488, Cat#53-9760-82) in PBS containing 1% BSA. Cells were ultimately stained with DAPI (100ng/ml, Sigma) and the fluorescence intensity signal was read using SpectraMax ® i3 reader.

Statistical analysis. Results are expressed as mean ± SEM. A one-way analysis of variance (One-way ANOVA) followed by Newman-Keuls multiple comparison test was used to determine significance when more than two groups were compared. A student's t-test was used to determine significance between two conditions. All statistical tests were performed using GraphPad Prism 7.0c (GraphPad Software, Inc). A $p<0.05$ was considered statistically significant.

Data availability. The datasets generated during and/or analysed during the current study are available from the corresponding author on reasonable request.

ACKNOWLEDGEMENTS

We sincerely thank the electron microscope facility (McMaster University, ON, Canada) for their exceptional training and technical service. We thank Christine King and Liliana De Sousa (Farncombe Metagenomics Facility, McMaster University, ON, Canada) for help with NanoString experiments. This work was performed with funding from the Ontario Thoracic Society (Canadian Lung Association). EAA is funded by the Canadian Institute of Health Research (#140358). CDR is a professor of pathology and molecular medicine and a division director of the McMaster Immunology Research Centre. RCA is a Career Investigator of the Heart and Stroke Foundation of Ontario and holds the Amgen Canada Research Chair in the Division of Nephrology at St. Joseph's Healthcare and McMaster University.

AUTHOR CONTRIBUTIONS: Conception and design: EAA and KA; Performed experiments: EAA, KT, PP, AD, PSK, JM, SL; Analysis and interpretations: EAA, KT, PP, AD, ADG, JM, PSK, SL, JGD, RCA, MRJ, CDR and KA; Drafting the manuscript: EAA and KA; Edited and revised manuscript: EAA, KT, PP, AD, ADG, JM, PSK, SL, JGD, RCA, MRJ, CDR and KA. All authors read and approved the final version.

COMPETING FINANCIAL INTERESTS: All authors declare no competing financial interests.

FIGURE LEGENDS

Figure 1. IL-6 addition promotes macrophage M2 polarization and spliced XBP1 induction. Bone marrow derived macrophages were exposed to the M2 polarization cocktail IL-4/IL-13 alone (open circles) and with the addition of IL-6 (closed circles). The cell lysates were assessed for (A) arginase activity at 2, 4, 7, 15, 24 and 30 hours expressed as mM urea per well and (B) arginase-1 protein. (C) In a separate experiment, mRNA was extracted from cell lysates and assessed for the appearance of spliced XBP1 at 2, 4, 7, 15, 24 and 30 hours. A one-way ANOVA was used to assess the effect of each treatment and to identify at which time point each treatment was different from their respective controls (2 hour) and indicated with *. Data are presented as mean ± SD, each time point was assessed in quadruplicates. #,* indicates $p<0.05$; ###,*** indicates $p<0.001$.

Figure 2. IL-6 addition to IL-4/IL-13 promotes expansion of the ER and mitochondrial membranes. Bone marrow derived macrophages were exposed to the M2 polarization cocktail IL-4/IL-13 alone, or with the addition of IL-6, for 30 hours. TEM images showing BMDMs polarized towards the M2 and M2+IL-6. The blue and red arrowheads show mitochondria and endoplasmic reticulum, respectively; the yellow asterisks indicate the location of the nucleus. Scale bar = 100nm.

Figure 3. Inhibition of IRE1-XBP1 splicing reduces macrophage alternative activation following their hyper-polarization with IL-6. Bone marrow-derived cells were harvested from C57BL/6 mice and cultured for 7 days in MCSF for differentiation into macrophages. Cells were then cultured for an additional 30 hours with IL-4/IL-13 or

IL-4/IL-13+IL-6, alone or in combination with STF-083010 (6 and 60μM). M2 cocktail included IL-4 (20ng/ml) and IL-13 (50ng/ml), with or without IL-6 (5ng/ml). (A) Arginase activity, which is reflective of the M2 macrophage phenotype, was assessed in cell lysates, and later accompanied with (B) RT-PCR of sXBP1. (C) Representative flow cytometric plots of selected samples showing the frequency of arginase-1/CD206 positive cells during macrophage polarization with/without STF-083010. Bars represent mean ± SEM from 4 replicates per group and graph is representative of two independent experiments. Two black filled columns are included, in which one serves as reference control for IL-4/IL-13 stimulated groups and other for IL-3/IL-13/IL-6 stimulated groups. *:P<0.05; **:P<0.01; ***:P<0.001, where * represent a difference between white-filled columns and the reference control.

Figure 4. Principal component analysis plot and hierarchical clustering of the samples showing the ability of STF-083010 to normalize the transcriptional signature of hyper IL-4/IL-13/IL-6 stimulated macrophages to IL-4/IL-13 stimulated macrophages. IL-6BMDMs were cultured for 30 hours with with IL-4/IL-13, IL-4/IL-13+IL-6 and IL-4/IL-13+IL-6+STF-083010 and subsequently subjected for RNA isolation and NanoString gene expression. (A) Principal Component Analysis (PCA) plot, presenting the 4 groups. (B) Dendrogram, obtained from hierarchical clustering of the same samples (using euclidean distance and average linkage).

Figure 5. Significantly regulated gene numbers and functional networks with different modules and comparisons of interest showing down-regulation of certain pro-fibrotic related genes in hyper M2 macrophage treated with STF-083010.

BMDMs were treated for 30 hours with IL-4/IL-13, IL-4/IL-13+IL-6 and IL-4/IL-13+IL-6+STF-083010 phenotype and subsequently subjected for RNA isolation and NanoString gene expression. (A) Showing comparison of regulated and unregulated genes between different pairwise comparisons of interests. (B) Functional network and its regulation and (C) Gene list within each module. The network is consistent across all comparisons, while the regulation is marked by colours: up-regulated genes are shown in red, down-regulated - in green, and genes that were not found to be differentially expressed in the comparison of interest are shown in white. Functional network with different modules shown in different colours and marked by ellipses. Each ellipse is contains the module ID and functional annotation. (D) Selected significantly regulated pro-fibrotic related genes.

Figure 6. STF-083010 reduces ER size and the hyper pro-fibrotic M2 phenotype of human macrophages. Human monocytic cell line were differentiated into macrophages using PMA and then stimulated with IL-4/IL-13 and IL-6, alone or in combination with STF-083010 (for 72 hours). (A) ER tracker (blue dye) and TEM displaying the ER compartment on cells following 72 hours of polarization. (B-C) In a separate experiment, CCL18 secretion and transcription was assessed as well as (D) the pro-fibrotic related marker, *Fn1*. A one-way ANOVA was used to assess the effect of each treatment. Gene expression by NanoString is presented as normalized counts. Data are presented as mean ± SD, each time point was assessed in quadruplicates. #,* indicates $p<0.05$; ###,*** indicates $p<0.001$.

Figure 1

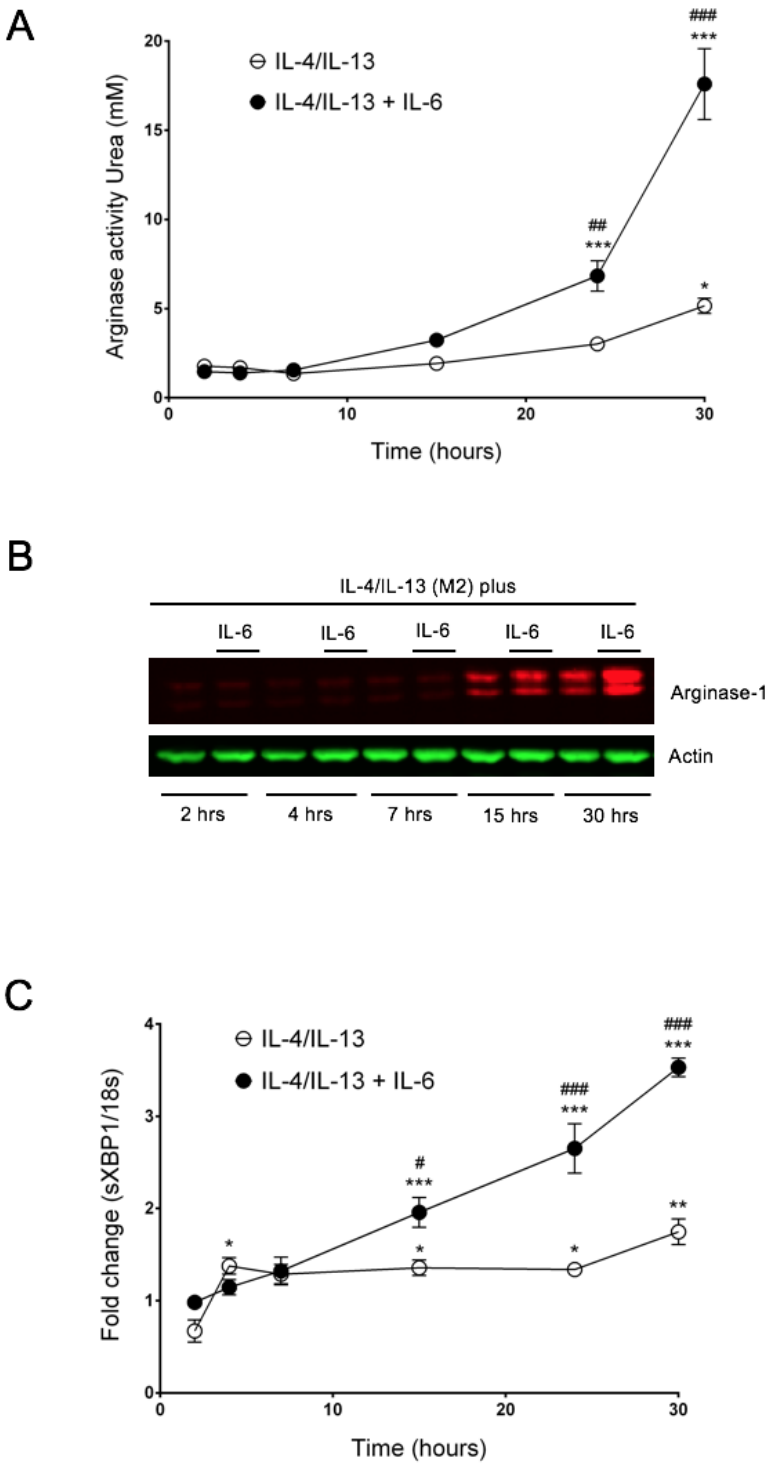
A
IL-4/IL-13
IL-4/IL-13 + IL-6
Arginase activity Urea (mM)
Time (hours)
B
IL-4/IL-13 (M2) plus
IL-6
Arginase-1
Actin
2 hrs
4 hrs
7 hrs
15 hrs
30 hrs
C
IL-4/IL-13
IL-4/IL-13 + IL-6
Fold change (sXBP1/18s)
Time (hours)

Figure 2

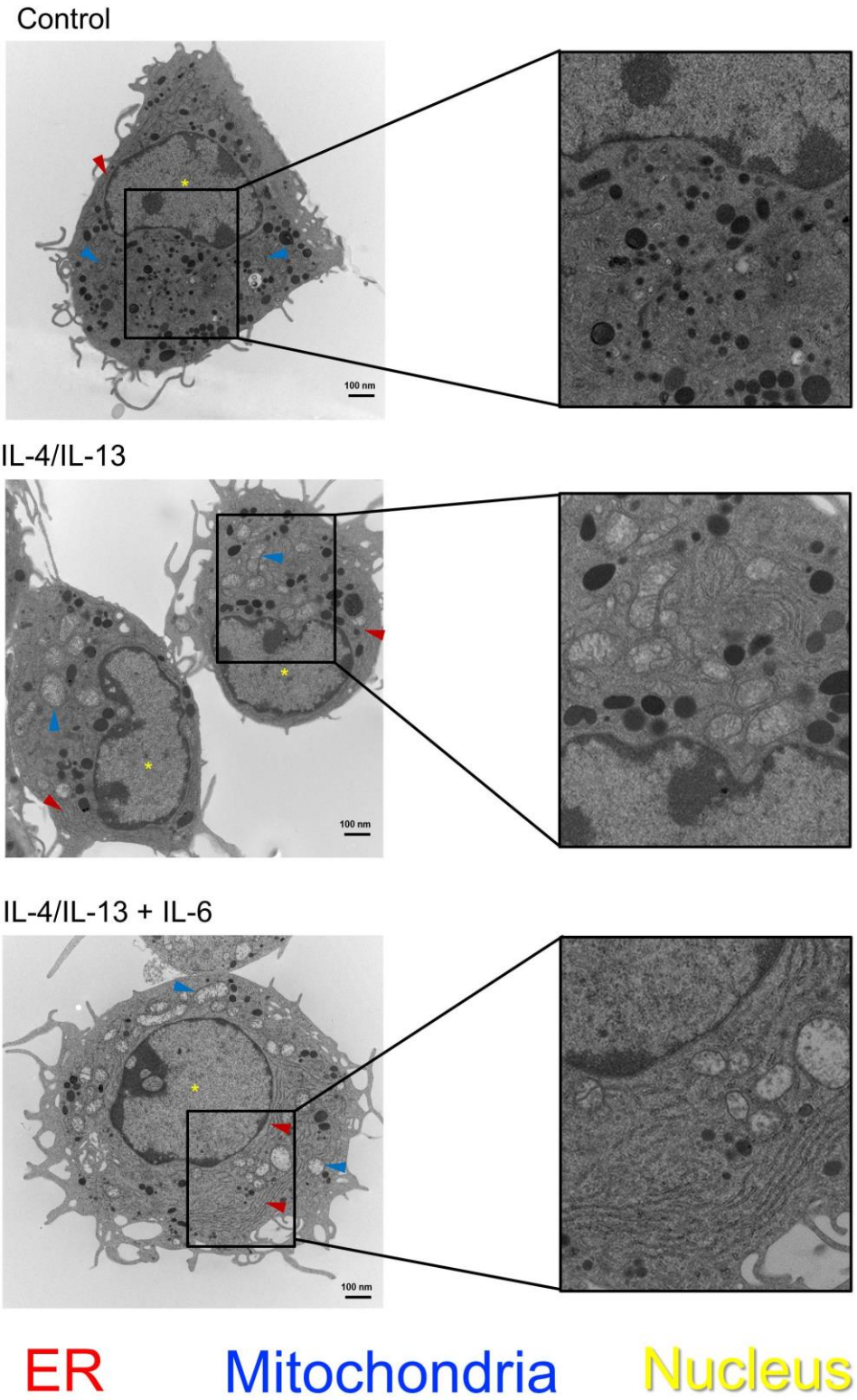
Control
100 nm
IL-4/IL-13
100 nm
IL-4/IL-13 + IL-6
100 nm
ER
Mitochondria
Nucleus

Figure 3

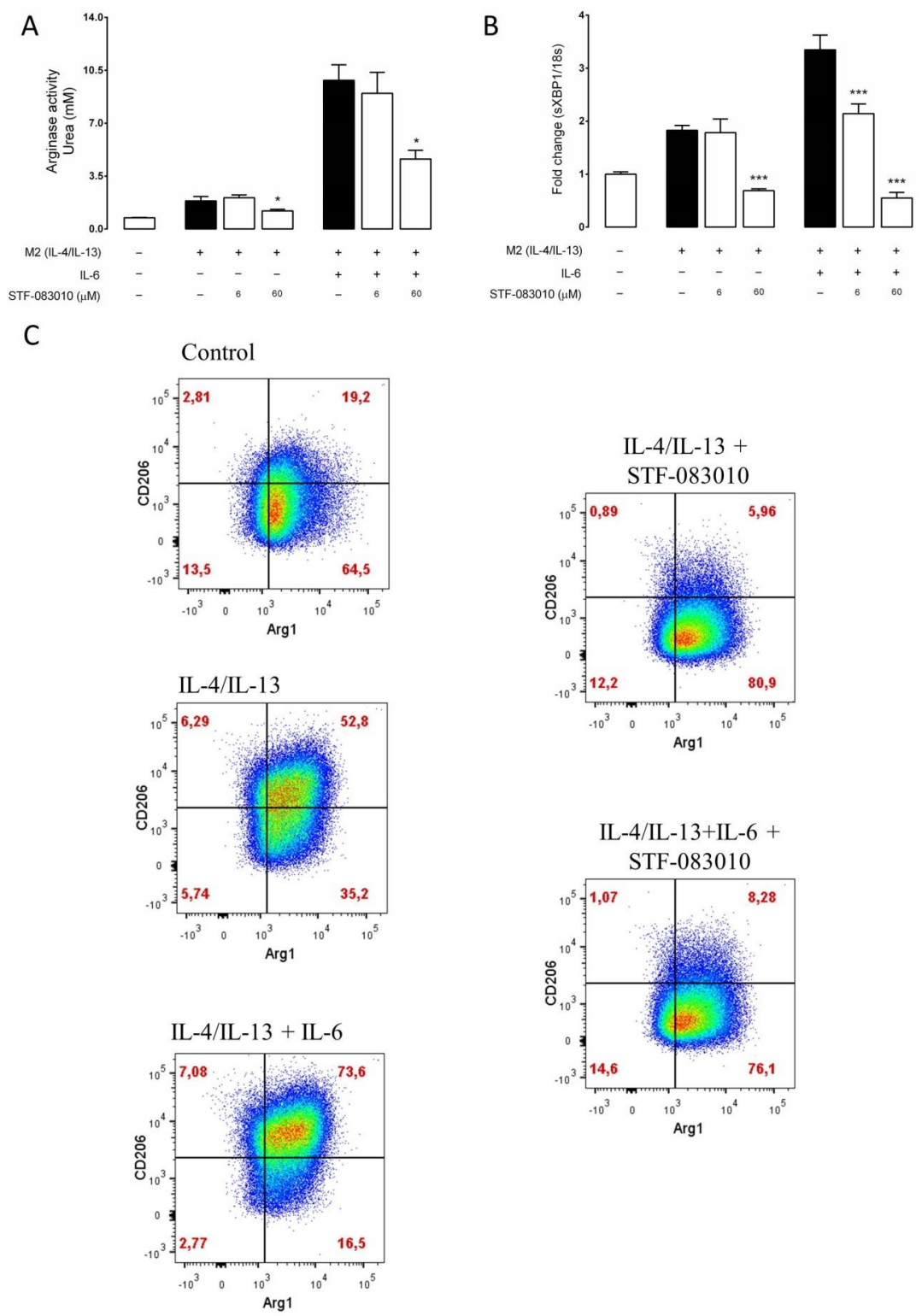
A
Arginase activity
Urea (mM)
14.0
10.5
7.0
3.5
0.0
M2 (IL-4/IL-13)
IL-6
STF-083010 (μM)
B
Fold change (sXBP1/18s)
C
Control
IL-4/IL-13
IL-4/IL-13 + IL-6
IL-4/IL-13 + STF-083010
IL-4/IL-13+IL-6 + STF-083010
CD206
Arg1
2,81
19,2
13,5
64,5
6,29
52,8
5,74
35,2
7,08
73,6
2,77
16,5
0,89
5,96
12,2
80,9
1,07
8,28
14,6
76,1

Figure 4

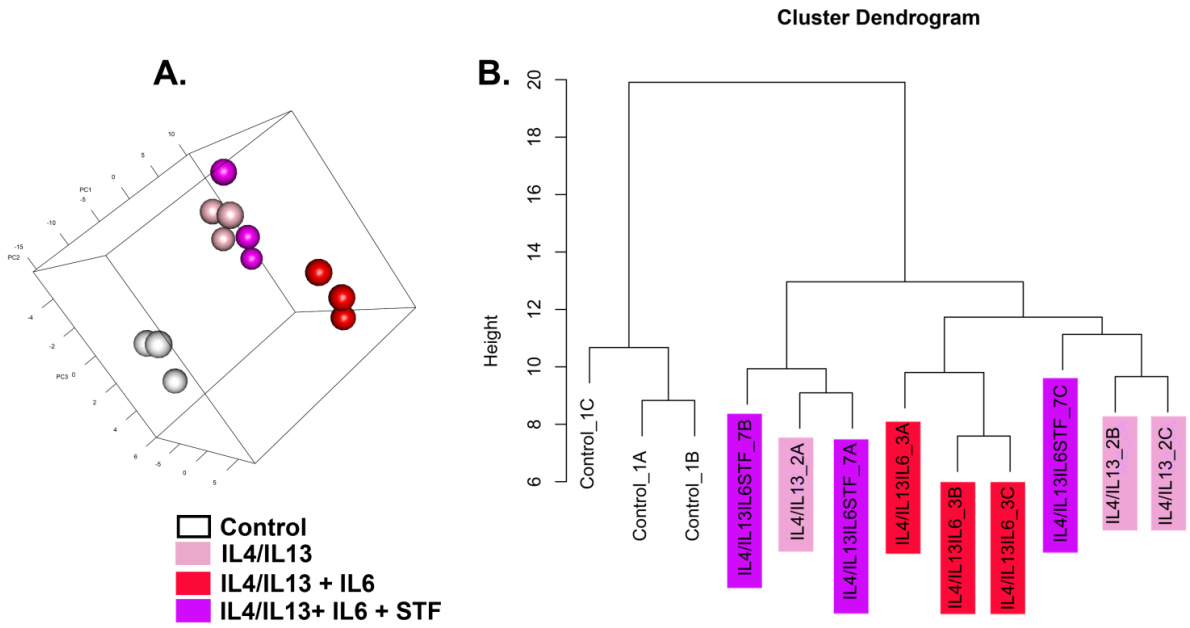
A.
Control
IL4/IL13
IL4/IL13 + IL6
IL4/IL13+ IL6 + STF
B.
Cluster Dendrogram
Height
6
8
10
12
14
16
18
20
Control_1C
Control_1A
Control_1B
IL4/IL13IL6STF_7B
IL4/IL13_2A
IL4/IL13IL6STF_7A
IL4/IL13IL6_3A
IL4/IL13IL6_3B
IL4/IL13IL6_3C
IL4/IL13IL6STF_7C
IL4/IL13_2B
IL4/IL13_2C

Figure 5

A

	m1 vs control	il4/il13 vs m1	il4/il13 vs control	il4/il13il6 vs control	il4/il13il6stf vs control	il4/il13il6 vs il4/il13	il4/il13il6stf vs il4/il13
Down	52	24	26	35	32	10	10
n.s.	42	49	74	64	69	95	99
Up	19	40	13	14	12	8	4

B

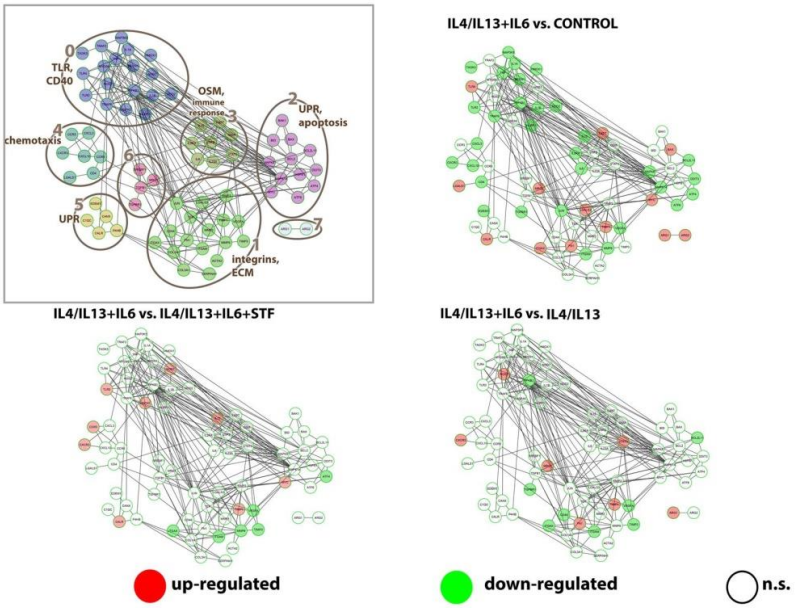

C

Module	Number of nodes	Node List
0	18	BECN1, HMOX1, HSPA5, IL1A, IL1B, MAP3K5, MYD88, NFKB1, NLRP3, NOD1, NOD2, NOS2, TAOK3, TLR2, TLR4, TNF, TRAF2, TRAF6
1	17	ACTA2, CD44, COL1A1, COL3A1, FN1, ITGAM, ITGAX, JUN, LGALS3, MMP2, MMP3, MMP9, SERPINH1, TEK, TIMP1, TIMP3, VEGFA
2	12	ATF4, ATF6, BAK1, BAX, BCL2, BCL2L11, BID, DDIT3, HSPB1, MAPK14, MAPK8, MYC
3	8	CSF2, IL15, IL23A, IL2RA, IL6, IL6ST, OSM, STAT3
4	7	CCR3, CCR5, CD4, CXCL10, CXCL3, CXCR3, LGALS1
5	5	C1QC, CALR, CANX, EDEM1, P4HB
6	4	MRC1, SREBF1, TGFB1, TGFBR1
7	2	ARG1, ARG2

D

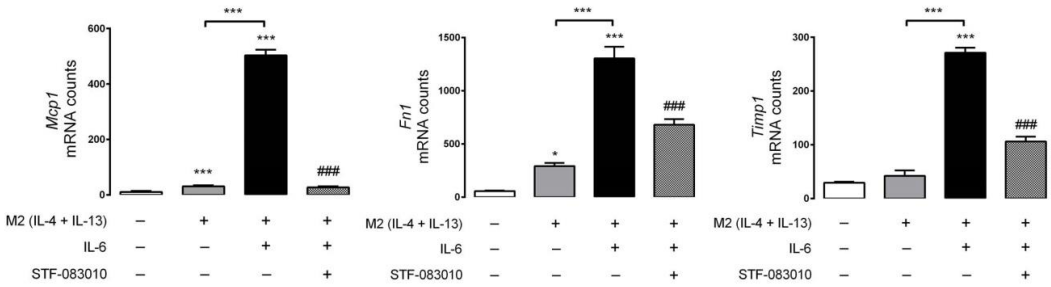

Figure 6

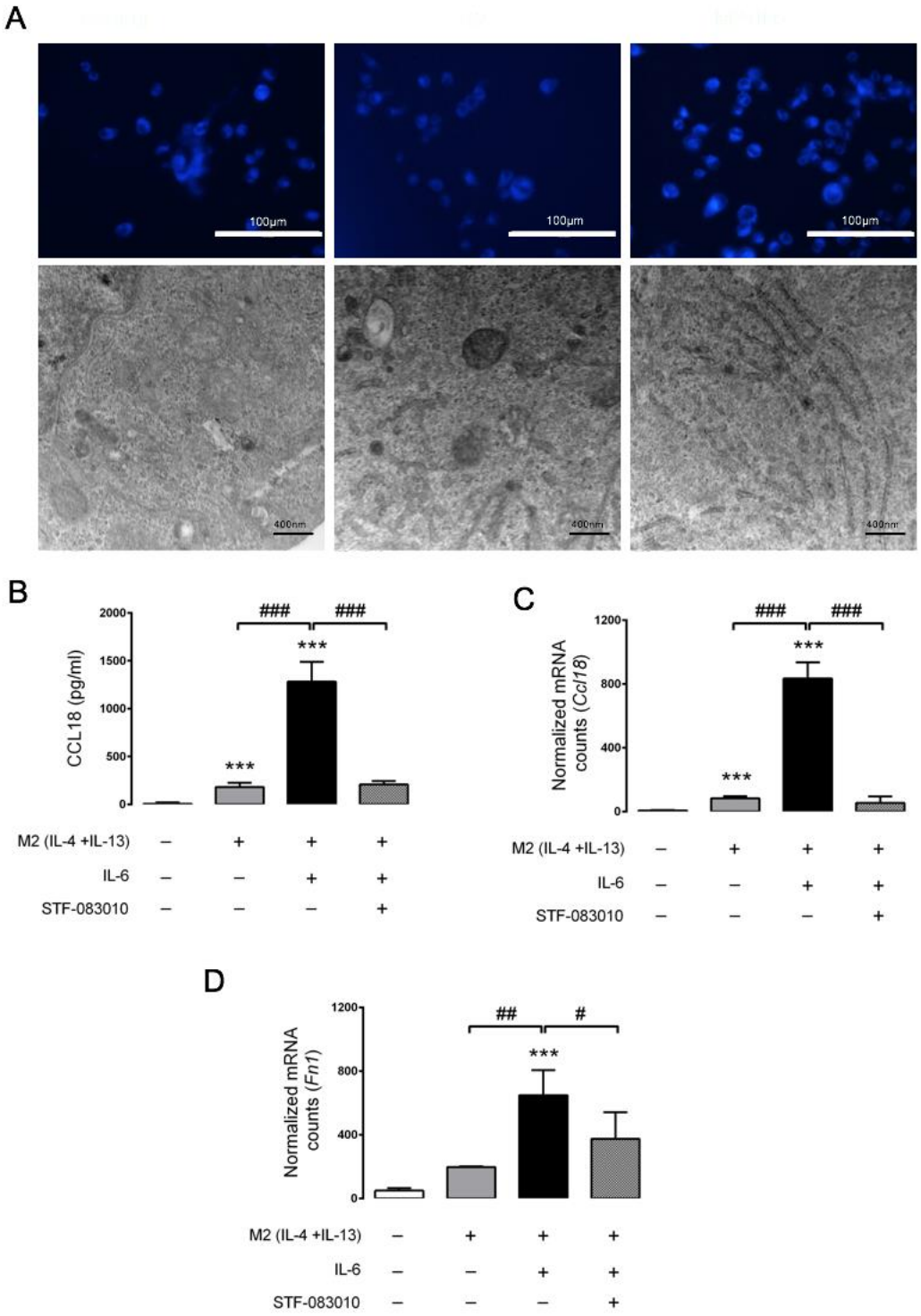
A
100µm
400nm
B
CCL18 (pg/ml)
###
***
M2 (IL-4 +IL-13)
IL-6
STF-083010
C
Normalized mRNA counts (Ccl18)
D
Normalized mRNA counts (Fn1)
##
#

Supplementary information

IL-6 mediates ER expansion and hyperpolarization of alternatively activated macrophages

Ehab E Ayaub [1,3], Karun Tandon [1,3], Pavithra Parthasarathy [1,3], Anisha Dubey[3], Anna Dvorkin-Gheva[3], James Murphy[1,3], Philipp S Kolb [1,3], Sarka Lhotak[2], Jeffrey G Dickhout[2], Rick C Austin[2], Martin RJ Kolb[1], Carl D Richards[3] and Kjetil Ask*[1,3].

Supplementary Table 1: Gene symbols and reference sequence details in nanoString codeset used to investigate gene expression patterns in the bone marrow-derived macrophages.

Supplementary Figure 1. Direct contact of IL-4/IL-13/IL-6-stimulated macrophages promotes fibroblast-to-myofibroblast differentiation. NIH-3T3 fibroblasts were cultured alone, and with TGFβ1 (2.5ng/ml). Fibroblasts were also co-cultured with IL-4/IL-13/IL-6-stimulated macrophages (following 30 hours of stimulation) and with the only conditioned media from IL-4/IL-13/IL-6-stimulated macrophages. Following 48 hours of (co)-culture, fibroblasts were fixed and subsequently stained with αSMA conjugated with Alexa Fluo 488 . The mean fluorescent intensity signal was read and illustrated as indicated above. . Data are presented as mean ± SD, each condition was assessed in triplicates. * indicates $p<0.05$; **indicates $p<0.01$; *** indicates $p<0.001$.

Supplementary Figure 2. Effect of STF-083010 on cellular viability of polarized BMDMs. Bone marrow-derived cells were harvested from C57BL/6 mice and cultured for 7 days in MCSF for differentiation into BMDMs. Cells were then cultured for an additional 30 hours with IL-4/IL-13and IL-4/IL-13+IL-6, alone or in combination with STF-083010 (6 and 60μM). To assess viability, cells were then directly cultured with CellTiter 96® AQ_{ueous} One solution for 3.5 hours and absorbance values were read at 490 nm. OD values were later normalized to ones from unstimulated cells and relatively presented as percent cellular viability. Two black filled columns are included, in which one serves as reference control for IL-4/IL-13 stimulated groups and other for IL-3/IL-13/IL-6 stimulated groups. *:$P<0.05$; **:$P<0.01$; ***:$P<0.001$.

Supplementary Figure 3. Representative plots showing gating strategy for flow cytometry analysis. BMDMs were first gated using SSC-A vs. FSC-A to show the sample population, then subsequently gated for singlets (SSC-A vs. SSC-H). The single cell gate was further analysed for its ability to express F4/80, thus demonstrating the frequency of F4/80+ cells from all assessed samples. Cellular expression of arginase-1 and/or CD206 was later determined from the F4/80 gated population.

Supplementary Figure 4. Functional network with different modules shown in different colours and marked by ellipses. Each ellipse contains the module ID (consistent throughout the manuscript) and functional annotation.

Supplementary Table 1

HUGO Gene	NSID
Actb	NM_007393.3:1138
B2m	NM_009735.3:177
Gapdh	NM_001001303.1:890
Gusb	NM_010368.1:1735
Hprt	NM_013556.2:30
Ipo8	NM_001081113.1:3496
Pgk1	NM_008828.2:36
Polr2a	NM_009089.2:2220
Ppia	NM_008907.1:390
Rplp2	NM_026020.6:146
Tbp	NM_013684.3:70
Tuba1a	NM_011653.2:1378
Ubc	NM_019639.4:21
Ywhaz	NM_011740.2:455
Xbp1	NM_013842.2:825
Atf6	NM_001081304.1:4765
Ddit3	NM_007837.3:255
Hspa5	NM_022310.2:2157
Canx	NM_007597.3:3930
Calr	NM_007591.3:551

HUGO Gene	NSID
P4hb	NM_011032.2:595
Edem1	NM_138677.2:610
Fkbp2	NM_008020.3:163
Taok3	NM_001081308.2:530
Map3k5	NM_008580.4:640
Atf4	NM_009716.2:812
C1qc	NM_007574.2:708
Tnf	NM_013693.1:1135
Nfkb1	NM_008689.2:2125
Il6	NM_031168.1:40
Osm	NM_001013365.2:579
Ccl12	NM_011331.2:56
Cxcl3	NM_203320.2:275
Il1b	NM_008361.3:1120
Il1a	NM_010554.4:225
Il10	NM_010548.1:985
Tgfb1	NM_011577.1:1470
Acta2	NM_007392.2:45
Fn1	NM_010233.1:2627
Col1a1	NM_007742.3:215
Col3a1	NM_009930.1:4370

HUGO Gene	NSID
Serpinh1	NM_009825.2:1845
Hspb1	NM_013560.2:630
Fkbp10	NM_010221.2:264
Loxl2	NM_033325.2:3700
Ccl20	NM_016960.1:120
Ccr3	NM_009914.4:2290
Ccr4	NM_009916.2:1670
Ccr5	NM_009917.5:1340
Ccr8	NM_007720.2:426
Cd4	NM_013488.2:950
Cd44	NM_009851.2:3075
Cd8a	NM_001081110.2:355
Csf2	NM_009969.4:452
Cxcl10	NM_021274.1:115
Cxcr3	NM_009910.2:605
Cxcr6	NM_030712.4:650
Ifng	NM_008337.1:95
Il17a	NM_010552.3:205
Il2	NM_008366.2:485
Il2ra	NM_008367.2:325
Il4	NM_021283.1:345

HUGO Gene	NSID
Itgae	NM_008399.2:3108
Jun	NM_010591.2:2212
Tlr2	NM_011905.2:255
Tlr4	NM_021297.2:2510
Mmp1a	NM_032006.3:954
Mmp2	NM_008610.2:2376
Mmp3	NM_010809.1:1575
Mmp7	NM_010810.4:350
Mmp9	NM_013599.2:1570
Mmp14	NM_008608.3:554
Timp1	NM_011593.2:436
Timp3	NM_011595.2:2460
Vegfa	NM_001025250.3:3015
Tek	NM_013690.2:3580
Lrp5	NM_008513.3:1680
Lrp6	NM_008514.3:3315
Myc	NM_010849.4:630
Bcl2	NM_009741.3:1844
Traf2	NM_009422.2:1334
Bax	NM_007527.3:735
Bak1	NM_007523.2:470

HUGO Gene	NSID
Mapk8	NM_016700.3:970
Bcl2l11	NM_001284410.1:236
Bad	NM_007522.3:1146
Bbc3	NM_133234.1:1461
Bid	NM_007544.3:1307
Myd88	NM_010851.2:1595
Traf6	NM_009424.2:980
Mapk14	NM_001168513.1:114
Kcnn4	NM_008433.4:275
Calca	NM_007587.2:221
Hmox1	NM_010442.2:610
Ido1	NM_008324.1:521
Lgals1	NM_008495.2:40
Lgals3	NM_001145953.1:1005
Lgals9	NM_010708.1:355
Fcer2a	NM_001253737.1:1770
Osmr	NM_011019.3:395
Il6ra	NM_010559.2:2825
Il6st	NM_010560.2:2325
Arg1	NM_007482.3:626
Arg2	NM_009705.2:249

HUGO Gene	NSID
Mrc1	NM_008625.1:3992
Il13	NM_008355.2:425
Cxcl17	NM_153576.2:0
Tnfsf13b	NM_033622.1:225
Grem1	NM_011824.4:1085
Stat3	NM_213659.2:2130
Tgfbr1	NM_009370.2:4425
Sh3glb1	NM_019464.2:1060
Becn1	NM_019584.3:1145
Nos2	NM_010927.3:3715
Itgam	NM_001082960.1:3025
Itgax	NM_021334.2:327
Emr1	NM_010130.1:995
Cd68	NM_009853.1:636
Ly6g	XM_909927.2:91
Il15	NM_008357.2:854
Il21	NM_021782.2:230
Il22	NM_016971.1:477
Il23a	NM_031252.1:360
Nod1	NM_172729.2:1446
Nod2	NM_145857.2:2890

HUGO Gene	NSID
Nlrp3	NM_145827.3:2745

Supplementary Figure 1

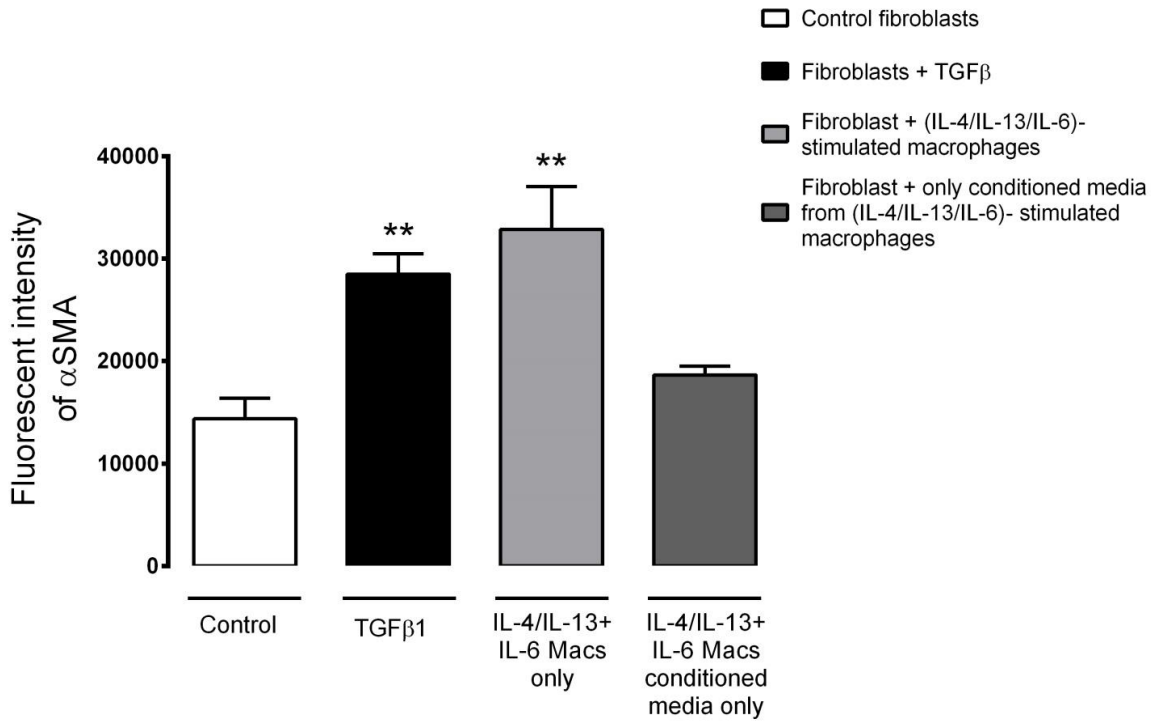

Supplementary Figure 2

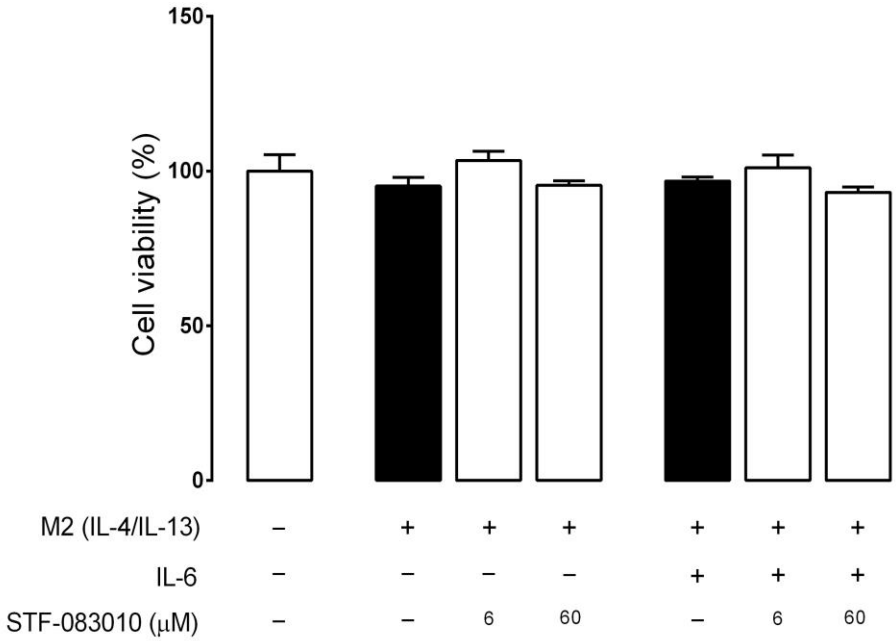

Supplementary Figure 3

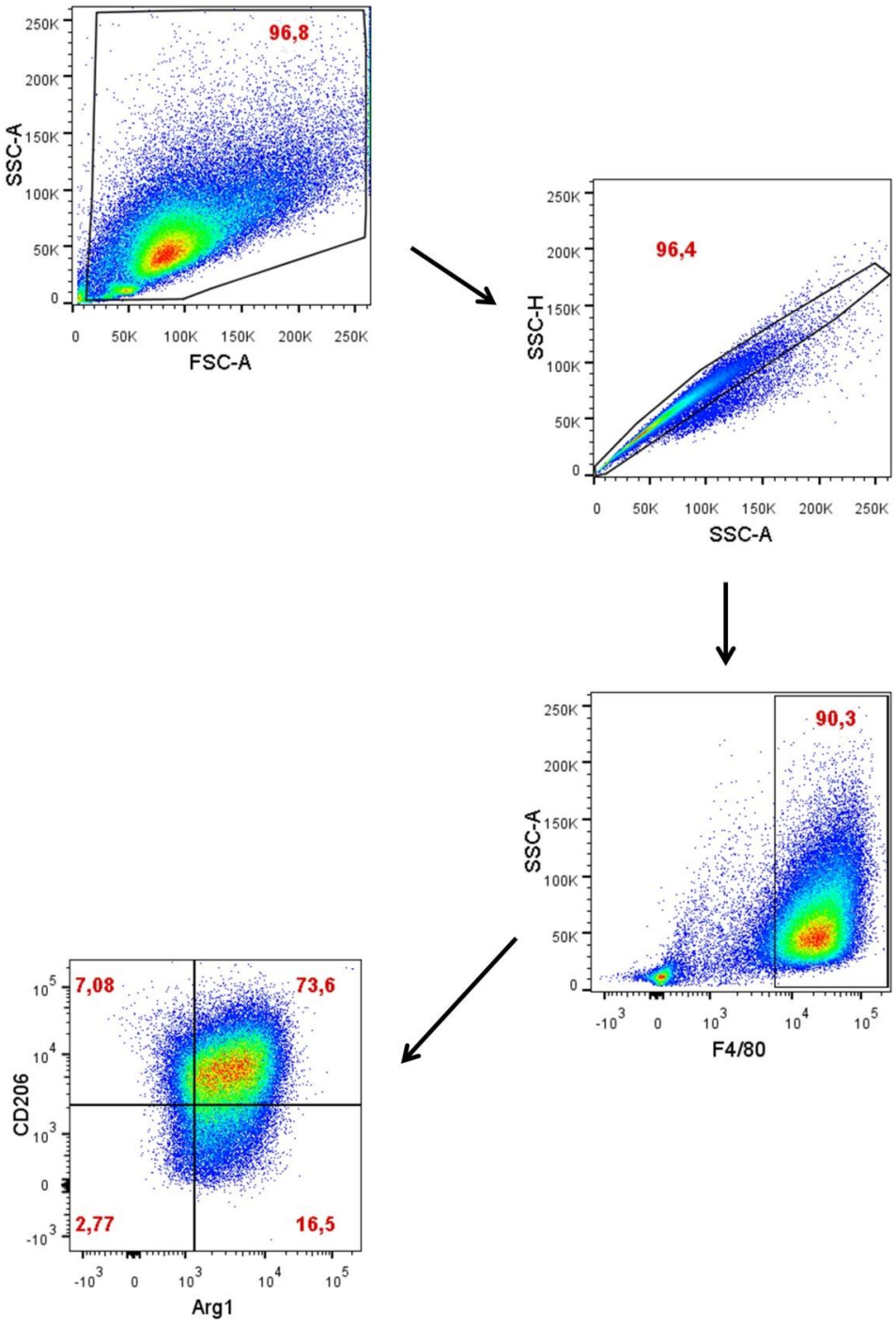

Supplementary Figure 4

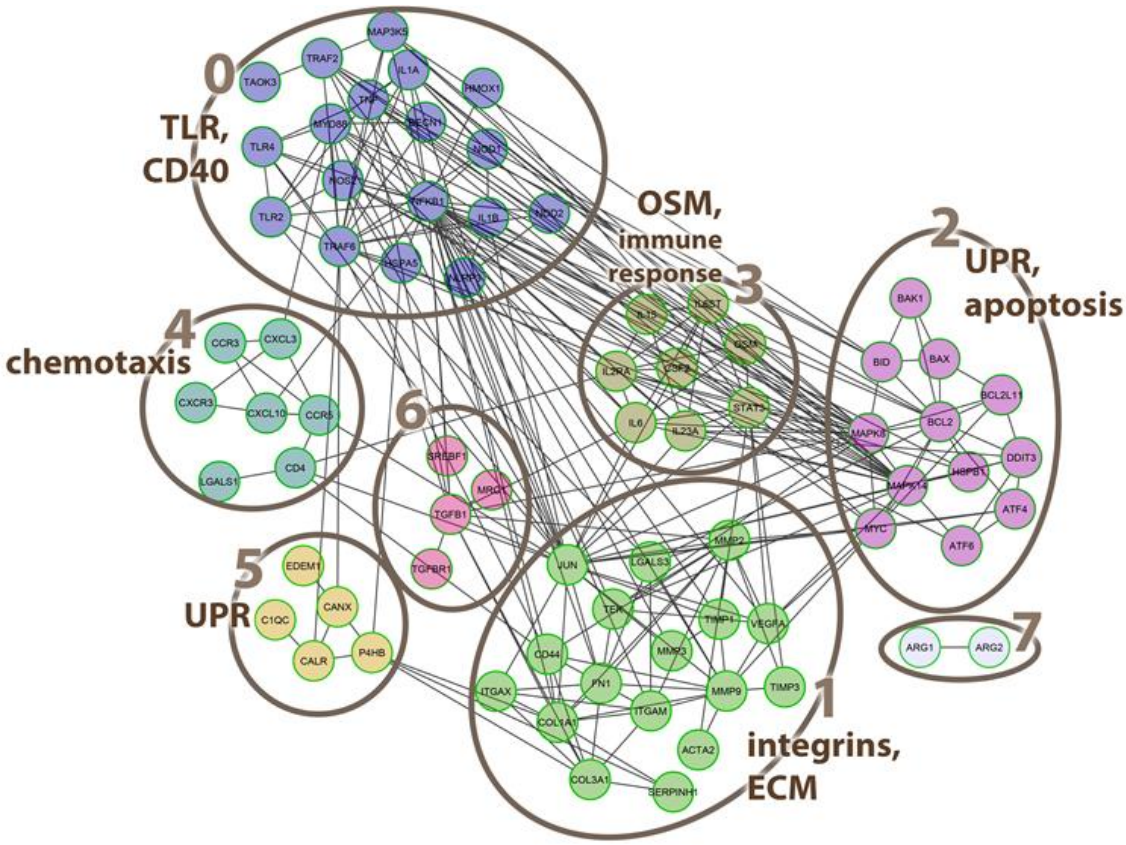

Chapter 4

Overexpression of OSM and IL-6 impacts the polarization of pro-fibrotic macrophages and the development of bleomycin-induced lung fibrosis

Summary and Significance

The increased accumulation of pro-fibrotic M2 macrophages has been associated with the pathogenesis of IPF and accelerated disease progression, demonstrating an urgent need to understand the mechanisms contributing to M2 macrophage programming and their role in fibrosis. Here, we have examined the role of gp130 cytokines IL-6 and Oncostatin M (OSM) in macrophage activation and their effect on bleomycin-induced pulmonary fibrosis. We hypothesized that exposure to IL-6 and OSM would enhance M2 macrophage programming *in vivo* and be associated with increased fibrotic disease severity. Our findings indicated that overexpression of IL-6 or OSM augmented ECM deposition and myofibroblast accumulation, which coincided with increased lung stiffness and differential regulation of chemokine mediators. These findings were mirrored by enhanced expression of well-known M2 macrophage markers, arginase-1 and CD206. To further support the M2 macrophage involvement, we immunophenotyped bleomycin-injured lungs at the inflammatory phase. As a result, the data demonstrated elevated levels of different M2 subtypes in response to bleomycin exposure with either IL-6 or OSM. Additional investigation into the mechanism of polarization demonstrated a direct action of IL-6, but not OSM, in potentiating the pro-fibrotic phenotype of M2 macrophage. These findings suggest a novel action of the gp130 cytokines, IL-6, and

OSM, in skewing macrophages towards an M2 phenotype and exacerbating the fibrotic lung disease. This study suggested that therapeutic strategies targeting these cytokines or their receptors may be beneficial in preventing the accumulation of M2 macrophages in pulmonary fibrosis and other M2-mediated diseases.

Overexpression of OSM and IL-6 impacts the polarization of pro-fibrotic macrophages and the development of bleomycin-induced lung fibrosis

Ehab A Ayaub[1,2], Anisha Dubey [2], Jewel Imani [1,2], Fernando Botelho [2], Martin RJ Kolb [1], Carl D Richards[2], Kjetil Ask *[1,2]

1. *Department of Medicine, Firestone Institute for Respiratory Health, McMaster University and The Research Institute of St. Joe's Hamilton, Hamilton, ON, Canada*
2. *Department of Pathology and Molecular Medicine, McMaster Immunology Research Centre, McMaster University, Hamilton, ON, Canada*

***Corresponding author:** Dr. Kjetil Ask, Department of Medicine, McMaster University and The Research Institute of St. Joe's Hamilton, Firestone Institute for Respiratory Health, Luke Wing, Rm L314-5, 50 Charlton Ave East, Hamilton, Ontario, Canada L8N 4A6, Ph. (905) 522 1155 ext. 33683; Fax (905) 521 6183; E-mail: askkj@mcmaster.ca

Running title: The role of OSM and IL-6 axis in lung fibrosis

This work was funded partly by the Canadian Institute of Health Research (CIHR; Grant No. 137013) and the Ontario Thoracic Society (Canadian Lung Association) awarded to KA and CDR. EAA is funded by the Canadian Institute of Health Research (CIHR; Grant No. 140358). AA is funded by Ontario Graduate Scholarships (OGS) and by Eva Eugenia Lillian Cope Graduate scholarship.

ABSTRACT

Although recent evidence indicates that gp130 cytokines, Oncostatin M (OSM) and IL-6 are involved in alternative programming of macrophages, their role in lung fibrogenesis is poorly understood. Here, we investigated the effect of transient adenoviral overexpression of OSM or IL-6 in mice during bleomycin-induced lung fibrosis.

Lung fibrosis and M2-like macrophage accumulation were assessed by immunohistochemistry, western blotting, gene expression and flow cytometry. *Ex-vivo* isolated alveolar and bone marrow-derived macrophages were examined for M2-like programming and signalling. Airway physiology measurements at day 21 demonstrated that overexpression of OSM or IL-6 exacerbated bleomycin-induced lung elastance, consistent with histopathological assessment of extracellular matrix and myofibroblast accumulation. Flow cytometry analysis at day 7 showed increased numbers of M2-like macrophages in lungs of mice exposed to bleomycin and OSM or IL-6. These macrophages expressed the IL-6Rα, but were deficient for OSMRβ, suggesting that IL-6, but not OSM, may directly induce alternative macrophage activation.

In conclusion, the gp130 cytokines IL-6 and OSM contribute to the accumulation of profibrotic macrophages and enhancement of bleomycin-induced lung fibrosis. This study suggests that therapeutic strategies targeting these cytokines or their receptors may be beneficial to prevent the accumulation of M2-like macrophages and the progression of fibrotic lung disease.

Keywords: gp130 cytokines, Interleukin 6, Oncostatin M, macrophage polarization, pulmonary fibrosis

INTRODUCTION

Interstitial fibrotic lung diseases are characterized by excessive tissue remodelling and accumulation of extracellular matrix (ECM)[1-6], leading to a progressive loss of function. Although intensive research over the past few decades have led to increased understanding of the pathobiology of lung fibrosis and the first approvals of antifibrotic drugs[7], the cellular and molecular mechanisms involved in the variable progression of fibrosis in patients diagnosed with lung fibrosis are still unclear. The accumulation of myofibroblasts that synthesize and deposit ECM is a hallmark feature of fibrotic lung disease[8-10]. Although it is poorly understood how myofibroblasts differentiate in the lung parenchyma, recent data suggest that alternatively activated macrophage (AAMs) may be critical in the myofibroblast transformation process[11-15].

Gp130 cytokines, also referred to as the IL-6 family, are involved in various inflammatory and immunoregulatory mechanisms. They elicit their cellular effects by binding to specific receptor complexes that include the signal transducing molecule, glycoprotein 130 (gp130) and play a critical role in various cellular processes such as cell differentiation, proliferation, and hematopoiesis[16-19]. *In vivo*, hyper-activation of the gp130/STAT3 signalling pathway (following genetic manipulation) causes excessive pulmonary fibrosis in murine models and occurs independently of the canonical TGFβ/SMAD3 signalling pathway[20]. Concerning macrophage polarization, IL-6 has recently been shown to induce an alternatively activated phenotype in macrophages derived from adipose tissue by enhancing IL-4Rα expression and augmenting the IL-4

response[21]. Additionally, Komori *et al* (2015) demonstrate that OSM facilitates M2 programming *in vitro* using adipose tissue-derived macrophages[22]. Moreover, OSM has previously been shown to induce IL-6 cytokine expression *in vivo*, following OSM overexpression in murine models[23]. Recently, cellular response to OSM was associated with enhanced IL-6 production and worse outcomes in inflammatory bowel disease[24], providing a point of convergence to induce IL-6-mediated signalling and rationalizes the implication of these two cytokines in driving pathological wound repair processes. In this study, we utilized an adenovirus over-expression system to assess the effects of OSM and IL-6 on bleomycin-induced lung injury and fibrosis in C57BL/6 mice. Our results demonstrate that over-expression of OSM (AdOSM) or IL-6 (AdIL-6) *in vivo* is associated with alternative macrophage accumulation and an increased fibrogenic response to bleomycin. This data suggests that targeting both gp130 cytokines and alternative programming of macrophages may be a viable strategy to prevent lung fibrogenesis.

METHODS

Animals and administration of bleomycin and adenoviral vectors

8-12 week wild type female C57BL/6 mice were purchased from Charles River Laboratories and housed in the Central Animal Facility. The animals were kept on a 12 h light/12 h dark cycle at a temperature of 20–25°C, humidity of ~50% and fed *ad libitum*. All work was conducted under the guidelines of the Canadian Council on Animal Care and approved by the Animal Research Ethics Board of McMaster University under Protocol #160414. Transient overexpression of OSM or IL-6 was achieved using adenovirus expression vectors, AdOSM and AdIL-6. Vector construction and validation were performed in-house based on previously published work[25-27]. Briefly, mice were anaesthetized under gaseous isoflurane while AdOSM ($2x10^7$ pfu/mouse) and AdIL-6 ($1x10^7$ pfu/mouse) was intratracheally administered in a volume of 50µl sterile saline. Control mice received an empty control vector, AdDL70 ($2x10^7$ pfu/mouse). Experimental pulmonary fibrosis was induced using intratracheal intubation of bleomycin (Hospira Healthcare Corp., NDC 61703-332-18) at 0.03 U/mouse in a volume of 50µl sterile saline. Bleomycin was either given alone or with AdOSM, AdIL-6 or AdDL70. The mice were then sacrificed after 7 days (injury phase) and 21 days (fibrotic phase).

Airway Physiology measurements

Quasi-static lung elastance was measured using a rodent mechanical ventilator (flexiVent®, SCIREQ, Montreal, PQ, Canada) as described earlier[15].

Collection of mouse specimens

Mice were anesthetized with gaseous isoflurane and exsanguinated by surgically severing the descending aorta. The trachea was cannulated, the lung excised and washed with phosphate-buffered saline (600µl per mouse) for broncheoalveolar lavage fluid (BALF) collection and analysis. The four lobes of the right lung were tied up with a surgical thread, excised and either placed in cold DMEMF12 media or frozen in liquid nitrogen. These lobes were enzymatically digested to generate a single cell suspension and subsequently stained for flow cytometry. The frozen lobes were subjected to protein and RNA isolation assays. The left lung was removed and inflated with 10% neutral buffered formalin solution under a pressure of 30 cmH_2O. The lungs were fixed for 48–72 hours before histological analysis.

Homogenization of lung tissues

The snap-frozen right lobes of the excised lungs were placed into a stainless-steel mortar and crushed into a fine powder with a stainless-steel pestle while submerged in liquid nitrogen. Approximately one-third of each finely ground lung tissue was placed in 1 ml of TRIzol reagent (Invitrogen, cat# 15596-026), with two-thirds being placed into 1 ml (RIPA) lysis buffer supplemented with protease inhibitors (1× PBS, 1% IGEPAL CA-130, 0.5% Na-deoxycholate, 0.1% SDS and 1mM Na-orthovanadate, 5 µg/ml aprotinin, 1mM phenylmethylsulphonylfluoride and 1mM dithiothreitol). The powdered lungs in the lysis buffer and TRIzol solutions were then mechanically sheared using a homogenizer (Ultra-Turrax® T25) and later processed for protein and RNA work.

Western Blotting

Protein concentration of lung homogenates or cell lysates was measured by Bradford Assay (Bio-Rad). Samples were prepared with 15 or 20ug of total protein, ddH_2O and 5x loading dye, for a final volume of 20uL. 4-20% Tris-Glycine Sodium deoxysulfate-polyacrylamide gels (SDS-PAGE) were prepared fresh and used immediately or stored at 4°C overnight. Samples were loaded onto gels and run at 95V for 12 minutes, then at 120V for 1 hour by electrophoresis. Protein was then transferred onto nitrocellulose membranes at 400 mA for 1 hour. Blocking buffer (1:1 TBS: Odyssey blocking Buffer) was added to membranes for 1 hour at room temperature. Following blocking, primary antibodies including mouse anti-arginase-1 (BD Biosciences, cat# 610708), rabbit anti-pSTAT3 (Cell Signaling, Cat# 9145), rabbit anti-total STAT3 (Cell Signaling, Cat# 4904), rabbit anti-pSTAT6 (Cell Signaling, Cat# 9361), rabbit anti-total STAT6 (Santa Cruz Biotechnology, Cat# sc-981) and goat anti-actin (Santa Cruz Biotechnology, Cat# sc-1616) were added to blots overnight at 4°C. Blots were then washed using TBS+ 0.15% Tween-20, and secondary antibodies (donkey anti-goat (Mandel Scientific, Cat# LIC92668074), Donkey anti-rabbit (Mandel Scientific, Cat# LIC92632213), or Donkey anti-mouse (Mandel Scientific, Cat# LIC92632212)) were added for 45 minutes, away from light. Blots were then imaged using Odyssey LI-COR® Imaging technologies. Quantification of protein signals were measured by densitometry using Image Studio Lite Ver 5.2.

Immunohistochemistry

Immunohistochemistry was performed at McMaster's Histology Core Facility as previously described[15]. Briefly, formalin-fixed tissues were cut at 5 µm sections and

stained with Masson's trichrome for ECM, anti-αSMA (Dako, cat# M0851) for the identification of αSMA-positive myofibroblasts and anti-fibronectin (Abcam, cat# ab2413) for the assessment of pro-fibrotic factors. Lung tissue sections were also stained with anti-arginase-1 (BD Biosciences, cat# 610708) for the identification of alternatively activated macrophages. We used the Dako ARK^{TM} (Animal Research Kit) Peroxidase (cat# K3954) to execute immunohistochemical stains involving mouse primary antibodies on mouse lung tissues. As for tissues that contain endogenous biotin (such as liver and kidney and other tissues), a step involving avidin/biotin block (Vector Laboratories, cat# SP2001) was conducted prior to immunohistochemical staining of the lung tissues. Diluent and IgG negative controls as well as non-treated tissue controls were included to ensure precision of the staining protocol and optimal antibody concentrations.

Immunofluorescence

Immunostaining of arginase-1 was performed on BALF cellular infiltrates mounted on cytospin slides. Briefly, BALF cells were first fixed in 4% paraformaldehyde solution, followed by permeabilization with 0.1% Triton X-100 PBS solution and subsequent blocking with 5% BSA solution. Cells were then incubated with anti-arginase-1 antibody (BD Biosciences, cat# 610708) for 1 hour before the application of a secondary antibody (Donkey anti-mouse Alexa 488 (Abcam, Cat# Ab150105) for 30 minutes. Slides were mounted in Prolong-gold/ DAPI before imaging.

Acquisition and analysis

Microscope slides were digitalized using an Olympus VS120-L100-W slide scanner microscope, and subsequent images were acquired to illustrate representative areas. Semi-

quantitative assessment of the severity of fibrosis using the Ashcroft grading procedure was performed based on Masson's trichrome staining, as described previously[15]. For αSMA, the main bronchus and larger airways were excluded by ImageJ. For both arginase-1 and αSMA, once thresholding was applied to specifically display the stained regions, the analyze particle function was then used to determine the total area of the stained regions. Image analysis was performed on image J to demonstrate the percentage of arginase-1 and αSMA staining normalized to the whole tissue area.

Lung single cell isolation and purification

Following sacrifice, the lungs were isolated, minced into small pieces and digested with 150 U/ml collagenase type I (Gibco, Cat# 17100-017) in warm DMEMF12 media for 1 h at 37°C with agitation. The digested lung pieces were then pushed through a 45 µm filter (BD Falcon) and the single cell suspension was treated with ACK lysis buffer for 1-2 min at 4^{o}C to lyse all erythrocytes. Lung cells were subsequently suspended in media and total number of viable cells and percent viability was determined using the Countess automated cell counter (Invitrogen).

Flow cytometry

Approximately $2x10^{6}$ viable lung cells or bone marrow derived macrophages were suspended in cell staining buffer (0.3% BSA in PBS). Non-antigen-specific binding of immunoglobulins to Fcγ II/III receptor on lung cells was blocked using purified rat anti-mouse CD16/32 antibody (Mouse FC Block) (BD Pharmingen, Cat# 553142). Next, lung cells were subjected to surface antibody staining solution, containing a mix of anti-mouse

CD45 (APC-Cy7, Biolegend, Cat#103116), anti-mouse CD206 (MMR) (BV650, Biolegend, Cat# 141723), anti-mouse CD11b (PE, eBiosciences, Cat# 12-0112-81) and anti-mouse F4/80 (BV605, Biolegend, Cat# 123133). BMDMs were stained with anti-mouse CD206, anti-mouse F4/80 and anti-mouse CD124 (IL-4Rα) (PE, BD Pharmingen, Cat# 552509). All cells were then fixed and permeabilized using a BD Cytofix/Cytoperm kit (BD Biosciences, Cat# 554722) prior to performing intracellular staining with anti-mouse/human arginase-1 (APC, R&D Systems, Cat# IC5868A) suspended in 1x BD Perm/Wash buffer solution (BD Biosciences, Cat# 554723). Cells were finally suspended in cell staining buffer for flow cytometry and data was collected using a BD LSRFortessa^{TM} and FACSDiva software from BD Biosciences. Data were analyzed using FlowJo vX Software from Treestar.

Murine alveolar macrophages isolation

Following exposure to the above conditions, lungs were harvested and BALF was collected as described above. Collected cells were then cultured in Dulbecco's Modified Eagle Medium (F12) containing 10% Fetal Bovine Serum. After 40 minutes in culture, adherent cells were selected by washing the non-adherent cell population. Macrophage-enriched cells were then lysed and RNA was isolated for nanoString gene expression analysis.

Isolation and alternative activation of bone marrow-derived macrophages

Bone marrow-derived macrophages (BMDMs) were isolated and cultured as described previously[15]. Briefly, bone marrow cells from wild type C57BL/6 mice were isolated

from the tibias and femurs and treated with 20 ng/ml of recombinant mouse macrophage colony stimulating factor (Murine M-CSF, PeproTech Canada) for 7 days. After 7 days, bone marrow derived macrophages were treated for either 18 or 30 hours with recombinant IL-4 (20 ng/ml), IL-13 (50 ng/ml), alone, or in combination with OSM (50 ng/ml) or IL-6 (50 ng/ml) (PeproTech Canada). Alternative activation of macrophages was assessed in the cell lysate by measuring arginase-1 protein by western blotting and by arginase-1 and CD206 by flow cytometry. In some instances, BMDMs were lysed and RNA was isolated for NanoString gene expression analysis.

Arginase assay

The arginase assay was adapted and optimized from a previously established protocol[23]. Following the seeding of BMDMs (80,000 cells/per well of a 96-well plate) and their subsequent stimulation with the above cytokine cocktails, supernatant was collected and cells were washed twice with ice-cold PBS. Next, cells were lysed in 25-100 µl of 0.1% Triton X-100 supplemented with protease inhibitors (200 mM sodium orthovanadate, 0.1 M PMSF, 1 M DTT and 5 µg/ml and bovine lung aprotinin). A 1:1 dilution with 25 mM of Tris-HCl (pH 7.5) was later performed. 25 µl of this mixture was transferred to a 96-well PCR plate, with the addition of 2.5 µl of 10 mM manganese chloride. The PCR plate was then placed in a thermal cycler programmed to heat at 56 degrees Celsius for 10 minutes. Afterwards, 25 µl of 0.5 M L-arginine was mixed with the pre-heated mixture and the entire plate was then re-incubated at 37 degrees Celsius for 30 minutes. An eight-point urea standard curve was then established (0 to 15 mM). 200 µl of acid solution (63.6% water, 9.1% concentrated sulphuric acid and 27.3% concentrated phosphoric

acid), followed by 10 µl of 9% alpha-isonitrosopropiophenone, were added to both samples and the urea solutions. The contents of each well were mixed thoroughly and the plate was incubated at 95 degrees Celsius for 30 minutes, followed by 10 minutes of cooling at 20 degrees Celsius. 150-200 µl of each sample was removed and placed in a new, clear, flat bottom, 96-well plate for absorbance reading at 550 nm.

RNA isolation and nanoString gene expression

RNA was isolated from adhered alveolar macrophages and BMDMs using NucleoSpin RNA plus (Macherey Nagel, Cat# 740984.250). Here, we used a nanoString custom designed panel focusing on selected genes including Il4ra, Arg1, Ccl2, Il6ra, Timp1, Osmr, Col1a1, Col1a3, Fn1, Mrc1. Analysis of raw mRNA counts was performed using nSolver v2.6. Background subtraction was performed using geometric mean of negative controls, followed by normalization to geometric mean of positive controls. Results were analyzed and normalized to housekeeping genes (Actb, Pgk1, Ppia and Ywhaz) and with the nanoString total counts method as described in the nCounter Expression Analysis Guide, producing similar results. Gene expression data is here shown as normalized to total counts.

GEO database analysis

Publically available dataset containing *Osmrβ* expression profiles of monocyte/macrophage populations were obtained Misharin *et. al*[28]. Briefly, following bleomcyin administration, wild type C57BL6 (Casp8flox/flox) mice were sacrificed after 14 and 19 days and lung cells were flow-sorted to isolate monocytes, interstitial macrophages, and alveolar macrophages (distinguished by high or low expression of

Siglec F). For naïve mice, Siglec F high Alveolar macrophages were isolated. Normalized counts were log2-transformed, and then the distribution of the Osmr Log2-normalized counts was compared to the distribution of Log2-normalized counts pooled across all genes and all samples. Plots were built by using R environment.

ELISA and Multiplex analysis of mediators

BALF total TGFβ1 was measured using a commercially available ELISA, according to the manufacturer's protocol (R&D Systems, Cat# DY1679). We also quantified 32 different mediators in the BALF and cell culture supernatant by using a Discovery Assay® (Mouse Cytokine and Chemokine Array 32-Plex, Eve Technologies Corp, Calgary, AB, Canada). The multiplex assay was performed at Eve Technologies using the Bio-Plex™ 200 system (Bio-Rad Laboratories, Inc., Hercules, CA, USA) and a Milliplex Mouse Cytokine/Chemokine kit (Millipore, St. Charles, MO, USA) according to Evetech protocol. The 32-plex consisted of eotaxin, G-CSF, GM-CSF, IFN-γ, IL-1α, IL-1β, IL-2, IL-13, IL-4, IL-5, IL-6, IL-7, IL-9, IL-10, IL-12 (p40), IL-12 (p70), IL-13, IL-15, IL-17, IP-10, KC, LIF, LIX, MCP-1, M-CSF, MIG, MIP-1α, MIP-1β, MIP-2, RANTES, TNFα, and VEGF. The assay sensitivities of these markers range from 0.1 pg/ml to 33.3 pg/ml. Individual analytes' values and other assay details are available on Eve Technologies' website and in the Milliplex protocol.

Sircol Collagen Assay

Following lung homogenization, the supernatant from the homogenized lung tissues in RIPA buffer was used to assess soluble lung collagen content, according to the manufacturer's instructions (Sircol^{TM} Soluble Collagen Assay, Biocolor, UK).

Statistical analysis

Results are expressed as mean ± SEM. A one-way analysis of variance (One-way ANOVA) followed by Newman-Keuls multiple comparison test was used to determine significance when more than two groups were compared. A student's t-test was used to determine significance between two conditions. All statistical tests were performed using GraphPad Prism 7.0c (GraphPad Software, Inc). A $p<0.05$ was considered statistically significant.

Data availability: The datasets generated during and/or analysed during the current study are available from the corresponding author on reasonable request.

RESULTS

Overexpression of OSM and IL-6 intensifies bleomycin-induced lung fibrosis

To determine the effects of OSM and IL-6 on bleomycin-induced lung fibrosis, wild-type C57BL/6 mice were intratracheally administered adenovirus control vector or adenovirus encoding OSM or IL-6 to induce transient overexpression of OSM or IL-6, alone or in combination with bleomycin (0.03U/mouse). The BALF was collected after 7 and 21 days and assessed for either OSM or IL-6 by ELISA. As expected, we observed elevated levels of IL-6 (**Figure 1A**) and OSM (**Figure 1B**) in the BALF of mice treated with AdIL-6 or AdOSM, respectively, confirming consistent vector administration and cytokine overexpression. Mice treated with AdOSM alone or in combination with bleomycin showed elevated levels of IL-6 in the BALF, compared to AdDL70, confirming OSM induction of IL-6 as previously shown[23]. Both IL-6 and OSM levels were undetectable in BALF during the fibrotic phase (day 21) of the bleomycin-induced injury model (data not shown). After 21 days, the assessment of quasi-static lung elastance (Est) revealed that both AdOSM and AdIL-6 addition to bleomycin resulted in a significant increase in elastance as compared to control vectors (AdDL70) and to the adenoviral vectors AdOSM and AdIL-6 alone (**Figure 1C**). As shown in Figure 1C, the administration of bleomycin alone resulted in a similar response to bleomycin plus control vector (AdDL70). Therefore, all further experiments were conducted with AdDL70 as a control. The increase in lung stiffness was associated with increased c*ollagen content* (**Figure 1D**) and Ashcroft fibrotic score based on Masson's Trichrome staining **(Figure 1E)**. Histological examination confirmed increased deposition of ECM

(Masson's Trichrome) and accumulation of alpha smooth muscle actin (αSMA) positive myofibroblasts in the lung parenchyma (**Figure 1F)** of mice exposed to bleomycin and AdOSM and AdIL-6. By excluding large airways and blood vessels, digital analysis of αSMA confirmed enhanced parenchymal αSMA (Please see supplementary material, Figure 1). Overall, these findings suggest that the overexpression of OSM and IL-6 results in an increased fibrotic response to bleomycin.

Elevation of OSM and IL-6 lead to differential regulation of soluble mediators during bleomycin-induced lung injury

To investigate how OSM and IL-6 overexpression led to the increased fibrogenic response in bleomycin-induced fibrosis, we assessed pro-fibrotic and inflammatory mediators in the broncheoalveolar fluid (BALF) at day 7 after the administration of bleomycin and the adenovectors. Total TGFβ1 and G-CSF were increased in the lungs of mice exposed to both bleomycin plus AdOSM or AdIL-6 **(Figure 2A-B).** In contrast, even though bleomycin caused a general increase in monokine-induced by gamma-interferon (MIG), interferon-gamma inducible-protein-10 (IP-10) and monocyte chemoattractant protein-1 (MCP-1/CCL2), mice receiving both bleomycin and AdIL-6 had an enhanced level of increase in these mediators (**Figure 2C-2E**), suggesting a selective capacity of IL-6 in their regulation. Even though leukemia inhibitory factor (LIF) was increased in response to bleomycin challenge, it was not further modulated by OSM or IL-6 overexpression **(Figure 2F)**. All other mediators assessed were below the threshold limit of detection (not shown). Overall, these findings indicate that OSM and IL-6 over-expression leads to a differential induction of inflammatory chemokines during

bleomycin-induced lung injury, suggesting that their individual fibrogenic properties might be different.

OSM and IL-6 enhance the induction of markers associated with alternative programming of macrophages

As both IL-6 and OSM have been reported to influence alternative programming of macrophages, we next examined the presence of AAM in lungs of mice exposed to bleomycin plus OSM or IL-6 adenoviral vectors. As expected, 7 days after administration, at the peak of adenoviral expression, increased levels of phospho-STAT3 were observed in total lung homogenates **(Figure 3A)**, confirming activation of the STAT3 pathway by overexpressed IL-6 or OSM in absence of bleomycin. This activation was not associated with a marked increase in arginase-1 expression **(Figure 3A)**, as opposed to lungs exposed to bleomycin plus AdOSM or AdIL-6 **(Figure 3B)**. Interestingly, the overall levels of pSTAT3 were not maintained in total lung homogenates exposed to both bleomycin and adenoviral control vectors, suggesting that the activation of the STAT3 pathway was not altered at this time-point **(Figure 3B)**. For full-length pictures of western blots, please see supplementary Figure 6-9. To specifically examine the presence of AAMs in this model we proceeded with an immunohistochemical analysis of lungs exposed to adenoviral vectors alone or in combination with bleomycin at the same time-point. As observed on western blots in Figure 3A, arginase-1 positive cells were not present in lungs exposed to the control vector or by AdOSM and AdIL-6 expression alone **(Figure 3C)**. The specificity of the arginase-1 antibody was confirmed by the use of IgG (negative control) and positive

controls (see supplementary material, Figure 2). The addition of bleomycin resulted in the appearance of multiple arginase-1 positive macrophage-like cells **(Figure 3C)**. The quantification of the percentage of arginase-1 positive stain **(Figure 3D)** in left lungs showed virtually identical outcome as the western blot observation noted above. These findings were also consistent with mRNA assessment of Arginase 1 from the corresponding right lungs **(Figure 3E)**, confirming the presence of alternative programming of macrophages in lungs exposed to bleomycin plus AdOSM or AdIL-6. We then examined arginase expression on macrophages isolated from lungs by flow cytometry.

Increased accumulation of CD206+Arg1+ macrophages in response to OSM and IL-6 during bleomycin-induced lung injury

The expression of CD206 and arginase-1 were assessed on lung-derived macrophages by flow cytometry at day 7, as both CD206 and arginase-1 expression peaks during the injury phase of the bleomycin[29,30]. In addition to anti-CD206 and anti-arg1, we included anti-CD45, anti-CD11b and anti-F4/80 to further characterize the AAM population. A total number of viable cells and the frequency of the population of interest was used to extrapolate absolute numbers. Consistent with the immunohistochemical assessment of arginase-1 positive cells described above, an increase of CD206+Arg1+ macrophages were found in lungs exposed to bleomycin plus AdOSM or AdIL-6 **(Figure 4A)**. Gene expression and immunofluorescence assessment of macrophages isolated from the alveolar spaces indicated that mice exposed to both IL-6 and bleomycin had increased levels of *arginase-1* mRNA (**Figure 4B**) and protein (**Figure 4C**) as compared to mice

receiving control vector only. As it was recently shown that IL-6 mediates alternative activation of macrophages through the induction of *Il-4rα*[21], we confirmed that *Il-4rα* gene expression was increased in alveolar macrophages (AMs) derived from AdIL-6 exposed lungs at Day 7 (**Figure 4D**). Of note, mice receiving AdIL-6 alone did not show arginase-1 positive cells (data not shown).

IL-6, but not OSM, directly acts on macrophages to induce M2 macrophage activation

To further investigate the molecular mechanisms involved in the alternative programming of macrophages, we resorted to using bone marrow-derived macrophages for the following reasons. a) primary alveolar macrophages do not have the capacity to polarize *in vitro* (data not shown); b) alternatively activated pro-fibrotic macrophages were recently shown to originate from the bone marrow[31]. Figure 5A shows a 5.7-fold increase in arginase activity when IL-6 is added to the conventional alternative programming cocktail, IL-4 and IL-13, which resulted in a 2.5-fold increase compared to non-stimulated cells. The administration of IL-6 alone did not have any effect on polarization in this assay. Importantly, the increased arginase activity was associated with increased levels of CD206+Arg1+ cells, as assessed by flow cytometry **(Figure 5B)**. These data were consistent with the findings in lungs of mice exposed to bleomycin plus IL-6 shown above. We then assessed their ability to express IL-4Rα. IL-6 alone, or in combination with IL-4/IL-13, increased IL-4Rα expression on CD206+Arg1+ macrophages **(Figure 5C-5D)**. To further examine the mechanism associated with IL-6 and OSM signalling, we stimulated BMDMs with IL-4/IL-13, alone or in combination with OSM or IL-6 for 18

hours and assessed STAT3 activation. Cell lysates were probed for arginase-1, phosphorylated STAT6 and phosphorylated STAT3 by Western Blot (**Figure 5E**). Arginase-1 and phospho-STAT6 were induced in BMDMs following stimulation with IL-4/IL-13 (**Figure 5E- 5G**). These results are consistent with previous studies demonstrating that Th2 cytokines, IL-4/IL-13, can activate the STAT6 pathway and induce an M2 macrophage phenotype[32-34]. Interestingly, IL-6 in combination with IL-4 and IL-13, (but not IL-6 alone) lead to robust increase in arginase-1 protein signal (**Figure 5E and 5G**). These findings demonstrate the capacity of IL-6 to enhance the M2 macrophage polarization process. Activation of the STAT3 pathway was also observed by BMDMs stimulated with IL-6, but not OSM, suggesting that IL-6 may directly activate these cells (**Figure 5E and 5H)**. For full-length pictures of western blots, please see supplementary Figure 10-12. The inability of OSM to augment phospho-STAT3 production in the BMDMs was consistent with mRNA data demonstrating differential receptor expression **(Figure 5I)**. The mRNA for the IL-6 receptor, *Il-6rα,* was highly expressed in control unstimulated BMDMs and AMs, while mRNA counts for the OSM receptor (*Osmr*) were below the detection limit. Of note, when we looked at *Il-6rα* and *Osmr* expression in IL-4/IL-13, IL-4/IL-13/IL-6 stimulated BMDMs as well as bleomycin-exposed AMs, similar results were observed (see supplementary material, Figure 3A, B). To examine Osmrβ expression profile on various macrophage ontology groups within the lung, we used publically available dataset obtained from Misharin *et. al*[28]. The log2-transformed counts demonstrate that Osmrβ was barely expressed on the different macrophage populations within the lung (see supplementary material, Figure

3C). These findings suggest that OSM is likely not acting directly on BMDMs or AMs to induce changes in phenotype.

IL-6 potentiates the pro-fibrotic phenotype of M2 macrophages

To examine the potential pro-fibrotic effect of IL-6 addition to the conventional M2 polarization cocktail (IL-4/IL-13), we performed gene expression analysis of selected pro-fibrotic related genes. Subsequently, we assessed 32 different mediators in the cell culture supernatant using a mouse cytokine/chemokine array. Nanostring gene expression analysis indicated that the addition of IL-6 to IL-4/IL-13 led to a robust increase in the pro-fibrotic related genes fibronectin 1 (*Fn1*), mannose receptor 1 (*Mrc1*), tissue inhibitor of metalloproteinase 1 (*Timp1*) and monocyte chemoattractant protein 1 (*Mcp-1*) **(Figure 6A-6D)**. Of note, both *Col1a1* and *Col3a1* were undetected in the IL-4/IL-13 condition, with or without IL-6 (data not shown). The multiplex array data showed that the assessed pro-inflammatory related cytokines were undetected in IL-4/IL-13/IL-6 exposed BMDM's while secreted MCP-1 was strongly increased, confirming the gene expression data **(Figure 6E)**. While fibronectin staining was absent in the parenchyma in non-bleo exposed tissues, the staining appears to be extracellular (incorporated into the ECM) and intracellular (on macrophage-like cells) in bleomycin exposed samples at day 7 (**Figure 6F**; see also supplementary material, Figure 4). At day 21, the majority of fibronectin staining was observed in the ECM in fibrotic areas (see supplementary material, Figure 5). Of note, in all conditions, fibronectin staining was also seen around the airways and blood vessels, but an additive effect of staining was observed in mice exposed to bleomycin plus AdOSM or AdIL-6 compared bleomcyin plus empty vector. Overall,

these data suggest unique phenotypic differences between IL-4/IL-13 (M2) - and IL-4/IL-13/IL-6- stimulated macrophages and different intensity of fibronectin staining *in vivo*.

DISCUSSION

Overall, we have shown that the gp130 cytokines, OSM and IL-6, potentiate bleomycin-induced lung injury and fibrosis. Overexpression of OSM or IL-6, in combination with bleomycin, resulted in an increase in lung elastance, collagen content and fibrotic score. Additionally, increased expression of these cytokines led to an increase in pulmonary M2-like macrophage accumulation *in vivo*, as demonstrated by induction of arginase-1 and CD206 expression. Our *in vitro* studies indicate that the enhancement of the M2-like phenotype is likely due to a direct activation of membrane-bound IL-6Rα by IL-6 and is associated with the activation of the STAT3 pathway as shown earlier[21], in addition to the required STAT6 pathway activated by IL-4 and IL-13. The ability of IL-6 to directly augment the production of pro-fibrotic factors in the macrophage population suggests a possible *in vivo* pro-fibrotic function of the CD206+Arg1+ macrophage population. Together, these results suggest a novel role of gp130 cytokines signalling in modulating macrophage function and fibrogenesis that may be relevant for patients diagnosed with fibrotic lung disease (please see **Figure 7** for additional illustration an illustration summarizing the results of this study).

Although enhanced levels of OSM and IL-6 have previously been implicated in models of fibrotic disease[35-38], our findings indicate that the overexpression of these cytokines alone (at the doses used) did not contribute to a fibrogenic response. Instead, we propose that bleomycin-induced injury primes the lung to OSM- and IL-6-driven pro-fibrotic functions. In the lungs exposed to either AdIL-6 or AdOSM and bleomycin, the high level of IL-6 that coincided with a marked increase in TGFβ1, could suggest an

intricate crosstalk between the two cytokines as proposed by previous studies[39-41]. For example, it is possible that the high level of BALF IL-6 is augmenting the trafficking of TGFβ1 receptors to the cell surface and is, therefore, enhancing TGFβ1 Smad signalling on fibroblasts. Alternatively, based on other published evidence, it is also possible that TGFβ1 may have acted on fibroblast to mediate endogenous IL-6 release, contributing to enhanced macrophage programming. Although these mechanistic explanations could potentiate TGFβ1 and IL-6 pro-fibrotic effects, further investigations was required to imply a causative role in the pathogenesis of fibrosis. It was evident that a comparable level of induction of M2-like (Arg1+) population was observed in lungs exposed to both cytokines plus bleomycin even though AdOSM-induced levels of IL-6 were found to be almost 10-fold lower than those in mice exposed to AdIL-6. One plausible explanation for this phenotype could be attributed to the ability of OSM to increase IL-4 expression, as we have shown earlier[42]. In the present work, a lower dose of adenovirus vectors was used to induce a significant but limited elevation of cytokines. This change in dose reflects the absence of pathology observed in the AdOSM-treated mice, compared to our previous work[43].

Although M2-like macrophages have been implicated in the fibrotic process, there is still ambiguity on the uniqueness of the markers that can precisely depict the origin and function of pro-fibrotic macrophages. Here we show that increased numbers of CD206+Arg1+ are associated with increased severity of pathology in the lung. However, it is not clear yet if these macrophages stemmed from the circulatory pool and if they are required for fibrogenesis to occur. Although CD206 is considered a marker of M2-like

macrophages and that recently, *Satoh et al.* elegantly demonstrated that bone marrow-derived atypical monocytes expressed CD206 were required for fibrogenesis[31], some reports suggest that naïve AMs may also express CD206[44]. Therefore, we cannot exclude the possibility that some CD206 resident macrophages underwent alternative activation in the bleomycin-exposed lungs, as opposed to increased infiltration of circulatory monocytes that were subsequently activated within the local tissue environment. The role of arginase-1 positive macrophages in fibrogenesis is debated. We showed recently that UPR-mediated apoptosis in the M2-like macrophage population was associated with decreased arginase-1 expression in the lung and complete protection from bleomycin-induced fibrosis[15]. However, Pesce *et. al* elegantly demonstrated that conditional arginase-1 deletion in the myeloid linage resulted in exacerbated *Schistosoma mansoni-induced* fibrosis, questioning the functional role of arginase-1 in the fibrotic process[45]. To have a better understanding of the exact role of CD206+Arg1+ macrophages in lung fibrosis, selective deletion strategies need to be developed and evaluated.

Previous studies have implicated both classical and trans-signalling of IL-6 in mediating the pathogenesis of fibrosis; Thanh-Thuy *et al.*, demonstrated that blockade of IL-6 trans-signalling using the gp130 Fc antagonist attenuates bleomycin-induced lung fibrosis[20,46]. However, only classical signalling, mediated by direct IL-6 activity on membrane-bound IL-6Rα, was responsible for the enhanced alternative activation of macrophages in the presence of IL-4[21]. Our data demonstrate that unlike the OSMRβ, which was undetected on pulmonary macrophages and BMDMs, the IL-6Rα was abundantly expressed. Furthermore, based on the robust ability of IL-4/IL-13/IL-6-exposed macrophages to

augment the induction of AAM markers such as arginase-1, arginase activity, Fn1, Mrc1, Timp1 and Mcp1, it would not be unreasonable to refer to these macrophages as "hyperpolarized AAM". As such, the findings that IL-6 leads to a hyperpolarized macrophage, as opposed to OSM, suggest that OSM acts indirectly on macrophages in mice exposed to bleomycin. The high level of fibronectin expression in hyperpolarized macrophages and the enriched ECM-linked fibronectin seen in the fibrotic lungs suggest that these macrophages contributes to the deposition of fibronectin as previously described[47,48]. The increased expression of IL-4Rα on the macrophage-enriched BALF cells and BMDMs in response to IL-6 stimulation was likely rendering monocytes/macrophages more sensitive to alternative programming by IL-4/IL-13. When overexpressed *in vivo*, both OSM and IL-6 led to increased STAT3 activation, as examined on whole lung tissues. Our *in vitro* data showed that only IL-6 induced STAT3 activation in BMDMs, as opposed to OSM. Thus, it is tempting to speculate that the difference observed in the STAT3 signalling activation *in vivo* and *in vitro* could be attributable to the selective localization of IL-6 and OSM receptors within different cell-types. It was previously shown that OSMRβ is primarily located on stromal or epithelial cells[17,49,50], whereas IL-6Rα (via IL-6) is present on leukocytes[51].

Overall, the findings from these experiments suggest that IL-6Rα, IL-4Rα and OSMRβ are potential cellular targets to reduce macrophage polarization and fibrotic disease progression. Although IL-4 is known to directly stimulate fibroblast proliferation and activation *in vitro*[52,53], its role *in vivo* is less clear. A previous study has shown that reduction of IL-4- and IL-13-responsive macrophages and mononuclear cells using IL-13-

Pseudomonas exotoxin A fusion protein attenuates bleomycin-induced lung fibrosis in mouse models[54]. Additionally, therapeutic blockade of IL-4 in a mice model of scleroderma leads to reduced dermal collagen deposition and fibrosis[55]. However, further experimentation is needed to validate the use of anti-IL-6Rα, anti-IL-4Rα and anti-OSMRβ in disease models driven primarily by M2-like macrophages.

The effect of the addition of IL-6 may also be relevant to better understand the molecular mechanisms of acute exacerbations in IPF (AE-IPF)[56] as IL-6 has been indicated as a putative prognostic marker for AE-IPF[57,58]. AE-IPF associated mortality occurs in over 70% of patients with biopsy-confirmed IPF and over 90% in patients requiring ventilator assistance[56,59]. Various pro-inflammatory cytokines are elevated in the BALF in response to bacterial and viral infections, which are hypothesized to contribute to acute exacerbation[60] and could constitute a valid therapeutic target to prevent progression of disease. Schupp *et al.* recently demonstrated that mechanisms regulating M2-like macrophage polarization could act as triggers of pathological wound healing and repair processes in patients with acute exacerbation of IPF[61]. While IL-6 may also elicit its action on fibroblasts to modulate fibrotic lung disease[62], its direct involvement in alternative macrophage activation in the context of bleomycin-induced lung injury yields a novel and a potentially clinically relevant pathophysiological property of IL-6. This is consistent with the beneficial use of IL-6 neutralizing antibodies that were previously demonstrated to influence fibrotic outcomes during bleomycin-induced lung injury. Here, Kobayashi *et al*. showed that IL-6 blockade during the injury phase prevented the apoptosis of type II pneumocytes and markedly accelerated fibrosis, while IL-6 blockade

at the early fibrotic phase ameliorated lung fibrosis. Of note, transient overexpression of IL-6 or OSM using the adenoviral delivery system, leads to a gradual increase in pulmonary transgene expression until approximately day 7-10, potentially explaining the differences observed by Kobayashi *et al.* Our data suggests that IL-6 alone does not impact the M2 polarization of macrophages, both *in vivo* and *in vitro*. As bleomycin exposure creates a TH2-like pro-fibrotic milieu, we believe that the addition of IL-6 synergizes with this milieu to enhance alternative programming and exacerbate fibrotic disease (please see **Figure 7** for additional illustration). Combined, our data suggest that increased levels of OSM and IL-6 may be involved in promoting the accumulation of alternatively activated macrophages and subsequently fibrogenesis. As the bleomycin model is a reversible model, how the IL-6/OSM axis contributes to fibrotic disease resolution and whether it impacts the phenotypic characterization of macrophage subtypes would be an important avenue to consider. Therapeutic strategies targeting these cytokines or their receptors may be beneficial to limit the accumulation of pro-fibrotic macrophages and to prevent progression of fibrotic lung disease.

ACKNOWLEDGEMENTS

We sincerely thank the central animal facility, McMaster Immunology Research Centre's Core Histology Facility (Mary Jo Smith); Bioinformatic Core Facility (Dr. Anna Dvorkin-Gheva) and Flow Cytometry Facility (Hong Liang) (McMaster University, ON, Canada) for their exceptional technical training and service; Nirob Saha for making the cartoon that illustrates the key findings of the paper (Figure 7); Xueya Feng for constructing the adenoviral expression vectors (AdOSM and AdIL-6); Jennifer Wattie for excellent technical assistance and flexiVent assessments; Anmar Ayoub, Karun Tandon, Pavithra Parthasarathy and Nafis Wazed for their helpful support and constructive feedback.

AUTHOR CONTRIBUTIONS: Conception and design: EAA, AD, MRJK, CDR and KA; Performed experiments: EAA, AD, JI, FB; Analysis and interpretations: EAA, AD, JI, FB, CDR and KA; Drafting the manuscript: EAA, AD, CDR, KA; Edited and revised manuscript: EAA, AD, JI, MRJK, CDR and KA. All authors read and approved the final version.

COMPETING FINANCIAL INTERESTS: All authors declare no competing financial interests.

FIGURE LEGENDS

Figure 1. OSM and IL-6 worsen bleomycin-induced increase in lung elastance and bleomycin-induced fibrotic changes. Mice were intubated with AdDL70, AdOSM and AdIL-6, alone, or in combination with bleomycin (0.03 U/mouse). Additional control groups were included, receiving bleomycin plus saline with no adenovectors. Mice were sacrificed following 7 and 21 days of exposure, with the fibrotic outcome was assessed at day 21. (A-B) IL-6 and OSM were assessed in the BALF by ELISA (day 7). (C) Elastance derived from pressure-driven pressure volume loops are shown and graphed as an average value of all the animals per group. (D) Lung collagen content was assessed by Sircol collagen assay. (E) Ashcroft score demonstrating the grade of fibrosis and (F) representative images from Masson's trichrome and αSMA stained lung sections. Bar graphs represent mean ± SEM from 5-8 mice per group. All samples were derived at the same time and processed in parallel. This figure shows one of two representative experiments. *:P<0.05; **:P<0.01; ***:P<0.001; #:P<0.05; ##:P<0.01; ###:P<0.001; * represent a difference between bleomycin-exposed groups and their respective controls (Saline-Bleo vs. Saline, AdDL70- Bleo vs. AdDL70, AdOSM-Bleo vs. AdOSM, AdIL-6-Bleo vs. AdIL-6); # represent a difference between the indicated groups. Significance was established using GraphPad, Prism 7.0 with one-way ANOVA using Newman-Keuls Multiple Comparison test.

Figure 2. Enhanced production of several mediators in the lungs of bleomycin-exposed mice during IL-6 or OSM overexpression. Following intratracheal intubation of AdDL70, AdOSM and AdIL-6 alone, or in combination with bleomycin (0.03

U/mouse), mice were sacrificed after 7 days. Different cytokine/chemokine mediators were assessed in the BALF, either by ELISA or multiplex assay. The differentially regulated factors include (A) TGFβ1 (B) G-CSF (C) MIG (D) IP-10 (E) MCP-1 and (F) LIF. All other mediators were below the level of detection, and are therefore not included in this figure. Bar graphs represent mean ± SEM from 3-5 mice per group, *:P<0.05; **:P<0.01; ***:P<0.001; #:P<0.05; ##:P<0.01; ###:P<0.001; * represent a difference between bleomycin-exposed groups and their respective controls (AdDL70- Bleo vs. AdDL70, AdOSM-Bleo vs. AdOSM, AdIL-6-Bleo vs. AdIL-6); # represent a difference between the indicated groups. Significance was established using GraphPad, Prism 7.0 with one-way ANOVA using Newman-Keuls Multiple Comparison test.

Figure 3. Increased induction of arginase-1 in the lungs of bleomycin-exposed groups during IL-6 or OSM overexpression. Following intratracheal intubation of AdDL70, AdOSM and AdIL-6, alone, or in combination with bleomycin (0.03 U/mouse), mice were sacrificed after 7 and 21 days. (A-B) Immunoblot images and densitometry analyses of STAT3, pSTAT3 and arginase-1 of lung homogenates following 7 days of exposure. (C-E) Representative arginase-1 immunostaining and quantification as well as arginase-1 mRNA signal in lung tissues following 7 days of exposure. Bar graphs represent mean ± SEM from 3-6 mice per group. All samples were derived at the same time and processed in parallel. The appropriate Western blot area depicting the antibody band was cropped and enclosed by black boxes, as indicated above. *:P<0.05; **:P<0.01; ***:P<0.001; #:P<0.05; ##:P<0.01; ###:P<0.001; * represent a difference between bleomycin-exposed groups and their respective controls (AdDL70- Bleo vs. AdDL70,

AdOSM-Bleo vs. AdOSM, AdIL-6-Bleo vs. AdIL-6); # represent a difference between the indicated groups. Significance was established using GraphPad, Prism 7.0 with one-way ANOVA using Newman-Keuls Multiple Comparison test.

Figure 4. Increased accumulation of CD206+Arg1+ macrophages in the lungs of bleomycin-exposed mice during IL-6 or OSM overexpression. Following intratracheal intubation of AdDL70, AdOSM and AdIL-6, alone, or in combination with bleomycin (0.03 U/mouse) mice were sacrificed after 7 days. Lungs were processed for flow cytometry and AMs derived from BALF cells were isolated by adhesion and subsequently subjected to RNA analysis and Nanostring gene expression. (A) A graph showing absolute numbers of CD45+CD206+CD11b+Arg1+F4/80+ cells. (B-C) graphs showing *Arg1* mRNA expression of adhered AMs and arginase-1/DAPI immunofluorescence staining of BALF cells. (D) *Il-4rα* mRNA expression of adhered AMs. All samples were derived at the same time and processed in parallel. Bar graphs represent mean ± SEM from 3-5 mice per group, *:P<0.05; **:P<0.01; ***:P<0.001; #:P<0.05; ##:P<0.01; ###:P<0.001; * represent a difference between bleomycin-exposed groups and their respective controls (AdDL70- Bleo vs. AdDL70, AdOSM-Bleo vs. AdOSM, AdIL-6-Bleo vs. AdIL-6); # represent a difference between the indicated groups. Significance was established using GraphPad, Prism 7.0 with one-way ANOVA using Newman-Keuls Multiple Comparison test.

Figure 5. IL-6, but not OSM, directly acts on macrophages to potentiate their alternatively activated phenotype. Bone-marrow derived macrophages were cultured from naïve C57BL/6 for either 18 or 30 hours with recombinant OSM, IL-6, IL-4/IL-13,

alone or in combination as indicated. AMs were isolated from naïve mice by adherence. BMDMs were either lysed and processed for (A) arginase activity assay, or analysed by flow cytometry to show (B) percentage of arg1+CD206+ macrophages, (C-D) fold change of percentage of IL-4Rα+ cells from the arg1+CD206+ population relative to controls. At least 100,000 events were captured per condition, and repeated twice. (E) Western blot analysis of cell lysates probed for arginase-1, pSTAT6, pSTAT3, and Actin. (F) Densitometry of pSTAT6 (corrected to STAT6), (G) arginase-1 (corrected to actin) and (H) pSTAT3 (corrected to STAT3) represented as a fold-change relative to control. (I) Normalized mRNA counts of *Osmrβ* and *Il6rα* from control (unstimulated) BMDMs and AMs. Flow cytometry and western blot results are from experiments completed in duplicates. The appropriate Western blot area depicting the antibody band was cropped and enclosed by black boxes, as indicated above. All samples were derived at the same time and processed in parallel. For Nanostring gene expression, lower than 5 counts was considered not detected "ND". Bar graphs represent mean ± SEM from 2-3 replicates per group (showing one of two representative experiments), *:P<0.05; **:P<0.01; ***:P<0.001; #:P<0.05; ##:P<0.01; ###:P<0.001; * represent a difference between any sample relative to the control (control vs. IL-4/IL-13, IL-6 vs. IL-4/IL-13 + IL-6); # represent a difference between the indicated groups. Significance was established using GraphPad, Prism 7.0 with One-way ANOVA and non-parametric independent Student's t-test.

Figure 6. IL-6 increases the expression of pro-fibrotic factors in IL-4/IL-13 stimulated BMDMs. BMDMs were cultured from naïve C57BL/6 for 30 hours with

recombinant IL-6 plus IL-4/IL-13. The harvested RNA and cellular supernatant were later examined for gene expression and cytokine/chemokine mediators, respectively. Anti-fibronectin antibody was used to stained lung tissues (Day 7). Significantly regulated pro-fibrotic related genes include (A) *Fn1* (B) *Mrc1* (C) *Timp-1 and* (D) *Mcp-1*. Analysis of mediators showed (E) MCP-1 protein level to be differentially regulated. (F) Representative images showing fibronectin positive staining. Bar graphs represent mean ± SEM from 3-5 samples per group, *:P<0.05; **:P<0.01; ***:P<0.001; #:P<0.05; ##:P<0.01; ###:P<0.001; * represent a difference between any sample relative to the control (control vs. IL-4/IL-13 or IL-4/IL-13/IL-6); # represent a difference between the indicated groups. Significance was established using GraphPad, Prism 7.0 with One-way ANOVA using Newman-Keuls Multiple Comparison test.

Figure 7. An illustration suggesting OSM or IL-6 presence in the lung acts as stimuli to further potentiate fibrotic disease development. Bleomycin exposure initiate epithelial injury, leading to the recruitment of immune cells and pro-fibrotic alternative macrophage polarization. Our data suggest that both gp130 cytokines, OSM or IL-6, have the capacity to enhance the fibrotic response to bleomycin, associated with an increased number of alternatively activated macrophages. We show further that IL-6 have the capacity to act directly on pulmonary macrophages as opposed to OSM, as macrophages do not express the OSM receptor.

Figure 1

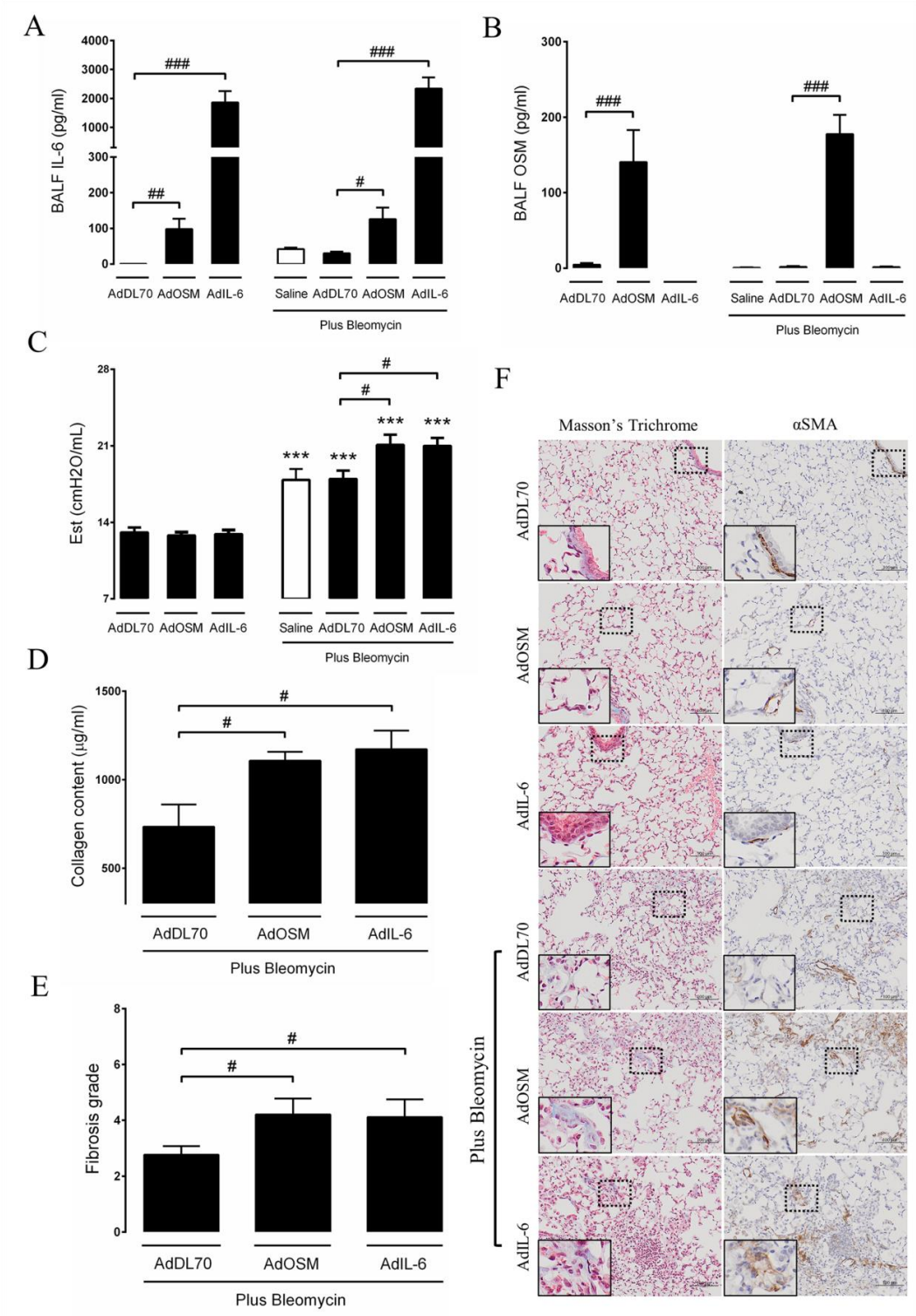
A
BALF IL-6 (pg/ml)
4000
3000
2000
1000
300
200
100
0
###
##
#
AdDL70 AdOSM AdIL-6
Saline AdDL70 AdOSM AdIL-6
Plus Bleomycin
B
BALF OSM (pg/ml)
300
200
100
0
###
AdDL70 AdOSM AdIL-6
Saline AdDL70 AdOSM AdIL-6
Plus Bleomycin
C
Est (cmH2O/mL)
28
21
14
7
#
***
AdDL70 AdOSM AdIL-6
Saline AdDL70 AdOSM AdIL-6
Plus Bleomycin
D
Collagen content (µg/ml)
1500
1000
500
#
AdDL70 AdOSM AdIL-6
Plus Bleomycin
E
Fibrosis grade
8
6
4
2
0
#
AdDL70 AdOSM AdIL-6
Plus Bleomycin
F
Masson's Trichrome
αSMA
AdDL70
AdOSM
AdIL-6
Plus Bleomycin

Figure 2

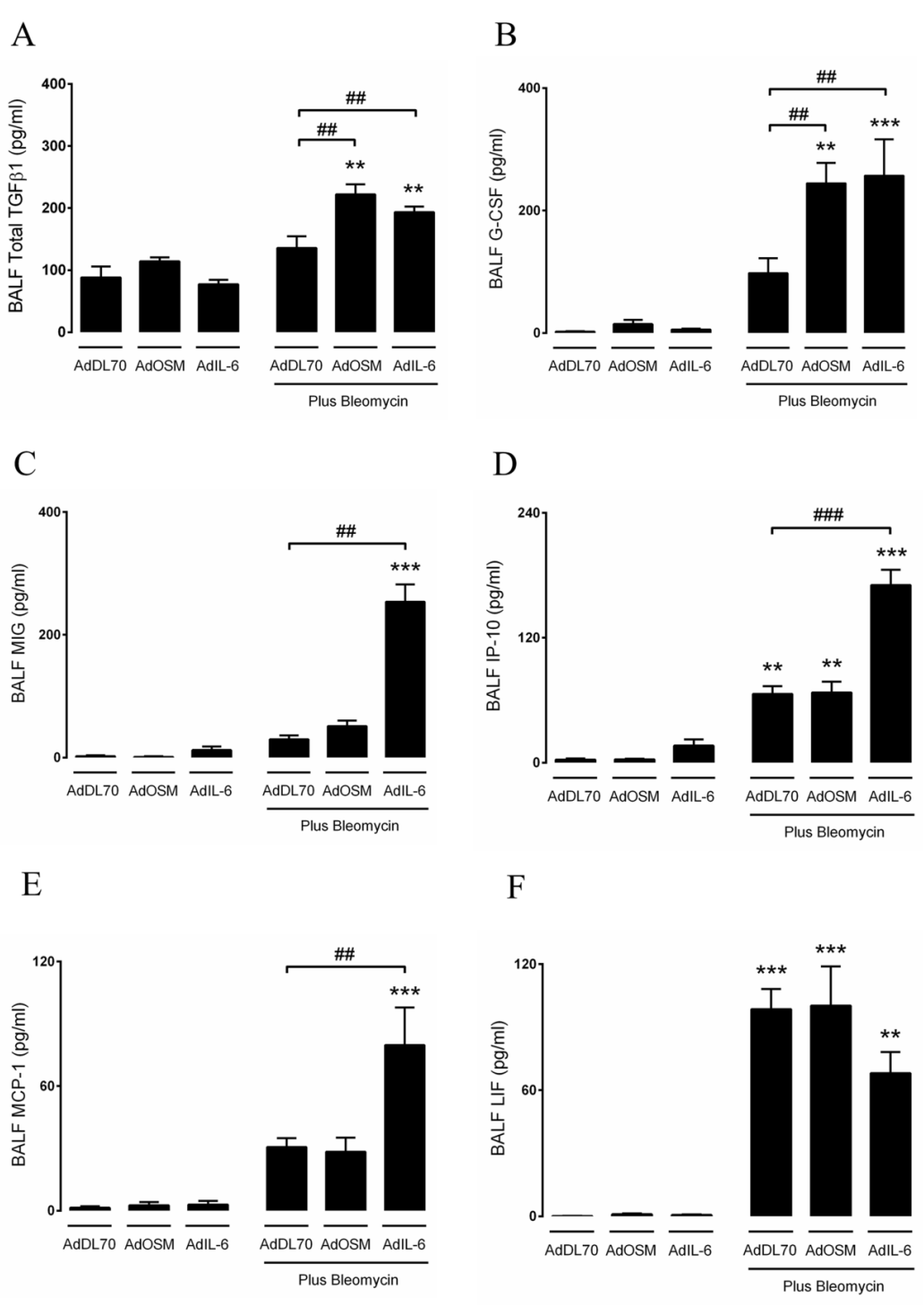
A
BALF Total TGFβ1 (pg/ml)
400
300
200
100
0
##
##
**
**
AdDL70 AdOSM AdIL-6 AdDL70 AdOSM AdIL-6
Plus Bleomycin
B
BALF G-CSF (pg/ml)
400
200
0
##
##
**
***
AdDL70 AdOSM AdIL-6 AdDL70 AdOSM AdIL-6
Plus Bleomycin
C
BALF MIG (pg/ml)
400
200
0
##
***
AdDL70 AdOSM AdIL-6 AdDL70 AdOSM AdIL-6
Plus Bleomycin
D
BALF IP-10 (pg/ml)
240
120
0
###
***
**
**
AdDL70 AdOSM AdIL-6 AdDL70 AdOSM AdIL-6
Plus Bleomycin
E
BALF MCP-1 (pg/ml)
120
60
0
##
***
AdDL70 AdOSM AdIL-6 AdDL70 AdOSM AdIL-6
Plus Bleomycin
F
BALF LIF (pg/ml)
120
60
0
***
***
**
AdDL70 AdOSM AdIL-6 AdDL70 AdOSM AdIL-6
Plus Bleomycin

Figure 3

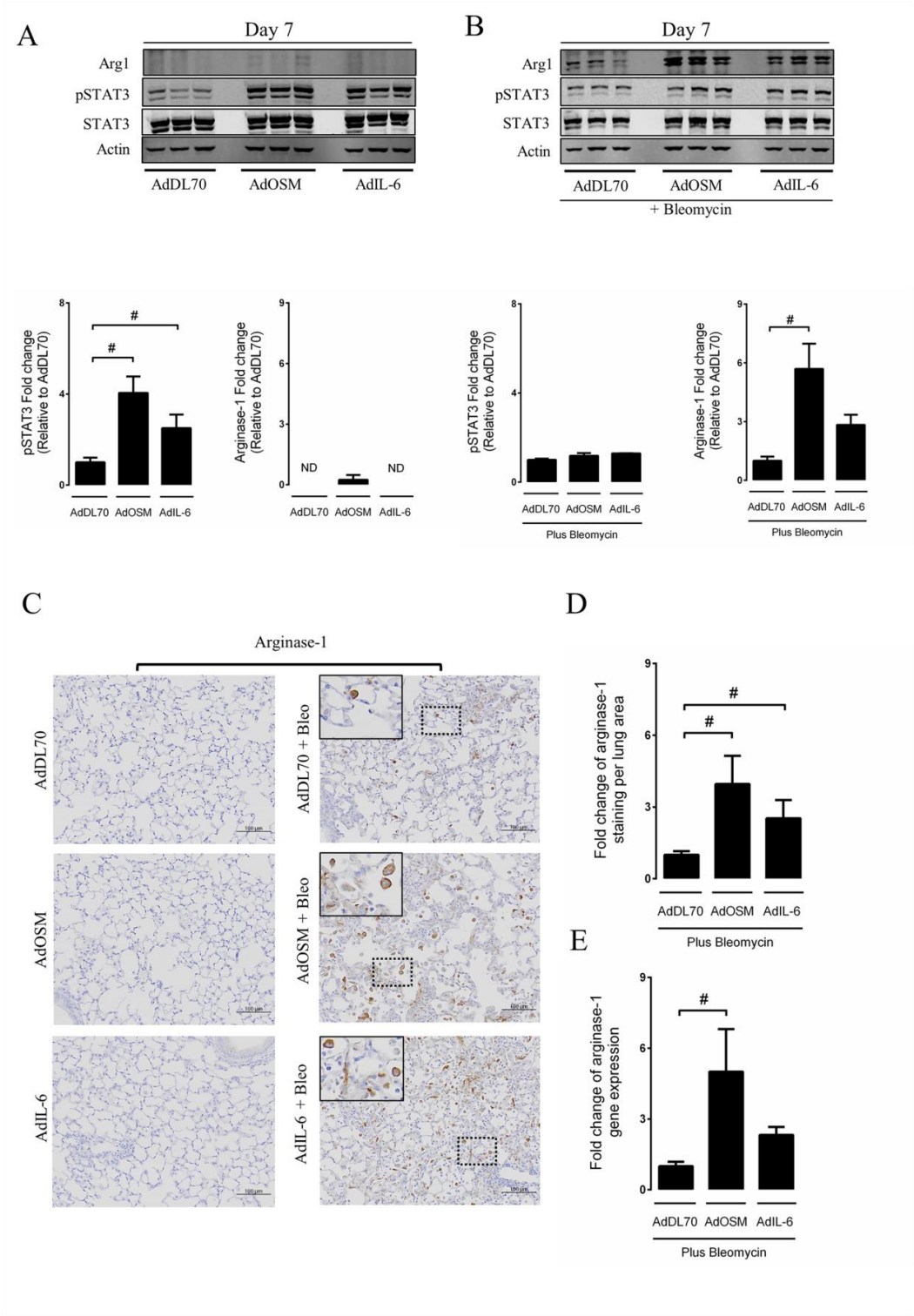
A
Day 7
Arg1
pSTAT3
STAT3
Actin
AdDL70
AdOSM
AdIL-6
B
Day 7
Arg1
pSTAT3
STAT3
Actin
AdDL70
AdOSM
AdIL-6
+ Bleomycin
pSTAT3 Fold change (Relative to AdDL70)
Arginase-1 Fold change (Relative to AdDL70)
ND
ND
Plus Bleomycin
C
Arginase-1
AdDL70
AdOSM
AdIL-6
AdDL70 + Bleo
AdOSM + Bleo
AdIL-6 + Bleo
D
Fold change of arginase-1 staining per lung area
E
Fold change of arginase-1 gene expression

Figure 4

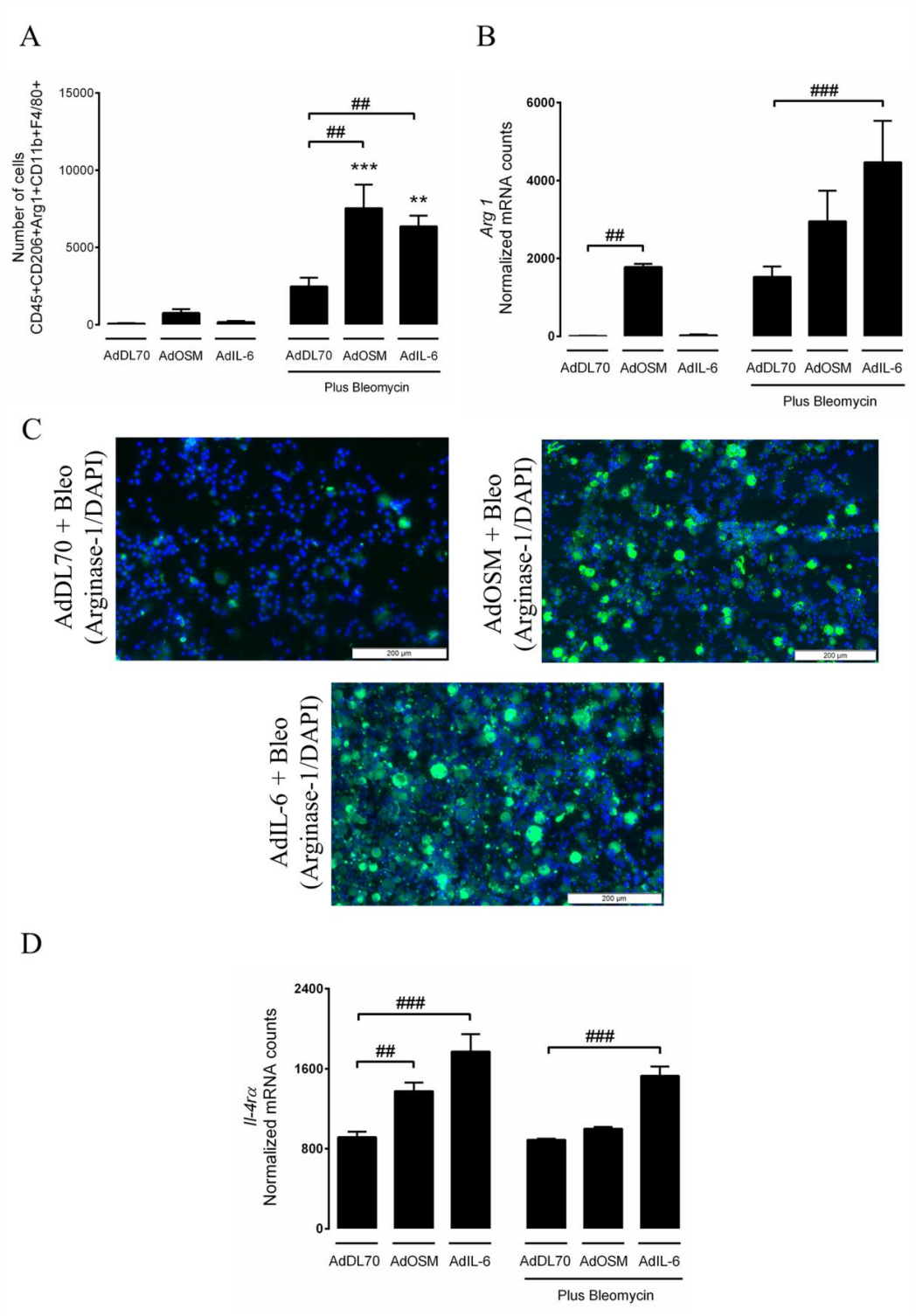
A
B
Number of cells
CD45+CD206+Arg1+CD11b+F4/80+
15000
10000
5000
0
##
##
***
**
AdDL70
AdOSM
AdIL-6
AdDL70
AdOSM
AdIL-6
Plus Bleomycin
Arg 1
Normalized mRNA counts
6000
4000
2000
0
##
###
AdDL70
AdOSM
AdIL-6
AdDL70
AdOSM
AdIL-6
Plus Bleomycin
C
AdDL70 + Bleo
(Arginase-1/DAPI)
AdOSM + Bleo
(Arginase-1/DAPI)
AdIL-6 + Bleo
(Arginase-1/DAPI)
200 µm
200 µm
200 µm
D
Il-4rα
Normalized mRNA counts
2400
1600
800
0
##
###
###
AdDL70
AdOSM
AdIL-6
AdDL70
AdOSM
AdIL-6
Plus Bleomycin

Figure 5

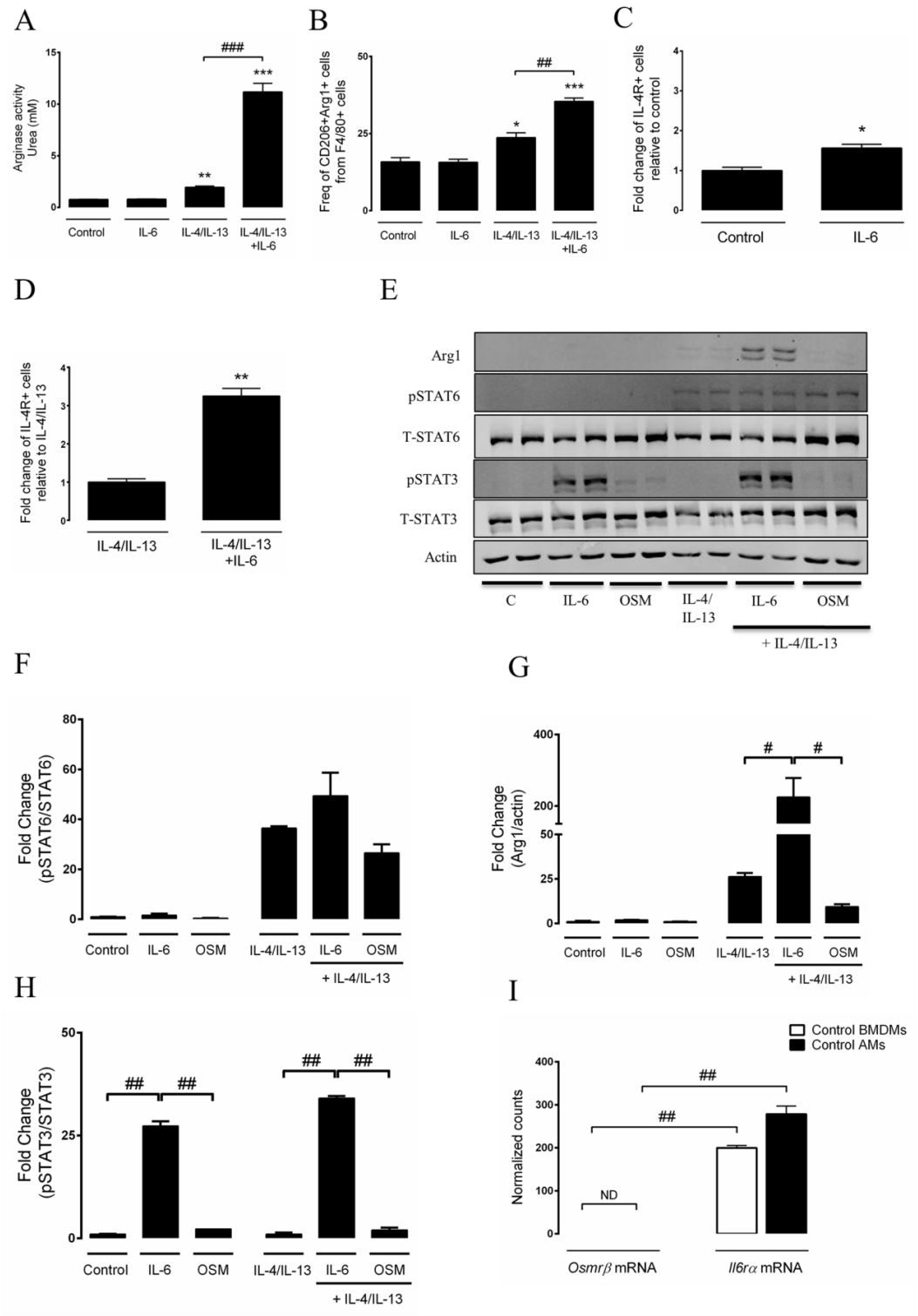
A
Arginase activity Urea (mM)
###
***
**
Control
IL-6
IL-4/IL-13
IL-4/IL-13 +IL-6
B
Freq of CD206+Arg1+ cells from F4/80+ cells
##
***
*
Control
IL-6
IL-4/IL-13
IL-4/IL-13 +IL-6
C
Fold change of IL-4R+ cells relative to control
*
Control
IL-6
D
Fold change of IL-4R+ cells relative to IL-4/IL-13
**
IL-4/IL-13
IL-4/IL-13 +IL-6
E
Arg1
pSTAT6
T-STAT6
pSTAT3
T-STAT3
Actin
C
IL-6
OSM
IL-4/ IL-13
IL-6
OSM
+ IL-4/IL-13
F
Fold Change (pSTAT6/STAT6)
Control
IL-6
OSM
IL-4/IL-13
IL-6
OSM
+ IL-4/IL-13
G
Fold Change (Arg1/actin)
#
#
Control
IL-6
OSM
IL-4/IL-13
IL-6
OSM
+ IL-4/IL-13
H
Fold Change (pSTAT3/STAT3)
##
##
##
##
Control
IL-6
OSM
IL-4/IL-13
IL-6
OSM
+ IL-4/IL-13
I
Control BMDMs
Control AMs
Normalized counts
##
##
ND
Osmrβ mRNA
Il6rα mRNA

Figure 6

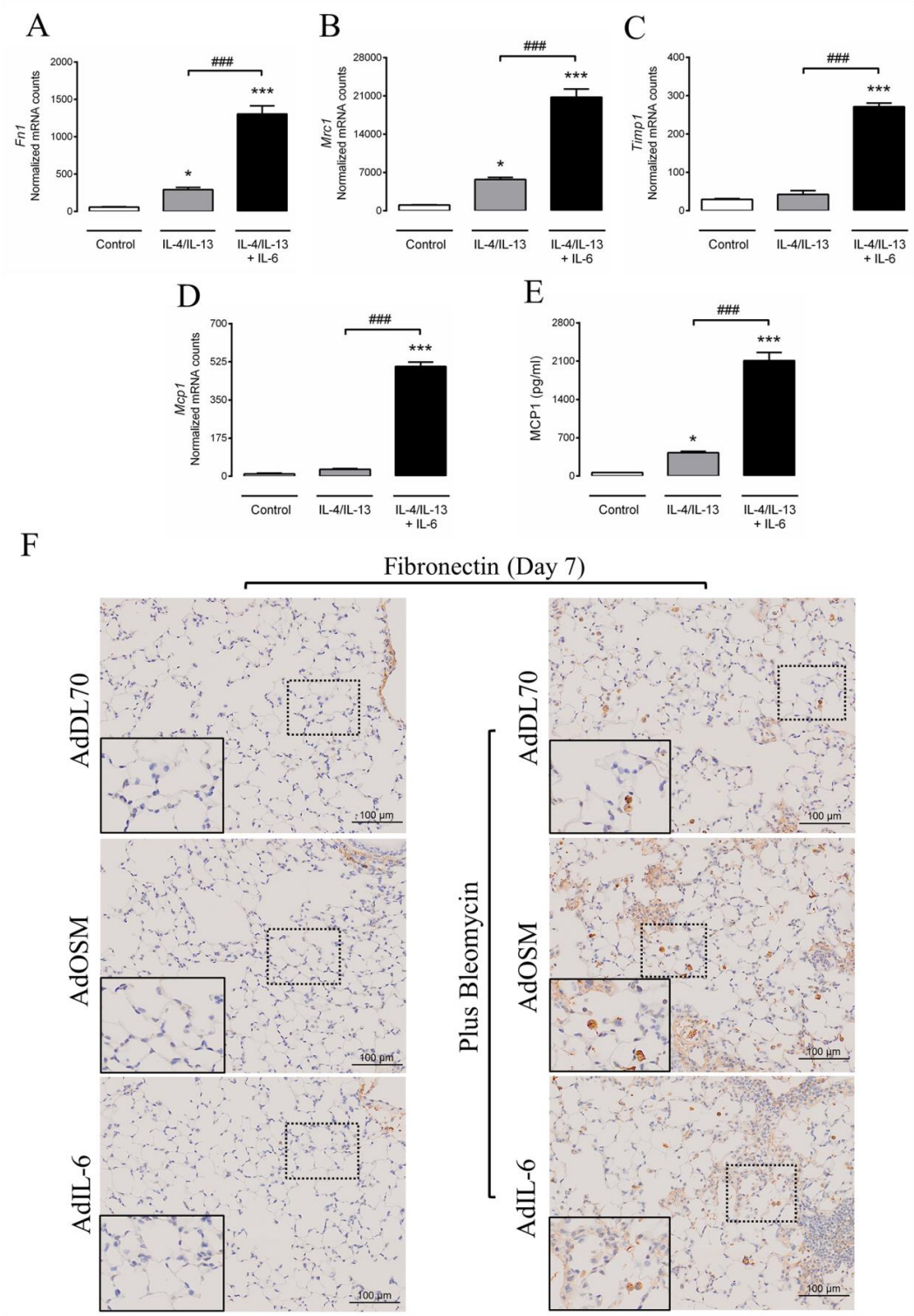
A
B
C
D
E
F
Fn1
Normalized mRNA counts
Mrc1
Timp1
Mcp1
MCP1 (pg/ml)
Control
IL-4/IL-13
IL-4/IL-13 + IL-6
###
***
*
Fibronectin (Day 7)
AdDL70
AdOSM
AdIL-6
Plus Bleomycin
100 µm

Figure 7

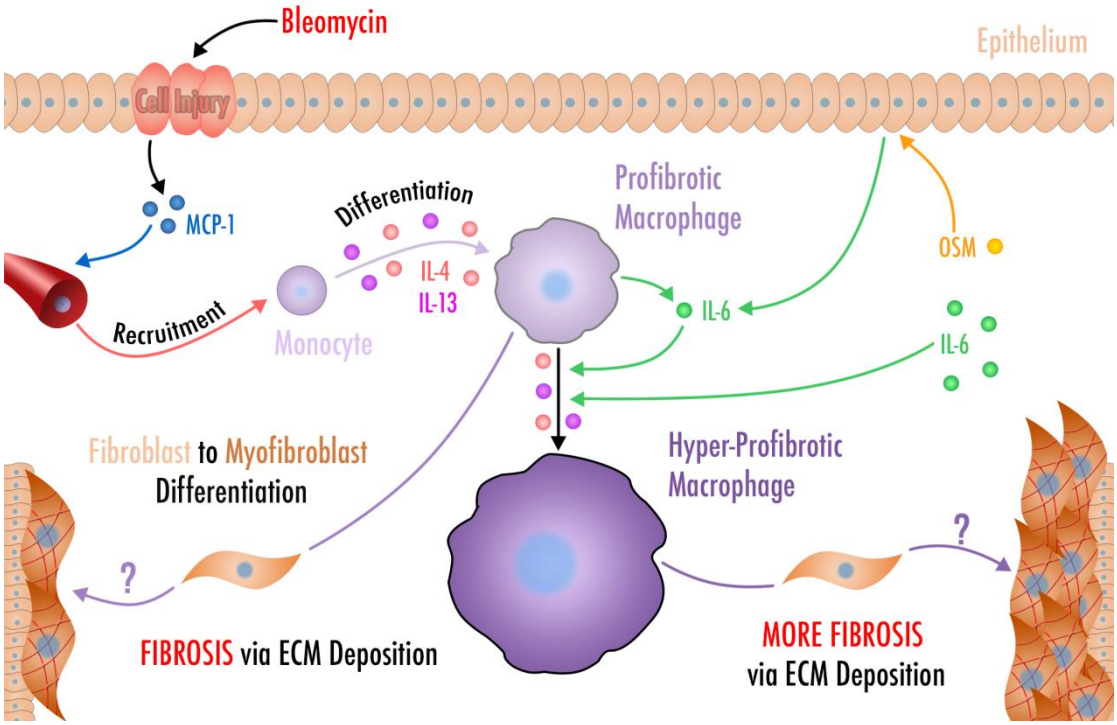
Bleomycin
Epithelium
Cell Injury
MCP-1
Differentiation
Profibrotic Macrophage
OSM
IL-4
IL-13
Recruitment
Monocyte
IL-6
IL-6
Fibroblast to Myofibroblast Differentiation
Hyper-Profibrotic Macrophage
?
?
FIBROSIS via ECM Deposition
MORE FIBROSIS via ECM Deposition

REFERENCES

1 Sgalla, G., Biffi, A. & Richeldi, L. Idiopathic pulmonary fibrosis: Diagnosis, epidemiology and natural history. *Respirology (Carlton, Vic.)* **21**, 427-437, doi:10.1111/resp.12683 (2016).

2 Gifford, A. H., Matsuoka, M., Ghoda, L. Y., Homer, R. J. & Enelow, R. I. Chronic inflammation and lung fibrosis: pleotropic syndromes but limited distinct phenotypes. *Mucosal Immunol* **5**, 480-484, doi:10.1038/mi.2012.68 (2012).

3 Bringardner, B. D., Baran, C. P., Eubank, T. D. & Marsh, C. B. The role of inflammation in the pathogenesis of idiopathic pulmonary fibrosis. *Antioxid Redox Signal* **10**, 287-301, doi:10.1089/ars.2007.1897 (2008).

4 Ask, K., Martin, G. E., Kolb, M. & Gauldie, J. Targeting genes for treatment in idiopathic pulmonary fibrosis: challenges and opportunities, promises and pitfalls. *Proceedings of the American Thoracic Society* **3**, 389-393, doi:10.1513/pats.200602-021TK (2006).

5 Moeller, A., Ask, K., Warburton, D., Gauldie, J. & Kolb, M. The bleomycin animal model: a useful tool to investigate treatment options for idiopathic pulmonary fibrosis? *The international journal of biochemistry & cell biology* **40**, 362-382, doi:10.1016/j.biocel.2007.08.011 (2008).

6 Park, S. & Lee, E. J. Recent advances in idiopathic pulmonary fibrosis. *Tuberculosis and respiratory diseases* **74**, 1-6, doi:10.4046/trd.2013.74.1.1 (2013).

7 Travis, W. D. *et al.* An official American Thoracic Society/European Respiratory Society statement: Update of the international multidisciplinary classification of the idiopathic interstitial pneumonias. *Am J Respir Crit Care Med* **188**, 733-748, doi:10.1164/rccm.201308-1483ST (2013).

8 Fernandez, I. E. & Eickelberg, O. The impact of TGF-beta on lung fibrosis: from targeting to biomarkers. *Proc Am Thorac Soc* **9**, 111-116, doi:10.1513/pats.201203-023AW (2012).

9 Selman, M., Pardo, A., Richeldi, L. & Cerri, S. Emerging drugs for idiopathic pulmonary fibrosis. *Expert Opin Emerg Drugs* **16**, 341-362, doi:10.1517/14728214.2011.565049 (2011).

10 Coward, W. R., Saini, G. & Jenkins, G. The pathogenesis of idiopathic pulmonary fibrosis. *Therapeutic advances in respiratory disease* **4**, 367-388, doi:10.1177/1753465810379801 (2010).

11 Gibbons, M. A. *et al.* Ly6Chi monocytes direct alternatively activated profibrotic macrophage regulation of lung fibrosis. *American journal of respiratory and critical care medicine* **184**, 569-581, doi:10.1164/rccm.201010-1719OC (2011).

12 Wynn, T. A. *et al.* Quantitative assessment of macrophage functions in repair and fibrosis. *Current protocols in immunology / edited by John E. Coligan ... [et al.]* **Chapter 14**, Unit14 22, doi:10.1002/0471142735.im1422s93 (2011).

13 Wynn, T. A., Chawla, A. & Pollard, J. W. Macrophage biology in development, homeostasis and disease. *Nature* **496**, 445-455, doi:10.1038/nature12034 (2013).

14 Wynn, T. A. & Barron, L. Macrophages: master regulators of inflammation and fibrosis. *Seminars in liver disease* **30**, 245-257, doi:10.1055/s-0030-1255354 (2010).
15 Ayaub, E. A. *et al.* GRP78 and CHOP modulate macrophage apoptosis and the development of bleomycin-induced pulmonary fibrosis. *J Pathol* **239**, 411-425, doi:10.1002/path.4738 (2016).
16 Pedersen, B. K. Muscles and their myokines. *The Journal of experimental biology* **214**, 337-346, doi:10.1242/jeb.048074 (2011).
17 Richards, C. D. The enigmatic cytokine oncostatin m and roles in disease. *ISRN inflammation* **2013**, 512103, doi:10.1155/2013/512103 (2013).
18 Silver, J. S. & Hunter, C. A. gp130 at the nexus of inflammation, autoimmunity, and cancer. *Journal of leukocyte biology* **88**, 1145-1156, doi:10.1189/jlb.0410217 (2010).
19 Sims, N. A. & Walsh, N. C. GP130 cytokines and bone remodelling in health and disease. *BMB reports* **43**, 513-523 (2010).
20 O'Donoghue, R. J. *et al.* Genetic partitioning of interleukin-6 signalling in mice dissociates Stat3 from Smad3-mediated lung fibrosis. *EMBO molecular medicine* **4**, 939-951, doi:10.1002/emmm.201100604 (2012).
21 Mauer, J. *et al.* Signaling by IL-6 promotes alternative activation of macrophages to limit endotoxemia and obesity-associated resistance to insulin. *Nat Immunol* **15**, 423-430, doi:10.1038/ni.2865 (2014).
22 Komori, T. *et al.* Oncostatin M is a potential agent for the treatment of obesity and related metabolic disorders: a study in mice. *Diabetologia* **58**, 1868-1876, doi:10.1007/s00125-015-3613-9 (2015).
23 Lauber, S. *et al.* Novel function of Oncostatin M as a potent tumour-promoting agent in lung. *Int J Cancer* **136**, 831-843, doi:10.1002/ijc.29055 (2015).
24 West, N. R. *et al.* Oncostatin M drives intestinal inflammation and predicts response to tumor necrosis factor-neutralizing therapy in patients with inflammatory bowel disease. *Nat Med* **23**, 579-589, doi:10.1038/nm.4307 (2017).
25 Braciak, T. A., Mittal, S. K., Graham, F. L., Richards, C. D. & Gauldie, J. Construction of recombinant human type 5 adenoviruses expressing rodent IL-6 genes. An approach to investigate in vivo cytokine function. *J Immunol* **151**, 5145-5153 (1993).
26 Kerr, C. *et al.* Adenovirus vector expressing mouse oncostatin M induces acute-phase proteins and TIMP-1 expression in vivo in mice. *Journal of interferon & cytokine research : the official journal of the International Society for Interferon and Cytokine Research* **19**, 1195-1205, doi:10.1089/107999099313145 (1999).
27 Richards, C. D., Braciak, T., Xing, Z., Graham, F. & Gauldie, J. Adenovirus vectors for cytokine gene expression. *Annals of the New York Academy of Sciences* **762**, 282-292; discussion 292-283 (1995).
28 Misharin, A. V. *et al.* Monocyte-derived alveolar macrophages drive lung fibrosis and persist in the lung over the life span. *The Journal of experimental medicine* **214**, 2387-2404, doi:10.1084/jem.20162152 (2017).

29 Sester, D. P. *et al.* A novel flow cytometric method to assess inflammasome formation. *J Immunol* **194**, 455-462, doi:10.4049/jimmunol.1401110 (2015).

30 Endo, M. *et al.* Induction of arginase I and II in bleomycin-induced fibrosis of mouse lung. *Am J Physiol Lung Cell Mol Physiol* **285**, L313-321, doi:10.1152/ajplung.00434.2002 (2003).

31 Satoh, T. *et al.* Identification of an atypical monocyte and committed progenitor involved in fibrosis. *Nature* **541**, 96-101, doi:10.1038/nature20611 (2017).

32 Stein, M., Keshav, S., Harris, N. & Gordon, S. Interleukin 4 potently enhances murine macrophage mannose receptor activity: a marker of alternative immunologic macrophage activation. *The Journal of experimental medicine* **176**, 287-292 (1992).

33 Nair, M. G., Guild, K. J. & Artis, D. Novel Effector Molecules in Type 2 Inflammation: Lessons Drawn from Helminth Infection and Allergy. *The Journal of Immunology* **177**, 1393-1399, doi:10.4049/jimmunol.177.3.1393 (2006).

34 Mylonas, K. J., Hoeve, M. A., MacDonald, A. S. & Allen, J. E. Alternative activation of macrophages by filarial nematodes is MyD88-independent. *Immunobiology* **218**, 570-578, doi:10.1016/j.imbio.2012.07.006 (2013).

35 Mozaffarian, A. *et al.* Mechanisms of oncostatin M-induced pulmonary inflammation and fibrosis. *J Immunol* **181**, 7243-7253 (2008).

36 Nagahama, K. Y. *et al.* Oncostatin M modulates fibroblast function via signal transducers and activators of transcription proteins-3. *Am J Respir Cell Mol Biol* **49**, 582-591, doi:10.1165/rcmb.2012-0460OC (2013).

37 Scaffidi, A. K. *et al.* Oncostatin M stimulates proliferation, induces collagen production and inhibits apoptosis of human lung fibroblasts. *British journal of pharmacology* **136**, 793-801, doi:10.1038/sj.bjp.0704769 (2002).

38 Saito, F. *et al.* Role of interleukin-6 in bleomycin-induced lung inflammatory changes in mice. *American journal of respiratory cell and molecular biology* **38**, 566-571, doi:10.1165/rcmb.2007-0299OC (2008).

39 Zhang, X. L., Topley, N., Ito, T. & Phillips, A. Interleukin-6 regulation of transforming growth factor (TGF)-beta receptor compartmentalization and turnover enhances TGF-beta1 signaling. *The Journal of biological chemistry* **280**, 12239-12245, doi:10.1074/jbc.M413284200 (2005).

40 Eickelberg, O. *et al.* Transforming growth factor-beta1 induces interleukin-6 expression via activating protein-1 consisting of JunD homodimers in primary human lung fibroblasts. *The Journal of biological chemistry* **274**, 12933-12938 (1999).

41 Elias, J. A., Lentz, V. & Cummings, P. J. Transforming growth factor-beta regulation of IL-6 production by unstimulated and IL-1-stimulated human fibroblasts. *J Immunol* **146**, 3437-3443 (1991).

42 Fritz, D. K. *et al.* A mouse model of airway disease: oncostatin M-induced pulmonary eosinophilia, goblet cell hyperplasia, and airway hyperresponsiveness are STAT6 dependent, and interstitial pulmonary fibrosis is STAT6 independent. *J Immunol* **186**, 1107-1118, doi:10.4049/jimmunol.0903476 (2011).

43 Wong, S., Botelho, F. M., Rodrigues, R. M. & Richards, C. D. Oncostatin M overexpression induces matrix deposition, STAT3 activation, and SMAD1 Dysregulation in lungs of fibrosis-resistant BALB/c mice. *Laboratory investigation; a journal of technical methods and pathology* **94**, 1003-1016, doi:10.1038/labinvest.2014.81 (2014).

44 Hussell, T. & Bell, T. J. Alveolar macrophages: plasticity in a tissue-specific context. *Nature reviews. Immunology* **14**, 81-93, doi:10.1038/nri3600 (2014).

45 Pesce, J. T. *et al.* Arginase-1-expressing macrophages suppress Th2 cytokine-driven inflammation and fibrosis. *PLoS Pathog* **5**, e1000371, doi:10.1371/journal.ppat.1000371 (2009).

46 Le, T.-T. T. *et al.* Blockade of IL-6 Trans Signaling Attenuates Pulmonary Fibrosis. *The Journal of Immunology Author Choice* **193**, 3755-3768, doi:10.4049/jimmunol.1302470 (2014).

47 Gratchev, A. *et al.* Alternatively activated macrophages differentially express fibronectin and its splice variants and the extracellular matrix protein betaIG-H3. *Scandinavian journal of immunology* **53**, 386-392 (2001).

48 Rennard, S. I., Hunninghake, G. W., Bitterman, P. B. & Crystal, R. G. Production of fibronectin by the human alveolar macrophage: mechanism for the recruitment of fibroblasts to sites of tissue injury in interstitial lung diseases. *Proceedings of the National Academy of Sciences of the United States of America* **78**, 7147-7151 (1981).

49 Cichy, J., Rose-John, S. & Pure, E. Regulation of the type II oncostatin M receptor expression in lung-derived epithelial cells. *FEBS letters* **429**, 412-416 (1998).

50 Tamura, S., Morikawa, Y., Tanaka, M., Miyajima, A. & Senba, E. Developmental expression pattern of oncostatin M receptor beta in mice. *Mechanisms of development* **115**, 127-131 (2002).

51 Hunter, C. A. & Jones, S. A. IL-6 as a keystone cytokine in health and disease. *Nature immunology* **16**, 448-457, doi:10.1038/ni.3153 (2015).

52 Saito, A., Okazaki, H., Sugawara, I., Yamamoto, K. & Takizawa, H. Potential Action of IL-4 and IL-13 as Fibrogenic Factors on Lung Fibroblasts in vitro. *International Archives of Allergy and Immunology* **132**, 168-176 (2003).

53 Postlethwaite, A. E., Holness, M. A., Katai, H. & Raghow, R. Human fibroblasts synthesize elevated levels of extracellular matrix proteins in response to interleukin 4. *Journal of Clinical Investigation* **90**, 1479-1485 (1992).

54 Jakubzick, C. *et al.* Therapeutic attenuation of pulmonary fibrosis via targeting of IL-4- and IL-13-responsive cells. *J Immunol* **171**, 2684-2693 (2003).

55 Ong, C., Wong, C., Roberts, C. R., Teh, H. S. & Jirik, F. R. Anti-IL-4 treatment prevents dermal collagen deposition in the tight-skin mouse model of scleroderma. *European journal of immunology* **28**, 2619-2629, doi:10.1002/(sici)1521-4141(199809)28:09<2619::aid-immu2619>3.0.co;2-m (1998).

56 Song, J. W., Hong, S. B., Lim, C. M., Koh, Y. & Kim, D. S. Acute exacerbation of idiopathic pulmonary fibrosis: incidence, risk factors and outcome. *The*

European respiratory journal **37**, 356-363, doi:10.1183/09031936.00159709 (2011).

57 Collard, H. R. *et al.* Plasma biomarker profiles in acute exacerbation of idiopathic pulmonary fibrosis. *Am J Physiol Lung Cell Mol Physiol* **299**, L3-7, doi:10.1152/ajplung.90637.2008 (2010).

58 Bhatti, H., Girdhar, A., Usman, F., Cury, J. & Bajwa, A. Approach to acute exacerbation of idiopathic pulmonary fibrosis. *Annals of thoracic medicine* **8**, 71-77, doi:10.4103/1817-1737.109815 (2013).

59 Collard, H. R. *et al.* Acute exacerbations of idiopathic pulmonary fibrosis. *Am J Respir Crit Care Med* **176**, 636-643, doi:10.1164/rccm.200703-463PP (2007).

60 Chen, W. H. *et al.* Potential Role for Alternatively Activated Macrophages in the Secondary Bacterial Infection During Recovery from Influenza. *Immunology letters* **141**, 227-234, doi:10.1016/j.imlet.2011.10.009 (2012).

61 Schupp, J. C. *et al.* Macrophage Activation in Acute Exacerbation of Idiopathic Pulmonary Fibrosis. *PLOS ONE* **10**, e0116775, doi:10.1371/journal.pone.0116775 (2015).

62 Hendrayani, S. F., Al-Khalaf, H. H. & Aboussekhra, A. The cytokine IL-6 reactivates breast stromal fibroblasts through transcription factor STAT3-dependent up-regulation of the RNA-binding protein AUF1. *The Journal of biological chemistry* **289**, 30962-30976, doi:10.1074/jbc.M114.594044 (2014).

Supplementary Information

Overexpression of OSM and IL-6 impacts the polarization of pro-fibrotic macrophages and the development of bleomycin-induced lung fibrosis

Ehab A Ayaub[1,2], Anisha Dubey [2], Jewel Imani [1,2], Fernando Botelho [2], Martin RJ Kolb [1], Carl D Richards[2], Kjetil Ask *[1,2]

1. *Department of Medicine, Firestone Institute for Respiratory Health, McMaster University and The Research Institute of St. Joe's Hamilton, Hamilton, ON, Canada*
2. *Department of Pathology and Molecular Medicine, McMaster Immunology Research Centre, McMaster University, Hamilton, ON, Canada*

***Corresponding author:** Dr. Kjetil Ask, Department of Medicine, McMaster University and The Research Institute of St. Joe's Hamilton, Firestone Institute for Respiratory Health, Luke Wing, Rm L314-5, 50 Charlton Ave East, Hamilton, Ontario, Canada L8N 4A6, Ph. (905) 522 1155 ext. 33683; Fax (905) 521 6183; E-mail: askkj@mcmaster.ca

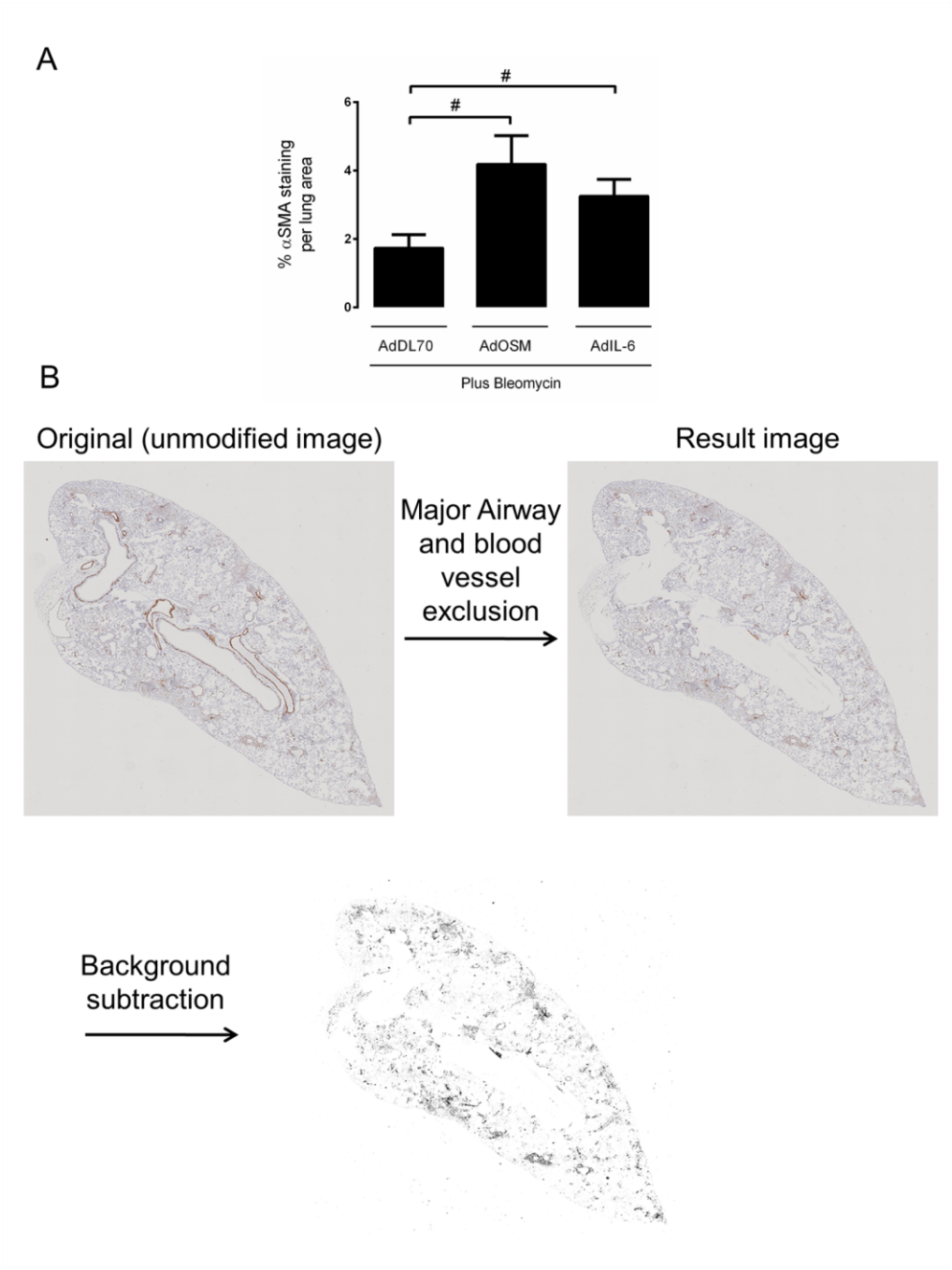

Supplementary Figure 1. Quantification of parenchymal αSMA staining in bleomycin-exposed lungs. Following the exclusion of major airways and blood vessels, (A)

parenchymal αSMA was assessed and shown as a percentage of the lung region. (B) Example of airway/vessel exclusion and thresholding method.

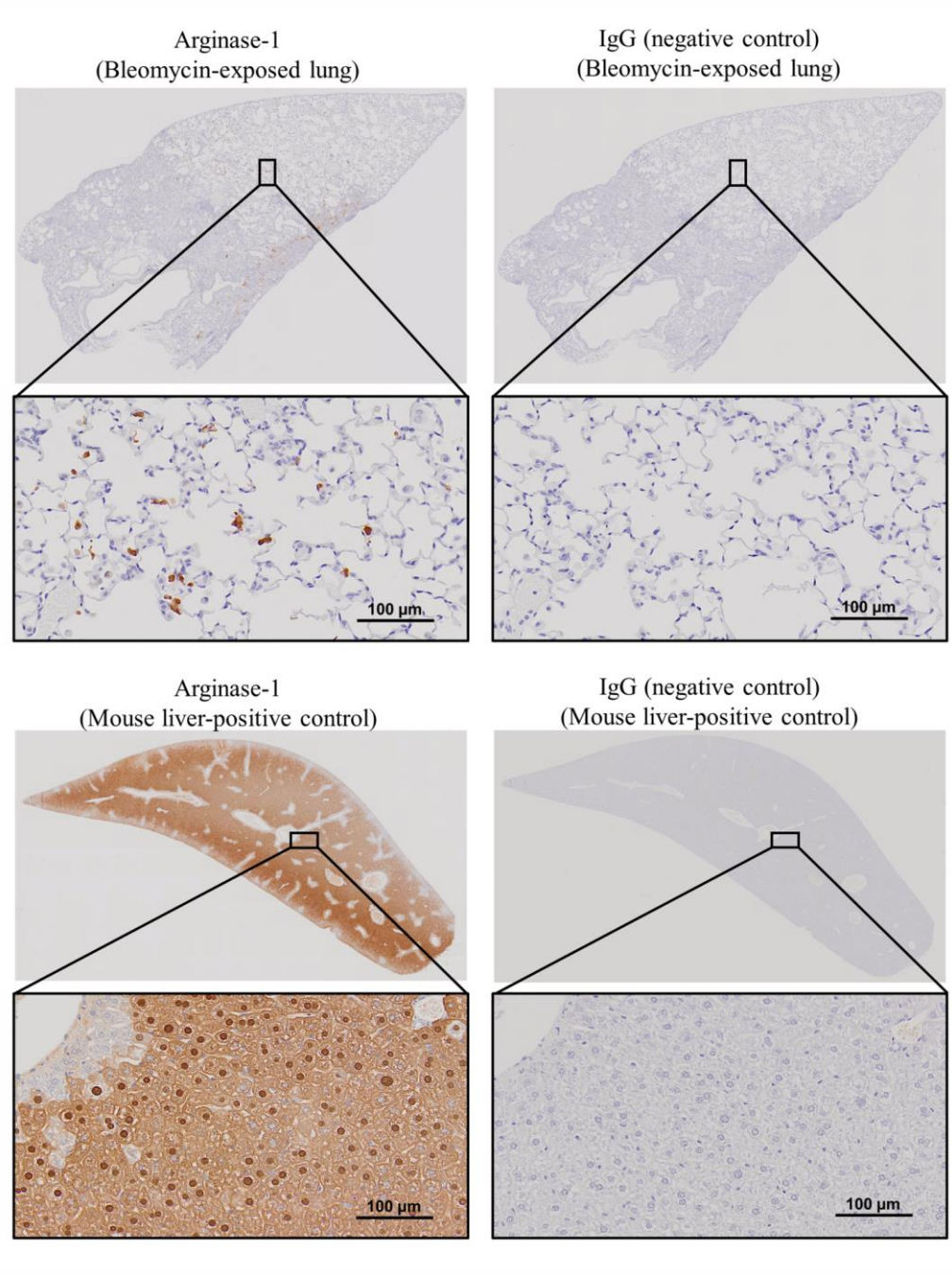

Supplementary Figure 2. Validation of mouse immunohistochemical staining of arginase-1 using positive and negative controls. Formalin-fixed sections of bleomycin-

exposed lung tissues and control liver tissues were stained with anti-arginase-1 antibody and a control (anti-IgG) antibody. Full tissue images and large scale inserts are shown.

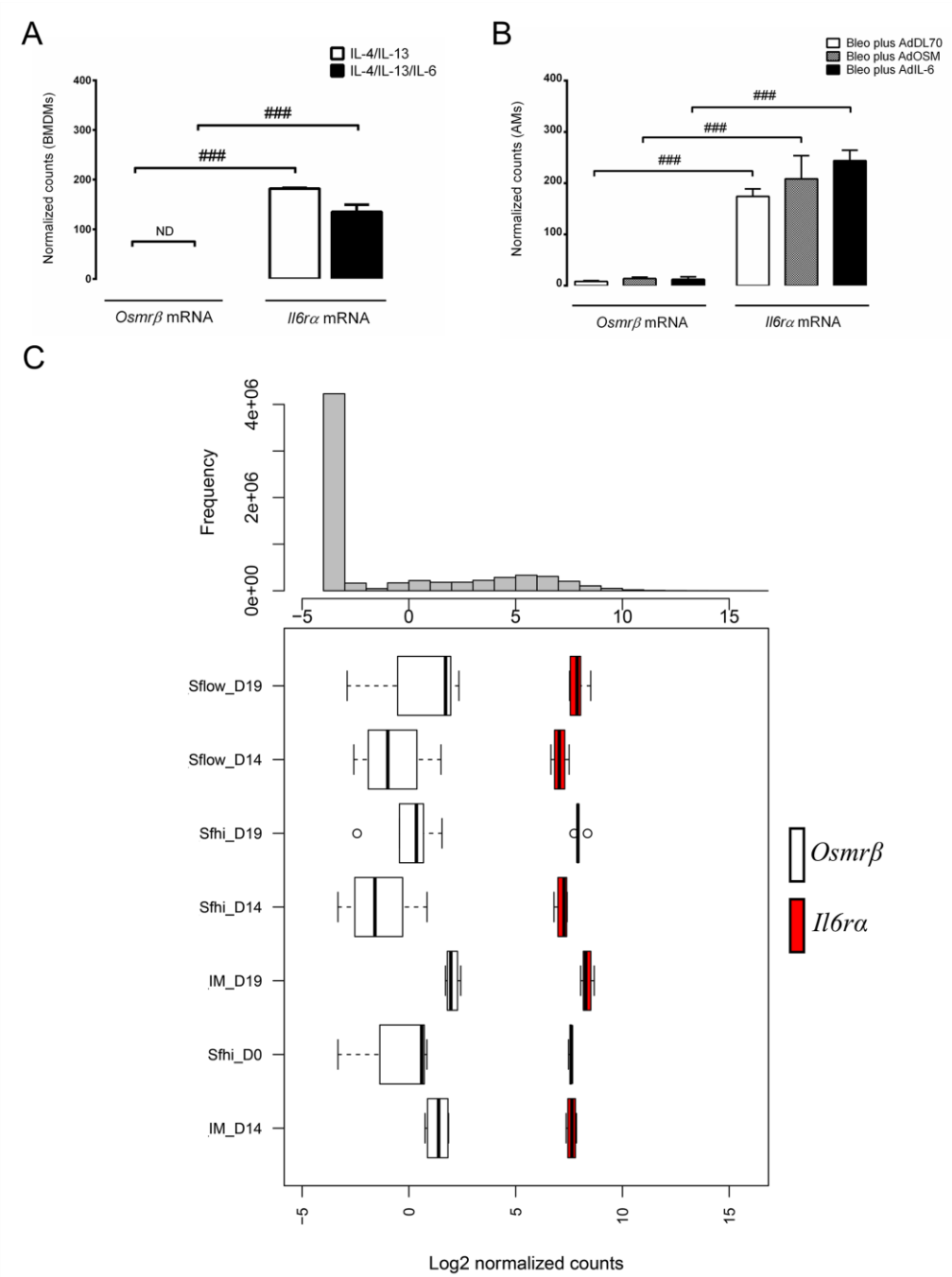

Supplementary Figure 3. Comparison of the expression of *Osmrβ* and *Il6rα* in BMDMs and lung macrophages. (A) *Osmrβ* and *Il6rα* mRNA expression from BMDMs exposed to IL-4/IL-13 and IL-4/IL-13/IL-6 for 30 hours. (B) *Osmrβ* and *Il6rα* mRNA expression from BALF AMs following 7 days of exposure to bleomycin plus AdDL70, AdOSM or AdIL-6. (C) Analysis of publically available GEO database showing overall gene expression frequency profile as well as expression of *Osmrβ* (white-bars) and *Il6rα* (red-bars) in different macrophage populations within the lung. Sflow and Sfhi= Siglec F low and high alveolar macrophages, IM= interstitial macrophages, D0=non-bleomycin exposed lungs and D14/19= days of bleomycin exposure before sacrifice. Bar graphs represent mean ± SEM from 3-5 samples per group, ###:P<0.001 and significance was established using GraphPad, Prism 7.0 with one-way and two ANOVA using Newman-Keuls Multiple Comparison test. For Nanostring gene expression, lower than 5 counts was considered not detected "ND". Log2 transformed counts were analysed and plotted using R environment.

.

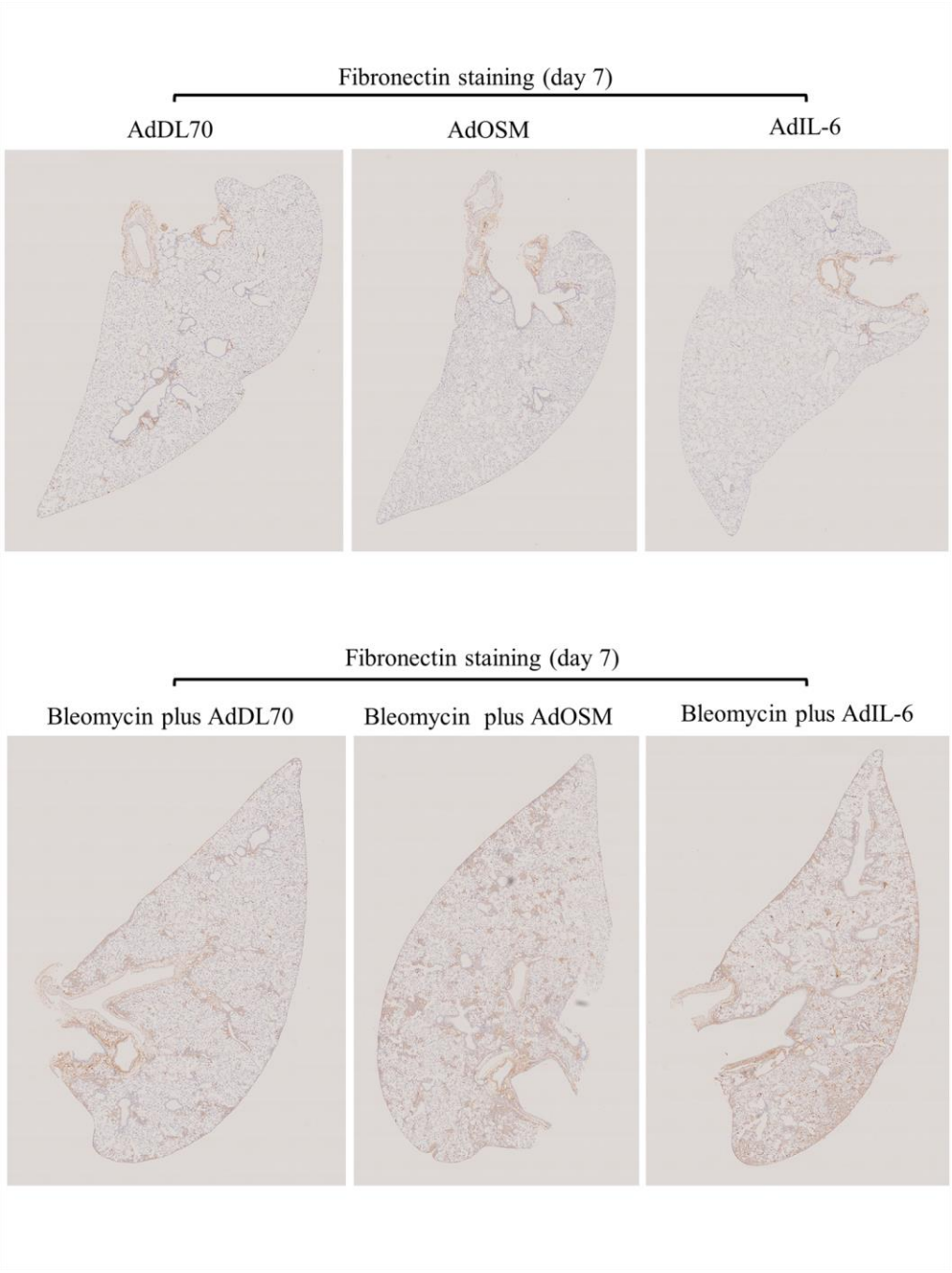

Supplementary Figure 4. Lung immunohistochemical staining of fibronectin in mice following in mice exposed to bleomycin plus AdOSM or AdIL-6 after 7 days of exposure of adenoviral vectors alone and with bleomycin.

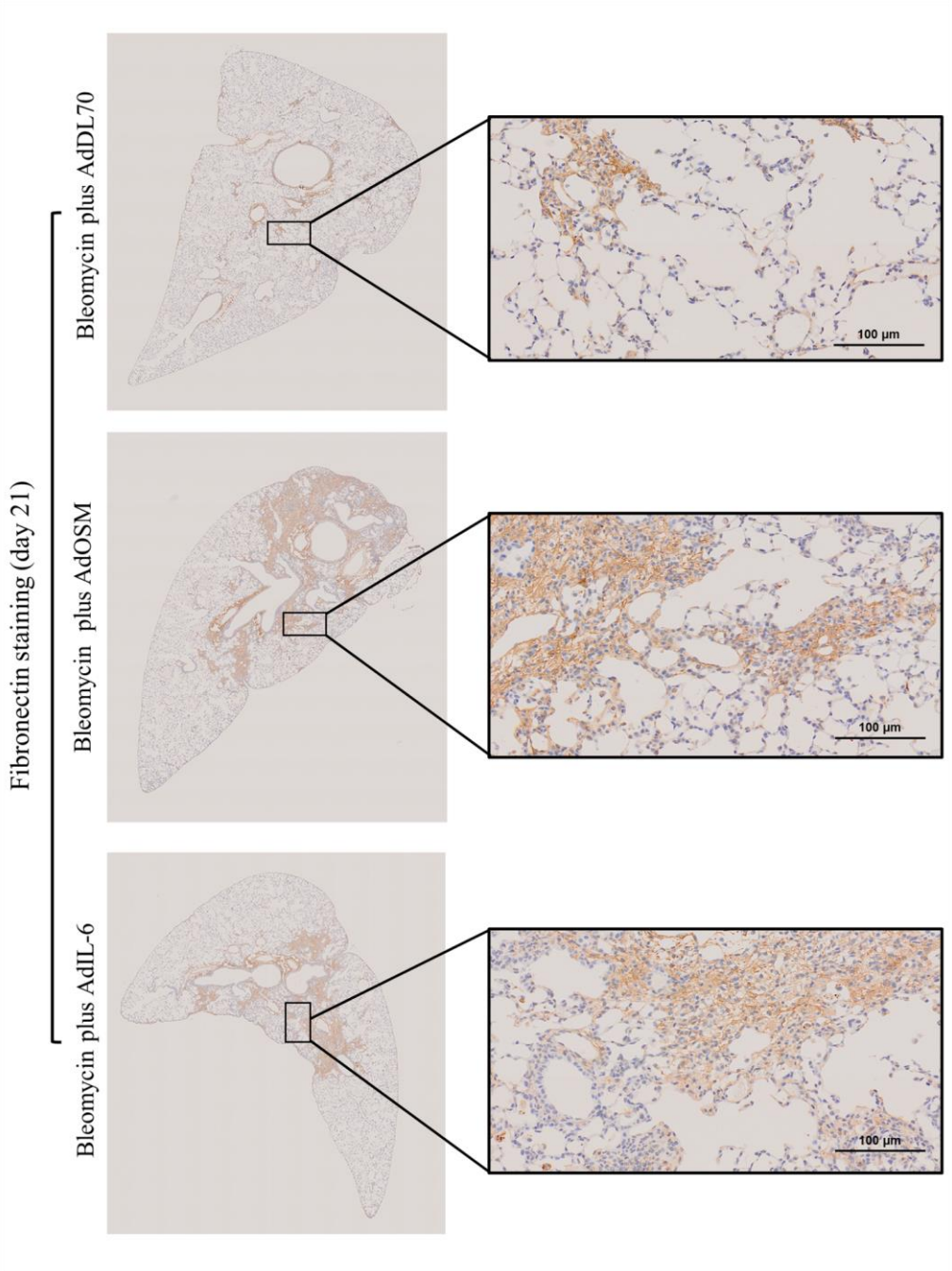

Supplementary Figure 5. Lung immunohistochemical staining of fibronectin in mice exposed to bleomycin plus AdOSM or AdIL-6 after 21 days of exposure.

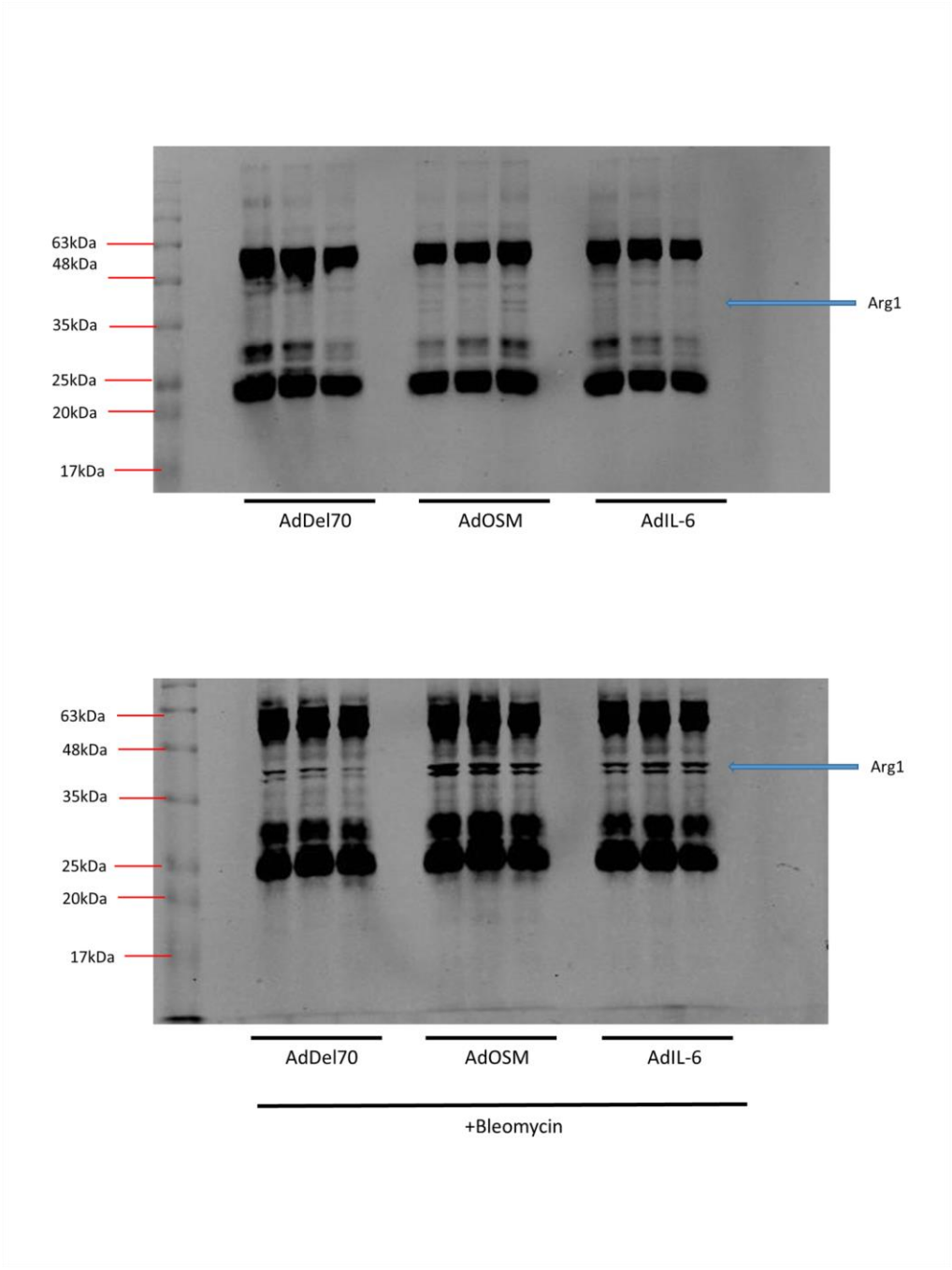

Supplementary Figure 6. Arginase-1 full length blots for figure 3A-3B

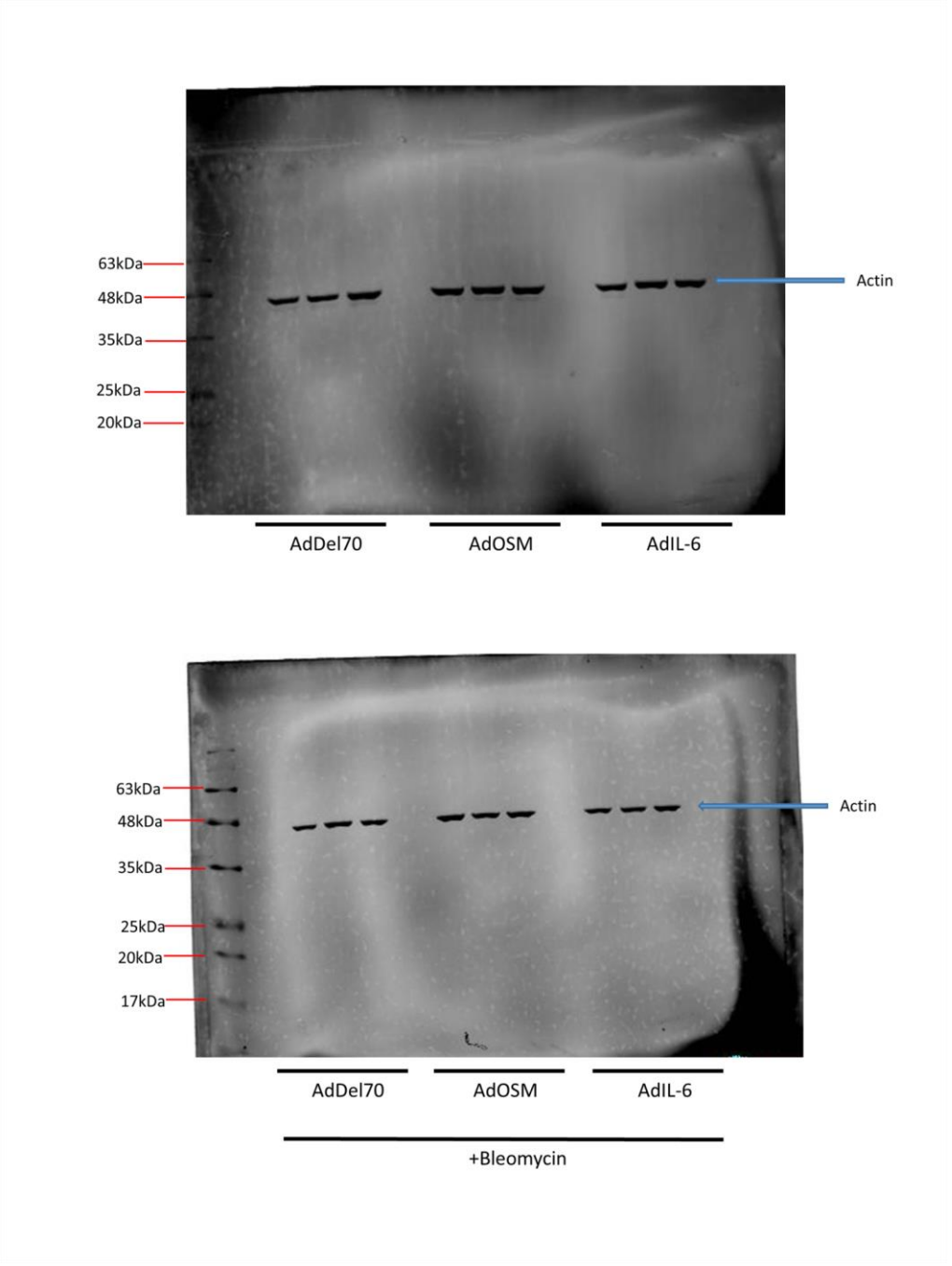

Supplementary Figure 7. Actin full length blots for figure 3A-3B

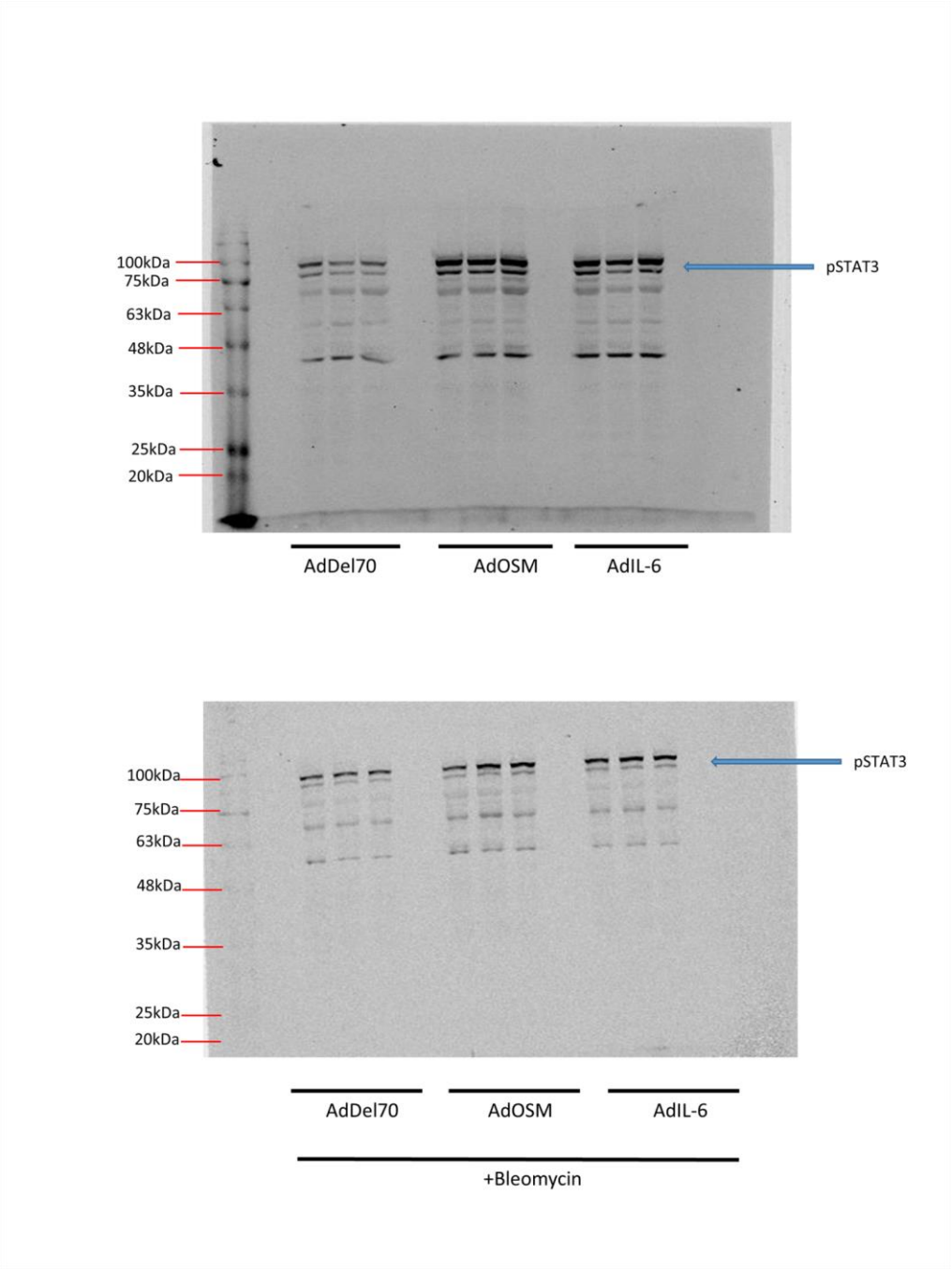

Supplementary Figure 8. pSTAT3 full length blots for figure 3A-3B

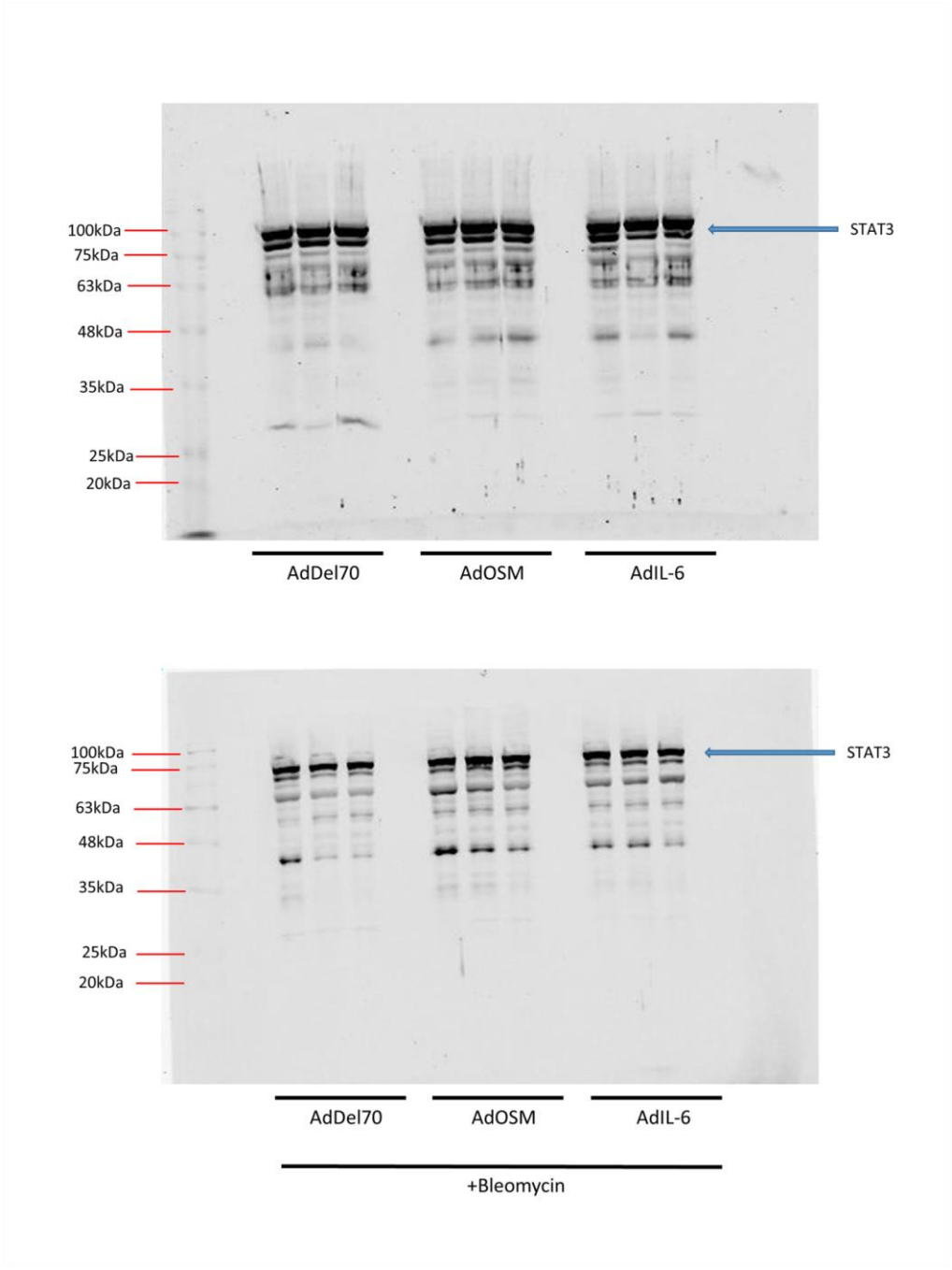

Supplementary Figure 9. STAT3 full length blots for figure 3A-3B

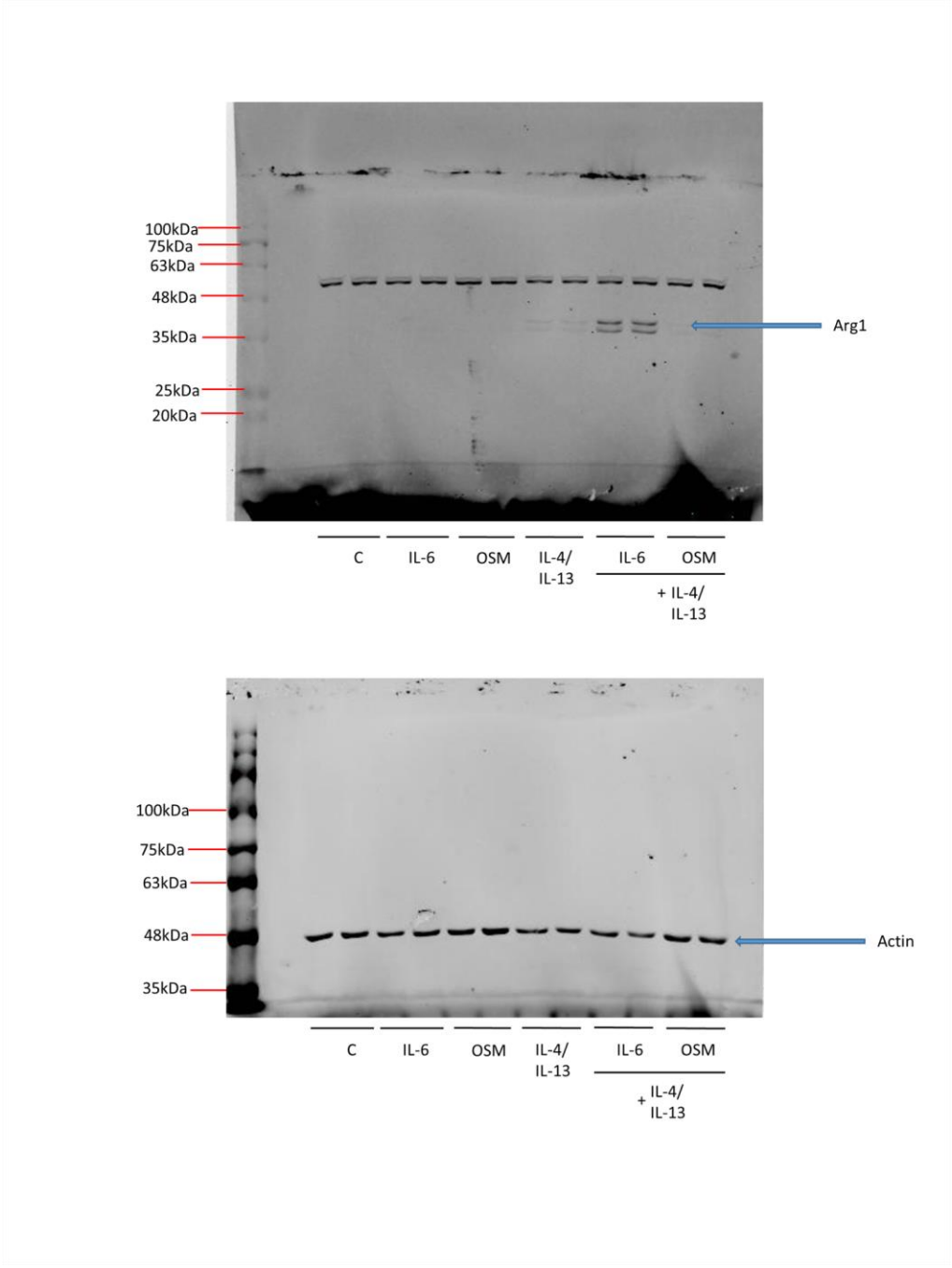

Supplementary Figure 10. Arginase-1 and Actin full length blots for figure 5E

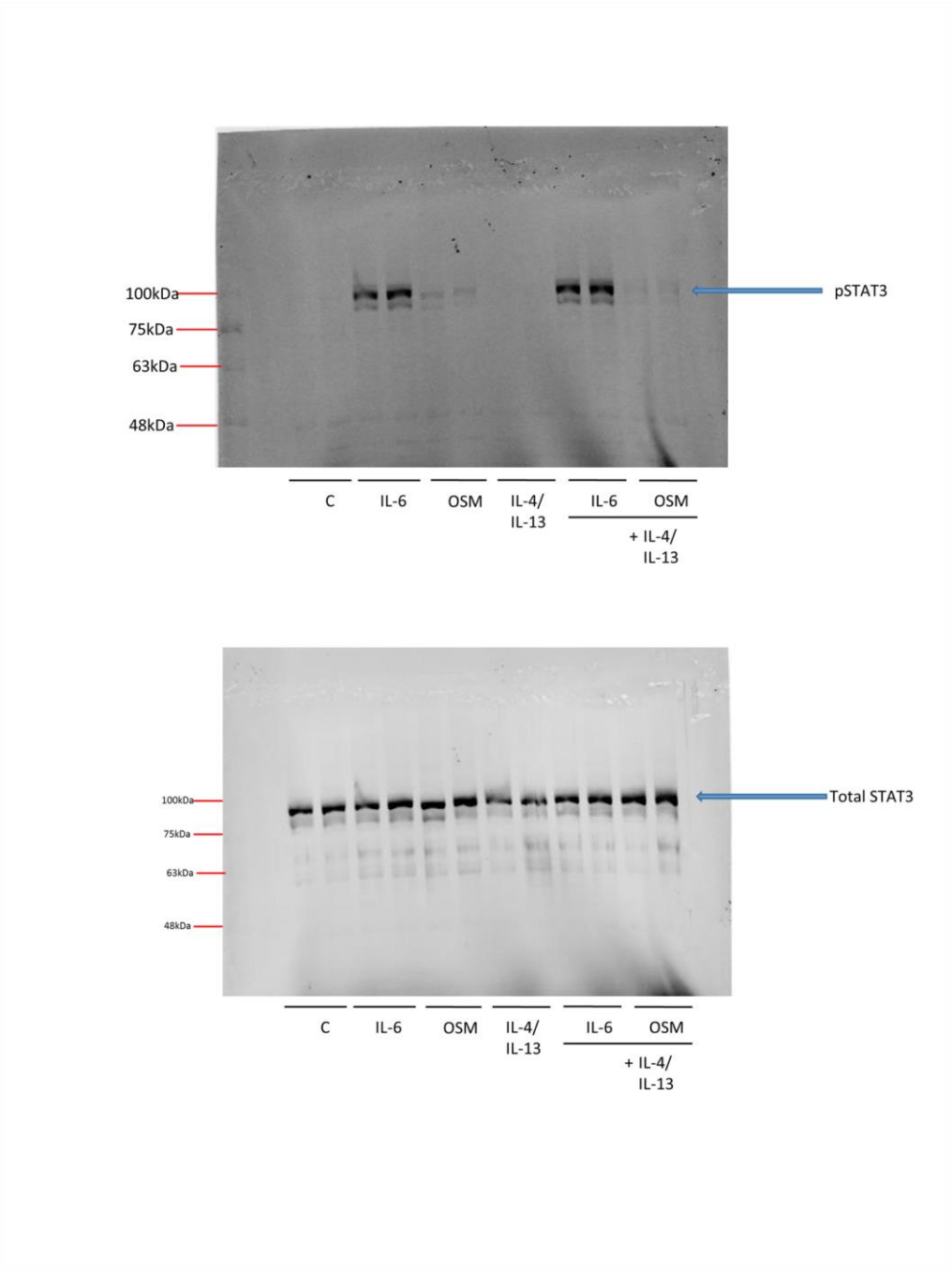

Supplementary Figure 11. pSTAT3 and STAT3 full length blots for figure 5E

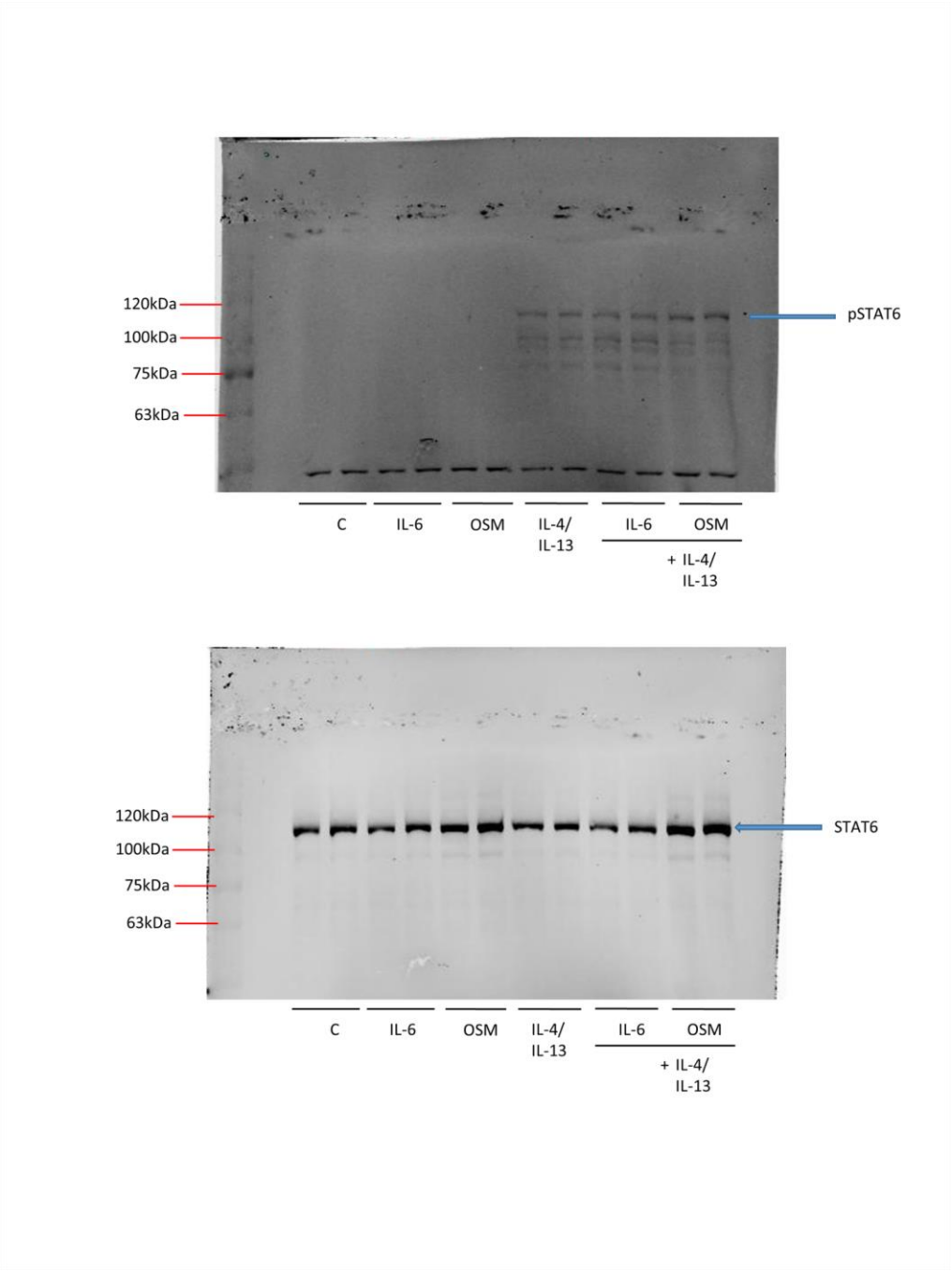

Supplementary Figure 12. pSTAT6 and STAT6 full length blots for figure 5E

Chapter 5

Discussion

In this chapter, the main findings of the previous chapters (2-4) will be discussed in the context of current findings in the literature. The rationale and major findings of the previous three studies have been extensively discussed in their respective chapters. Therefore, the goal of this section is to:

- Articulate the key findings of the thesis in the context of the literature
- Elaborate on how chapters 2-4 conceptually led to each other
- State how the work presented in this thesis contributes to the advancement of knowledge in the understanding of macrophage biology in chronic fibrotic lung disease
- Outline future directions for identifying the precise molecular mechanisms to understand macrophage pro-fibrotic function

ER stress-mediated apoptosis in fibrosis

Fibrosis is a major disease process involved in the pathogenesis of many chronic diseases, and impairs the function of many organs such as the kidney, lung, heart and liver [23]. While there is abundant research implicating a wide variety of cells and cellular mediators in perpetuating the fibrotic process, the exact molecular mechanisms that contribute to scarring in the lung remain to be fully understood.

The findings from chapter 2 identified a novel central approach to modulate fibrogenesis by altering macrophage function. Initially, we hypothesized that the hyper-active UPR, mediated by GRP78 partial loss, would lead to increased accumulation of myofibroblasts and epithelial cell death, ultimately resulting in worsened severity of fibrotic disease. On the contrary, Grp78 heterozygosity attenuated the fibrotic response in the lung but was nonetheless associated with high levels of ER stress markers and increased level of apoptosis (based on TUNEL positivity). This observation was initially puzzling considering that ER stress has been implicated in chronic tissue injury and triggering aberrant fibrotic processes in IPF patients [64, 72]. Upon further investigation, it was determined that the dying cells were apoptotic macrophages and not epithelial cells, reflected by reduced F4/80+ and Arg1+ macrophage cell numbers. The protected mice had a reduced accumulation of M2-like macrophages, thought to be the primary macrophage cell type implicated in promoting fibrosis [100]. Therefore, our findings further implicate M2-like macrophages in the fibrotic process and identify UPR activation in macrophages as a key pathway in fibrosis.

In the context of fibrosis where various immune and non-immune cellular contributors exist, cellular responses to UPR activation varies depending on the type of cells. Our data showed that UPR- and Chop-mediated apoptosis of macrophages protected animals from bleomycin-induced lung fibrosis. These results are consistent with the work of Malhi et al. on a mouse model of steatohepatitis. These authors elegantly demonstrated that deficiency in Chop, which is normally induced by ER stress and mediates apoptosis, rendered macrophages less susceptible to UPR-mediated apoptosis, resulting in augmented liver fibrosis [101]. In these cases, lack of UPR-mediated apoptosis appears to have a role in facilitating fibrotic disease processes. Alternatively, UPR-mediated apoptosis also serves as a physiological host defence response against the intracellular pathogen, especially during infection, such as with *Mycobacterium tuberculosis*, which exploits the host cellular machinery to their benefit [102]. By inducing apoptosis, the host can minimize bacterial proliferation and risk to the host's normal function. Aside from macrophage apoptosis, increasing evidence also suggests that alveolar epithelial cell apoptosis through ER-stress is a key event that elicits and progresses fibrosis in the lung parenchyma [64]. Pharmacological targeting of caspases, genetic removal of pro-apoptotic signalling genes, and the administration of ligands that mediate apoptosis in the animal model, have all been promising in abrogating lung fibrogenesis mediated by pro-fibrotic insults [103-106]. Collectively, these observations suggest that ER stress-mediated cell death in the affected cells could be either advantageous or detrimental,

depending on the precise cellular function and magnitude of stress within the diseased tissue.

Macrophage apoptosis, which can be mediated by a multitude of pathways, has been suggested to be central to the fibrotic process and regulation of the main effector cells, the myofibroblasts. In our fibrosis semi-resistant *Grp78*$^{+/-}$ lungs, the number of apoptotic macrophages increased with reduced number of αSMA-positive myofibroblasts, suggesting a possible direct or indirect link between these two cell types. As with our findings which demonstrated that the UPR-mediated macrophage apoptosis is an anti-fibrotic target, other molecular pathways programming macrophage apoptosis have been found to elicit a similar function. For instance, Akt1 (Akt Serine/Threonine kinase 1) activation during bleomycin-induced fibrosis elicited ROS-mediated TGFβ1 expression, activated mitophagy (engulfment of dysfunctional mitochondria by autophagosomes) and promoted macrophage survival [107]. In contrast, macrophage-specific deletion of Akt1 disrupted the mitophagy program and reduced fibrosis by enhancing macrophage apoptosis [107]. Macrophage apoptosis can also be mediated by liposome-encapsulated clodronate, which is thought to induce cascades and signals leading to the loss of mitochondrial inner membrane and cellular apoptosis [108]. When clodronate was administered during the fibrotic phase of bleomycin-induced lung fibrosis, the fibrotic outcome was significantly attenuated while their depletion during recovery phase delayed fibrotic disease resolution [54]. This finding is consistent with previous studies suggesting that macrophages are critical in influencing ECM degradation during the resolution of

liver fibrosis [109]; and alveolar macrophages contribute immensely to the uptake of collagen and the reversibility of bleomycin induced-lung fibrosis [56]. This constellation of evidence complements our findings that macrophage apoptosis during the early fibrotic phase (Day 7) was associated with a reduced fibrotic outcome in the *Grp78*$^{+/-}$ mice, while macrophage resistance to apoptosis in the *Chop*$^{-/-}$ mice was associated with enhanced ECM deposition in the lung. Whether macrophage resistance to undergo apoptosis in the *Chop*$^{-/-}$ mice is associated with decreased collagen degradation and reduced reversibility of bleomycin-induced fibrosis remains to be further investigated in future studies. Apoptotic cell death could have a protective or pathologic outcome on fibrosis depending on the type and phenotype of cells undergoing programmed suicide and mechanisms regulating timing of apoptosis. Pharmacological strategies aimed at selectively targeting the UPR to promote macrophage apoptosis or reducing macrophage activity can be utilized to provide novel anti-fibrotic targets.

UPR-mediated ER expansion during M2 macrophage polarization

The protective pro-fibrotic effect of UPR-mediated apoptosis of macrophages (as demonstrated in Chapter 2) revealed that the UPR can be targeted to promote macrophage apoptosis in response to injury-repair processes and modulate the polarization of macrophages towards the M2-like phenotype. Although ER stress has been implicated in alternative programming of macrophages and in foam cell formation (lipid-loaded macrophages in the atherosclerotic plague) [110, 111], the precise UPR pathway exploring this process has not been investigated. Our findings from Chapter 2 revealed

that M2-like macrophages are likely the subtype required for fibrogenesis. Our findings showed that Grp78 haplo-insufficiency promoted XBP1 induction in M2 macrophages, suggesting that the polarization process may be mediated by the IRE1-XBP1 arm of the UPR. Interestingly, IL-6 has recently been implicated in dramatically promoting macrophage polarization toward the M2-like phenotype in an obesity-associated model of inflammation [112]. How IL-6 affects the pro-fibrotic function and phenotype of macrophages and whether there is a targetable molecular process remains unclear. Together with these findings and our results from Chapter 2, the IL-6/M2 programming model provided us with a unique and compelling tool to study how UPR-mediated XBP1 expression is essential in the hyperpolarization of macrophages towards the M2-phenotype. Since IL-6 has been shown to increase IL-4Rα expression on macrophages [112], it can sensitize macrophages to IL-4-mediated effects and UPR-mediated XBP1 splicing. We have chosen to further investigate this process by primarily using murine bone marrow-derived macrophages (BMDMs) for a few reasons. a) Primary alveolar macrophages are limited in quantity and do not have the capacity to polarize towards the M2 phenotype *in vitro* (data not shown); b) Pro-fibrotic M2-like macrophages are thought to have a circulating progenitor and were recently shown to originate in the bone marrow [113]; and c) Similar to *ex-vivo* isolated pulmonary macrophages derived from murine models of fibrosis, BMDMs are responsive to IL-4/IL-13 to activate downstream signalling, leading to the expression of comparable molecules of interest (such as arginase-1, CD206 and fibronectin 1).

Our findings from Chapter 3 identified that IL-6-mediated programming of M2 macrophages increased ER expansion, induced XBP1 and generated a hyper-pro-fibrotic macrophage phenotype. Our results proposed the following scenario: Macrophage polarization into the alternatively activated phenotype activates the UPR, which expands the ER to accommodate the production, expression and secretion of pro-fibrotic products. During this process, XBP1 splicing occurs to promote the expansion process and further enhance UPR activation which supports the protein folding load within the ER. When IL-6 is present, it acts concurrently with IL-4 to synergize the above effects, thus further augmenting the UPR, ER expansion and pro-fibrotic potential of the macrophage. Although the literature has carefully examined and implicated the process of ER expansion in different cell types, little to no evidence explored this process in pro-fibrotic M2-like macrophages. We believe that we have addressed this gap in knowledge and provided a considerable amount of evidence to implicate IRE1-XBP1 pathway with ER expansion in M2 macrophages. Overall, our data showed that the IL-6/XBP1 axis could be a key to mediate macrophage pro-fibrotic functions.

The link between the relatively late timing of IRE1-XBP1 induction and the process of M2 polarization could suggest that there is an IRE1-independent pathway that is implicated in the polarization process. Due to the late induction during the polarization process, as we have showed, it is tempting to speculate that XBP1 promotes the expression of molecular chaperones needed to maintain ER homeostasis, and may not solely be responsible for the polarization process. Given that ER expansion is a complex

molecular process that requires the cooperation of many signals within the cell, other UPR stress sensors could further engage in ER membrane biogenesis [61]. It has been reported by Bommiasamy et al. that UPR-mediated ATF6α activation could also promote ER expansion and phospholipid biosynthesis, independent of XBP1-splicing [61]. The mechanisms acted by ATF6α could be distinct from those previously shown by XBP1, suggesting that a redundant pathway executes a vital cellular task. Since this process was investigated in stromal cells like NIH-3T3 (a fibroblast cell line derived from a mouse embryo) and CHO (an epithelial cell line derived from a Chinese hamster ovary), it remains unclear whether this pathway applies to the myeloid compartment or promotes macrophage pro-fibrotic activation. Overall, multiple UPR arms could facilitate a concerted effort in activating macrophage-ER expansion program, leading to enhanced pro-fibrotic capacity.

Fibroblast-to-myofibroblast conversion process is believed to be the most prevailing pathological process directly impacting fibrotic disease progression. As such, understanding the mechanisms and signals by which M2-like macrophages modulate this process is crucial for the development of novel anti-fibrotic targets. Our results, which showed a heightened αSMA positivity signal induced by IL-6-stimulated M2 macrophages, suggests a true pro-fibrotic nature of this unique macrophage subtype. To our knowledge, the direct co-culture approach employed by our study is the first in literature to address whether the close proximity between macrophages and fibroblasts can functionally contribute to the differentiation of fibroblasts to myofibroblasts. The

findings that neither the conditioned medium of M1 or M2+IL-6 macrophages nor M1 macrophages themselves influenced fibroblast-to-myofibroblast differentiation likely suggest the involvement of surface markers in fibroblast activation/differentiation. It is possible that without the physical co-existence of these cells, these hyper-pro-fibrotic macrophages are insufficient to drive fibroblasts-to-myofibroblasts differentiation solely with their secreted soluble mediators. However, it is still possible that the secreted factors from these pro-fibrotic macrophages activate fibroblasts to secrete soluble ECM products without causing fibroblasts-to-myofibroblast differentiation, as shown by Ploeger et al. [44]. Additionally, it could be logical to speculate that the crosstalk between fibroblasts and macrophages could be mediated by activated surface markers on hyper M2 macrophages to directly activate fibroblasts. Whether UPR activation (XBP1 splicing or ATF6 phosphorylation) contributes to the M2-mediated pro-fibrotic effect on fibroblasts remains under investigation. In this regard, targeting the ER expansion program genetically or pharmacologically would be helpful to better understand the macrophage function during wound healing. Overall, M2 polarization, enhanced by IL-6, is associated with increased ER expansion. This key finding suggest that IL-6 signalling and mechanism of ER expansion may serve as putative therapeutic targets to counter fibrosis.

IL-6 as a key promoter of macrophage pro-fibrotic function *in vivo*

In Chapter 3, it was determined that hyper M2 macrophages (IL-6–mediated polarization) exerted pro-fibrotic function. To directly address whether IL-6 can recapitulate such effects in a pro-fibrotic environment *in vivo*, we used adenoviruses to overexpress IL-6

(AdIL-6) and OSM (AdOSM) during bleomycin-mediated lung injury. In murine models of OSM overexpression, OSM has been shown to induce IL-6 cytokine expression *in vivo* [114], thus providing a unique way to induce IL-6-mediated signalling and rationalizing the implication of these two cytokines in driving fibrotic processes. These two cytokines enhanced the fibrotic response to bleomycin, as shown by a sizable accumulation of AAMs and pro-fibrotic factors. Our data suggests that while IL-6 acts directly on macrophages to promote the M2-like phenotype, OSM acts indirectly perhaps by acting on OSMR-sufficient cells to promote IL-6 release. These findings suggest that anti-IL-6Rα or anti-OSMRα could be utilized to modulate macrophage phenotypes, and subsequently reduce the extent of the fibrotic process.

Our findings from Chapter 4 are novel and support current thoughts in the literature that markers of M2-like macrophages increase during fibrotic disease exacerbation and progression. Previous studies in IPF patients have shown that a level of human M2 cytokine called BALF CCL18 elevates during acute exacerbation and predicts the development of a future exacerbation [6]. CCL18 is preferentially produced by human M2 macrophages and involved in the development of IgG4-DS – a Th2-driven fibrotic disease characterized by glandular swelling and extensive fibrosis [115]. M2-CCL18 production increases collagen production from lung fibroblasts [116] and even though it is not regarded as a murine M2 marker, its expression co-localizes on cells that are functionally and phenotypically viewed as M2-like cells. Interestingly, as with our murine models, IL-6 potentiated the M2 phenotype by augmenting CCL18 production in human

macrophage cell lines exposed to IL-4/IL-13. Our findings are consistent with the findings that M2-like macrophages are key producers of CCL18 [117]. Intriguingly, factors other than IL-6 have been shown to modulate the cellular release of CCL18. Prasse et al. showed that collagen type 1 could also upregulate CCL18 level in the injured lungs [49]. Based on this finding, one can speculate that the presence of IL-6 in a pro-fibrotic Th-2 like microenvironment could have an additional co-stimulatory effect on the macrophage M2 phenotype. Overall, our findings in the murine system (Chapter 4) uncovered, for the first time, a novel preclinical and biological link on how IL-6 may function in a pro-fibrotic *in vivo* setting.

The current knowledge from this project provides new and exciting future directions to uncover the true identity of M2-like macrophages in driving fibrotic lung disease. The strong association between IL-6-mediated accumulation of AAMs and the extent of the fibrotic process is promising in unmasking the true pro-fibrotic macrophage pathways directly responsible for laying down the ECM. Investigating the unique macrophage subtype within the Arg1+CD206+ population could clarify varying roles of AAM subtypes within the injury lungs. As demonstrated by Pesce et al., arginase-1 expressing macrophages have a suppressive effect on inflammation and fibrosis in a Th2-inducing infection model in the liver [118]. However, the precise action of these cells in the lungs remains to be further explored; one possible way by which their action could be tested is with the generation of myeloid specific knockout of arginase-1. While it is probable that the M2-like macrophages induced by IL-6 drives fibrogenesis, it is not currently feasible

to prove this speculation. The precise identification of the unique M2 polarized subpopulation that provokes pro-fibrotic effects remains unclear and requires new models and functional assays. Such knowledge is needed to specifically pinpoint the type of macrophage that promotes ECM build-up versus the type of macrophage that promotes collagen degradation and fibrotic disease resolution. To further elucidate the precise function of macrophages or monocytes elicited by IL-6, one possible experimental design would be to adoptively transfer these cells at each stage of bleomycin-induced lung injury (inflammatory phase vs. fibrotic phase vs. resolution phase) and further observe their impact on the fibrotic outcome. As there is a growing list of various chronic fibrotic diseases in which IL-6 is a key pleiotropic cytokine implicated in out-of-control fibrotic processes [119-122], our findings regarding IL-6 and macrophage pro-fibrotic activation may extend our knowledge to a broader spectrum of diseases, ranging from systemic fibroproliferative diseases (such as systemic sclerosis) and organ specific-fibrotic disorders (such as lung, liver, cardiac and kidney fibrosis). Thus, the need for a joint effort to identify and target the unique pro-fibrotic macrophage subtype may lead to the development of effective anti-fibrotic agents.

Aside from macrophages, pro-fibrotic monocytes can be recruited to the lung to directly impact the development of the fibrotic process. In our data, we have not assessed or quantitated monocytes and thereby cannot rule out the involvement of these cells in the pathology observed in bleomycin plus AdIL-6-exposed mice. Recently, Satoh et al. discovered that atypical monocytes with granulocytes characteristics, called SatM

(Ceacam1+Msr1+Ly6C-F4/80-Mac1+) monocytes, make up a novel subset of monocytes that are critical for fibrosis [113]. The generation of these monocytes is primarily controlled by the transcription factor C/EBPβ from a granulocyte/macrophage progenitor. Interestingly, C/EBPβ can also positively regulate IL-6 production [123], further implicating IL-6 in regulating the differentiation of SatM progenitors during pathological wound repair. Alternatively, IL-6 abundance in the injured tissue may yield a unique disease-specific subtype of monocytes or macrophages that differs in their characteristics and functionality. While we have not explored this possibility in our study, it would be worth to examine the IL-6/SatM axis in bleomycin-injured mouse lungs, which may allow us to move a step closer to understanding how IL-6 mediates pro-fibrotic effects.

All in all, our studies from Chapter 2-4 led to major findings in the field of macrophage biology and fibrosis: First of all, M2-like macrophages are likely the subtype required for the progression of fibrosis; pro-fibrotic macrophages polarization is enhanced with the addition of IL-6 and is associated with their increased capacity to produce fibrogenic factors and increased ER expansion; and lastly, the addition of IL-6, a key factor involved in the progression of fibrosis, increases fibrogenesis *in vivo*. These findings are novel and contribute to the advancement of knowledge by identifying M2-like macrophages, ER expansion and IL-6 as putative therapeutic targets to counter fibrotic disease progression.

Concluding remarks

The research discussed in Chapters 2-4 included: 1) A genetic manipulation study implicating GRP78- and UPR-mediated macrophage polarization and apoptosis in the pathobiology of lung fibrosis; 2) a mechanistic (pharmacological) approach to understanding how IL-6 contribute to UPR-mediated ER expansion and the generation of a hyper-pro-fibrotic macrophage phenotype; and 3) An adenoviral-directed over-expression of IL-6 and OSM investigating the role of IL-6 on macrophage pro-fibrotic function and the fibrotic response to bleomycin-induced pulmonary fibrosis.

The idea that the UPR is a targetable molecular pathway that can be utilized to modulate macrophage function is a novel finding with immense translational therapeutic potential. The opposing effects mediated by Grp78 and Chop on macrophage function and fibrosis provide a proof-of-principle platform that the UPR can be further scrutinized to either induce macrophage apoptosis or to manipulate their polarizing pro-fibrotic phenotype. Nonetheless, more research is needed to better understand and expand upon these findings in the context of basic science and translational realms. The *in vitro* study pertaining to IL-6 and ER expansion provides insights into the precise molecular machinery by which macrophages acquire a hyper-pro-fibrotic role, and how they might influence the downstream trans-differentiation of fibroblasts into scar-producing myofibroblasts. The ability to further explore the exact UPR pathway(s) to undermine this process will allow the understanding of a fundamental cellular switch and open up more avenues to explore diseases where macrophages are the primary cellular contributors. Future directions would be also to continue to understand the precise phenotype and

source of these pro-fibrotic M2-like cells and the factors that regulate their preferential homing to the fibrotic areas. Another important aspect of this work would be to look into cells that are upstream orchestrators of the fibrotic process (such as T cells) and identify the pro-fibrogenic phenotype of T cells that activate macrophages. Identifying the specific population of macrophages that transcribes and functionally elicits pro-fibrotic role, and understanding specific signalling that may modify macrophage phenotype will enhance targeted cellular therapies. Such knowledge will have clinical implications for IPF and possibly other diseases of chronic tissue remodelling and fibrosis**.**

References for Chapters 1 & 5

1. Lee, J.S. and H.R. Collard, *Idiopathic pulmonary fibrosis: continuing to make progress.* Lancet Respir Med, 2015. **3**(12): p. 921-3.
2. Robert Davidson. *Idiopathic Pulmonary Fibrosis - Patient Information Guide*. 2016; Available from: http://cpff.ca/wp-content/uploads/2016/05/IPF_Guide_2012_EN_Rev_Feb_2106_ForWeb.pdf.
3. Collard, H.R., et al., *Acute exacerbations of idiopathic pulmonary fibrosis.* Am J Respir Crit Care Med, 2007. **176**(7): p. 636-43.
4. Song, J.W., et al., *Acute exacerbation of idiopathic pulmonary fibrosis: incidence, risk factors and outcome.* Eur Respir J, 2011. **37**(2): p. 356-63.
5. Kim, D.S., *Acute exacerbations in patients with idiopathic pulmonary fibrosis.* Respir Res, 2013. **14**: p. 86.
6. Schupp, J.C., et al., *Macrophage activation in acute exacerbation of idiopathic pulmonary fibrosis.* PLoS One, 2015. **10**(1): p. e0116775.
7. Fernandez, I.E. and O. Eickelberg, *The impact of TGF-beta on lung fibrosis: from targeting to biomarkers.* Proc Am Thorac Soc, 2012. **9**(3): p. 111-6.
8. Selman, M., et al., *Emerging drugs for idiopathic pulmonary fibrosis.* Expert Opin Emerg Drugs, 2011. **16**(2): p. 341-62.
9. Coward, W.R., G. Saini, and G. Jenkins, *The pathogenesis of idiopathic pulmonary fibrosis.* Ther Adv Respir Dis, 2010. **4**(6): p. 367-88.
10. Barnes, P.J., *Inhaled corticosteroids are not beneficial in chronic obstructive pulmonary disease.* Am J Respir Crit Care Med, 2000. **161**(2 Pt 1): p. 342-4; discussioin 344.
11. Nickerson, M. and R.A. Marrie, *The multiple sclerosis relapse experience: patient-reported outcomes from the North American Research Committee on Multiple Sclerosis (NARCOMS) Registry.* BMC Neurol, 2013. **13**: p. 119.
12. King, T.E., Jr., et al., *A phase 3 trial of pirfenidone in patients with idiopathic pulmonary fibrosis.* N Engl J Med, 2014. **370**(22): p. 2083-92.
13. Richeldi, L., et al., *Efficacy and safety of nintedanib in idiopathic pulmonary fibrosis.* N Engl J Med, 2014. **370**(22): p. 2071-82.
14. Klingberg, F., B. Hinz, and E.S. White, *The myofibroblast matrix: implications for tissue repair and fibrosis.* J Pathol, 2013. **229**(2): p. 298-309.
15. Chapman, H.A., *Epithelial-mesenchymal interactions in pulmonary fibrosis.* Annu Rev Physiol, 2011. **73**: p. 413-35.
16. Lee, K. and C.M. Nelson, *New insights into the regulation of epithelial-mesenchymal transition and tissue fibrosis.* Int Rev Cell Mol Biol, 2012. **294**: p. 171-221.
17. Piera-Velazquez, S., F.A. Mendoza, and S.A. Jimenez, *Endothelial to Mesenchymal Transition (EndoMT) in the Pathogenesis of Human Fibrotic Diseases.* J Clin Med, 2016. **5**(4).
18. Piera-Velazquez, S., Z. Li, and S.A. Jimenez, *Role of endothelial-mesenchymal transition (EndoMT) in the pathogenesis of fibrotic disorders.* Am J Pathol, 2011. **179**(3): p. 1074-80.
19. Keeley, E.C., B. Mehrad, and R.M. Strieter, *The role of fibrocytes in fibrotic diseases of the lungs and heart.* Fibrogenesis Tissue Repair, 2011. **4**: p. 2.

20. Bellini, A. and S. Mattoli, *The role of the fibrocyte, a bone marrow-derived mesenchymal progenitor, in reactive and reparative fibroses.* Lab Invest, 2007. **87**(9): p. 858-70.
21. Kendall, R.T. and C.A. Feghali-Bostwick, *Fibroblasts in fibrosis: novel roles and mediators.* Front Pharmacol, 2014. **5**: p. 123.
22. Todd, N.W., I.G. Luzina, and S.P. Atamas, *Molecular and cellular mechanisms of pulmonary fibrosis.* Fibrogenesis Tissue Repair, 2012. **5**(1): p. 11.
23. Wynn, T.A. and T.R. Ramalingam, *Mechanisms of fibrosis: therapeutic translation for fibrotic disease.* Nat Med, 2012. **18**(7): p. 1028-40.
24. Kolahian, S., et al., *Immune Mechanisms in Pulmonary Fibrosis.* Am J Respir Cell Mol Biol, 2016. **55**(3): p. 309-22.
25. Helene, M., et al., *T cell independence of bleomycin-induced pulmonary fibrosis.* J Leukoc Biol, 1999. **65**(2): p. 187-95.
26. Christensen, P.J., et al., *Induction of lung fibrosis in the mouse by intratracheal instillation of fluorescein isothiocyanate is not T-cell-dependent.* Am J Pathol, 1999. **155**(5): p. 1773-9.
27. Feghali-Bostwick, C.A., et al., *Cellular and humoral autoreactivity in idiopathic pulmonary fibrosis.* J Immunol, 2007. **179**(4): p. 2592-9.
28. Papiris, S.A., et al., *Relationship of BAL and lung tissue CD4+ and CD8+ T lymphocytes, and their ratio in idiopathic pulmonary fibrosis.* Chest, 2005. **128**(4): p. 2971-7.
29. Daniil, Z., et al., *CD8+ T lymphocytes in lung tissue from patients with idiopathic pulmonary fibrosis.* Respir Res, 2005. **6**: p. 81.
30. Okazaki, T., et al., *Impairment of bleomycin-induced lung fibrosis in CD28-deficient mice.* J Immunol, 2001. **167**(4): p. 1977-81.
31. Gilani, S.R., et al., *CD28 down-regulation on circulating CD4 T-cells is associated with poor prognoses of patients with idiopathic pulmonary fibrosis.* PLoS One, 2010. **5**(1): p. e8959.
32. Simonian, P.L., et al., *gammadelta T cells protect against lung fibrosis via IL-22.* J Exp Med, 2010. **207**(10): p. 2239-53.
33. Keane, M.P., et al., *IL-12 attenuates bleomycin-induced pulmonary fibrosis.* Am J Physiol Lung Cell Mol Physiol, 2001. **281**(1): p. L92-7.
34. Wilson, M.S., et al., *Bleomycin and IL-1beta-mediated pulmonary fibrosis is IL-17A dependent.* J Exp Med, 2010. **207**(3): p. 535-52.
35. Saito, A., et al., *Potential action of IL-4 and IL-13 as fibrogenic factors on lung fibroblasts in vitro.* Int Arch Allergy Immunol, 2003. **132**(2): p. 168-76.
36. Boveda-Ruiz, D., et al., *Differential role of regulatory T cells in early and late stages of pulmonary fibrosis.* Immunobiology, 2013. **218**(2): p. 245-54.
37. Garibaldi, B.T., et al., *Regulatory T cells reduce acute lung injury fibroproliferation by decreasing fibrocyte recruitment.* Am J Respir Cell Mol Biol, 2013. **48**(1): p. 35-43.
38. Maggi, E., et al., *Thymic regulatory T cells.* Autoimmun Rev, 2005. **4**(8): p. 579-86.

39. Adegunsoye, A., et al., *Skewed Lung CCR4 to CCR6 CD4+ T Cell Ratio in Idiopathic Pulmonary Fibrosis Is Associated with Pulmonary Function.* Front Immunol, 2016. **7**: p. 516.
40. Atamas, S.P., et al., *Production of type 2 cytokines by CD8+ lung cells is associated with greater decline in pulmonary function in patients with systemic sclerosis.* Arthritis Rheum, 1999. **42**(6): p. 1168-78.
41. Brodeur, T.Y., et al., *IL-21 Promotes Pulmonary Fibrosis through the Induction of Profibrotic CD8+ T Cells.* J Immunol, 2015. **195**(11): p. 5251-60.
42. Slosman, D.O., et al., *Bleomycin primes monocytes-macrophages for superoxide production.* Eur Respir J, 1990. **3**(7): p. 772-8.
43. Lehnert, B.E., et al., *Stimulation of rat and murine alveolar macrophage proliferation by lung fibroblasts.* Am J Respir Cell Mol Biol, 1994. **11**(4): p. 375-85.
44. Ploeger, D.T., et al., *Cell plasticity in wound healing: paracrine factors of M1/ M2 polarized macrophages influence the phenotypical state of dermal fibroblasts.* Cell Commun Signal, 2013. **11**(1): p. 29.
45. Murray, P.J., et al., *Macrophage activation and polarization: nomenclature and experimental guidelines.* Immunity, 2014. **41**(1): p. 14-20.
46. Martinez, F.O., et al., *Macrophage activation and polarization.* Front Biosci, 2008. **13**: p. 453-61.
47. Laskin, D.L., et al., *Macrophages and tissue injury: agents of defense or destruction?* Annu Rev Pharmacol Toxicol, 2011. **51**: p. 267-88.
48. Pechkovsky, D.V., et al., *Alternatively activated alveolar macrophages in pulmonary fibrosis-mediator production and intracellular signal transduction.* Clin Immunol, 2010. **137**(1): p. 89-101.
49. Prasse, A., et al., *A vicious circle of alveolar macrophages and fibroblasts perpetuates pulmonary fibrosis via CCL18.* Am J Respir Crit Care Med, 2006. **173**(7): p. 781-92.
50. Zhu, Z., et al., *Alternatively activated macrophages derived from THP-1 cells promote the fibrogenic activities of human dermal fibroblasts.* Wound Repair Regen, 2017.
51. Vannella, K.M. and T.A. Wynn, *Mechanisms of Organ Injury and Repair by Macrophages.* Annu Rev Physiol, 2017. **79**: p. 593-617.
52. Wynn, T.A. and K.M. Vannella, *Macrophages in Tissue Repair, Regeneration, and Fibrosis.* Immunity, 2016. **44**(3): p. 450-62.
53. Migliaccio, C.T., et al., *The IL-4Ralpha pathway in macrophages and its potential role in silica-induced pulmonary fibrosis.* J Leukoc Biol, 2008. **83**(3): p. 630-9.
54. Gibbons, M.A., et al., *Ly6Chi monocytes direct alternatively activated profibrotic macrophage regulation of lung fibrosis.* Am J Respir Crit Care Med, 2011. **184**(5): p. 569-81.
55. Okuma, T., et al., *C-C chemokine receptor 2 (CCR2) deficiency improves bleomycin-induced pulmonary fibrosis by attenuation of both macrophage infiltration and production of macrophage-derived matrix metalloproteinases.* J Pathol, 2004. **204**(5): p. 594-604.

56. Atabai, K., et al., *Mfge8 diminishes the severity of tissue fibrosis in mice by binding and targeting collagen for uptake by macrophages.* J Clin Invest, 2009. **119**(12): p. 3713-22.
57. Wang, M. and R.J. Kaufman, *Protein misfolding in the endoplasmic reticulum as a conduit to human disease.* Nature, 2016. **529**(7586): p. 326-35.
58. Zhang, L.H. and X. Zhang, *Roles of GRP78 in physiology and cancer.* J Cell Biochem, 2010. **110**(6): p. 1299-305.
59. Hendershot, L.M., *The ER function BiP is a master regulator of ER function.* Mt Sinai J Med, 2004. **71**(5): p. 289-97.
60. Ron, D. and P. Walter, *Signal integration in the endoplasmic reticulum unfolded protein response.* Nat Rev Mol Cell Biol, 2007. **8**(7): p. 519-29.
61. Bommiasamy, H., et al., *ATF6alpha induces XBP1-independent expansion of the endoplasmic reticulum.* J Cell Sci, 2009. **122**(Pt 10): p. 1626-36.
62. Kaufman, R.J., *Orchestrating the unfolded protein response in health and disease.* J Clin Invest, 2002. **110**(10): p. 1389-98.
63. Tanjore, H., W.E. Lawson, and T.S. Blackwell, *Endoplasmic reticulum stress as a pro-fibrotic stimulus.* Biochim Biophys Acta, 2013. **1832**(7): p. 940-7.
64. Korfei, M., et al., *Epithelial endoplasmic reticulum stress and apoptosis in sporadic idiopathic pulmonary fibrosis.* Am J Respir Crit Care Med, 2008. **178**(8): p. 838-46.
65. Torres-Gonzalez, E., et al., *Role of endoplasmic reticulum stress in age-related susceptibility to lung fibrosis.* Am J Respir Cell Mol Biol, 2012. **46**(6): p. 748-56.
66. Wei, J., et al., *Protein misfolding and endoplasmic reticulum stress in chronic lung disease.* Chest, 2013. **143**(4): p. 1098-105.
67. Horowitz, J.C. and A.H. Limper, *Stress in the ER (endoplasmic reticulum): a matter of life and death for epithelial cells.* Am J Respir Crit Care Med, 2008. **178**(8): p. 782-3.
68. Selman, M. and A. Pardo, *Idiopathic pulmonary fibrosis: an epithelial/fibroblastic cross-talk disorder.* Respir Res, 2002. **3**: p. 3.
69. Roberson, E.C., et al., *Influenza induces endoplasmic reticulum stress, caspase-12-dependent apoptosis, and c-Jun N-terminal kinase-mediated transforming growth factor-beta release in lung epithelial cells.* Am J Respir Cell Mol Biol, 2012. **46**(5): p. 573-81.
70. Somborac-Bacura, A., et al., *Cigarette smoke induces endoplasmic reticulum stress response and proteasomal dysfunction in human alveolar epithelial cells.* Exp Physiol, 2013. **98**(1): p. 316-25.
71. Watterson, T.L., et al., *Urban particulate matter causes ER stress and the unfolded protein response in human lung cells.* Toxicol Sci, 2009. **112**(1): p. 111-22.
72. Lawson, W.E., et al., *Endoplasmic reticulum stress enhances fibrotic remodeling in the lungs.* Proc Natl Acad Sci U S A, 2011. **108**(26): p. 10562-7.
73. Tanjore, H., et al., *Alveolar epithelial cells undergo epithelial-to-mesenchymal transition in response to endoplasmic reticulum stress.* J Biol Chem, 2011. **286**(35): p. 30972-80.

74. Baek, H.A., et al., *Involvement of endoplasmic reticulum stress in myofibroblastic differentiation of lung fibroblasts.* Am J Respir Cell Mol Biol, 2012. **46**(6): p. 731-9.
75. Ayala, P., et al., *Attenuation of endoplasmic reticulum stress using the chemical chaperone 4-phenylbutyric acid prevents cardiac fibrosis induced by isoproterenol.* Exp Mol Pathol, 2012. **92**(1): p. 97-104.
76. Riek, A.E., J. Oh, and C. Bernal-Mizrachi, *1,25(OH)(2) vitamin D suppresses macrophage migration and reverses atherogenic cholesterol metabolism in type 2 diabetic patients.* J Steroid Biochem Mol Biol, 2013.
77. Dickhout, J.G., et al., *Induction of the unfolded protein response after monocyte to macrophage differentiation augments cell survival in early atherosclerotic lesions.* FASEB J, 2011. **25**(2): p. 576-89.
78. Reimold, A.M., et al., *Plasma cell differentiation requires the transcription factor XBP-1.* Nature, 2001. **412**(6844): p. 300-7.
79. Iwakoshi, N.N., et al., *Plasma cell differentiation and the unfolded protein response intersect at the transcription factor XBP-1.* Nat Immunol, 2003. **4**(4): p. 321-9.
80. Ohmori, Y. and T.A. Hamilton, *STAT6 is required for the anti-inflammatory activity of interleukin-4 in mouse peritoneal macrophages.* J Biol Chem, 1998. **273**(44): p. 29202-9.
81. Heinrich, P.C., et al., *Principles of interleukin (IL)-6-type cytokine signalling and its regulation.* Biochem J, 2003. **374**(Pt 1): p. 1-20.
82. Hirano, T., *Interleukin 6 and its receptor: ten years later.* Int Rev Immunol, 1998. **16**(3-4): p. 249-84.
83. Cappelli, S., et al., *Interstitial lung disease in systemic sclerosis: where do we stand?* Eur Respir Rev, 2015. **24**(137): p. 411-9.
84. De Lauretis, A., et al., *Serum interleukin 6 is predictive of early functional decline and mortality in interstitial lung disease associated with systemic sclerosis.* J Rheumatol, 2013. **40**(4): p. 435-46.
85. Collard, H.R., et al., *Plasma biomarker profiles in acute exacerbation of idiopathic pulmonary fibrosis.* Am J Physiol Lung Cell Mol Physiol, 2010. **299**(1): p. L3-7.
86. Jones, S.A., J. Scheller, and S. Rose-John, *Therapeutic strategies for the clinical blockade of IL-6/gp130 signaling.* J Clin Invest, 2011. **121**(9): p. 3375-83.
87. Jones, S.A., et al., *IL-6 transsignaling: the in vivo consequences.* J Interferon Cytokine Res, 2005. **25**(5): p. 241-53.
88. Yu, H., D. Pardoll, and R. Jove, *STATs in cancer inflammation and immunity: a leading role for STAT3.* Nat Rev Cancer, 2009. **9**(11): p. 798-809.
89. Jostock, T., et al., *Soluble gp130 is the natural inhibitor of soluble interleukin-6 receptor transsignaling responses.* Eur J Biochem, 2001. **268**(1): p. 160-7.
90. Wong, S., et al., *Oncostatin M overexpression induces matrix deposition, STAT3 activation, and SMAD1 Dysregulation in lungs of fibrosis-resistant BALB/c mice.* Lab Invest, 2014. **94**(9): p. 1003-16.

91. Yu, Y., et al., *Leukemia inhibitory factor attenuates renal fibrosis through Stat3-miR-29c.* Am J Physiol Renal Physiol, 2015. **309**(7): p. F595-603.
92. Dong, Z., et al., *IL-27 alleviates the bleomycin-induced pulmonary fibrosis by regulating the Th17 cell differentiation.* BMC Pulm Med, 2015. **15**: p. 13.
93. Le, T.T., et al., *Blockade of IL-6 Trans signaling attenuates pulmonary fibrosis.* J Immunol, 2014. **193**(7): p. 3755-68.
94. Saito, F., et al., *Role of interleukin-6 in bleomycin-induced lung inflammatory changes in mice.* Am J Respir Cell Mol Biol, 2008. **38**(5): p. 566-71.
95. Smith, R.E., et al., *TNF and IL-6 mediate MIP-1alpha expression in bleomycin-induced lung injury.* J Leukoc Biol, 1998. **64**(4): p. 528-36.
96. Kobayashi, T., et al., *Bidirectional role of IL-6 signal in pathogenesis of lung fibrosis.* Respir Res, 2015. **16**: p. 99.
97. Castranova, V., et al., *The alveolar type II epithelial cell: a multifunctional pneumocyte.* Toxicol Appl Pharmacol, 1988. **93**(3): p. 472-83.
98. Desallais, L., et al., *Targeting IL-6 by both passive or active immunization strategies prevents bleomycin-induced skin fibrosis.* Arthritis Res Ther, 2014. **16**(4): p. R157.
99. Khanna, D., et al., *Safety and efficacy of subcutaneous tocilizumab in adults with systemic sclerosis (faSScinate): a phase 2, randomised, controlled trial.* Lancet, 2016. **387**(10038): p. 2630-40.
100. Lech, M. and H.J. Anders, *Macrophages and fibrosis: How resident and infiltrating mononuclear phagocytes orchestrate all phases of tissue injury and repair.* Biochim Biophys Acta, 2013. **1832**(7): p. 989-97.
101. Malhi, H., et al., *C/EBP homologous protein-induced macrophage apoptosis protects mice from steatohepatitis.* J Biol Chem, 2013. **288**(26): p. 18624-42.
102. Seimon, T.A., et al., *Induction of ER stress in macrophages of tuberculosis granulomas.* PLoS One, 2010. **5**(9): p. e12772.
103. Kuwano, K., et al., *Attenuation of bleomycin-induced pneumopathy in mice by a caspase inhibitor.* Am J Physiol Lung Cell Mol Physiol, 2001. **280**(2): p. L316-25.
104. Wang, R., et al., *Abrogation of bleomycin-induced epithelial apoptosis and lung fibrosis by captopril or by a caspase inhibitor.* Am J Physiol Lung Cell Mol Physiol, 2000. **279**(1): p. L143-51.
105. Budinger, G.R., et al., *Proapoptotic Bid is required for pulmonary fibrosis.* Proc Natl Acad Sci U S A, 2006. **103**(12): p. 4604-9.
106. Hagimoto, N., et al., *Induction of apoptosis and pulmonary fibrosis in mice in response to ligation of Fas antigen.* Am J Respir Cell Mol Biol, 1997. **17**(3): p. 272-8.
107. Larson-Casey, J.L., et al., *Macrophage Akt1 Kinase-Mediated Mitophagy Modulates Apoptosis Resistance and Pulmonary Fibrosis.* Immunity, 2016. **44**(3): p. 582-96.
108. Lehenkari, P.P., et al., *Further insight into mechanism of action of clodronate: inhibition of mitochondrial ADP/ATP translocase by a nonhydrolyzable, adenine-containing metabolite.* Mol Pharmacol, 2002. **61**(5): p. 1255-62.

109. Duffield, J.S., et al., *Selective depletion of macrophages reveals distinct, opposing roles during liver injury and repair.* J Clin Invest, 2005. **115**(1): p. 56-65.
110. Oh, J., et al., *Endoplasmic reticulum stress controls M2 macrophage differentiation and foam cell formation.* J Biol Chem, 2012. **287**(15): p. 11629-41.
111. Yao, S., et al., *Endoplasmic reticulum stress promotes macrophage-derived foam cell formation by up-regulating cluster of differentiation 36 (CD36) expression.* J Biol Chem, 2014. **289**(7): p. 4032-42.
112. Mauer, J., et al., *Signaling by IL-6 promotes alternative activation of macrophages to limit endotoxemia and obesity-associated resistance to insulin.* Nat Immunol, 2014. **15**(5): p. 423-30.
113. Satoh, T., et al., *Identification of an atypical monocyte and committed progenitor involved in fibrosis.* Nature, 2017. **541**(7635): p. 96-101.
114. Lauber, S., et al., *Novel function of Oncostatin M as a potent tumour-promoting agent in lung.* Int J Cancer, 2015. **136**(4): p. 831-43.
115. Furukawa, S., et al., *Preferential M2 macrophages contribute to fibrosis in IgG4-related dacryoadenitis and sialoadenitis, so-called Mikulicz's disease.* Clin Immunol, 2015. **156**(1): p. 9-18.
116. Luzina, I.G., et al., *CCL18-stimulated upregulation of collagen production in lung fibroblasts requires Sp1 signaling and basal Smad3 activity.* J Cell Physiol, 2006. **206**(1): p. 221-8.
117. Chen, J., et al., *CCL18 from tumor-associated macrophages promotes breast cancer metastasis via PITPNM3.* Cancer Cell, 2011. **19**(4): p. 541-55.
118. Pesce, J.T., et al., *Arginase-1-expressing macrophages suppress Th2 cytokine-driven inflammation and fibrosis.* PLoS Pathog, 2009. **5**(4): p. e1000371.
119. Khan, K., et al., *Clinical and pathological significance of interleukin 6 overexpression in systemic sclerosis.* Ann Rheum Dis, 2012. **71**(7): p. 1235-42.
120. Choi, I., et al., *IL-6 induces hepatic inflammation and collagen synthesis in vivo.* Clin Exp Immunol, 1994. **95**(3): p. 530-5.
121. Melendez, G.C., et al., *Interleukin 6 mediates myocardial fibrosis, concentric hypertrophy, and diastolic dysfunction in rats.* Hypertension, 2010. **56**(2): p. 225-31.
122. Fielding, C.A., et al., *Interleukin-6 signaling drives fibrosis in unresolved inflammation.* Immunity, 2014. **40**(1): p. 40-50.
123. Hungness, E.S., et al., *Transcription factors C/EBP-beta and -delta regulate IL-6 production in IL-1beta-stimulated human enterocytes.* J Cell Physiol, 2002. **192**(1): p. 64-70.

Appendix

COPYRIGHT INFORMATION

Part of this thesis consists of a reprint of a previously published original article. This includes Chapter 2, as indicated below:

TERMS AND CONDITIONS

This copyrighted material is owned by or exclusively licensed to John Wiley & Sons, Inc. or one of its group companies (each a"Wiley Company") or handled on behalf of a society with which a Wiley Company has exclusive publishing rights in relation to a particular work (collectively "WILEY"). By clicking "accept" in connection with completing this licensing transaction, you agree that the following terms and conditions apply to this transaction (along with the billing and payment terms and conditions established by the Copyright Clearance Center Inc., ("CCC's Billing and Payment terms and conditions"), at the time that you opened your RightsLink account (these are available at any time at http://myaccount.copyright.com).

Terms and Conditions

- The materials you have requested permission to reproduce or reuse (the "Wiley Materials") are protected by copyright.
- You are hereby granted a personal, non-exclusive, non-sub licensable (on a stand-alone basis), non-transferable, worldwide, limited license to reproduce the Wiley Materials for the purpose specified in the licensing process. This license, **and any CONTENT (PDF or image file) purchased as part of your order,** is for a one-time use only and limited to any maximum distribution number specified in the license. The first instance of republication or reuse granted by this license must be completed within two years of the date of the grant of this license (although copies prepared before the end date may be distributed thereafter). The Wiley Materials shall not be used in any other manner or for any other purpose, beyond what is granted in the license. Permission is granted subject to an appropriate acknowledgement given to the author, title of the material/book/journal and the publisher. You shall also duplicate the copyright notice that appears in the Wiley publication in your use of the Wiley Material. Permission is also granted on the understanding that nowhere in the text is a previously published source acknowledged for all or part of this Wiley Material. Any third party content is expressly excluded from this permission.
- With respect to the Wiley Materials, all rights are reserved. Except as expressly granted by the terms of the license, no part of the Wiley Materials may be copied, modified, adapted (except for minor reformatting required by the new Publication), translated, reproduced, transferred or distributed, in any form or by any means, and no derivative works may be made based on the Wiley Materials without the prior permission of the respective copyright owner.**For STM Signatory Publishers clearing permission under the terms of the STM Permissions Guidelines only, the terms of the license are extended to include subsequent editions and for editions in other languages, provided such editions are for the work as a whole in situ and does not involve the separate exploitation of the permitted figures or extracts,** You may not alter, remove or suppress in any manner any copyright, trademark or other notices displayed by the Wiley Materials. You may not license, rent, sell, loan, lease, pledge, offer as security, transfer or assign the Wiley Materials on a stand-alone basis, or any of the rights granted to you hereunder to any other person.
- The Wiley Materials and all of the intellectual property rights therein shall at all times remain the exclusive property of John Wiley & Sons Inc, the Wiley Companies, or their respective licensors, and your interest therein is only that of having possession of and the right to reproduce the Wiley Materials pursuant to Section 2 herein during the continuance of this Agreement. You agree that you own no right, title or interest in or to the Wiley Materials or any of the intellectual property rights therein. You shall have no rights hereunder other than the license as provided for above in Section 2. No right,

- Any fee required for this permission shall be non-refundable after thirty (30) days from receipt by the CCC.
- These terms and conditions together with CCC's Billing and Payment terms and conditions (which are incorporated herein) form the entire agreement between you and WILEY concerning this licensing transaction and (in the absence of fraud) supersedes all prior agreements and representations of the parties, oral or written. This Agreement may not be amended except in writing signed by both parties. This Agreement shall be binding upon and inure to the benefit of the parties' successors, legal representatives, and authorized assigns.
- In the event of any conflict between your obligations established by these terms and conditions and those established by CCC's Billing and Payment terms and conditions, these terms and conditions shall prevail.
- WILEY expressly reserves all rights not specifically granted in the combination of (i) the license details provided by you and accepted in the course of this licensing transaction, (ii) these terms and conditions and (iii) CCC's Billing and Payment terms and conditions.
- This Agreement will be void if the Type of Use, Format, Circulation, or Requestor Type was misrepresented during the licensing process.
- This Agreement shall be governed by and construed in accordance with the laws of the State of New York, USA, without regards to such state's conflict of law rules. Any legal action, suit or proceeding arising out of or relating to these Terms and Conditions or the breach thereof shall be instituted in a court of competent jurisdiction in New York County in the State of New York in the United States of America and each party hereby consents and submits to the personal jurisdiction of such court, waives any objection to venue in such court and consents to service of process by registered or certified mail, return receipt requested, at the last known address of such party.

WILEY OPEN ACCESS TERMS AND CONDITIONS

Wiley Publishes Open Access Articles in fully Open Access Journals and in Subscription journals offering Online Open. Although most of the fully Open Access journals publish open access articles under the terms of the Creative Commons Attribution (CC BY) License only, the subscription journals and a few of the Open Access Journals offer a choice of Creative Commons Licenses. The license type is clearly identified on the article.

The Creative Commons Attribution License

The Creative Commons Attribution License (CC-BY) allows users to copy, distribute and transmit an article, adapt the article and make commercial use of the article. The CC-BY license permits commercial and non-

Creative Commons Attribution Non-Commercial License

The Creative Commons Attribution Non-Commercial (CC-BY-NC)License permits use, distribution and reproduction in any medium, provided the original work is properly cited and is not used for commercial purposes.(see below)

Creative Commons Attribution-Non-Commercial-NoDerivs License

The Creative Commons Attribution Non-Commercial-NoDerivs License (CC-BY-NC-ND) permits use, distribution and reproduction in any medium, provided the original work is properly cited, is not used for commercial purposes and no modifications or adaptations are made. (see below)

Use by commercial "for-profit" organizations
Use of Wiley Open Access articles for commercial, promotional, or marketing purposes requires further explicit permission from Wiley and will be subject to a fee.
Further details can be found on Wiley Online Library
http://olabout.wiley.com/WileyCDA/Section/id-410895.html

Other Terms and Conditions:

v1.10 Last updated September 2015

Questions? customercare@copyright.com or +1-855-239-3415 (toll free in the US) or +1-978-646-2777.